Deliverable 16.1: MAGIC - T1 - Initial State of the Art on the chemo-mechanical evolution of cementitious materials in disposal conditions

Work Package 16

This project has received funding from the European Union's Horizon 2020 research and innovation programme 2014-2018 under grant agreement N°847593.

Document information

Project Acronym	**EURAD**
Project Title	**European Joint Programme on Radioactive Waste Management**
Project Type	**European Joint Programme (EJP)**
EC grant agreement No.	**847593**
Project starting / end date	**1st June 2019 – 30 May 2024**
Work Package No.	**16**
Work Package Title	**Chemo-Mechanical AGIng of Cementitious materials**
Work Package Acronym	**MAGIC**
Deliverable No.	**16.1**
Deliverable Title	**Initial State of the Art on the chemo-mechanical evolution of cementitious materials in disposal conditions**
Lead Beneficiary	**IRSN**
Contractual Delivery Date	**May 2022**
Actual Delivery Date	**November 2022**
Type	**Report**
Dissemination level	**PU**
Authors	**Alexandre Dauzères (IRSN), Olivier Helson (ANDRA), Sergey Churakov (PSI), Vanessa Montoya (UFZ;SCK-CEN), Jad Zghondi (ANDRA), Erika Neeft (COVRA), Jianfu Shao (LAMCUBE), Andrea Cherkouk (HZDR), Kristel Mijnendonckx (SCK-CEN), Alain Sellier (LMDC), Guido Deissmann (FZJ), Thuro Arnold (HZDR), Laurie Lacarrière (LMDC), Michele Griffa (EMPA), Thierry VIDAL (LMDC), Mejdi Neji (IRSN), Xavier Bourbon (ANDRA), Layla Ibrahim (LMDC), Nicolas Seigneur (Mines Paris Tech), Stéphane Poyet (CEA), Benoit Bary (CEA), Yannick Linard (ANDRA), Trung Le Duc (TUL), Veronika Hlavackova (TUL), Antoine Pasteau (ANDRA), Kyra Jantschik (GRS), Marvin Middelhoff (GRS), Janez Perko (SCK-CEN), Quoc Tri Phung (SCK-CEN), Suresh Seetharam (SCK-CEN), Wanqing Shan (LAMCUBE), Ananya Singh (UNIMAN), Jon Lloyd (UNIMAN), Victor Vilarrasa (CSIC)**

To be cited as:

Dauzères A., Helson O., Churakov S., Montoya V., Zghondi J., Neeft E., Shao J., Cherkouk A., Mijnendonckx K., Sellier A., Deissmann G., Arnold T., Lacarrière L., Griffa M., VIDAL T., Neji M., Bourbon X., Ibrahim L., Seigneur N., Poyet S., Bary B., Linard Y., Le Duc T., Hlavackova V., Pasteau A., Jantschik K., Middelhoff M., Perko J., Tri Phung Q., Seetharam S., Shan W., Singh A., Lloyd J., Vilarrasa V. (2022): Initial State of the Art on the chemo-mechanical evolution of cementitious materials in disposal conditions. Final version as of 09/11/2022 of deliverable D16.1 of the HORIZON 2020 project EURAD. EC Grant agreement no: 847593.

Acknowledgement

This document is a deliverable of the European Joint Programme on Radioactive Waste Management (EURAD). EURAD has received funding from the European Union's Horizon 2020 research and innovation programme under grant agreement No 847593.

Status of deliverable		
	By	Date
Delivered (Lead Beneficiary)	Alexandre Dauzères (IRSN)	May 2022
Reviewed (internal review)	MAGIC board members	May – August 2022
Verified (WP Leader)	Alexandre Dauzères (IRSN)	August – September 2022
Reviewed (Reviewers)	Andres Idiart	September 2022
Approved (PMO)	Bernd Grambow	November 2022
Submitted to EC (Coordinator)	Louise Théodon (ANDRA)	November 2022

Executive Summary

This report is an initial State-of-The-Art (SOTA) literature review in the MAGIC WP (Work Package) dedicated to synthetize the knowledge on cementitious materials evolution in radioactive waste geological disposal conditions.

The European Union (EU) member states (MS)' disposal contexts are not considered in the present report. Existing previous SOTA reports are listed in this document.

This SOTA has the following objectives:

1) Sharing a collective overview of the main disturbances, from the nanoscale to the macroscale, in terms of chemistry (with consequences on transport) but also in terms of mechanics and microbial activity, which will prevail for concrete structure emplaced in clayey and crystalline environment;
2) Identifying the limitations and gaps especially for chemo-mechanics modelling but also for microbial impact in representative conditions, in order to update more precisely the perspectives and adapt the road map of MAGIC's WP.

MAGIC's participants contributed to the different SOTA chapters' writing. The structure is divided in four parts: Part 1 is a synthesis of key processes controlling the evolution of chemical and transfer properties of cementitious materials placed in deep disposal environments. Due to the numerous previous SOTA on this topic, especially on the chemical evolution of concrete in saturated environment, this part focuses on the key reactive pathways identified in previous studies. The multiscale mechanical behaviours related to the disturbances imposed in geological disposal environments is detailed in Part 2. Part 3 highlights the existing knowledge on the chemo-mechanical (C/M) modelling approach on concrete. Finally, the influence of microbial activity on the chemo-mechanical behaviour of concrete is detailed in Part 4.

Table of content

Executive Summary 4

Table of content 5

List of figures 7

List of Tables 11

Glossary 12

General introduction 15

1. Synthesis of key processes controlling the evolution of chemical and transfer properties of cementitious materials placed in deep disposals environments 17

1.1 Interaction of cementitious materials in unsaturated environments representative of the evolution during the operation of a geological disposal facility 17

1.1.1 The carbonation process 17

1.1.2 Consequences of carbonation 20

1.2 Cements interactions in saturated environments representative of post-closure evolution in geological disposal 23

1.2.1 Geochemical evolution of cementitious materials exposed to geological disposal environment 23

1.3 Feedback of Reactive Transport (RT) modelling on cementitious materials in geological disposal 33

1.3.1 RT modelling of cementitious materials evolution in saturated environments 33

1.3.2 RT modelling of cementitious materials evolution in unsaturated environments 41

1.4 Synthesis and identified gaps 48

1.5 References for part 1 49

2. Multiscale mechanical behaviour related to the disturbances imposed in geological disposal environments 68

2.1 Mechanical constraints applied to concrete in a geological disposal 68

2.2 Mechanical behaviour of concrete at the nano/microscale exposed to geological disposal environments 69

2.2.1 Experimental developments and key results 69

2.2.2 Modelling approaches and key results 73

2.3 Mechanical behaviour of concrete at the meso/macroscale exposed to geological disposal environments 76

2.3.1 Experimental developments and key results 76

2.3.2 Modelling approaches and key results 80

2.4 Synthesis and identified gaps 88

2.5 References for part 2 89

3. Existing knowledge on the chemo-mechanical (C/M) modelling of concrete including parallel applications 97

3.1 C/M modelling at the pore scale/microstructure scale in saturated and unsaturated environment 97
3.1.1 Reactive transport at pore scale 97
3.1.2 Mechanical pore-scale models 100
3.1.3 Hydro-(thermo)-mechanical pore-scale models 101
3.1.4 Chemo-mechanical pore-scale models 101
3.2 C/M modelling at the macroscale (in saturated and unsaturated environment) 104
3.2.1 Saturated environment 104
3.2.2 Unsaturated environment 110
3.3 Synthesis and identified gaps 115
3.3.1 Pore-scale models 115
3.3.2 Up-scaling of mechanical properties versus cement alteration 116
3.3.3 Impact of chemo-mechanics damages on transfer properties 116
3.3.4 Reinforcement chemo-mechanical damage 116
3.3.5 Implementation of the improvements in finite element codes 116
3.4 References for part 3 117
4. Microbial activity influence on the chemo-mechanical behaviour of concrete 124
4.1 Knowledge synthesis of microbial impact on cementitious materials in various contexts (sewage pipes, marine structures) 124
4.1.1 Biodeterioration of sewage systems 125
4.1.2 Deterioration and biofouling of marine structures 126
4.1.3 Microbial induced calcite precipitation 126
4.2 Assessment of microbial populations likely to be encountered in geological disposals and to create problems for concrete structures. 128
4.2.1 Physiochemical factors that influence microbial activity 128
4.2.2 Physiology of relevant types of microorganisms 132
4.2.3 Natural analogous sites representing cement systems 135
4.3 Preliminary studies on the degradation of concrete due to microbial activity in geological disposals. 137
4.4 Synthesis and identified gaps 141
4.5 References for part 4 142
Conclusion 151
5. Appendix A 155
Natural water compositions in the host rocks 155
6. Appendix B 159
Poisson-Nernst-Planck equation 161
6.1 References for appendixes 170

List of figures

Figure 1-1: Molar fraction of $H2CO3$, $HCO3-$, $CO32-$ (Thiery, 2005) 18

Figure 1-2: Carbonation front of a mortar cement CEM II detected by phenolphthalein pulverisation after 211 days of accelerated carbonation with 10% CO2 content (Hyvert, 2009). 19

Figure 1-3: Evolution of carbonation depth for different carbon dioxide content (Hyvert et al., 2010).. 19

Figure 1-4: Distribution of pores sizes of a cement paste W/C=0.4 (Houst, 1993) 20

Figure 1-5: Aqueous corrosion: oxide formation on the surface of a metal in an aerated (a) or anoxic conditions (b). 21

Figure 1-6: Potential-pH simplified diagram for iron at 25°C (Pourbaix, 1963) 22

Figure 1-7: (a) Average corrosion kinetics (µm) after one year, (b) Deformed shape of corrosion layer after one year (Millard and L'Hostis, 2012) 23

Figure 1-8: 3D microstructure evolution (porosity value) modelling obtained with Yantra-LB code coupled to geochemical solver PhreeqC. Microstructure modelling (Patel et al., 2018). 41

Figure 1-9: Representation of sorption isotherm data with Van Genuchten expression for different temperature and cement composition, from Poyet (2016) 44

Figure 2-1: Indentation modulus vs. silicon to calcium (Si/Ca) ratio for the hydrates of the (a) the reference cement paste and the (b) interior, (c) middle, and (d) outer zone of the decalcified cement paste (Brown et al., 2018). 73

Figure 2-2: Evolution of Young's modulus as a function of the calcium concentration in the liquid phase (Gérard, 1996) 76

Figure 2-3: Degradation depth after 153 days of accelerated leaching with NH_4NO_3 solution 6M (Nguyen, 2005)..... 77

Figure 2-4: Evolution of compressive strength as a function of degradation (Nguyen, 2005). 77

Figure 2-5: The stress-strain curves of the compression test at different chemical degradation stages (Nguyen, 2005). 78

Figure 2-6: Evolution of creep curves for the sound concretes and leached ones (Sellier et al., 2011). 78

Figure 2-7: Evolution of leached calcium quantity as a function of square root of time (Camps, 2008). 78

Figure 2-8: Evolution of deviatoric failure stress with carbonation ratio during triaxial compression tests of concrete (Takla, 2010; Takla et al., 2011) 81

Figure 2-9: Diminution of elastic modulus of cement paste due to chemical leaching in triaxial compression tests (Yurtdas et al., 2011) 82

Figure 2-10: Diminution of deviatoric failure stress of cement paste due to chemical leaching in triaxial compression tests (Yurtdas et al., 2011) 82

Figure 2-11: Two typical micro-structural representations of concrete materials (Ghorbanbeigi, 2014) 82

Figure 2-12: Illustration of three steps of analytical homogenization 83

Figure 2-13: Failure envelops of cement paste samples with different carbonation ratios (experimental data from Takla, 2010; Takla et al., 2011) 85

Figure 2-14: Evolution of uniaxial compression strength with carbonation time (experimental data from Chang and Chen (2005) 86

Figure 2-15: Stress-strain curves in uniaxial compression tests of concrete samples with different carbonation ratios (experimental data from Chang and Chen (2005)) 86

Figure 2-16: Failure envelops of concrete samples with different chemical leaching ratios 87

Figure 2-17: Stress-strain curves in uniaxial compression tests of concrete samples with different chemical leaching ratios (experimental data from Nguyen, 2005) 87

Figure 3-1: Modelling of leaching of cement paste with de-ionised water (left boundary condition). Portlandite is marked with red colour, C-S-H phases with grey and clinkers with blue. The cross-section represents dissolved Ca concentration (Perko et al., 2020). 98

Figure 3-2: (a) Node and mesh generation procedure; (b) an example of the overlay procedure for cement paste, shown in 2D for simplicity (pink – outer product, red – inner product, light blue – unhydrated cement), adapted from (Šavija et al., 2019). 100

Figure 3-3: Heat transfer model notations and geometric considerations for fluid flow, advection, and conduction models. The figure is taken from (Caulk et al., 2020). 101

Figure 3-4: Idealized concrete representation involves three different length scales: the macroscale, the mesoscale, and the microscale. ITZ stands for interfacial transition zone. 103

Figure 3-5: Life cycle of concrete in aggressive solution (Buffo-Lacarrière and Sellier, 2011) 104

Figure 3-6: Thermodynamic equilibrium curve of solid/liquid calcium (Gérard et al., 1998) 105

Figure 3-7 : Degradation depth of concrete in contact with water and in the case in presence of bentonite (Yokozeki et al., 2004) 105

Figure 3-8: The concentration of calcium in interstitial water after 106of leaching (Sellier et al., 2011) 106

Figure 3-9: Distribution of the (a) calcium concentration c in the pore solution, (b) concentration of calcium in the skelton s, (c) scalar damage parameter *dm* in a concrete pane (Bangert et al.,2003) 106

Figure 3-10:The finite element mesh (a) for the concrete, (b) for the reinforcements ans stirrups in the concrete member. (Choi et al.,2018) 107

Figure 3-11 :Load-displacement curve (w/c = 0.5) of test results and calculated curves considering a partial reduction of the flexural compressive strengh due to the leaching effect. (Choi et al., 2018) .. 107

Figure 3-12: Stress-strain curve (w/c=0.5) of the damaged members for different ration of degradation (*Ad/At*) (Choi et al.,2018) 107

Figure 3-13: The simulation of tensile behaviour for sound and leached concrete (Lacarrière et al., 2006) 108

Figure 3-14: The simulation of compressive behaviour for sound and leached concrete (Lacarrière et al., 2006) 109

Figure 3-15: Volumetric change due to creep in CEMI based concrete (Sellier et al., 2011) 109

Figure 3-16 : Progress of carbonation depth for different w/c ratio (Ishida and Li, 2008) 112

Figure 3-17: Profiles of calcium concentration in interstitial water for different stage of degradation (Bary and Sellier, 2004) 112

Figure 3-18: Profiles of porosity for different stage of degradation (Bary and Sellier, 2004) 113

Figure 3-19: Evolution of carbonation depth as a function of carbon dioxide content for different types of cement (Hyvret et al., 2010) 114

Figure 4-1: Part of the sewer network and cross-sections of a pumped section and a gravity pipe with the main biological reactions that result in concrete deterioration. Figure adapted from (Li et al. 2017) and created with BioRender.com. 125

Figure 4-2: Principle of biofouling. (1-2) microbial film formation allows (3-4) the growth of diatoms, algae, invertebrates and other eukaryotes. Figure adapted from (Hayek et al. 2021) and created with Biorender.com. 126

Figure 4-3: a) Original accelerated test where cemented waste is exposed to sterile growth medium are to a combination of biomass and spent medium; b) modified accelerated test were cemented waste pre-exposed to sterile medium or to microbial cells is further exposed to sterile medium (Rogers et al. 1996, Rogers et al. 2003). 139

Figure 4-4: Accelerated cement biodegradation test with semicontinuous cultures. Cement cubes are exposed to a medium with (above) or without (below) $5x10^8$ cells. Samples are incubated 4 days at 30°C at 100 rpm. Afterwards, the spent medium is analysed and the cement cubes are transferred to fresh exposure medium with or without cells and the steps are repeated. 139

Figure 5-1: Chemical composition of the crystalline host rock groundwater. 155

Figure 6-1: Schematic representations of the modified Gouy–Chapman (MGC) model (left) and the triple layer (TL) model (right) (Lyklema, 1995). Surface sites are shown by pink (negatively charged, (-)) and light blue (zero charged) spheres surrounded by black circles. The net negative surface charge emerges due to deprotonation of surface sites, controlled by the pH in solution. The distribution of ions charge in the diffuse layer is described by the Poisson Boltzmann equation for external electrostatic potential $\Psi(x)$. 159

Figure 6-2: Simulation of a steady state ion distribution in a nanoscale pore with charged surfaces resembling the surface charge of illite/smectite particles. At the beginning of the simulations, two reservoirs separated by narrow pores are filled with 5 mol/m³ and 1 mol/m³ NaCl solution, respectively. Results of the calculation show a redistribution of cationic and anionic species and formation of diffused double layer as a result of the salt concentration gradient and the electrostatic potential due to the presence of the charged mineral surface (Hax Damiani et al., 2020). 162

Figure 6-3: Conceptualisation of modified GC model and ζ-potential measurements of effective surface charge (A). Ions in the Sterner layer are tightly attached to the surface and contribute to the net surface charge. In an applied electric field, the colloidal particles of C-S-H move in direction of the field strength or opposite to it depending on the surface charge. (B) Concentration profile of positive and negative species in DDL according to Poisson Boltzmann equation. PB-model predicts negative effective potential due to depletion of anionic species and limited sorption of cation. Accordingly, PB-model always predicts a net repulsive force between charged surface at short distances, if noticeable overlap of DDLs takes place (C). Reactive Monte Carlo simulations of C-S-H surface charge indicate strong dependence of surface ζ-potential as function of pH and concentration of divalent cations (e.g. Ca) (Churakov and Labbez, 2017; Churakov et al., 2014; Jonsson et al., 2005; Labbez et al., 2009). Simulations and measurements demonstrate that with increasing Ca concentration the surface potential change from negative to positive. In a 20mM $Ca(OH)_2$ solution (e.g.) in equilibrium with portlandite, positive ζ-potential (surface overcharge), leads to co adsorption of anionic species (E). Furthermore, the ion-ion correlation leads to attractive force between C-S-H surfaces at short distances, the phenomena that are not captured by PB-theory. 163

Figure 6-4: The electrical potential (A) and ion concentration distribution (B) with respect to the distance normal to the surface of charged surface calcium-silicate-hydrates. The red lines represent predictions of the Monte Carlo simulations, which account for the ion-ion correlations and the finite size of the ions. Black lines are results from the conventional Poisson Boltzmann Nernst -Planck theory (PB-NP) modelling chain. Blue lines are predictions of a modified PNP model (MPB). Solid and dashed lines represent cationic and anionic species, respectively. The system corresponds to a mix of 10 mol/m³ NaCl with 20 mol/m³ $Ca(OH)_2$. Adopted from (Yang et al., 2019) 165

Figure 6-5: A: Multiscale modelling approach for the assessment of diffusive mobility of water and cation in cement paste taking into account molecular scale interaction of ions with surface of C-S-H phases and the heterogeneous microstructure of cement paste (Yang et al., 2019).. The normalised effective diffusion coefficients for Na^+, H_2O and Cl^- obtained with the classical PB-NP model (dashed lines) and the modified MPB-NP model, taking into account the activity of the cationic and anionic species (B). Estimation of diffusion parameter at the scale of cement grains (anhydrous phases)..... 165

Figure 6-6: Lattice models: (a) two dimensional 9-velocity lattice (D2Q9); (b) three dimensional 27-velocity lattice (D3Q27). Only next-neighbours communication is required for these space-filling lattices. 166

Figure 6-7: Schematic of the Gibbs free energy (ΔG) for homogeneous (HON) and heterogeneous (HET) nucleations as a function of the radius of spherical nuclei. As soon as a critical nucleus is formed ($r_{critical}$) and the energetic barrier is exceeded (at the maximum of the ΔG curve) further growth of the nucleus is more favourable than its disaggregation and precipitation starts. (Prasianakis et al., 2017) 168

Figure 6-8: Initial distribution of portlandite and C-S-H in cement phase (left) and the evolution of portlandite dissolution front followed by carbonate precipitation front after 1 day of reaction time (Right). The simulations are performed in a 250 μm × 250 μm × 450μm with 435 $\mu m3$ grid resolution (Patel et al., 2021)..... 169

List of Tables

Table 1-1: Summary of simulation studies addressing i) laboratory and in situ experiments on and ii) long term predictions of cement/clay interactions. (Deissmann & Ait Mouheb; 2021**)** 37

Table 2-1*: Examples from the literature of estimates of linear elastic moduli of cement-based composites, obtained with Resonant Ultrasound Spectroscopy, with indications of specimen scale/size, composite type and study target*..... 70

Table 2-2: Elastic moduli of individual cement and cement paste phases, taken from several sources in the literature..... 71

Table 2-3: Evolution of physical properties in sound specimen at T_0 and after 9 and 18 months of decalcification 79

Table 5-1: The chemical composition (main anions and cations) of S25 groundwater..... 156

Table 5-2: Measured pore water chemistries in granitic rocks (Neeft et al., 2020)..... 156

Table 5-3: Parameter for "Konrad-solution" at 25°C (Herold et al., 2020) 156

Table 5-4: Composition for synthetic “Konrad-solution” at 25°C 157

Table 5-5: Chemical composition of the clayey host rock groundwater. 157

Glossary

AAR	Alkali aggregate reactions
ASR	Alkali silica reactions
ASTM	American Society for Testing and Materials
ATP	Adenosine Triphosphate
BSA	Biogenic sulphuric acid
CASH	Calcium Aluminate silicate Hydrates
CDF	Cumulative Distribution Function
CEBAMA	Cement Based Materials
CEM	Cement (CEM I, CEM II…)
CFL	Courant-Friedrichs-Lewy
CH	Calcium hydroxyde: Portlandite
CI	Cement-clay Interaction
CIGEO	Industrial Centre for Geological Disposal in France
CKD	Cement kiln dust
CNT	Classical Nucleation Theory
CORI	Cement Organic Radionuclide Interactions
COX	Callovo-Oxfordian clay rock
CSH	Calcium Silicates Hydrates
DDL	Diffuse double layer
DEM	Discrete Element Method
EC	European Commission
EDS	Energy dispersive spectroscopy
EPS	Extracellular Polymeric Substances
EPS	Extracellular polymeric substances
ESEM	Environmental Scanning Electron Microscopy
EU	European Union
EURAD	European Joint Programme on Radioactive Waste Management
FDM	Finite difference method
FE	Finite Element
FEM	Finite Element Method

FFT	Fast fourier transform
GC	Gouy-Chapman (model)
GDF	Geological disposal facilities
GEM	Gibbs Energy Minimization
HET	Heterogeneous
HLW	High-level waste
HON	Homogeneous
HPF	Hyperalkaline Plume in Fractured Rock
ILW	Intermediate level waste
ISA	Iso-Saccharinic Acid
ITZ	Interfacial Transtion zone
LAC	Low Alkaline Cement
LB	Lattice Boltzmann (method)
LBM	Lattice Boltzman Modelling
LCS	Long -term cement studies project
LLW	Low level waste
LMA	Law of Mass Action
MAGIC	The chemo-mechanical aging of cementitious materials
MGC	Modified Gouy Chapman model
MICP	Microbial induced calcite precipitation
MS	Member states
MSH	Magnesium silicate hydrate
NN	Neural Networks
NRUS	Nonlinear Resonant Ultrasound Spectroscopy
NS	Navier-Stokes
OPA	Opalinus clay
OPC	Ordinary Portland Cement
PB	Poisson Boltzmann
PDF	Probability density function
R&D	Research and Development
REV	Representative Elementary Volume
RH	Relative humidity

RUS	Resonant Ultrasound Spectroscopy
SCM	Surface Complexation Model
SEM	Scanning Electron Microscope
SNT	Supersaturation-Nucleation-Time
SOB	Sulphur-oxidizing bacteria
SOTA	State of the art
SRB	Sulfate reducing bacteria
THM	Thermo-hydro-mechanical
URL	Underground Rock Laboratory
VFA	Volatil fatty acids
XAS	X-ray absorbtion spectroscopy
XRD	X-ray diffraction analysis

General introduction

In many radioactive waste disposal concepts, cementitious materials are widely used, for example as structural support material for access galleries and disposal drifts or cells (e.g., concrete/shotcrete), as well as grouts/mortars used as containment material for low and intermediate level wastes (Neeft et al. 2020). Thus, these cementitious materials can be in contact with both, the host rock clay or granitic formation as well as bentonite components (NEA, 2012; Neeft et al., 2020; Szabó-Krausz et al., 2021). Concretes, mortars and grouts are used for structural and isolation purposes in high-level and low-intermediate level radioactive waste repositories. Cement-based materials are envisaged for a large number of disposal facilities for intermediate level wastes across Europe and are already used as liners in disposal cells or as part of waste containers in many member states' existing facilities for low-level waste / near-surface disposal. Extensive feedback on the durability of concrete is available from the vast experience in civil engineering. However, a specific approach during the design and construction of a repository in terms of stringent safety requirements is of key importance. In addition, further understanding is required to support their use as a backfill material for high level wastes in geological disposal, particularly to understand their contribution to the overall system performance during late post-closure time frames.

The mechanical behaviour of cementitious materials is strongly influenced by the boundary conditions imposed by the geotechnical system and the host rock (i.e. water saturation, temperature, etc.), during both the operational phase and the post-closure transient period (period with saturation progress). To assess the performance of the cementitious components, studies must be extended over long periods of time, considering various operating conditions. Cementitious materials are planned to be used as disposal barriers (i.e. buffer, plugs), as conditioning materials (waste packages and waste matrices) and as structural elements. These multiple uses require further understanding of their long-term behaviour, taking into account the mechanical initial state and including the impacts of all relevant physical and bio-geochemical processes (e.g. microbes) on their degradation. Furthermore, over the long term, ground- and pore-waters, with aggressive chemical ions, are a key driving factor for cementitious materials deterioration. The mineralogical and microstructural changes generated by these aggressive environments might have consequences on the mechanical behaviour of the cement matrix.

The HORIZON 2020 European CEBAMA project studied the long-term safety of cement-based materials in nuclear waste disposal applications and the ability to build complex components for the engineering barrier system (i.e. buffer). It focused mostly on the chemical degradation of cementitious materials in contact with other geotechnical barriers or components with different composition (i.e. bentonite, host rocks) in representative environments of geological disposal. Plugs and seals (building and physical behaviour) was the purpose of yet another European project named DOPAS.

The present document is a state-of-the-art (SOTA) review of the chemo-mechanical behaviour of cementitious materials exposed to various representative disturbances including the microbial one, for use in deep geological nuclear waste repositories. Two types of host rocks are considered in the present document, i.e. the clayey and the crystalline rocks.

The first main objective of this SOTA review is **to share a collective overview of the main disturbances which will prevail for concrete structure emplaced in clayey and crystalline environments. It considers all relevant scales (from nano to macro) in terms of chemistry (processes, nature of mechanisms and extension with time) but also in terms of mechanics and microbial activity.** The second main objective is **to identify the limitations and gaps especially for the coupled chemo-mechanical modelling but also for microbial impact on the chemo-mechanical behavior in representative conditions, in order to update more precisely the perspectives and adapt the road map of the MAGIC WP.**

To reach this level of knowledge, the SOTA is structured in four parts allowing a progressive increase in complexity from the chemical consideration to the mechanical one and their coupling, without forgetting the consideration of a disturbance (microbial activity) rarely tested.

The first part of this document is dedicated to a synthesis of key processes controlling the evolution of chemical and transfer properties of cementitious materials placed in deep disposal environments. The SOTA of CEBAMA and of the CORI WP (EURAD) and numerous review papers already focused on these literature aspects. Thus, Subpart 1.1 is dedicated to the interactions in unsaturated conditions representative of the operational period in disposal facilities. A detailed review of existing literature is developed. It mainly focuses on the carbonation processes of materials based on highly blended cements (i.e. low hydration heat/ low-pH cements) and Portland cements and its consequences on rebars corrosion. The Subpart 1.2, dedicated to identify the chemical evolutions of cementitious materials in saturated conditions, was summarized and only the key mechanisms considered useful for MAGIC's WP remain in this part. The Subpart 1.3 offers a feedback on reactive transport modelling applied to cementitious materials emplaced in deep repositories in saturated and unsaturated conditions. It also considers the pore scale approach and try to list the current limitations and perspectives in this field.

The second part is focused on the multiscale mechanical behaviour related to the disturbances imposed in geological disposal environments. Subpart 2.1 lists the main mechanical constraints applied to concrete in geological disposal conditions (including natural loading of the host rock) to consider in the MAGIC WP. Subparts 2.2 and 2.3 provide a review of key studies on concrete mechanical behaviour at the nano/mesoscale and meso/macroscale. Both subparts consider experimental and numerical studies.

The third part concerns the core of MAGIC's WP with a review of the existing knowledge on the coupled chemo-mechanical (C/M) modelling of concrete. Subparts 3.1 and 3.2 deal with the chemo-mechanical modelling at the pore/microstructure scales in saturated and unsaturated environment and at the macroscale, respectively. Subpart 3.3 synthetically suggests a discussion on the limitations and gaps identified in this field.

The fourth and last part is dedicated to the influence of microbial activity on the chemo-mechanical behaviour of concrete. By considering other environments, such as concrete emplaced in sewage pipes or used for marine structures, subpart 4.1 provides a knowledge synthesis of the microbial impact on cementitious materials. Subpart 4.2 is dedicated to an assessment of microbial populations likely to be encountered in geological disposals and potentially problematic for concrete structures. If the studies as part of geological disposal including concrete degradation due to microbial activity are scarce, subpart 4.3 details the preliminary experiments (in previous project) and results relative to biodegradation of cementitious materials. Subpart 4.4 identifies gaps to study the concrete durability in relation to bacterial activity in the repository context.

Due to the large existing SOTA on concrete degradation (CEBAMA SOTA – Vehmas and Holt, 2016) detailing the context on concrete in geological disposal, the present document will not cover the formulation and chemistry of concrete planned to be used in the geological disposal and the repository concept already reviewed in the CEBAMA initial SOTA.

This deliverable constitutes a basis for the work to be carried out in MAGIC's WP, in terms of experiments and modelling. MAGIC's participants contributed to the SOTA different chapters' writing.

1. Synthesis of key processes controlling the evolution of chemical and transfer properties of cementitious materials placed in deep disposals environments

The following part highlights the key reactive mechanisms identified in the cement/disposal environment interactions. The objective is rather to have an overview of the mechanisms that may play a role on the mechanical behaviour dealt within MAGIC's WP than to have a detailed description of the reactivity (already existing in the CEBAMA SOTA, see Vehmas and Holt, 2016). This synthesis is divided in three parts. The first one focuses on unsaturated conditions. The second one is dedicated to the key processes experimentally observed when cementitious materials are placed in saturated environment (directly with the rock or a representative groundwater)., while the last part is dedicated to the reactive transport modelling of cementitious materials under both conditions.

1.1 Interaction of cementitious materials in unsaturated environments representative of the evolution during the operation of a geological disposal facility

LMDC, LamCube, ANDRA

During the 120-year operational phase of the waste disposal facility, the concrete in the industrial centre for geological disposal (Cigéo) will be subjected to a period of ventilation in order to ensure safe operation and to remove the heat from the exothermic wastes (Trotignon et al., 2011). Ventilation will lead to 'dry' air conditions (relative humidity of around 50% considered in the calculations) and thus to desaturation of the concrete, which will promote the atmospheric carbonation process.

1.1.1 The carbonation process

Carbonation is a natural phenomenon due to the dissolution of carbon dioxide from the air into the interstitial solution of the cementitious material. Under the effect of a concentration gradient, atmospheric carbon dioxide diffuses into the pores of the concrete and dissolves in the interstitial solution to form calcium carbonate $Ca\mathrm{CO}_3$ from portlandite $Ca(OH)_2$ and other calcium-bearing cementitious minerals.

Carbon dioxide is a gas present in the atmospheric air at about 0.04% by volume fraction. When this gas is in contact with an aqueous solution, carbon dioxide dissolves in the solution to form carbonic acid H_2CO_3 according to Henry's law.

The reactions of the dissolution of CO_2 in water are written below:

$$\begin{aligned} CO_2 + H_2O &\rightarrow H_2CO_3 \\ H_2CO_3 + H_2O &\rightarrow HCO_3^- + H_3O^+ \\ HCO_3^- + H_2O &\rightarrow CO_3^{2-} + H_3O^+ \end{aligned} \qquad \text{1-1}$$

The molar fractions of carbonic acid H_2CO_3, hydrogen carbonate HCO_3^- and carbonate ion CO_3^{2-} at equilibrium as a function of pH are given in Figure 1-1 (recovering from the thesis of Thiery, 2005). At 20°C, for a pH above 10.3, the ion CO_3^{2-} predominates, and for pH between 6.3 and 10.3, HCO_3^- is instead the predominant ion. Then, during the carbonation process, the pH of the interstitial solution of concrete decreases from a basic value around 13 to a value below 9. For this reason, the separate predominance interval has an important impact on carbonation.

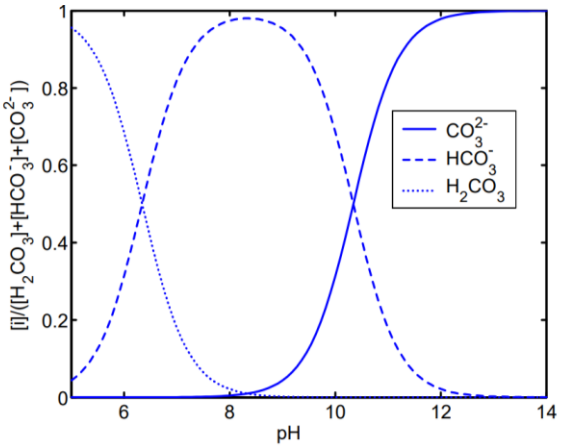

Figure 1-1: Molar fraction of $\mathrm{H_2CO_3}$, $\mathrm{HCO_3^-}$, $\mathrm{CO_3^{2-}}$ (Thiery, 2005)

The CO_2 penetrates concrete by gaseous diffusion through the pores or through cracks. It then reacts with the hydrated cement paste fraction of concrete. This chemical reaction, called carbonation, transforms the hydration products, particularly portlandite, into calcium carbonates.

1.1.1.1 Carbonation of portlandite

During the hydration of cement paste, the clinker phases C_2S and C_3S dissolve to form portlandite: $Ca(OH)_2$. Portlandite is the fastest carbonating hydrate, and its carbonation affects the pH of the pore solution. The pH of the pore solution remains at about 12.5 until portlandite is exhausted. The dissolved CO_2 in the interstitial solution decreases the pH by using the ions hydroxyl OH^-. To restore the basicity of the pore solution, portlandite dissolves according to the following equation:

$$Ca(OH)_2 \leftrightarrow Ca^{2+} + 2OH^- \qquad 1\text{-}2$$

Thus, the calcium ions released precipitate with the carbonate ions CO_3^{2-} to form the calcium carbonate according to the reaction:

$$Ca^{2+} + CO_3^{2-} \rightarrow CaCO_3 \qquad 1\text{-}3$$

In a simplified approach, the reaction mechanism of carbonation of $Ca(OH)_2$ is synthesised by the following heterogeneous chemical reaction:

$$Ca(OH)_2 + CO_2 \rightarrow CaCO_3 + H_2O \qquad 1\text{-}4$$

1.1.1.2 Carbonation of Calcium silicate hydrate C-S-H

Other hydrated compounds are also susceptible to carbonate (Berner, 1992; Bary and Sellier, 2004; Hyvert et al., 2010; Kangni-Foli et al., 2021). The calcium silicate hydrates (C-S-H) resulting from the hydration of C_2S and C_3S, carbonate to form calcium carbonate, silica gel and water according to the following reaction:

$$\mathrm{CaO}_x(\mathrm{SiO}_2)_y(H_2O)_z + \mathrm{x}H_2CO_3 \rightarrow \mathrm{x}CaCO_3 + \mathrm{y}\mathrm{SiO}_2.\mathrm{t}H_2O + (\mathrm{x}-\mathrm{t}+\mathrm{z})H_2O \qquad 1\text{-}5$$

After total portlantdite carbonation, atmospheric carbonation results in neutralization of calcium silicate hydrates. The decrease in the C/S ratio of C-S-H has long been demonstrated on C_3S or CEM I pastes, indicating a non-congruent dissolution of C-S-H to calcite formation (Groves et al., 1991; Richardson et al., 1993; Al-Kadhimi et al., 1996). In the case of blended cements, C-S-H are also strongly altered and decalcified in the same way after natural and accelerated carbonation (Auroy et al., 2018).

The carbonation of C-S-H affects the microstructure of the cement pastes and modifies its physical and mechanical properties. Therefore, this process has to be taken into account in models predicting carbonation.

Usually, the depth of carbonation of mortar or concrete is measured experimentally after wetting the fresh surfaces and spraying with a phenolphthalein solution. The phenolphthalein solution reveals the interface between the healthy zone with a pH higher than 9 and the carbonated zone where the pH is below 9: its pink colouring becomes colourless upon contact with the carbonated zones (Hyvert, 2009).

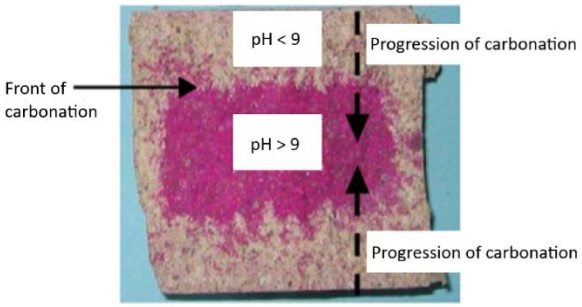

Figure 1-2: Carbonation front of a mortar cement CEM II detected by phenolphthalein pulverisation after 211 days of accelerated carbonation with 10% CO2 content (Hyvert, 2009).

Many studies show that the kinetics of carbonation depends on the cement type for different partial pressure of carbon dioxide (e.g. Hyvert et al., 2010). For CEM II (clinker and limestone filler) and CEM III (clinker and slag) cement paste, where the quantity of portlandite is less than that of CEM I (Portland cement), the depth of carbonation is more important. From a kinetic point of view, the reactivity is the same. For blended cement pastes fixing less carbonate, the depth of carbonation is for a given time greater because the amount of reactive calcium for carbonation is lower and the CO_2 penetrates deeper. The analysis involves mass balance calculations. This effect can be reproduced by an empirical model proposed by Hyvert et al. (2010) which allows identifying the depth of carbonation for different partial pressures of carbon dioxide by taking into account the quantities of carbonatable elements of the hydrated cement. This model is validated through the experimental results Figure 1-3.

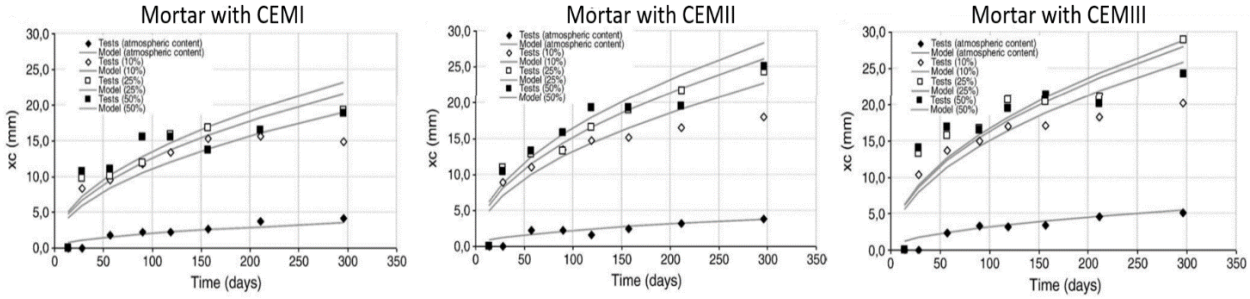

Figure 1-3: Evolution of carbonation depth for different carbon dioxide content (Hyvert et al., 2010).

Progress of carbonation fronts is known to depend on gas diffusion and relative humidity (Steiner et al., 2020; Russell et al., 2001; Leemann and Moro, 2017; Winter, 2009; Ashraf, 2016) and is fastest for relative humidity between 60-80%. Under such conditions, the concrete is de-saturated to such a degree that relatively fast diffusion of atmospheric CO_2 is possible and still enough water in contact with the cement phases exist to allow dissolution of reactants.

Experimental investigations show that carbonation fronts are not sharp (Parrott and Killoh, 1989; Thiery et al., 2007), which is in part attributed to the influence of chemical reaction kinetics (Morandeau et al., 2014; Thiery et al., 2007). The role of the ratio between the characteristic time of carbonation reaction to a characteristic diffusion time was discussed for example by Muntean et al. (2011). In general, if the characteristic time for reaction is much longer than the time for diffusion of CO_2, then the size of the reaction zone is small, compared to the progress of the reaction front. This case leads to a reduction of porosity due to carbonation and is frequently observed for OPC-based materials (Meier et al., 2007; Muntean et al., 2011).

A study carried out on cement pastes highlights the influence of the cement type and the temperature on the depth of carbonation with time. The results underline the accelerating effect of temperature by thermoactivation of transport and retrograde solubility of calcite with temperature (the higher the temperature, the lower the solubility; Drouet et al., 2019).

1.1.2 Consequences of carbonation

1.1.2.1 Microstructural impact

The carbonation process modifies the microstructure and the mineralogy of the cement paste by the dissolution of CH, decalcification of C-S-H and formation of calcite. The total porosity of cement paste decreases by filling the pores with calcite (Figure 1-4). This decrease is greater for low W/C ratio (Houst, 1993; Thiery, 2005). Experimental studies have shown (Ngala and Page, 1997; Bary and Sellier, 2004; Hyvert et al., 2010; Kangni-Foli et al., 2021) that the reduction in porosity is due to the carbonation of not only portlandite but also of other hydrates. Then, the chemical zoning of the carbonation process can be simplified by four main zones (Bary and Sellier, 2004):

- Zone 0: it corresponds to the sound material;
- Zone 1: CH is dissolved linearly; also, the other hydrates (C-S-H, AFt, AFm) start to react, and calcite precipitates;
- Zone 3: CH and the aluminates are totally carbonated, the C-S-H is present with C/S ratio between 0.85-0.90;
- Zone 4: it corresponds to the area where all the carbonatable calcium is carbonated and precipitates as calcite.

From a mechanical point of view, the densification induced by $CaCO_3$ precipitation improves the mechanical properties (increase in strength and modulus) (Jerga, 2004; Ahmad et al., 2017; Merah and Krobba, 2017; Zhang et al., 2020) but also tends to make concrete more brittle (Merah and Krobba, 2017; Tschegg et al., 2011; Xiao et al., 2022). The main drawback is carbonation shrinkage (Jerga, 2004; Verbeck, 1958; Swenson and Sereda, 1968; Suda et al., 2019) and the consequent (micro-) cracking (Auroy et al., 2018; Borges et al., 2010; Auroy et al., 2015; Wan et al., 2014). Carbonation shrinkage appears to be due to C-S-H decalcification and silica polymerization (Swenson and Sereda, 1968; Chen et al., 2006; Kangni-Foli et al., 2021) and the combination of carbonation and drying shrinkage is the main reason for (micro-)cracking.

Carbonation then generates two adverse effects: (1) porosity reduction that tends to decrease the transport properties, and (2) shrinkage and (micro-) cracking that tends to increase them knowing that this phenomenon is less significant on a concrete scale than a cement paste scale. The opposing results about the consequences of carbonation on transport (either increase or decrease in transport properties after carbonation) highlight the competition between these two adverse effects that depends on the initial mineralogical composition of the cementitious material that is carbonated (Auroy et al., 2015; Kangni-Foli et al., 2021; Dutzer et al., 2019).

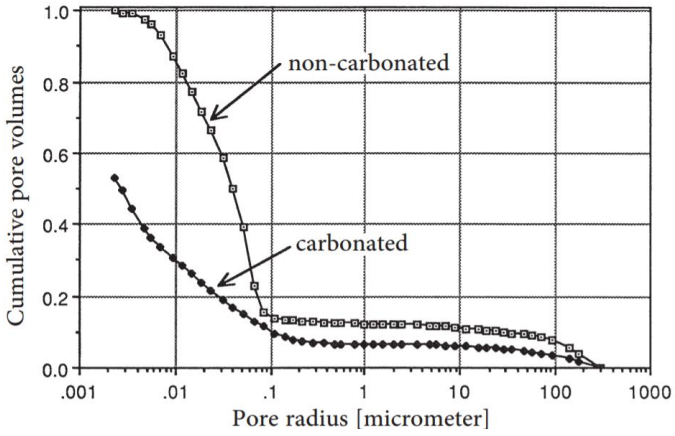

Figure 1-4: Distribution of pores sizes of a cement paste W/C=0.4 (Houst, 1993)

1.1.2.2 Corrosion of reinforcement due to carbonation

In the Cigéo context, reactive transport models have been used to simulate atmospheric carbonation of intermediate-level long-lived radioactive waste (ILW) concrete packages (Thouvenot et al., 2013). Based on the portlandite and calcite fronts, the results show that the concrete alteration is about 2 to 3 cm over a period of 100 years. This depth of carbonation is in practice compared to the thickness of the

concrete cover, in order to assess the risk of coupling with the corrosion process of the steel reinforcements.

- Process of corrosion

Steel corrosion is one of the main factors in the degradation of reinforced concrete structures. In the case of reinforced concrete, corrosion is due to an electrochemical reaction of steel, and an ion transfer occurs at the interface.

Aqueous corrosion is the result of two simultaneous electrochemical reactions:

The dissolution of the metal in contact with water by an anodic process (oxidation of iron):

$$Fe \rightarrow Fe^{2+} + 2e^{-} \qquad 1\text{-}6$$

The cathodic process is represented by consuming the electrons released from the anodic reaction in the presence of oxygen:

$$O_2 + 2H_2O + 4e^{-} \rightarrow 4OH^{-} \qquad 1\text{-}7$$

The products of the two half-reactions react with each other to form an insoluble ferrous hydroxide, which is then transformed to the more stable hydrated hydroxide, according to the reactions below:

$$Fe^{2+} + 2OH^{-} \rightarrow Fe(OH)_2$$
$$Fe(OH)_2 + H_2O + \frac{1}{2}O_2 \rightarrow 2Fe(OH)_3 \qquad 1\text{-}8$$

Figure 1-5 illustrates generalised corrosion in the very simple case of a metal which, in the presence of water and oxygen, oxidises with oxide formation. In the case of deep geological disposal, the environment tends to reach anoxic conditions, so water plays the role of oxidant (Figure 1-5). The layer of corrosion products formed is heterogeneous and consists of Goethite, Maghemite and Ferrihydrite. (Poupard et al., 2006; Dehoux et al., 2015) The phenomenology of aqueous corrosion can be relatively complex, since, depending on the environmental conditions, the formation of sulphur, carbonate, chloride or silicate compounds is possible.

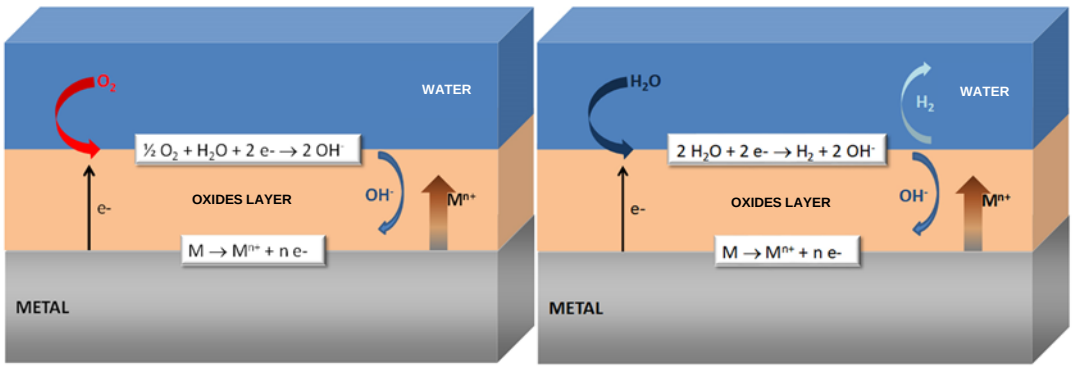

Figure 1-5: Aqueous corrosion: oxide formation on the surface of a metal in an aerated (a) or anoxic conditions (b).

- Condition of corrosion:

The stability of a metal in water depends on the pH of the solution and also on the electrical potential of the metal compared to the solution. The diagram of Pourbaix (1963) divides into zones the state of iron according to the pH and potential (Figure 1-6).

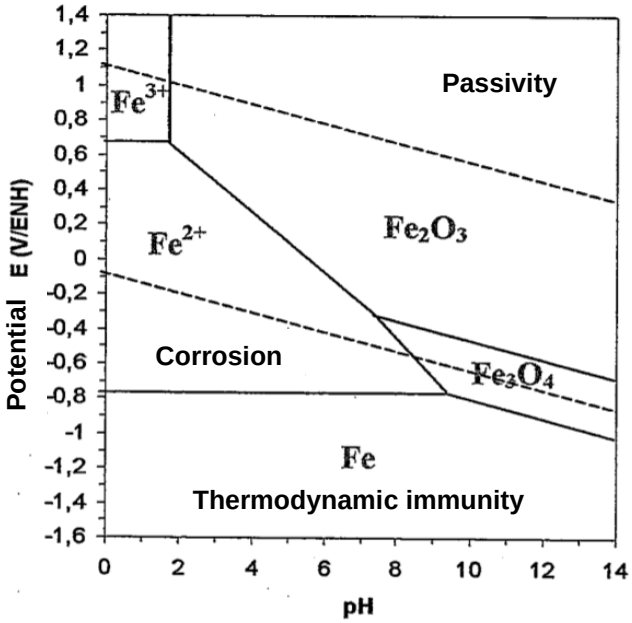

Figure 1-6: Potential-pH simplified diagram for iron at 25°C (Pourbaix, 1963) (Diagram only valid for a given dissolved Fe concentration in aqueous solution)

The interstitial concrete solution has high alkalinity, but during carbonation and dissolution of Portlandite, the pH decreases to a value below 9. In the presence of water and oxygen, the electrical potential of the reinforcement drops to negative values, which leads to the depassivation of reinforcement bars, and it finds itself in a corrosion zone. The pathology that appears is generalised corrosion leading to a progressive reduction of the reinforcement section, which causes a loss of bearing capacity of the reinforced concrete elements. In addition, the formation of expansive corrosion products applies pressure on the concrete surrounding the reinforcement. This pressure is often sufficient to cause concrete cracking and then the concrete cover to burst. Corrosion also leads to a loss of steel ductility and a reduction in bonding between concrete and steel, with an effect on the structural behaviour of the structure (Zhu et al., 2017).

- Kinetics of corrosion

Different approaches exist to model the corrosion rate of concrete reinforcement. In the case of reinforced concrete, corrosion is driven by oxygen diffusion, which is one reason for the importance of the concrete cover. Hence, the modelling of corrosion kinetics is based on a material balance where the consumption of a species drives the corrosion reaction and its rate (Huet, 2005; Millard and L'Hostis, 2012). The following model proposed by Millard and L'Hostis (2012) considers different parameters influencing the corrosion process. In Equation 1-9 the corrosion rate $V_{corr}(x,t)$, depends on the availability of oxygen in terms of oxygen concentration $[O_2](x,t)$; it also depends on the water saturation rate at the interface $S_r(x,t)$, the porosity φ and the kinetics of the chemical reaction K. M_{Fe} represents the molar mass of iron and ρ_{Fe} its density :

$$V_{corr}(x,t) = \frac{4}{3}.\frac{M_{Fe}}{\rho_{Fe}}.K.\varphi.S_r(x,t).[O_2](x,t) \qquad 1\text{-}9$$

Eq 1-9 model is especially valid in the operational phase (dry and carbonated concrete) for an already depassivated steel with corrosion products already formed.

The above model is applied to a concrete slab that contains a rebar shown in Figure 1-7, the point closest to the external atmosphere is called Pext and Pint is the point at the internal part of the slab. The corrosion rate is measured as the layer of corrosion produced at the interface that causes deformations in the concrete over time. The results obtained show that oxygen is the main factor that affects the corrosion kinetics (Figure 1-7), where the kinetics is 40% higher in the area exposed to atmospheric air (Pext). As a results, the deformed shape of the corrosion layer is not uniform around the rebar interface (Figure 1-7b).

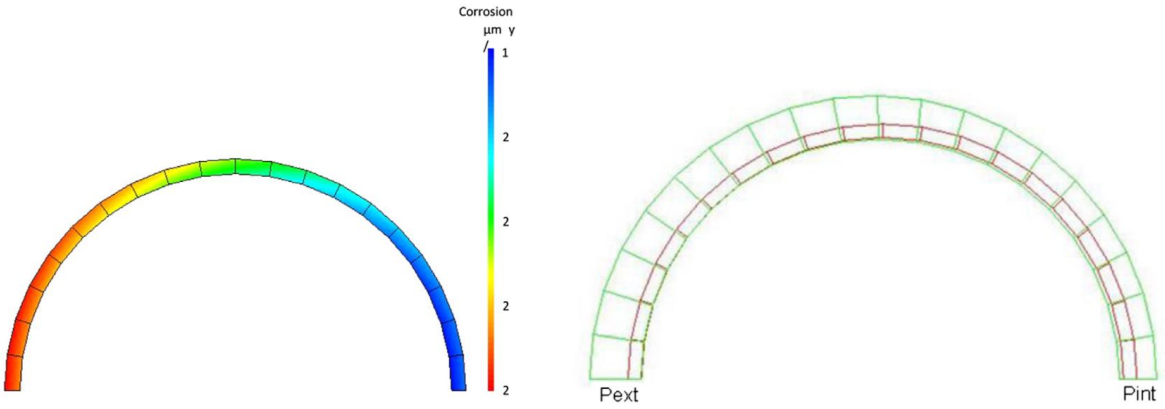

(a) (b)

Figure 1-7: (a) Average corrosion kinetics (µm) after one year, (b) Deformed shape of corrosion layer after one year (Millard and L'Hostis, 2012)

A sufficient concrete cover delays, minimizes and sometimes even prevents oxygen reaching the steel bar. A sufficient concrete cover has been defined for a wide range of exposure environments in EN 206. The available knowledge has been translated into practical executable requirements European codes such as EN 206. The corrosion rate of steel is minimized if steel is exposed to a reducing, alkaline conditions since a passivation layer on the steel surface that limits corrosion is stable at these chemical conditions. Water is used then as an oxidant instead of oxygen during anaerobic corrosion of steel. The corrosion rate becomes equal to the dissolution rate of the precipitated iron if the steel is passivated. Consequently, there is no volume increase of the iron precipitating products at the rebar. The stress intensity between the rebar and surrounding concrete is then too small for spallation of concrete. The dissolution rate of iron highly depends on the presence of minerals that can uptake iron by chemisorption or the formation of a solid solution with iron. The kinetics of this iron uptake by cementitious minerals, as well as the impact of the concrete strength by this iron uptake, are unknown.

1.2 Cement interactions in saturated environments representative of post-closure evolution in geological disposal

A part dedicated to the presentation of porewaters composition is included in Appendix A in support to the next development.

1.2.1 Geochemical evolution of cementitious materials exposed to geological disposal environment

1.2.1.1 Context and boundary conditions

ANDRA, GRS, FZJ

Cement/clay interaction has been intensively investigated in the framework of radioactive waste disposal (Bildstein et al., 2019; Seigneur et al., 2019; Wilson et al., 2021; Gaucher and Blanc 2006; Savage et al., 2020; Idiart et al., 2020; Marty et al., 2015; Jenni and Mäder, 2021; González-Santamaría et al. 2020b; 2020a). Within the context of deep geological disposal, these interactions have been investigated for more than three decades by means of laboratory and *in situ* experiments, studies on natural and industrial analogues, and reactive transport modelling. Comprehensive reviews on various aspects of these interactions have already been published in the past decades (Metcalfe and Walker, 2004; Michau, 2005; Gaucher and Blanc, 2006; Savage et al., 2007; Savage, 2009, 2011; Sidborn et al., 2014; Dauzères, 2016; Claret et al., 2018; Savage and Cloet, 2018; Bildstein et al., 2019, CEBAMA, 2019). All details relative to the previous studies are covered in these studies and especially in the CEBAMA

EC project achieved in 2019. As part of the MAGIC WP, the main objective is to identify the key chemical reactive processes, which will play a role in the mechanical evolution of cementitious materials. For this reason, the present part will summarize the key reactive pathways that may have an impact on the long-term evolution of various concretes in contact with representative clayey environment, in order to drive the future studies in the WP.

During the operating period and the initial post-closure period, the geochemical processes in the repository will be dominated first by a drying transient (*in situ* elements and the host rock in contact). During this period, tunnels are connected to the surface atmosphere, which will control the atmosphere parameter in the underground facility (pressure, humidity, O_2/CO_2 partial pressure,…). These conditions will lead to a loss of water (drying of all the materials) and oxidation of reduced species, especially of chemically reduced minerals such as pyrite (FeS_2) present in clay rocks, leading to an acidification of the pore solution and a mobility of sulphate ions. The oxidising conditions prevailing during the operating period and few years after, will change to reducing conditions once the reduction of the entrapped oxygen is completed. These conditions may have a potential impact on the microbial activity. In the longer term, the post-closure period leads to a progressive resaturation of the concrete structures in contact with the clay host rocks. The process kinetics depend on the site location, the structure design, the hydraulic state and evolution. The cementitious materials of the structures will be exposed to *in situ* porewater after a very long period of partially water saturated condition.

Underground concrete structures are in chemical imbalance with the geological media, especially clay host rocks (i.e. COx, OPA, Boom clay). The strong (geo-) chemical differences between cement and clay materials causes solute transport and chemical transformation in both materials, leading to the formation of alteration fronts. Concrete will therefore chemically change over time according to the expected chemical reactions, and according to the chemistry of the geological medium. These chemical degradations are coupled and their extension is highly dependent on boundary conditions and other types of perturbations, especially mechanical loadings and steel reinforcement corrosion. Also the temperature in the underground repository may range from about 18 to 50 °C depending on the location (localization and depth of the host rock). A short-term temperature rise in the host rock, in the range of 5 to 10 °C due to hydration of cementitious materials, is expected to have a negligible effect on chemical or physical processes. Cement formulations will be adjusted to have low temperature increase during the setting period (e.g. massive concrete plug).

Cementitious materials are employed for various purposes also in waste repositories in crystalline (granitic) rocks (Neeft et al., 2020). For example, the disposal tunnels are sealed with concrete end plugs to ensure mechanical and hydrological isolation of different compartments. In the Finnish final repository for HLW (i.e., spent nuclear fuel), several thousand tons of Ordinary Portland Cement (OPC)–based grouts, shotcrete and rock bolt mortars will be present in structural applications and for sealing of fractures. Also, in the LLW repository in Finland (as the SFR for LILW in the Swedish repository), isolation is achieved by a combination of cementitious barriers and the granitic host rock (Leivo, 2021). Processes occurring at the interface of cement/mortar/concrete and granite can change both the properties of the cementitious material and the granite at the interface.

In general, cement-based materials used in the groundwater environment are fundamentally unstable in a long-term perspective, due to thermodynamic disequilibrium with their environment. Thus, concretes and cementitious materials/barriers used in geological disposal facilities in crystalline or clay rocks will inevitably change (close to the interface) their mineralogical, chemical and physical properties in the long term, both as a consequence of recrystallisation and chemical interactions with their environment. With respect to the long-term evolution of cementitious materials at the interface to granitic/crystalline rock, interactions are mainly related to the contact with the groundwater present in the bedrock. Generally, groundwaters in granitic rocks can exhibit a wide range of chemical characteristics ranging from lowly mineralised waters (representing, e.g., also glacial meltwater) to higher saline brackish or marine waters, or basement brines, depending on repository site and depth. The processes occurring in the cementitious materials in a repository due to the contact with granitic groundwaters depend on the local environmental conditions (in particular the groundwater composition) and comprise the typical

processes described in detail in the respective literature in the context of the performance and degradation of cementitious construction materials in the subsurface (Taylor, 1997; Hewlett, 1998).

Whether in a clayey or granitic environment, the main degradation processes are the following:

- Removal of alkalis and partial neutralization leading to decalcification;
- Carbonation;
- Attack by aggressive species (e.g., magnesium, sulphate, chloride).

Alkali-silica reaction is not directly related to the interactions of concrete with clay or crystalline rock. Instead, it is an intrinsic reactivity of concrete and is therefore not considered in the following sections. Deleterious alkali-silica reactions can be prevented with a proper choice of cement and aggregates to manufacture concrete.

Typically, dissolution of cement hydrates and clay phases are observed in combination with precipitation of secondary mineral phases at or near the material interface. The thickness of the altered layers depend on the transport regime (diffusion vs. advection) and the magnitude of solute concentration gradient, as well as changes of porosity and transport properties of altered materials. Some experimental studies and nearly all reactive transport calculations of cement/clay interactions show significant porosity changes due to precipitation/dissolution of minerals on both sides of the interface. Most of the modelling studies investigate the geochemical evolution of interfaces in low permeability media where diffusive transport dominates. They calculate a strong porosity reduction in narrow zones. The clogging of the pore space leads to a strong decrease of transfer properties across the interface, which significantly slows down the geochemical alteration processes in the long term.

Benchmarking studies related to cement/clay interaction were conducted by Marty et al. (2015) and Idiart et al. (2020). In general, the results obtained with different numerical codes agree well with each other. This shows that differences in predictions by numerical simulations are caused mainly by the modelling assumptions in terms of primary and secondary mineral phase selection, kinetic constraints, and which type of coupling between transport and chemical processes is assumed. A benchmarking study specifically on the coupling between chemical and transport processes with respect to porosity, tortuosity and permeability evolution was conducted by Xie et al. (2015). It is concluded that the results do not depend on the reactive transport code used and the simulations are shown to be robust. In addition, 2D modelling allows local differences in porosity and mineralogical assembly to be taken into account, which leads to a better agreement between the codes compared to the 1D modelling problem despite the increase in complexity.

1.2.1.2 Cement analogues

Natural analogues provide answers to complex problems such as the evolution of materials in underground disposal sites. Analogues can help identifying the key mechanisms to consider in modelling and provide information on the boundary conditions of the system over very long periods.

Characterising the archaeological cements of Pompeii and the concretes of a uranium mine lead to select the main alteration factors such as the migration of carbonate and sulphate ions, but also the saturation degree of the material (Rougeau, 1994). Hodgkinson & Hugues (1999) studied 1800-year-old Roman mortars from Hadrian's Wall. These authors highlight the role of CO_2 gas and carbonated water in the evolution of the cementitious materials. The initial C-A-S-H seems not to have changed significantly at low temperatures and appears preserved from carbonation in some cases. However, Si enrichment of the C-A-S-H is visible on contact with the flints. Calcite precipitation is abundant in Hadrian's Wall mortars. Analysis of the cement used to bind the stone blocks of the Hadrian's Wall shows some similarity to Portland cements as they contain calcium silicate hydrates. This is a qualitative indicator of the good stability and durability of modern cements (Miller et al., 2000). The study of Gallo-Roman cements older than 1500 years confirms long-term stability of the cementitious material as long as no major physical disturbances occur. C-S-H shows a low C/S ratio supporting the stability calculations with time (Thomassin et Rassineux, 1992). The condition of Roman concrete exposed for two thousand years to a marine environment provides information on the durability of pozzolanic

materials. This particular case cannot be extended to the different types of cements and is valid under specific curing conditions (Vola et al., 2011). The cementitious matrix decomposes into C-A-S-H, calcite, tobermorite and sulfo-aluminates, illustrating the reaction products between hydrated lime and seawater. Finally, a study of an unusual natural environment at Maqarin, northern Jordan, suggests that pH conditions within a deep geological repository may remain hyperalkaline for up to a thousand years (Vola et al., 2011). The result comes from the analysis of alkaline waters generated by the dissolution of a natural portlandite created by the natural combustion of a bituminous marl. Analogues are useful information for designing models that predict the long-term behaviour of cementitious matrices. However, the difficulty lies in the fact that the composition and initial state of the material are hard to figure out. The studies within the MAGIC project therefore focus on the analysis of cementitious materials in accelerated conditions and on analogues that are several decades old.

1.2.1.3 Key interactions of cementitious materials with clayey and crystalline rocks

Following processes dominate evolution of hydrated cement system (whatever the cement) in contact with clay or crystalline environment:

The Hydrolysis/neutralization: The leaching describes processes that result in the dissolution from the cement-matrix under a water flow. This leads to a loss of materials, dissolved in water without a reprecipitation process. This phenomenon is relevant for porous cementitious materials, which repeatedly are in contact with solutions (regularly submitted to a water flow), which are not in equilibrium with the cement. The pore solution pH of sound Portland concrete is in a range of 12.5 to 13.2, so the neutral pH (between 7 and 7.8 for clay pore water) of the geological water acts as an aggressive/acidic solution. The pH of the agressive solution influences the solubility (Jantschik et al., 2018) of all minerals (Portlandite, C-S-H…). The chemical stability of all major cementitious hydrates is highest in the pH range of 10.5 to 12.5. The hydrolysis of a cementitious material starts with the neutralisation of the alkalis contained in the pore solution and then leads to the neutralisation of the hydrates by dissolving the portlandite (CH), followed by calcium aluminate phases (AFm/AFt) decomposition and finally the decalcification of the calcium silicate hydrates (C-S-H). This results in a concomitant decrease of the pH of the pore solution. Initially, dissolution of KOH and NaOH within the cement will form a pore water with pH ~13. The pore water pH will then decrease to ~12.5 buffered by equilibration with portlandite (at 25 ºC). This pH will remain until all portlandite has dissolved, after which, pH will be controlled by equilibrium with the incongruent dissolution of the C-S-H gel and will decrease down to ~10.5. The ultimate residue (if all calcium is removed from the material) will consist essentially of hydrous forms of silica, alumina and iron oxide. By this stage, the cement paste will be disintegrated.

In contact with water from geological formations for long periods of time, decalcification by leaching, induces loss of mass and alkalinity. Leaching generally leads to an increase in porosity and transfer properties in cementitious materials. Calcite reprecipitation during the neutralization process generally leads to a decrease of the porosity and the transfer properties (see below the carbonation paragraph). In an OPC, due to the crystalline structure and display in the hydrated cement, C-S-H decalcification represents 1/3 of the increase in porosity against 2/3 for CH. The effect on mechanical strength is not on the same order of magnitude, as the decalcification of calcium hydroxides creates macroporosity and as a huge influence on the mechanical properties while that of the C-S-H has a lower impact (Carde et François, 1999).

Cementitious materials can be described with macroscopic chemical and physical states of degradation (from sound to neutralized). The state of alteration is characterised by the total Ca/Si ratio of the cementitious matrix, which progressively decreases under the effect of hydrolysis and leaching. Leaching of alkalis and decalcification causes changes of many physical and mechanical properties of cement-based materials such as porosity, elastic modulus, compressive strength and creep. Leaching of concrete by percolating or flowing water can cause severe damage, e.g., in dams, pipes or conduits, and is potentially important for the long-term evolution of repository systems for nuclear wastes. Note that the calcium concentration difference between Callovo-Oxfordian groundwater ($[Ca^{2+}]$ = 5.4 mmol/L) and the pore water of sound CEM I concrete is lower than an order of magnitude (Sellier et al., 2011) and therefore less damaging in the long-term than deionised water. Decalcification by leaching is envisaged when the dissolved equilibrium calcium concentration of a cementitious material is higher than the equilibrium

dissolved calcium concentration in clay. The dissolved equilibrium calcium concentration reduces with the Ca/Si ratio (Berner, 1992) & Vehmas&Itala (2019). There are many host rocks whose equilibrium dissolved calcium concentration in pore water is larger than the dissolved equilibrium calcium concentration of a cementitious mineral, especially CSH-phases. In those circumstances, decalcification by leaching is highly unlikely.

It is possible to study the chemical degradation of a cementitious material under laboratory conditions by reproducing the underground conditions using an experimental device allowing CO_2 regulation in order to impose a constant pH to the leaching solution (Dauzères et al., 2014). Under these conditions, the composition of the hydraulic binder influences the degradation reacting with the COx pore water. The results show that the low hydration heat/low pH cement paste (37% CEM I cement, 30% fly ashes and 33% silica fume) is strongly degraded leading to a coarser porosity. By contrast, the degradation of the CEM I cement paste seems to be limited by the precipitation of a calcium carbonate crust (see next paragraph) on the surface, which reduces the exchange of soluble species and thus the degraded thickness. This illustrates the complexity of multi-ionic degradation as blended cements are usually known for their better chemical resistance. These results need to be verified under more representative conditions, i.e. for a cementitious material directly in contact with the rock. At a concrete scale, accelerated ammonium nitrate degradation of two “low heat of hydration and low pH” concretes clearly shows the interest of blended cements (ternary blast furnace slag mix and ternary fly ash mix). The results from Bes (2019) show that after 8 months of exposure to an ammonium nitrate solution concentrated at 6 mol/L, the decrease in mechanical properties is about 10% for low pH concrete compared to 60% for CEM I concrete. The mechanical performance of low pH concretes changes in a similar way to that of low pH cement pastes. For an equivalent degraded thickness, the mineralogical structure of the zones degraded by an accelerated ammonium nitrate process appears to be similar to deionized water degradation, therefore validating the use of this acceleration technique. Compared to real disposal conditions, chemical degradation under water is a condition maximising chemical degradation as the water supply is usually limited by the rock. In the context of the interaction between low pH concrete and the “Konrad-solution”, the dissolution of C-S-H seems to be relevant. C-S-H phases are instable in neutral and acid solution (Hagemann et al., 2009).

Carbonation under water: Carbon dioxide (CO_2) is an acid source after dissolving in pore water. Neutralisation of the interstitial solution causes a re-equilibrium with the cement hydrates and leads to their dissolution. Carbonation occurs when carbon dioxide dissolves in the pore solution of cement paste, producing CO_3^{2-}ions, which will react with Ca^{2+} and produce $CaCO_3$ (calcite) at the expense of portlandite. Later, when portlandite has totally reacted, C-S-H is first decalcified and later decomposed. Carbonation of a cementitious material under water leads to lixiviation by decreasing the pH of the interstitial solution, which leads to the solution of calcium and hydroxides (Badouix, 2000). This results in a reorganisation of the material in the altered layer (gradient) with the formation of calcite and carbo-aluminates (Revertégat et al., 1997). The AFm and AFt phases react with the carbonate anions and can form equivalent carbonate phases (e.g., thaumasite, $Ca_3Si(OH)_6SO_4CO_3{\cdot}12H_2O$). If pH is lowered further by addition of more carbon dioxide, these initially formed carbonate species will decompose. The residues from complete carbonation of cementitious materials are calcite, amorphous silica, hydrocarboaluminates and different Al- and Fe-hydroxides. The pH value of the carbonated cement paste first drops to around 10 when all portlandite is consumed and later to a pH around 8, when the other phases are decomposed.

These carbonation reactions are mostly happening at a slow rate and are expected to be especially pronounced during the operational phase of the repository, when the cementitious materials are partially unsaturated and in contact with gaseous CO_2 from the ventilated tunnels. In later stages of repository evolution, carbonation reactions take place due to CO_2 production from degrading organic wastes or due to interaction with carbonate-rich groundwaters. Due to microstructural changes, carbonation is often accompanied by a reduction of permeability and diffusivity of cementitious materials. Indeed, porosity in the cementitious material can be filled by the precipitation of calcium carbonate, which leads to a change in the transfer properties compared to the sound material.

In the case of carbonation in saturated conditions, the reactions and their sequencing do not differ from what is observed in atmospheric carbonation (see paragraphs 1.1.1.1 and 1.1.1.2), the products observed and their stability are the same (Revertégat et al., 1997). Atmospheric carbonation is significantly faster than underwater carbonation due to the several orders of magnitude gap between the gas and water phase transfer parameters.

It is particularly important to make a distinction between the carbonation rate, which refers to fixed CO_2, and the carbonation depth, which refers to the evolution of the pH. Carbonation kinetics is often associated with carbonation depth. The amounts of leached calcium are lower when the solution contains carbonates.

Exposure to a solution with 25 mmol/L $NaHCO_3$ maintained at a pH of 8.5 shows in particular that CEM V hydrated cements fix less carbonates and are less sensitive to clogging than CEM I cements (Richet et al., 2004). On a cement paste scale, the average effective diffusion coefficient of tritiated water is lower in the carbonated part (Richet et al., 2004). Exposure of a cementitious material to a carbonated solution can lead to the formation of ettringite behind the calcite precipitation front. Ettringite precipitation could be the cause of swelling phenomenon (Revertégat et al., 1997). In fact, the carbonate layer is not homogeneous, consisting of a dense surface layer mainly composed of calcite with limited diffusion of carbonates, followed by a porous alteration layer which is the place of ettringite formation and which evolves significantly with time (Badouix, 2000). The carbonation under water linked to the partial pressure of CO_2 in equilibrium with the the Callovo-Oxfordian clay will be maintained throughout the entire disposal period. In the Cigéo context, the partial pressure in equilibrium with the clay is about 20 times higher than the atmospheric value.

Attack by aggressive species: The transport and distribution of chlorides in a concrete structure are very much a function of the environmental exposure, i.e., chloride concentration and duration of exposure to solutions in contact with the concrete surface. Sulphate attack in concrete made with cement with a high C_3A content originates mainly from interaction with sulphate from rich groundwaters or bentonite barrier according to the concept. The damage to concrete structures resulting from external sulphate attack is related to the chemical reactions between sulphate ions and the solid cement hydration products. By migrating through the porosity of concrete by diffusion, sulphate ions can react with aluminates in the cementitious matrix and cause degradation under the effect of crystallisation pressures induced by the precipitation of sulfo-aluminates, especially ettringite ($Ca_6(Al,Fe)_2(OH)_{12}(SO_4)_3 \cdot 26H_2O$), and gypsum ($CaSO_4 \cdot 2H_2O$). This can lead to the generation of internal stresses as a result of the formation of the expansive products (calcium sulfo-aluminates), which in consequence results in a mechanical response of the bulk material, such as cracking. However, the potential effects of sulphate attack in cementitious repository materials can be mitigated by the utilisation of sulphate resisting cements that have a low C_3A content. Having low C_3A contents can delay the formation of ettringite but in the long term it will form wither way, although with less magnitude. These cements called SR cements, are worldwide commercially available. The presence of chlorides is known to limit the effects of sulphate attack by forming Friedel salts in addition to ettringite (e.g. marine environment). Sulphate degradation is also an interdependent process with hydrolysis leading to an increase in the porosity of concrete. This is one explanation of why concretes formulated with blended cements (slag, fly ash, pozzolanic addition...) are resistant to sulphates. The limited amount of C_3A in these binders and the consumption of portlandite (CH) during pozzolanic reactions also explain their better behaviour regarding sulphates. The effect of a sulphate-containing solution on the degradation of a CEM I paste was studied for a solution representative of Callovo-Oxfordian waters regarding sulphate concentration and pH (Planel et al., 2006). The results of the XRD analyses allow to distinguish a zone with dissolution of portlandite, a zone with gypsum precipitation accompanied by the formation of ettringite, and finally a zone where ettringite is the only crystallised phase. The quantities of ions exchanged are proportional to the square root of the time as in the case of hydrolysis with deionised water, which shows that the

process is diffusive through the degraded layer. The phenomenon is diffusive as long as no large pressure gradients are present. Load and tests with cycles of immersion and drying are well known to accelerate sulphate ingress. Prediction of long-term alteration of concrete requires numerical simulations due to the low kinetics involved. In the case of a Portland cement-based concrete barrier exposed to moderate sulphate attack (10 mM dissolved sulphate) and considering the ettringite precipitation front as an alteration indicator, degradation can reach 1.5-3 m over one million years according to modelling assumptions (reaction kinetics, approximation of local equilibrium, evolution of porosity). The degradation process leads to an internal zone where portlandite is dissolved but C-S-H remain mostly intact and an external zone with degradation of the C-S-H (Trotignon et al., 2005). As previously mentioned, sulphate reacts in contact with CH and C-S-H in the concrete. In the specific case of low-pH concrete, the reactions with sulphate are considered only with C-S-H due to the absence of portlandite (Herold et al., 2020). The reaction with the C-S-H precipitates gypsum and further reactions products depend on the cation which is bounded with sulphate. Equation 1-1 to 1-3 show the reaction of C-S-H with sodium sulphate (Na_2SO_4), potassium sulphate (K_2SO_4) and magnesium sulphate ($MgSO_4$). Sodium hydroxide and potassium hydroxide may increase the pH of the pore solution (Herold et al., 2020).

$$2CaO \cdot 2SiO_2 \cdot 3H_2O + 2Na_2SO_4 + 3H_2O \rightarrow 2(CaSO_4 \cdot H_2O) + 4NaOH + 2SiO_2 \quad \text{1-10}$$

$$2CaO \cdot 2SiO_2 \cdot 3H_2O + 2K_2SO_4 + 3H_2O \rightarrow 2(CaSO_4 \cdot H_2O) + 4KOH + 2SiO_2 \quad \text{1-11}$$

$$2CaO \cdot 2SiO_2 \cdot 3H_2O + 2MgSO_4 + 3H_2O \rightarrow 2(CaSO_4 \cdot H_2O) + 4Mg(OH)_2 + 2SiO_2 \quad \text{1-12}$$

There are significant differences between the reagents and products. The volume expansion causes strain in the cement matrix, which can result in a failure of the cement paste. However, a failure of the cement paste is only expected, if its stability is already affected by chemical attacks of the C-S-H for low-pH cement (Hagemann et al., 2009) (Kunther et al., 2013) and portlandite for Portland cement. The molar volume of gypsum ($CaSO_4$ $2H_2O$; 74 cm^3/mol) is 2.25 times larger than that of portlandite ($Ca(OH)_2$; 33 cm^3/mol. In addition, the molar volume of monosulfate (309 cm^3/mol) replaced with ettringite (707 cm^3/mol) indicates a similar increase. The dimensional variations are however not only explained by these volume increases, which led some authors to suggest the theory of crystallisation pressure. The magnesium-gypsum reaction (Equation 1-11;1-12) induces formation of gypsum and attack by magnesium ion at at the same time. Alteration processes occur simultaneously. Hence, the combined chemical process is very harmful to the cement (Biczok, 1968). Herold et al. (2020) describe a lower Ca/Si ratio in the C-S-H-phases in low-pH concretes compared to high-pH concretes resulting in a higher stability of low-pH concrete in presence of sulphate containing solutions. A part of the sulphur enrichment of the cementitious material is sometimes attributed to the oxidation of pyrite, e.g. in Opalinus (OPA) clay, which promotes the mobility of sulphates (Mäder et al., 2017). Concerning the chloride attack, at moderate temperatures (40°C) and high chloride ion concentrations (i.e. 10%), concrete can be degraded due to the formation of Friedel's salts. The leaching of calcium ions leads to the formation of calcium chloride and the formation of chloro-aluminates, which can lead to internal alteration, cracks and increased porosity (Abbas and Safeer, 2014).

Deterioration of material properties due to chloride ingress is one of the causes of concrete degradation worldwide. Concrete itself is generally not adversely affected by chloride ingress, though the formation of some chloride-bearing phases such as Friedel's salt ($Ca_4(Al,Fe)_2(OH)_{12}Cl_2 \cdot nH_2O$) at the expense of other AFm/AFt phases is possible. However, the steel reinforcement and other steel materials inside concrete can be corroded at elevated chloride concentrations, which may lead to the formation of (expansive) corrosion products accompanied by crack formation due to mechanical stress (Zhu et al., 2018). This is deemed to be more relevant under oxic conditions that may occur in concrete-granite systems when an insufficient concrete cover has been used or in the presence of glacial meltwaters.

In the presence of a source of sulphate and carbonate ions, a sufficiently low temperature (in the range of 5-10°C) and a pH of 10.5, thaumasite can be formed in cement-based concretes (Schmidt, 2007).

The Magnesium attack: The ingress of magnesium sulphate or magnesium chloride are specific forms of sulphate or chloride attack. The magnesium can exchange with calcium in the hydrated cement paste and causes enhanced degradation of cement material. Degradation caused by exchange reactions results in dissolution of portlandite and the decrease of pH. The attack by magnesium ions present in groundwaters can be particularly deteriorating for concrete structures, as it can cause a complete disintegration of the C-S-H phases in the long term. In contact with magnesium rich groundwaters, the magnesium replaces the calcium in the hydration phases leading to the formation of amorphous $Mg(OH)_2$, magnesium silicate hydrates (M-S-H) as well as Mg-containing SiO_2 gel, accompanied with a drop in pH to approx. 10.5 (Taylor, 1997; Eglinton, 1998). Calcium bearing phases are dissolved and could be replaced by magnesium bearing phases such as M-S-H without binding properties, brucite or other.

Granitic, clay, saline and bentonite waters cover many application cases. Recently, the alteration of a micromortar (CEM I 42.5 105 468, Silica fume, Blast furnace slag and Quartz filler) in contact with different interstitial waters representative of the groundwater from the nuclear waste disposal site was investigated. This include a granitic natural water occurring in the Josef underground laboratory (Czech Republic), a Callovo-Oxfordian clay formation pore water form underground research laboratory in Bure (France) and bentonite artificial porewater. The results show in all cases a depletion of calcium in the cementitious material by leaching. In the case of waters containing magnesium (clay pore water and bentonites) a magnesium enrichment is shown, which is explained by the strong chemical gradient between the pore water and the cementitious material (Vehmas et al., 2020).

The magnesium attack caused by $MgCl_2$ solutions leads to the formation of brucite and calcium chloride:

$$MgCl_2 \cdot 6H_2O + Ca(OH)_2 \rightarrow Mg(OH)_2 + CaCl_2 \cdot 6H_2O \qquad 1\text{-}13$$

Brucite can generate a film at the surface and can delay further degradation of the cement matrix. However, Biczók (1968) suggests that the brucite-film is stable in stagnant waters only because it will be leached and or neutralized quickly by advective flow. When the brucite is leached the degradation retarding effect is lost. Brucite and gypsum ($CaSO_4 \cdot 2H_2O$) are formed by the attack of magnesium sulphate ($MgSO_4$):

$$MgSO_4 \cdot 7H_2O + Ca(OH)_2 \rightarrow Mg(OH)_2 + CaSO_4 \cdot 2H_2O + 5H_2O \qquad 1\text{-}14$$

Brucite precipitates and forms a deposit at the surface of SiO_2-gel. In contrast to C-S-H-phases, magnesium-silicate-hydrate-phases (M-S-H) form notably in low-pH concrete, do not exert a stabilizing effect on the cement matrix, resulting in a lower mechanical stability. Moreover, M-S-H-phases do not form a stable compound with the cement matrix and are therefore to a much higher extent subject to leaching by ingressing solution (Jantschik et al., 2018).

The theory of calcium-magnesium exchange by dissolution/precipitation processes in the cement matrix is also described by investigations of (Dauzères et al., 2016; Neji et al., 2022 and Gaboreau et al., 2011). Investigations of the contact zone between OPA clay and low-pH concrete showed a decrease of calcium concentrations and increase of magnesium concentrations in the contact zone. Hence, a dissolution of C-S-H and formation of M-S-H may be assumed. Alonso et al. (2016) specify that magnesium enrichment in the concrete is expected if the leaching solution from the host rock includes > 3 mmol/l magnesium ions. A more recent publication (Bernard et al., 2019) shows, however, that M-S-H are rather precursors of clay minerals whereas C-S-H are cement hydrates. The structures are thus very different and invalidate the hypothesis of a Ca/Mg exchange previously implied.

1.2.1.4 Influence of the interface with the host rock

IRSN, ANDRA, FZJ, GRS

Short term laboratory (Adler et al., 1999; Adler, 2001; Dauzères et al., 2010, 2014; Fernandez et al., 2016; Balmer et al., 2017) and longer-term in situ experiments (up to about 20 years) at different underground research laboratories like HADES, Mol, Belgium (Read et al., 2001), Mont Terri, Switzerland (Jenni et al., 2014; Dauzères et al., 2016; Lerouge et al., 2017; Mäder et al., 2017), Bure, Department Meuse/Haute Marne, France (Gaboreau et al., 2011, 2012; Dauzères et al., 2016), or at the Tournemire site in France (Tinseau et al., 2006; Techer et al., 2012a,b; Bartier et al., 2013; Lalan et al., 2016), as well as the FEBEX experiment in the Grimsel test site in Switzerland (Alonso et al., 2017; Fernandez et al., 2017; Turrero and Cloet, 2017) have demonstrated that at the cement/clay interface, alteration of both cement paste and clay material takes place. This leads to mineralogical changes modifying the microstructure of the altered region, which may influence transport relevant properties such as porosity, diffusivity and permeability, or the radionuclide retention behaviour of the materials.

From a phenomenological point of view, the reactive mechanisms observed when the cementitious materials are in direct contact with the clayey host rock (in saturated conditions) are similar to those observed for interaction with representative clayey solution. The main impact is the kinetics of the chemical evolution on both sides of the interface. The thickness evolution of the degraded layers as a function of time is mainly controlled by the transfer properties in these layers. With the clogging of the porosity, the effective diffusion coefficient decreases. This leads to a strong decrease of the chemical exchanges and thus the chemical evolution in both materials (concrete and host rocks).

Hardened concrete interfacing clay

The nature of the interface affects all chemical reactions, including carbonation. As mentioned above, immerged in pure clayey solution, an exogeneous calcite crust is likely to be formed limiting the exchange of soluble species and then the degradation, especially for Portland cement (Dauzères et al., 2014; Kamali et al., 2008; Badouix et al., 2000; Albert et al., 2002; Planel et al., 2006). In contact with the clayey host rock with the same solution in the pore network, the reactive mechanisms are the same as those observed in the cement paste immersed in solution (sulphate attack, carbonation, leaching, Mg-attack…). However, heterogeneous calcite precipitates over 20 µm in the sulfate-resisting Portland cement paste and a diffuse carbonation of the cement materials is observed without clogging allowing a deepest altered zone (Dauzères et al., 2010). The assumption made in this particular case is that in contact with the mudstone, the reduction of the local carbonate concentration by calcium fixation from the dissolution of portlandite is followed by an insufficient carbonate flux to induce calcite precipitation. In this experiment, it should be noted that the cement paste is placed in contact with the saturated clay disc once hardened.

Poured concrete interfacing clay during hardening

Concerning the chemical evolution at the interface, the key parameters are the mineralogy and porewater composition of the clay material (which depends on the repository concept and site), as well as the cementitious ones, and their initial transport properties (e.g., porosity, diffusivity, incl. water saturation). The processes occurring at the cement/clay interface (sulphate attack, carbonation, leaching, Mg-attack…) as well as their kinetics will depend largely on the initial properties of the materials. The type of binder (OPC or mixed cement) has a significant impact compared to the nature of the host rock.

As part of the long-term FEBEX experiment, the analysis of shotcrete interacting for 13 years with granitic groundwater and porewater from FEBEX bentonite showed modifications in the concrete matrix over a thickness of 5 cm (Alonso et al., 2017; Fernandez et al., 2017; Turrero and Cloet, 2017). As the cement used is not sulphate resistant, the first centimeter of concrete is the most altered with the depletion of portlandite and the massive formation of ettringite in connection with the high amounts of sulphates brought by the bentonite. Measurement of soluble ions in the concrete pore water as a function of distance from the bentonite interface shows alkali leaching coinciding with a decrease in pH. However, the calcium concentration is higher in the first few centimeters in contact with the interface,

which is explained by the penetration of calcium provided during the saturation of the bentonite to the granite water (Fernandez et al., 2017).

Using sulphate resistant cements, leaching and carbonation are the key degradation processes of hardened concrete in contact with clay material with a low concentration in dissolved magnesium and calcium. As an order of magnitude, according to the ACED Deliverable 2.4 Belgian clay at Mol has a 50 to 100 times smaller dissolved magnesium and calcium concentration than other clay host rocks considered in France, Switzerland and Netherlands.

Formation of C-A-S-H and (amorphous) M-S-H at the interface between low-pH cement paste and Toacian clay rock affect porosity and transport properties (Dauzères et al., 2016). The replacement of portlandite, C-S-H gel and monosulphoaluminate by ettringite (Savage, 2014) were also observed. Note that in low-pH formulations, C-A-S-H can be present already as initial hydration phase. In low-pH cementitious materials, where portlandite may be lacking, and the decalcification of the C-(A)-S-H can proceed directly, leading to an earlier formation of amorphous silica as residue. Low-pH cementitious formulations with slag and micro silica, however, have a more refined pore structure leading to lower diffusivity and thus lower rates of mineral alteration. Low-pH concrete has a higher stability in contact with magnesium and ammonium rich solutions caused by the lower calcium content in the concrete (Herold et al., 2020). Hence, the dissolution of calcium from the cement hydrates (C-S-H with low Ca/Si ratio) has a lower influence on the stability of low-pH concrete compared with high-pH concrete.

For both OPC and low-pH concrete, the redistribution of sulphate towards the unaltered cementitious matrix due to the decrease in pH close to the interface with Opalinus clay for 2.2 and 4.9 years, destabilizing earlier formed Ca-Al-sulphates (ettringite, monosulphate (AFm)) that re-precipitate in the higher pH regions (Mäder et al., 2017). The dissolution of Ca(OH)2 followed by decalcification of C-S-H means a reduction in the Ca/Si ratio of the cementitious material. This change is accompanied by rapid precipitation of Ca-carbonates directly at the interface, such as aragonite and calcite, due to steep gradients in hydroxyl ion concentrations (higher on the cementitious material) and the partial pressure of carbon dioxide ($pCO_2(g)$ is higher in the clay rock formation) across the cement/clay-interface.

In the long term, some chemical reactions in contact with the rock lead to an increase in the porosity of the cementitious material as shown in the following examples:

- The evolution of low alkaline concrete in contact with OPA clay was analysed mineralogically and chemically after 5 years of interaction (Lerouge et al., 2017). The experiment involves a vertical borehole in the OPA, filled with three different concrete sections and a compacted bentonite section. The results show that the alteration of the concrete is limited to a very porous (≈75%) white crust of 1 mm thickness. The altered layer contains calcite, C-S-H with a low C/S ratio and Mg-rich phases (magnesium enrichment and slight calcium and sulphate depletion).
- At the Meuse/Haute-Marne URL, it was possible to sample 5-year-old interfaces between a cementitious material and the Callovo-Oxfordian clay (Gaboreau et al., 2012). The sample tested corresponds a class G cement paste injected into a borehole that remained in direct contact with the clay host rock (at 20°C, the geological temperature) for years. In the hydrodynamic test conditions, i.e saturated conditions and far from any mechanical perturbation, the porosity profile showed an opening of the cement paste porosity.
- Micro-tomography and autoradiography analysis of low-permeability high-pH concrete that has been in contact with Boom clay for 14 years in the Belgian Underground Clay Research Laboratory (HADES) also shows an increase in porosity at the interface in relation to calcium leaching (Phung et al., 2018).
- In OPC and LAC (Low Alkaline Cement) concretes, an increase of porosity towards the concrete/clay interface was measured and explained by decalcification. Gaboreau et al. (2011) suggest a porosity increase over a depth of up to 3.5 cm from the interface after 15 years of interaction in the Tournemire URL. The area of increased porosity clearly depend on the longer contact time and on the concrete composition. In OPC, portlandite dissolves and the Ca/Si ratio in the C-S-H is reduced from 1.5 – 2.0 to 0.8 (Gaboreau et al., 2011). In LAC, magnesium enriched in the porosity increased zone, while calcium migrates from the LAC to the clay (Lerouge et al., 2017).

Other specific conditions result in contrast in decreasing the porosity of the cementitious material:

- In the case of shotcrete lining taken from the base of a shaft (Gaboreau et al., 2012) for example, unsaturated conditions induced by the ventilation of the shaft lead to precipitation of gypsum, which results in porosity clogging at the interface. The results show a limit of mineralogical disturbance extension to a few hundred micrometers around the interface. The main processes observed are dissolution of portlandite, carbonation and decrease of the Ca/Si ratio suggesting a C-S-H decalcification.
- The reactivity of a Portland cement paste with argillite was investigated in IRSN laboratory using a diffusion cell at a temperature of 70°C (Lalan et al., 2019). In this experiment, the cementitious material is poured in contact with a clay disc. The reservoir behind the cementitious material and the clay is filled with alkaline water and a synthetic porewater from the clay rock, respectively. The experimental artefact of the alkaline reservoir (voluntary imposed) leads to a deeper decalcification front and less porosity reduction by carbonation. The results show a reduction in the porosity of the cementitious paste by carbonate precipitation despite the creation of macroporosity by dissolution of portlandite to a thickness of 400 µm after more than one year of interaction and hardening. At ambient temperature, the porosity is increasing while the effect of decalcification on the porosity of the cementitious material is countered by the temperature effect that enhances the carbonation process.

Regarding the effect of temperature, Glasser et al. (2001) conducted an experiment in the HADES undergound laboratory (Belgium). Cylinders of different concretes (CEM I, CEM I + fly ash, CEM I + slag) were placed in Boom clay at 85°C for 12 to 18 months. An over-coring was used to sample and characterise the cement/clay interface. The concrete alteration with a thickness of 100 to 250 µm zone shows an evolution with a loss of Ca and an enrichment in Mg, S, Al, Si in comparison to the unaltered cement material. The contact between the two materials can be distinguished by a line (10 µm) rich in Mg, Al, Si containing a complex gel of low crystallinity whose composition may correspond to a hydrotalcite and sepiolite.

Finally, the extent and significance of these processes will need to be assessed on a site-specific basis (NDA, 2016). Due to this complexity and diversity, it is difficult to establish a general sequence of secondary minerals forming in the cement domain due to the impact of the clay porewater. Details on experimental observations with respect to secondary phases formed at the interfaces between various cementitious materials and clays, clay rocks or bentonite have been compiled by Dauzères (2016) and Deissmann and Ait Mouheb (2021).

1.3 Feedback of Reactive Transport (RT) modelling on cementitious materials in geological disposal

1.3.1 RT modelling of cementitious materials evolution in saturated environments

PSI, UFZ

1.3.1.1 General overview on the reactive transport modelling

In the last 20 years, a substantial effort has been made in reactive transport simulations of cementitious materials evolution in contact with i) different clay rocks (i.e. Opalinus Clay, Callovo-Oxfordian and Boom-Clay), ii) bentonite and iii) crystalline rocks. Although most of the work is related to large scale modelling of repository systems (De Windt et al., 2004; Trogtignon et al., 2007; Marty et al., 2009, 2014, 2015; Berner et al., 2013; Kosakowski and Berner, 2013; Liu et al., 2014; Mon et al., 2017; Idiart et al., 2020) some work has also taken advantage of field scale experiments (Dauzères et al., 2016; Jenni et al., 2017; Jenni and Mäder, 2021) or natural analogues (De Windt et al., 2008; Watson et al., 2013; Soler, 2013) to identify key coupled processes (Yang et al., 2019; Galindez and Molinero, 2010; Oda et al., 2004; Fernández et al., 2007; Yuan et al., 2013; Liu and Jacques, 2017; Bildstein and Claret, 2015; Trapote-Barreira et al., 2016; Samper et al., 2018; Huang et al., 2018). Modelling studies up to 2020 have been summarised by Claret et al. (2018), Savage and Cloet (2018), Bildstein et al. (2019), De Windt and Spycher (2019), and Wilson et al. (2021).

During all these years, cement-clay interactions have been mainly modelled including various degrees of complexity. The main challenge of these models is related to the complexity of the chemical reactions involved with a large number of mineral phases, solid solutions and aqueous species participating in ion-exchange, surface complexation and dissolution/precipitation reactions kinetically and thermodynamically controlled. The earliest modelling attempts used as assumption local equilibrium for chemical reactions while other authors opted for coupling thermodynamic and kinetic approaches. Although thermodynamic equilibrium assumption is computationally efficient, in some cases this approach is not able to capture the fine structure of potential alteration zones in all the studied systems (Marty et al., 2009). New dual porosity transport modelling concepts, accounting for electrostatic effects in the clayrock side (Jenni et al. (2017) and Jenni and Mäder (2021)) or in the cement (Appelo, 2017, Yang et al. 2019) have also been recently described. On the other hand, Neretnieks (2014) proposed a simplified analytical model, which may be useful from a performance assessment point of view, but cannot reproduce the complex phenomena occurring at the cement interface. Comparison of the proposed simplified analytical model with reactive transport is described in Idiart et al. (2020a).

Different chemical thermodynamic databases have been used, including EQ3/6 (Wolery, 1983), CEMDATA2007 (Lothenbach and Winnefeld, 2006), Nagra/PSI database (Hummel et al., 2002; Thoenen et al., 2014), ThermoChimie (Giffaut et al., 2014) or Thermoddem (Blanc et al., 2012; Blanc 2017). In particular during the last years, the thermodynamic databases for hydration phases in cementitious materials, zeolites, which play a role in clay/cement interactions and clay minerals have been significantly improved (Blanc et al., 2015; Lothenbach et al., 2019, Ma and Lothenbach, 2020, Zhen-Wu et al. 2020).

Most of the simulations were performed at 25 °C; only in few cases the effects of temperature were investigated. Here, greater rates of dissolution of montmorillonite and other minerals were noted; however, leading to relatively little differences compared to simulation results at 25 °C (Savage and Cloet, 2018). Simulations accounting for non-saturated or evolving conditions with respect to saturation state has not been described extensively (Idiart et al. 2020b).

Another important aspect is that most of the studies mentioned before are related to the interaction of ordinary Portland cement with clay (bentonite barrier or clays host rocks), but very few effort has been dedicated to study 'low pH' cements/clay interaction (Berner et al., 2013; Dauzères, 2016; Idiart et al., 2020; Jenni et al., 2021).

With respect to the simulation of laboratory and in situ experiments, it can generally be concluded that reactive transport modelling shows a great capability for reproducing the experiments, e.g., regarding mineralogical transformation pathways and net porosity evolution (Bildstein et al., 2019). Despite the differences in the practice of long-term simulation approaches addressing cement-clay interactions carried out in the last years, there are general similarities in terms of the predicted thickness of the altered zones in the clay and cement domain, the types of secondary solid products and changes in porosity. The simulations show a narrow zone (mainly in the order of cm to dm) of perturbed mineral and fluid chemistry located close to the interface, for timescales up to and beyond 100 000 years (Savage and Cloet, 2018; Bildstein et al., 2019). Regarding the predicted mineral transformations there are recurring results, such as decalcification of the cementitious material (portlandite dissolution, decrease of the Ca/Si ratio in C-S-H), precipitation of ettringite in the presence of sulphates, and/or carbonation and smectite dissolution, dedolomitisation, and formation of C-(A)-S-H solids, clay minerals (illite, saponite), zeolites and carbonates in the clay domain.

Critical parameters identified in the various studies comprise dissolution/precipitation kinetics and the description of evolving reactive surface areas that can play an important role in sequential minerals' appearance or disappearance, the localization of porosity reduction and increase, the kinetics and the laws controlling the porosity/permeability and porosity/diffusivity feedback, and the inclusion of certain secondary phases (e.g., zeolites) and their thermodynamic/kinetic parameters. For example, thermodynamic data for M-S-H and C-A-S-H phases only became available recently (Roosz et al., 2018; Lothenbach et al., 2019), and were thus not be included in previous modelling studies.

Idiart et al. (2020) performed a benchmark study on the interaction of a low pH concrete (Cebama reference mix concrete) with a Callovo-Oxfordian clay rock (simulation time frame 100 000 years), comparing different codes, using a number of simulation cases with increasing complexity. Overall, the results showed a good agreement between different codes, demonstrating the applicability of reactive transport modelling to support safety assessments. The impact of including the (slow) dissolution kinetics of the clay minerals was shown to be negligible in the studied system, probably due to the low-pH nature of the cementitious system studied.

In general, the capability of currently available reactive transport modelling codes (PHREEQC (Parkhurst and Appelo, 1999), TOUGHREACT (Burnol et al., 2006; Xu et al., 2011), CRUNCH (Steefel et al., 2015), HYTEC (van der Lee et al., 2003), ORCHESTRA (Meeussen, 2003), MIN3P-THCm (Bea et al., 2011)) exceeds the level of understanding of the various geochemical processes in the system. Calculations are mostly done in 1 dimension (1D), but some codes have the capability to tackle 2-D or 3-D with longer simulation times (i.e. coupled PHREEQC v.3 - COMSOL v.6 (iCP) (Nardi et al., 2014), OpenGeoSys-GEM (Kosakowski and Watanabe, 2014), OpenGeoSys-Phreeqc (Montoya et al., 2021), Retraso (Saaltink et al., 1998), QPAC (Quintessa, 2012), CORE2D (Samper et al., 2003), HPx (Simunek et al., 2013); PFLOTRAN (Hammond, 2022). Nowadays, the same codes also have the capability to tackle the effects of changing porosity due to mineral precipitation and dissolution reactions on diffusion coefficients by the Archie´s law and permeability, but the exact relationship between these processes remains as open issue (Kosakowski et al., 2009). Additionally, Marty et al. (2009) have also emphasized the need to consider the refinement of computational meshes to accurately reproduce potential alteration in small scale. Nowadays, only few existing transport codes allow for diffusion in porewater affected by the negative clay sheet surface charge: CRUNCH (Steefel, 2009), PHREEQC (Appelo and Wersin, 2007), PFLOTRAN (Trinchero et al. 2022), iCP (Idiart et al. 2019) and an in-house development of Clay Technology AB (Birgersson and Karnland, 2009). In the new concept of Jenni et al. (2017), their approach can be implemented in any multicomponent transport code considering the Nernst-Planck equation.

Predictive modelling has shown to be very sensitive to parameters with large uncertainties (i.e geometric factors for the calculation of diffusive transport, dissolution kinetics, surface areas, initial conditions such as contents of hydrated and un-hydrated cement phases, and certain thermodynamic data). For example, the accuracy of the M-S-H and C-A-S-H thermodynamic data and the incorporation on thermodynamic databases is currently under discussion. The selection of secondary minerals in predictive modelling also has a large impact upon the estimated amount of alteration (Oda et al., 2004). In general, the selection of secondary minerals is based on expert judgement and knowledge and process understanding gained from laboratory and in-situ experiments and natural analogues (Savage, 2011) which increase the reliability and predictive capabilities of the simulations.

Modelling of cementitious materials degradation in contact with crystalline rocks has started already in the late 1980's (Haworth et al., 1987; Savage and Rochelle, 1993) and is still developing (Watson et al., 2017), using different modelling tools. Results are widely available for example in the HPF-Experiment modelling report (Soler et al., 2006) and the LCS modelling report (Watson et al., 2017). The present coupled calculational tools are adequate, although improvements could still be made (Alexander et al., 2013).

In reactive transport modelling, the importance of choosing the right and relevant boundary conditions is shown in (Chen et al., 2015).

Table 1-1 provides an overview on a number of reactive transport modelling studies on cement/clay interactions, including studies addressing the simulation of laboratory and in situ experiments as well as long-term predictive studies.

Generally, the simulations in table 1-1 show that:

- The model for the evolution of an alkaline perturbation in a clay host rock is largely consistent with experimental observations;

- Akaline pore water conditions generated by minerals analogous to those in cements can be long-lived (in excess of tens of thousands of years), depending on the site flow conditions and the nature of the cementitious material (e.g., dense, high performance cements or porous grouts, groundwater movement);
- Reactions between alkaline waters and the host rock mostly yield an increase in mineral volumes (although some initial porosity increase is possible during the early KOH/NaOH phase) and thus fractures could be sealed by the precipitation of secondary phases; however there still not enough evidences about this phenomena (Harris et al. 1998)
- The effects of the site hydrology (and tectonic/erosional processes) upon fracture sealing need to be considered on a repository site-specific basis (Alexander and Neall, 2007).

Table 1-1: Summary of simulation studies addressing i) laboratory and in situ experiments on and ii) long term predictions of cement/clay interactions. (Deissmann & Ait Mouheb; 2021**)**

Cementitious material	Clay	Simulation time	Code	Thermodynamic database	Temperature	Dimensions	Geometry	Conditions	Chemical reactions	Porosity update	Reference
CEM I	Boom Clay	1.5 y	RETRASO	EQ3/6 LLNL	25 °C / 85 °C	0.002 m	1D cartesian	saturated	local equilibrium and kinetics	Yes	Read et al., 2001
CEM I (concrete)	Toarcian clay	15 y	HYTEC	EQ3/6 LLNL	15 °C	0.20 m	1D radial	saturated	local equilibrium and kinetics	Yes	De Windt et al., 2008
CEM I	Toarcian clay	15 y	QPAC	LLNL	15 °C	0.5 m	1D radial	saturated	local equilibrium and kinetics	Yes	Watson et al., 2013
CEM I	Toarcian clay	15 y	CrunchFlow	LLNL	15 °C	1.155 m	1D/2D radial	saturated	local equilibrium and kinetics	Yes	Soler, 2013
CEM I	Toarcian clay	18 y	HYTEC	CHESS CEMDATA07	25 °C	0.044 m	1D cartesian	saturated	local equilibrium and kinetics	Yes	Bartier et al., 2013
CEM I	Toarcian clay	15 y	MC-CEMENT	Various Sources	15 °C	0.11 m	1D cartesian	saturated	local equilibrium and kinetics	Yes	Yamaguchi et al., 2013
LAC / ESDRED low-pH concrete	Opalinus Clay	5 y	HYTEC	CHESS CEMDATA07	25 °C	1 m	1D cartesian	saturated	local equilibrium and kinetics	Yes	Dauzères et al., 2016
CEM I, low pH concrete	Opalinus Clay	5 y	FLOTRAN	EQ3/6 LLNL + CEMDATA07	25 °C	0.25 m	1D cartesian	saturated	local equilibrium and kinetics	Yes	Jenni et al., 2017
CEM I (concrete)	FEBEX bentonite	1 y	CrunchFlow	extended LLNL	25 °C and 120 °C	0.029 m	1D cartesian	saturated	local equilibrium and kinetics	No	Fernandez et al., 2009
CEM I (concrete)	Toarcian clay	100 000 y	HYTEC	EQ3/6 LLNL	25 °C	20 m	1D cartesian	saturated	local equilibrium	Yes	De Windt et al., 2004
CEM I (concrete)	Toarcian clay	100 000 y	HYTEC	EQ3/6 LLNL	70 °C	35 m x 15 m	2D cylindrical	saturated	local equilibrium	not specified	De Windt et al., 2004
CEM I	Callovo-Oxfordian clay	2000 y	TOUGHREACT	EQ3/6	non isothermal	100 m	1D radial	unsaturated (evolving)	local equilibrium	No	Burnol et al., 2006
CEM I / CEM V (concrete)	Callovo-Oxfordian clay	1 000 000 y	HYTEC	EQ3/6 LLNL	25 °C	17.5 m	1D radial	saturated	local equilibrium	Yes	Trotignon et al., 2006
CEM I / CEM V (concrete)	Callovo-Oxfordian clay	1 000 000 y	HYTEC	EQ3/6 LLNL	25 °C	17.5 m	1D radial	saturated	local equilibrium and kinetics	Yes	Trotignon et al., 2007

CEM I	Callovo-Oxfordian clay	10 y	TOUGHREACT	Thermoddem	25 °C (initial)	40 m	1D radial	unsaturated / saturated	kinetic assumption	Yes	Troitignon et al., 2011
CEM I (concrete)	Callovo-Oxfordian clay	1 000 000 y	TOUGHREACT	Thermochimie	25 °C	10 m	1D cartesian	saturated	local equilibrium and kinetics	Yes	Marty et al., 2009
CEM I	Callovo-Oxfordian clay	100 000 y	PhreeqC	Thermochimie	25 °C	43 m / 45.4 m	1D cartesian and 1D radial	saturated	local equilibrium and kinetics	no/yes	Marty et al., 2014
CEM I	Callovo-Oxfordian clay	10 000 y	Toughreact, PhreeqC, CRUNCH, HYTEC, ORCHESTRA, MIN3P-THCm	Thermoddem	25 °C	43 m	1D radial	saturated	local equilibrium and kinetics	No	Marty et al., 2015
Concrete	Bentonite and clayrock	1 000 000	CORE2D	EQ3/6	Non isothermal	25 m	1D radial	saturated	local equilibrium and kinetics	Yes	Mon et al., 2017
CEBAMA low-pH concrete	Callovo-Oxfordian clay	100 000 y	iCP, CORE2D OpenGeoSys-GEM, ORCHESTRA, MIN3P	Thermochimie/ Thermoddem	25 °C	43 m	1D cartesian	saturated	local equilibrium and kinetics	yes *	Idiart et al., 2020

* depending on calculation case synthesis

PSI, Empa

1.3.1.2 Reactive transport modelling of cement paste reactivity at nano and micro scale

Depending on the focus of the reactive transport modelling and dominance of advective or diffusive transport mechanism and heterogeneities, the mass transport can be simulated following a continuum or pore scale approach.

Pore-scale simulation equations comprise:

Fluid flow based on the NS equation:

$$\frac{\partial u}{\partial t} + (u \cdot \nabla)u = -\frac{1}{\rho}\nabla p + \nu \Delta u, \qquad \nabla \cdot u = 0, \tag{1-15}$$

where u is the velocity vector, p is the pressure, ρ is the fluid density, and ν is the kinetic viscosity of the fluid.

Solute transport and chemical reactions:

$$\frac{\partial c_i}{\partial t} + \nabla \cdot J_i = R_i, \tag{1-16}$$

where c_i is the molar concentration of species i in solution and R_i is the reaction term. Total flux J_i of the species i can represents as the sum of advective and diffusive contributions, with D_i being the dispersion/diffusion coefficient:

$$J_i = (uc_i - D_i \nabla c_i) \tag{1-17}$$

The surface reactions:

$$-D_i \nabla c_i = \xi_{im} r_m, \tag{1-18}$$

where r_m denotes the surface reaction rate and ξ_{im} is the stoichiometric coefficient of the component i in each surface reaction m.

At the macroscopic scale, the porous medium is typically conceptualized as a continuum with bulk parameters that characterize its physical and chemical properties. At this scale, mobile and immobile phases are assumed to co-exist at each point in space. The Darcy's equation is applied as a momentum equation, while reactive transport is described by the mass balance equation of each species (Steefel et Lichtner, 1994).

The total flux (*J*) in porous (fully saturated) media is equal to the sum of fluxes induced by the different gradients that may be present: chemical potential, hydraulic head, electrical potential and temperature. However, the three most dominant mass transport phenomena are:

- Diffusion (created by a gradient in chemical potential, hence concentration);
- Advection (created by a gradient in hydraulic pressure);
- Electrochemical gradient due to charged mineral surfaces.

Diffusion is the movement of species as a result of a difference in the chemical potential (concentration gradient). The relationship between the diffusive flux and the concentration gradient is described by Fick's first law:

$$\boldsymbol{J} = -\boldsymbol{D_e}\frac{\partial \boldsymbol{C}}{\partial \boldsymbol{x}} \tag{1-19}$$

Where J is the solute flux [mol/m²s], D_e is the effective diffusion coefficient of the solute in the porous medium [m²/s] and C is the liquid phase solute concentration [mol/l].

The microstructure of cement phases acts as the key factor for controlling the effective diffusivity. The effective diffusion coefficient is expected to be smaller than the bulk diffusion coefficient due to the interaction with the mineral surfaces and the geometrical complexity of the pore space. Furthermore, only a small fraction of the porosity (e.g. inter-connected solute and solvent accessible porosity) is available for the transport in porous media. The effective diffusion coefficient D_e of each species can be related to the diffusion coefficient in bulk electrolyte, D_0, via the accessible porosity of the medium η [-] and a geometric factor G [-]:

$$\boldsymbol{D_e = \eta G D_0} \qquad \text{1-15}$$

The geometric factor is a lump parameter that accounts for the complex morphology of the pore structure. This term is often expressed as a ratio of two contributions, namely the tortuosity τ [-] and constrictivity δ [-]:

$$\boldsymbol{G = \frac{\delta}{\tau^2}} \qquad \text{1-16}$$

Tortuosity accounts for the increased diffusive path of molecules traveling through a labyrinth of connected and dead-end pores. Constrictivity accounts for pore narrowing and widening pores, which hinders the transport of particles. Neither constrictivity nor tortuosity can be independently measured in a single experiment. Only the geometric factor lumping both factors can be estimated from a diffusion experiment, provided the porosity is known from independent measurements.

The molecular diffusion coefficient D_0 depends essentially on the nature of the chemical species, the temperature and the viscosity of the fluid. Typical values for molecular diffusion coefficients in water are in the range of 10^{-9} and 10^{-10} m²/s (Li and Gregory, 1974). For comparison, the molecular diffusion coefficient of water is 2.3×10^{-9} m²/s at normal temperature and pressure conditions (Holz et al., 2000).

Detailed theoretical developments in this part relative to the special effect of the charged surfaces of cement minerals- double layer effects, the molecular scale limitations of classical Poisson-Nernst-Planck equation, the nucleation processes at pore scale and the application to Machine learning are included in Appendix B**.**

1.3.1.3 3D Microstructure modelling

Recent developments of efficient reactive transport codes based on Lattice Boltzman Modelling (LBM) approach enables to perform direct reactive transport simulation of cement paste microstructure evolution at pore scale. In these models the initial microstructure is normally obtained based on numerical cement hydration models (Bentz, 1997; Van Breugel, 1995a; 1995b). These models provide grid-based distribution of solid phases in hydrated cement paste and water filled porosity. Depending on the model resolution and the system setup, either macroscopic, capillary or even gel pores can be resolved explicitly, and the solid phase can be assigned to have specific transport properties according to the system composition. The reactivity of the solid phase is described using either kinetic or equilibrium approach.

Recently, LB code Yantra https://bitbucket.org/yantralbm/yantra/src/master/ coupling with geochemical solver PhreeqC, was used to simulate microstructure evolution due to Ca-leaching in 3D (Figure 1-8). The model was able to describe the increase of porosity related to capillary pores due to dissolution of portlandite and the increase of gel porosity due to the decalcification of C-S-H. The overall evolution of porosity was compared between initial structures of cement paste generated by two cement hydration models, CEMHYD3D and HYMSOTRUC, for three water-to-cement ratios. It was observed that the rate

of leaching is directly proportional to the ability of microstructure to transport calcium ions and higher fraction of percolated capillary pores results in higher rate of leaching. The model qualitatively reproduces experimentally observed changes in cement paste porosity and pore size distribution due to leaching. The quantitative comparison of the model prediction with experimental data is challenging due to large uncertainties in the initial microstructure model and disparity of the experimental and modelling time scales (Patel et al., 2018).

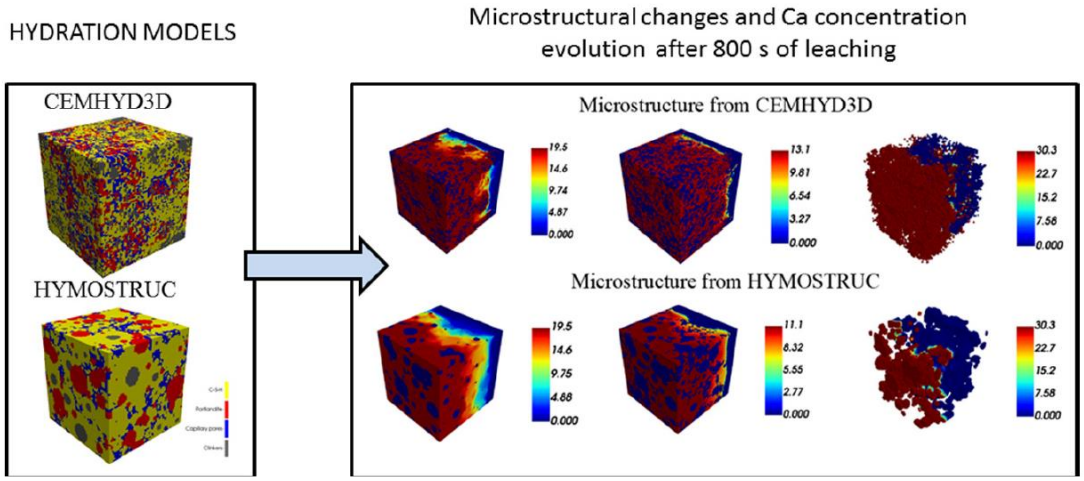

Figure 1-8: 3D microstructure evolution (porosity value) modelling obtained with Yantra-LB code coupled to geochemical solver PhreeqC. Microstructure modelling (Patel et al., 2018).

The model was further extended to include dissolution and precipitation phenomena caused by carbonation (Patel et al., 2021). The system setup represents a common scenario in which cementitious materials in underground constructions are exposed to CO_2-rich groundwater. Under such a condition, cement paste is exposed to combined effect of carbonation and calcium leaching. In the developed model, the capillary pores are explicitly resolved and the solid phases with intrinsic porosity (e.g. C-S-H) are treated as porous media. Governing equations are solved using a lattice Boltzmann method based reactive transport solver with chemical reaction under thermodynamic equilibrium. The two-dimensional scoping calculations on idealized microstructures revealed that carbon content and pH of boundary solution strongly affect degradation rates, location and thickness of precipitated calcite layer. Furthermore, reactive surface area plays a dominant role, while the tortuosity of porous media play rather a secondary role. The 3D simulations using simulated cement paste microstructure based on HYMOSTRUC model (Van Breugel, 1995b) show that degradation rate exhibits non-linear behaviour with square root of time. This implies that simple empirical relations for prediction of progression of reaction fronts are not applicable and use of numerical microscale reactive transport models is inevitable. The developed model qualitatively captures the progress of carbonation, leaching fronts and zonation as observed in experiments. Good quantitative agreement between modelling and experiments is obtained for initial stages of the front propagation (cf. Appendix B). At longer timescales, the modelling results and experimental observations diverge significantly. This discrepancy is likely due to the lack of consideration of kinetics of C-S-H dissolution and calcite precipitation (Patel et al., 2021).

1.3.2 RT modelling of cementitious materials evolution in unsaturated environments

Mines Paris Tech

1.3.2.1 General consideration and recent development in cement modelling exposed to unsaturated environment

Reactive transport modelling couples a thermodynamics based description of the reactivity of the cement hydrates to the advective-diffusive transport of aqueous and gaseous species within the pore space. By nature, reactive transport simulations are able to represent the evolution of a cementitious materials in a wide range of conditions. However, an accurate description of the numerous parameters (and their evolution) which are required for a simulation is challenging. Among others, porosity, gaseous and aqueous diffusion coefficients and permeability constitute the critical set of hydrodynamic parameters. While their characterization alone is challenging, they are likely to evolve as mineral reactions occur and modify the pore structure. For reactive transport modelling, many parameters are required to constrain the geochemical reactions. Solid properties (solubility, reaction rate, solid solutions, specific surface area, density, content...) and other geochemical properties (gas - liquid partioning, existence of aqueous complexes, activity coefficients) are critical to represent the equilibrium between the solid, the porewater and potential gas phase. We hereby review the general methodology devoted to the reactive transport modelling of cementitious materials in unsaturated conditions. This topic is particularly relevant in the context of nuclear waste disposal, but is also important in other contexts. For example, the integrity of wellbores in subsurface gas repository (Ajayi and Gupta, 2019), agressive gases may trigger cement degradation which may lead to fugitive gas migration (Cahill et al., 2019; Sandl et al., 2021).

Description of the physicochemical processes playing during the evolution of cementitious materials in unsaturated conditions

The volume of cementitious materials, V_{cem} is decomposed in the pore volume (porosity ω) and solid volume. The pore volume can be filled with water, i.e. in saturated conditions. In general, the fraction of the pore space occupied by liquid or gas is described by the liquid or gas saturation, S^l or S^g (with S^l+S^g = 1). The solid volume is constituted by the volume of the different cement hydrates (portlandite, C-S-H, monosulfoaluminate ...). These quantities are linked with the closure relation:

$$V_{water} + V_{gas} + V_{solid} = V_{cem} \qquad 1\text{-}22$$

$$\omega S^l + \omega S^g + \Sigma_{solid\ j}\phi_j = 1 \qquad 1\text{-}23$$

The behaviour of the fluid phases (phase α = liquid (l) or gas (g)) can be described by the multiphase flow equations, which describe the mass conservation in the two phases, with the Darcy-velocity and the definition of the capillary pressure:

$$\frac{\delta \omega S^l \rho^l}{\delta t} + \vec{\nabla}(\rho^l \vec{u}^l) = \rho^l R_v^l \quad 1\text{-}24$$

$$\frac{\delta \omega S^g \rho^g}{\delta t} + \vec{\nabla}(\rho^g \vec{u}^g) = \rho^g R_v^g \quad 1\text{-}25$$

$$\vec{u}^\alpha = -\frac{k_r^\alpha(S^\alpha)\kappa(\omega)}{\mu^\alpha}(\vec{\nabla}p^\alpha - \rho^\alpha \vec{g}) \quad 1\text{-}26$$

$$p^g - p^l = p_{cap}(S^l) \quad 1\text{-}27$$

In the previous equations, κ is the cementitious material permeability (m²), k_r^α is the relative permeability, μ^α is the fluid viscosity (kg m^{-1} s^{-1}), p_{cap} is the capillary pressure (Pa), sometimes referred to as suction, linking the difference between the pressure in the liquid p^l and gas p^g phase (Pa). ρ^α is the phase density (kg L$^{-}{}_{\alpha}{}^{1}$), $\vec{u}^\alpha$ is the Darcy-velocity in phase α (m s^{-1}), R_v^α is the volumetric source term of phase α (external or internal).

The relationship defining the capillary pressure, sometimes referred to as suction, $p_{cap}(S^l)$ is commonly referred to as the sorption isotherm, usually linking the liquid saturation S^l to the relative humidity RH, defined by (Morrow, 1970; Coussy et al., 2004; Seigneur et al., 2022):

$$RH = exp\left(-\frac{p_{cap}(S^l)}{\rho_l^n RT}\right) \quad 1\text{-}28$$

with ρ_l^n is the molar density of the liquid phase (mol L^{-1}_{α}), R is the thermodynamic gas constant (8.315 J mol^{-1} K^{-1}) and T is the temperature (K).

The transport of species can be described, in the total-concentration formalism (Lichtner, 1996; Seigneur et al., 2018), as

$$\frac{\partial(\omega S^l T_i^l + \omega S^g T_i^g)}{\partial t} = \vec{\nabla}\left(D^l(\omega, S^l)\vec{\nabla}T_i^l + D^g(\omega, S^g)\vec{\nabla}T_i^g - T_i^l\vec{u}^l - T_i^g\vec{u}^g\right) + R_i^s \quad 1\text{-}29$$

where $D^{\alpha}(\omega,S^{\alpha})$ represents the effective diffusion coefficient in phase α $(\mathrm{m}^2\ \mathrm{s}^{-1})$, T_i^{α} is the total concentration of species I (Ca, $CO^{=}_3$, Si, H_2O, ...) in phase α (mol L_{α}^{-1}). For example, for calcium:

$$T_{Ca}^l = [Ca^{++}] + [CaOH^+] + [CaCO_3(aq)] + [CaSO_4(aq)] + ... \quad 1\text{-}30$$

R_i is the production rate of species i by mineral dissolution/precipitation (mol L^{-1}_{cem} s^{-1})

$$R_i^s = -\omega S^l \sum_{solid\ j} \nu_{ij} R_j \quad 1\text{-}31$$

with ν_{ij} is the stoichiometric coefficient of species i within solid species j. R_j represents the kinetic rate of a solid species j (mol L_w^{-1} s^{-1}), usually described using a transition-state-theory based law (Lasaga, 1981); Seigneur et al., 2022):

$$R_j = k_j S_j \left(\frac{Q_j}{K_j} - 1\right) \quad 1\text{-}32$$

where k_j is a kinetic constant with (mol m^{-x} s^{-1}), S_j is the reactive surface area of the reaction (m^2 L^{-1}_{water}), Q_j is the ion activity product (-) and K_j is the thermodyanmic constant of mineral j (-). This reaction rate leads to a change in the volume fraction φ_j of mineral j linked to its molar volume V_j:

$$\frac{d\phi_j}{dt} = V_j R_j \quad 1\text{-}33$$

So that the change in porosity of the cementitious materials associated with mineral reactions can be written as

$$\frac{d\omega}{dt} = -\sum_{solid\ j} \frac{d\phi_j}{dt} \quad 1\text{-}34$$

Geochemical solvers are used to compute every species concentration to respect the mass balance and using mass action law.

Poyet (2016) has shown that sorption isotherms can be represented accurately on a wide range of temperature and for various cement formulations by the use of Van Genuchten expression:

$$p_{cap}(S^l) = p_e\left((S^l)^{-\frac{1}{m}} - 1\right)^{1-m} = -\rho_l^n RT \ln(RH) \quad 1\text{-}35$$

where p_e is the air-entry pressure (usually between 10 and 100 MPa) and m is an empirical parameter of Van Genuchten relations (usually between 0.3 and 0.6).

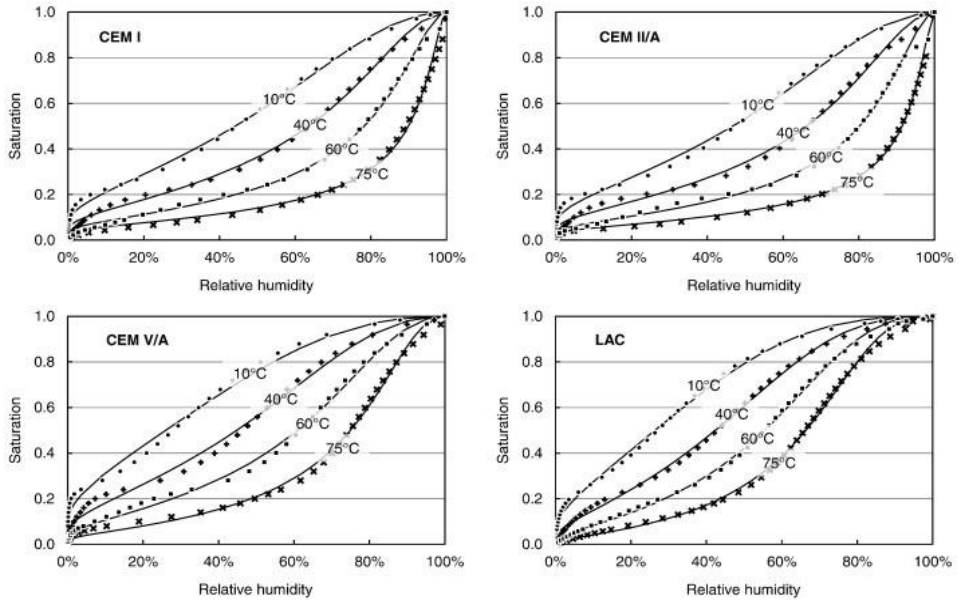

Figure 1-9: Representation of sorption isotherm data with Van Genuchten expression for different temperature and cement composition, from Poyet (2016)

When modelling cementitious materials in unsaturated conditions, sorption isotherms are critical, since they impose the equilibrium saturation of the system. They also control the vapor pressure and the drying / resaturation kinetics. At low RH, decrease in relative permeability of water inhibits advective fluxes of water to favor water transport through the gas phase Li et al. (2021).

The sorption isotherm is a macroscopic representation of the interaction between water and the solid surface down to the smallest pores (Sin and Corvisier, 2019). In the case of cementitious materials, the nanometric gel pores induce a very high capillary pressure. Thus, in the case of a chemical degradation, sorption isotherms may significantly change. For example, in the case of C-S-H decalcification, polymerisation reactions progressively turn the C-S-H structure into a silica gel, coarsening the pore structure. Auroy et al. (2015), Auroy et al. (2018), Soja et al. (2020) and Kangni-Foli et al. (2021) have shown that drying and carbonation have the potential to significantly coarsen the pore structure and modify the sorption isotherm, generally towards lower saturation. This implies that gas transport may be enhanced due to these effects (Georget et al., 2018).

As cement hydrates react, the pore structure evolves, altering the macroscopic properties of the cementitious material. Evolution of permeability κ and the effective diffusion coefficients in the liquid and gas phase are critical to take into account. Unfortunately, these evolutions are usually poorly constrained and empirical relations are used instead. In general, reactive transport models use Kozeny-Carman relations to describe the evolution of permeability, starting from an initial porosity ω_0 and initial permeability κ_0 (Xie et al., 2015; Poonoosamy et al., 2018; Seigneur et al., 2019)

$$\kappa = \kappa_0 \left(\frac{\omega}{\omega_0}\right)^3 \left(\frac{1-\omega_0}{1-\omega}\right)^2 \qquad 1\text{-}36$$

Evolution of diffusion is usually considered by the use of Millington-Quirk relation, which is an extension of Archie's law for unsaturated porous media:

$$D^\alpha(\omega, S^\alpha) = D_0^\alpha\,(\omega)^{a_\alpha}\,(S^\alpha)^{b_\alpha} \qquad 1\text{-}37$$

This expression suggests that diffusion both in the gas and liquid phase is dependent on the phase saturation, as observed experimentally (Dridi and Lacour, 2014; Georget et al., 2018).

In the case of reactive gases, such as CO_2 or H_2S (Omosebi et al., 2017), or when water transport occurs in the gas phase, both the sorption isotherm and gas diffusion parameters are critical to determine the degradation extent.

Reaction rate (Equation 1-32) is driven by the saturation of the porewater with respect to different minerals, and is controled by the reactive surface area, S_j. This parameter describes the fluid-solid surface on which the solid reaction may occur. Surface areas are notoriously variable and hard to constrain for cementitious materials. In the case of one type of degradation, these values can evolve in numerous ways. One example is the fact that portlandite grains can sometimes be passivated by the precipitation of calcite coating (Regnault et al., 2009; Ruiz-Agudo et al., 2013; Galan et al., 2015; Varzina et al., 2020), leading to residual non-reactive portlandite. Predicting such behaviour is not straightforward. In the context of carbonation, passivation will be favored when calcite precipitation kinetics exceed portlandite dissolution. Thus, this is more likely to occur with larger portlandite grains and higher fluxes of carbonates within the material, typically through CO_2 gaseous diffusion rather than under water carbonation. It may be necessary to be able to quantify the size distribution of the portlandite grains (Hernandez et al., 2018). This passivation is also observed for C-S-H gels. Scawt Hill (Northern Ireland) is such a location in which C-S-H gels have been formed about 58 million years ago. This analogue also showed that precipitated calcite as a result of carbonation may surround C-S-H gels by which these poorly-crystalline gels are protected from further carbonation (Knight, 2003).

During decalcification, C-S-H polymerization occurs, changing the internal structure of the cementitious materials, generally resulting in larger specific surface areas. Garcia-Lodeiro et al. (2021) indicate a change from 20 to 140 $m^2.g^{-1}$ after degradation. Also, variation in the kinetic rate coefficients are reported depending on the Ca/Si ratio (Trapote-Barreira et al., 2014) and various values can be found (Baur et al., 2004; De Windt et al., 2008; Marty et al., 2009; 2015; Tran et al., 2018; Zajac et al., 2020) for these parameters, as reported in Seigneur et al. (2022).

Chemical reactions within the porespace can induce mechanical stresses which may damage the cement material. For example, in saturated conditions, the delayed ettringite formation may induce swelling and cracks (Brunetaud et al., 2008; Sellier and Multon, 2018; Gu et al., 2019) if the C_3A content in cement is too high. In unsaturated conditions, however, presence of a gas phase may partly accomodate expanding reactions. However, significant cracking may be induced by shrinkage. Usually, two types of shrinkage are described: drying (Bisschop and Van Mier, 2002; Shiotani et al., 2003; Soja et al., 2020) and carbonation shrinkage (Ye et al., 2017). Borges et al. (2010), Han et al. (2013), Wan et al. (2014) and Kangni-Foli et al. (2021) have shown that the carbonation induced decalcification of C-S-H may lead to shrinkage (Swenson and Sereda, 1968; Chen et al., 2006), and formation of cracks in the cement paste. Drying shrinkage is associated with the dependence of the C-S-H structure on the water content (Li et al., 2021).

During carbonation, decalcification occurs and modify the internal structure of the C-S-H. This leads to a general volume decrease of the material, particularly at high degree of decalcification (Matsushita et al., 2004), generating internal stresses. Auroy et al. (2018) have shown that cracking in cement pastes appears both in the case of natural and accelerated carbonation. It was further shown by Kangni-Foli et al. (2021) that atmospheric carbonation of model cement pastes in controled conditions may induce severe crackings, particularly for low-pH cement formulation, specifically in the most decalcified regions.

Carbonation reactions are complex in the sense that, depending on the experimental conditions or cement formulations, they can lead to seemingly opposite effects (Dutzer et al., 2019). Carbonation has been able to seal fractures ((Harris et al. 1998); Wigand et al., 2009; Liteanu and Spiers, 2011; Jacquemet et al., 2012) and to induce cracking (Han et al., 2013; Ruiz-Agudo et al., 2013; Auroy et al., 2015; Ghantous et al., 2017; Dutzer et al., 2019; Kangni-Foli, 2019). Carbonation has been extensively studied, both experimentally (Ho and Lewis, 1987; Papadakis et al., 1991; Chang and Chen, 2006; Ati¸s, 2003; Leemann and Moro, 2017; Drouet et al., 2019) and numerically (Shen et al., 2013; Kari et al., 2014; Huang et al., 2018).

However, few attempts have been made on modelling the fully coupled system in unsaturated systems. Most studies use a variety of simplifications, the most common one being neglecting the appearance of cracks associated with geochemical reactions. Few studies also include a multiphase system with an accurate description of water (release, consumption, evaporation).

In recent years, several reactive transport modelling studies were based on a relatively complete description of all the processes mentioned above (Addassi and Johannesson, 2020; Xie et al., 2021; Seigneur et al., 2022).

In an attempt to model the experiments from Kangni-Foli et al. (2021), Seigneur et al. (2022) used a damage factor ξ in HYTEC (Van Der Lee et al., 2002, 2003; De Windt and Devillers, 2010) to model the evolution of gas transport as crack appear in their reactive transport approach:

$$D^g(\omega, S^g) = \xi D_0^g \left(\frac{\omega}{\omega_0}\right)^2 \left(\frac{S^g}{S_0^g}\right)^2 \quad \text{1-38}$$

This damage factor was constrained based on Dutzer et al. (2019), the damage factor would likely be in the range of 2.5 - 4. This damage factor was changed to 3 when amorphous silica started to precipitate. With this damage factor, the authors have managed to reproduce carbonation depths over 1 year. The model included a complete mass balance of water in the aqueous complex, gaseous and solid components. Parameters of this study were derived from dedicated experimental characterizations, and one single model successfully reproduced carbonation extents for the two different model materials (a C_3S hydrated paste and a C-S-H sample). The main simplification in their study is that the sorption isotherm was not modified during carbonation.

While Seigneur et al. (2022) focused on model materials, Addassi and Johannesson (2020) have presented a detailed analysis for a more complex cement paste in three different exposure conditions. They conclude that one single model fails to adequately represent all these different exposure conditions (Xie et al., 2021).

Huang et al. (2018) have suggested to use a look-up table, based on reactive transport simulations, to accelerate simulation of cement degradation. However, based on the wide variety of exposure and conditions, such methods may be limiting.

1.3.2.2 Modelling of cement materials degradation in unsaturated environment at the pore scale

PSI, Empa

Consideration of partial saturation in reactive transport simulations at pore scale brings yet another level of complexity compared to the corresponding 3D modelling at saturation conditions. Accordingly, the pore scale simulations of cement paste at partial saturation are essentially limited to the estimation of effective diffusivities of solutes, moisture distribution and effective permeability as function of saturation degree. The underlying models for the microstructure are either based on numerical simulation of cement paste hydration or obtained experimentally through x-ray CT and 1H NMR (Genty and Pot, 2014; Zalzale et al., 2013; Zhang et al., 2014; 2012). Most of the studies based on numerical microstructure are dealing with the early age cement paste. Despite the fact that the transformation of microstructure due to the mineral dissolution and re-precipitation are not considered in such studies, the simulations provide a basis for the upscaling of effective transport parameters for multiscale modelling including the mechanical damage of cement paste (Liu et al., 2021).

(Zhang et al., 2012) have systematically applied the Lattice Boltzmann method to model the diffusion process of the ionic species through the partially saturated cement paste. The simulated relative ionic diffusivity as a function of the degree of water saturation were found to be in good agreement with the experimental data available in the literature. Combination of X-ray CT and LB simulation was used to estimate the water distribution in cement paste at different degrees of saturation (Genty and Pot, 2014; Zhang, 2017; Zhang et al., 2014). A general trend between the decrease of the saturation and increase in the gas permeability could be well reproduced. The simulations suggest that the microstructure and,

in particular the pore network connectivity are the major factors controlling the moisture distribution and permeability. Each microstructure can be characterised by a critical water saturation at which the liquid-filled or gas-filled capillary porosity becomes disconnected leading to abrupt change in gas or liquid permeability. This critical water saturation is strongly related to microstructure model. Despite the fact that the numerical microstructure modelling or experimental estimation is subject of large uncertainties, the simulated permeabilities show good agreement with experimental data.

(Zalzale et al., 2013) combined ^{1}H nuclear magnetic resonance relaxation analysis used 3D lattice Boltzmann model for C-S-H paste to estimate the water and gas permeabilities in capillary pores as function of water saturation. The numerical model comprises explicit capillary pores and treated weakly-permeable nano-porous C-S-H as effective saturated porous media, whereas the capilary pore saturation was obtained from Kelvin-Laplace. It was concluded that the degree of capillary water saturation is the parameter controlling the variation of experimentally measured permeability of C-S-H paste. It could be further showed that consideration of partially permeable C-S-H matrix is essential for the agreement between modelled and measured permeabilities. Recently, Cl diffusivity in limestone blended cement paste was studied considering its 3D microstructure produced by voxel-based CEMHYD3D model at different saturation degree (Liu et al., 2022). The results indicate complex dependence of ionic diffusivity on the saturation degree of capillary pores their percolation and the underlying microstructure.

1.4 Synthesis and identified gaps

The still existing constructions built by the Romans two millenia ago provide the evidence that the chemo-mechanical ageing of concrete can be a very slow process if the concrete has been well manufactured in specific conditions. After three decades of research, the main reactive processes controlling the concrete chemical evolution in disposal environment are globally well understood: 1/ in saturated conditions: leaching, carbonation, magnesium and sulphate attack, sometimes chloride attack depending on the concentration in solution and type of cement (ingress of sulphates and chlorides does not necessarily lead to a detoriation of cementitious materials if a proper choice has been made of the materials that have been used to manufacture these materials); 2/ in unsaturated conditions: carbonation conducted to different carbonate phases depending on the cement formulation.

Their impact on the microstructure evolution and transport properties remains challenging. The rate of solute transport can be strongly delayed by clogging of pores with salt crystals (especially calcite and ettringite precipitation). The intensity of pore clogging is strongly influenced by the type and amount of salt and by the pore structure of the substrate. A better understanding of the salt-substrate interaction and of the connection between pore-clogging and damage (cracking), must be developed to predict these effects quantitatively. Long-term chemical degradation and eventually the mechanical stability of cementitious materials depend on the chemical gradients and the rate of ion diffusive transport at pore scale. Experimental results suggest that the effective diffusivity of the ions depends on the ion charge and the surface charge of the cement phases at pore scale, which can be attributed to the electrical double layer near the charged C-S-H surfaces. Several continuum scale reactive transport models have been developed to simulate carbonation and leaching processes in cementitious materials. The predictive capability of such models depend on the accuracy of input parameters such as reaction rate, diffusivity and permeability and their changes as the pore-structure evolves due to chemical interactions. If these essential parameters could be obtained from a pore-scale simulation able to resolve heterogeneities in cement paste microstructures, how to extract these essential parameters (relation between transport properties and changes in porosity and microstructure) is still an open issue.

Reactive transport models are used to understand the durability of cementitious materials since the early 2000s. However, proper coupled description of reactive transport in unsaturated systems, while accounting for mutliphase flow and transport, evaporation and porosity changes is only recent. There are a few limitations to using reactive transport models within cementitious materials under unsaturated conditions:

- The evolution of sorption isotherms is usually neglected. Also, limited data to constrain the evolution of these isotherms is available.
- Empirical laws to model diffusion in the liquid and gas phases have limited predictive capacities.
- There remain uncertainties in database parameters for the C-S-H phases (densities, surfaces ...). C-S-H are usually modelled based on a discrete set of Ca/Si ratios. A solid solution framework may be more suited for their description (some solid solution already available), provided that accurate data regarding their density, water intake are provided.

Reactive transport modelling usually describes one single value for porosity and water content, while the structure of the cement system expands over a large spatial scale. Hence, the validity of this approach may not be guaranteed by experimental data (Lothenbach et al., 2008; Blanc et al., 2010; Blanc, 2017; Blanc et al., 2012). A multi-scale model with lower scale REVs may be more appropriate.

1.5 References for part 1

Abbas, Safeer, "Structural and Durability Performance of Precast Segmental Tunnel Linings" (2014). Electronic Thesis and Dissertation Repository. 1865.

Addassi, M. and Johannesson, B. (2020). Reactive mass transport in concrete including for gaseous constituents using a two-phase moisture transport approach. Construction and Building Materials, 232:117148.

Adler, M. (2001). Interaction of claystone and hyperalkaline solutions at 30°C: A combined experimental and modelling study. Ph.D. thesis, University of Bern, Bern, Switzerland.

Adler, M., Mäder, U.K., Waber, H.N. (1999). High-pH alteration of argillaceous rocks: an experimental study. Schweizerische Mineralogische und Petrographische Mitteilungen 79, 445-454.

Agnel M., A. Vinsot, J-C. Robinet (2021). Experimental protocol for the synthesis of poral water in the Callovo-Oxfordian claystone at 25 °C. Technical Document. CGRPASTR210001.

Albert, B. Altération de matrices cimentaires par des eaux de pluie et des eaux sulfatées: approche expérimentale et thermodynamique, Thèse de doctorat, Ecole Nationale Supérieure des Mines de Saint Etienne et de l'Institut National Polytechnique de Grenoble, 2002, p. 294.

Al-Kadhimi, T. K. H., Banfill, P. F. G., Millard, S. G., Bungey, J. H. (1996) An Accelerated Carbonation Procedure for Studies on Concrete, Advances in Cement Research, 8 (30) 47–59.

Ahmad S., R.A. Assaggaf, M. Maslehuddin, O.S.B. Al-Amoudi, S.K. Adekunle, S.I. Ali, Effects of carbonation pressure and duration on strength evolution of concrete subjected to accelerated carbonation curing, Constr. Build. Mater. 136 (2017) 565–573. https://doi.org/10.1016/j.conbuildmat.2017.01.069.

Ajayi, T. and Gupta, I. (2019). A review of reactive transport modeling in wellbore integrity problems. Journal of Petroleum Science and Engineering, 175:785–803.

Alexander, M., Bertron, A., De Belie, N., 2013. Performance of cement based materials in aggressive aqueous environments. State of the Art Report RILEM TC 211, Springer, 471 p.

Alexander, R. (2012). The impact of a (hyper)alkaline plume on (fractured) crystalline rock. In: NEA, 2012. Cementitious materials in safety cases for geological repositories for radioactive waste: Role, evolution and interactions, NEA/RWM/R(2012)3/REV, 85-88.

Alexander, W.R. and Neall, F.B. (2007) Assessment of potential perturbations to Posiva's SF repository at Olkiluoto caused by construction and operation of the ONKALO facility. Posiva Working Report 2007-35, Posiva, Olkiluoto, Finland.

Alonso, M.C., García Calvo, J.L., Cuevas, J., Turrero, M.J., Fernández, R., Torres, E., Ruiz, A.I. (2017). Interaction processes at the concrete-bentonite interface after 13 years of FEBEX-Plug operation. Part I: Concrete alteration. Physics and Chemistry of the Earth, Parts A/B/C 99, 38-48.

Alonso, M.C., Garcia-Calvo,J.L. 2016: Concrete groundwater interactions in EBS. In: WP1 Experimental studies – State of the art literature review (M09 – Feb 2016], Deliverable D 1.03. CEBAMA (Conract Number: 662147)

Alt-Epping, P., Gimmi, T., Wersin, P. and Jenni, A. (2018) Incorporating electrical double layers into reactive-transport simulations of processes in clays by using the Nernst-Planck equation: A benchmark revisited. Applied Geochemistry 89, 1-10.

Appelo, C.A.J.; Wersin, P. (2007) Multicomponent diffusion modeling in clay systems with application to the diffusion of tritium, iodide, and sodium in Opalinus Clay. Environ. Sci. Technol., 41, 5002–5007

Appelo, C.A.J. (2017) Solute transport solved with the Nernst-Planck equation for concrete pores with 'free' water and a double layer. Cement and Concrete Research, 101, 102-113

Ashraf, Warda. (2016) "Carbonation of Cement-Based Materials: Challenges and Opportunities." Construction and Building Materials 120: 558–70.

Ati¸s, C. D. (2003). Accelerated carbonation and testing of concrete made with fly ash. Construction and Building Materials, 17(3):147–152.

Auroy M., Poyet, S., Le Bescop, P., Torrenti, J.M., Charpentier, T., Moskura, M., Bourbon, X. (2015) Impact of carbonation on unsaturated water transport properties of cement-based materials, Cem. Concr. Res. 74, 44–58. https://doi.org/10.1016/j.cemconres.2015.04.002.

Auroy M., S. Poyet, P. Le Bescop, J.-M. Torrenti, T. Charpentier, M. Moskura, X. Bourbon, Comparison between natural and accelerated carbonation (3% CO2): impact on mineralogy, microstructure, water retention and cracking, Cem. Concr. Res. 109 (2018) 64–80. https://doi.org/10.1016/j.cemconres.2018.04.012.

Badouix, F. (2000). Modelisation du comportement à long terme des bétons : prise en compte de la carbonatation. These de doctorat, ENS Cachan

Baker, A.J., Bateman, K., Hyslop, E.K., Ilett, D.J., Linklater, C.M., Milodowski, A.E., Noy, D.J., Rochelle, C.A., Tweed, C.J. (2002). Research on the alkaline disturbed zone resulting from cement-water-rock reactions around a cementitious repository. UK Nirex Limited Report N/054, UK Nirex Ltd., Harwell, Didcot, United Kingdom.

Balmer, S., Kaufhold, S., Dohrmann, R. (2017). Cement-bentonite-iron interactions on small scale tests for testing performance of bentonites as a barrier in high-level radioactive waste repository concepts. Applied Clay Science 135, 427-436.

Bartier, D., Techer, I., Dauzères, A, Boulvais, P., Blanc-Valleron, M.-B., Cabrera, J. (2013). In situ investigations and reactive transport modelling of cement paste/argillite interactions in a saturated context and outside an excavated disturbed zone. Applied Geochemistry 31, 94-108.

Bary, B., & Sellier, A. (2004). Coupled moisture—carbon dioxide–calcium transfer model for carbonation of concrete. Cement and Concrete Research, 34(10), 1859-1872. https://doi.org/10.1016/j.cemconres.2004.01.025

Bateman, K., Coombs, P., Noy, D.J., Pearce, J.M., Wetton, P., Haworth, A., Linklater, C. (1999). Experimental simulation of the alkaline disturbed zone around a cementitious radioactive waste repository: numerical modelling and column experiments. Geological Society of London, Special Publication 157, 183-194.

Baur, I., Keller, P., Mavrocordatos, D., Wehrli, B., and Johnson, C. A. (2004). Dissolutionprecipitation behaviour of ettringite, , and calcium silicate hydrate. Cement and concrete research, 34(2):341–348.

Bea, S.A., Mayer, K.U., MacQuarrie, K.T.B.: Modelling reactive transport in sedimentary rock environments - Phase II MIN3P-THCm code enhancements and illustrative simulations for a glaciation scenario. Technical report: NWMO TR-2011-13 (2011)

Bentz, D.P. (1997) Three-dimensional computer simulation of Portland cement hydration and microstructure development. Journal of the American Ceramic Society 80, 3-21.

Bernard, E., Lothenbach, B., Chlique, C., Wyrzykowski, M., Dauzères, A., Pochard, I., & Cau-Dit-Coumes, C. (2019). Characterization of magnesium silicate hydrate (M-S-H), Cement and Concrete Research, 116, 309-330.

Berner, U. (1992) Evolution of pore water chemistry during degradation of cement in a radioactive waste repository environment, Waste management, 12, 201-219.

Berner, U., Kulik, D.A., Kosakowski, G. (2013). Geochemical impact of a low-pH cement liner on the near field of a repository for spent fuel and high-level radioactive waste. Physics and Chemistry of the Earth Parts ABC 64, 46-56.

Bes. T. Etude du comportement des bétons bas-PH sous sollicitations chimiques. Matériaux. Université Paul Sabatier - Toulouse III, 2019.

Biczók, I.: Betonkorrosion – Betonschutz. Bauverlag GmbH, Wiesbaden - Berlin, Wiesbaden, 659 p., 1968.

Bildstein, O., Claret, F. (2015) Chapter 5 - Stability of Clay Barriers Under Chemical Perturbations, Developments in Clay Science, Elsevier, 6, 155-188,

Bildstein, O., Claret, F., Frugier, P. (2019). RTM for waste repositories. Reviews in Mineralogy and Geochemistry 85, 419-457, 2019.

Birgersson, M., Karnland, O. (2009) Ion equilibrium between montmorillonite interlayer space and an external solution—Consequences for diffusional transport, Geochimica et Cosmochimica Acta 73(7):1908-1923

Bisschop, J. and Van Mier, J. (2002). Drying shrinkage microcracking in cement-based materials. Heron, 47 (3), 2002.

Blanc, P. (2017). Thermoddem: Update for the 2017 version. In Report BRGM/RP-66811-FR.

Blanc, P., Vieillard, P., Gailhanou, H., Gaboreau, S., Marty, N., Claret, F., Madé, B. Giffaut, E. (2015) ThermoChimie database developments in the framework of cement/clay interactions, Applied Geochemistry, 55, 95-107

Blanc, P., Bourbon, X., Lassin, A., and Gaucher, E. C. (2010). Chemical model for cement-based materials: Temperature dependence of thermodynamic functions for nanocrystalline and crystalline c–s–h phases. Cement and Concrete Research, 40(6):851–866.

Blanc, P., Lassin, A., Piantone, P., Azaroual, M., Jacquemet, N., Fabbri, A., and Gaucher, E. C. (2012). Thermoddem: A geochemical database focused on low temperature water/rock interactions and waste materials. Applied geochemistry, 27(10):2107–2116.

Borges P.H.R., J.O. Costa, N.B. Milestone, C.J. Lynsdale, R.E. Streatfield, Carbonation of CH and C-S-H in composite cement pastes containing high amounts of BFS, Cem. Concr. Res. 40 (2010) 284–292. https://doi.org/10.1016/j.cemconres.2009.10.020.

Brunetaud, X., Divet, L., and Damidot, D. (2008). Impact of unrestrained delayed ettringite formation-induced expansion on concrete mechanical properties. Cement and concrete research, 38(11):1343–1348.

Bukovska, Z. at al.: 2020, Data acquisition from the deep horizons of the Rozna Mine. RAWRA Technical Report (No. 464/2020/ENG). Czech Radioactive Waste Repository Authority, Prague, 48 pp.

Burnol, A., Blanc, P., Xu, T., Spycher, N., Gaucher, E.C., 2006. Uncertainty in the reactive transport model response to an alkaline perturbation in a clay formation. TOUGH Symposium 2006, Berkeley, California.

Carde, C., François, R. (1999) Modelling the loss of strength and porosity increase due to the leaching of cement pastes. Cement and Concrete Composites, Elsevier, 21 (3), pp.181-188.

Cahill, A. G., Beckie, R., Ladd, B., Sandl, E., Goetz, M., Chao, J., Soares, J., Manning, C., Chopra, C., Finke, N., et al. (2019). Advancing knowledge of gas migration and fugitive gas from energy wells in northeast british columbia, canada. Greenhouse Gases: Science and Technology, 9(2):134–151.

CEBAMA (2019) CEBAMA: Cement-based materials, properties, evolution, barrier functions - IGD-TP | Safe Solutions for Radioactive Waste (igdtp.eu).

Chang, C.-F. and Chen, J.-W. (2006). The experimental investigation of concrete carbonation depth. Cement and Concrete Research, 36(9):1760–1767.

Chaparro, M.C., Saaltink, M.W., Soler, J.M. (2017). Reactive transport modelling of cement-groundwater-rock interaction at the Grimsel Test Site. Physics and Chemistry of the Earth 99, 64-76.

Chen J.J., J.J. Thomas, H.M. Jennings, Decalcification shrinkage of cement paste, Cem. Concr. Res. 36 (2006) 801–809. https://doi.org/10.1016/j.cemconres.2005.11.003.

Chen, X., Thornton, S.F., Small, J., (2015). Influence of hyper-alkaline pH leachate on mineral and porosity evolution in the chemically disturbed zone developed in the near-field host rock for a nuclear waste repository. Transport in Porous Media 107, 489-505.

Cheng, J. and Sprik, M. (2014) The electric double layer at a rutile TiO2 water interface modelled using density functional theory based molecular dynamics simulation. Journal of Physics-Condensed Matter 26.

Churakov, S.V. and Labbez, C. (2017) Thermodynamics and Molecular Mechanism of Al Incorporation in Calcium Silicate Hydrates. Journal of Physical Chemistry C 121, 4412–4419.

Churakov, S.V. and Prasianakis, N.I. (2018) Review of the current status and challenges for a holistic process-based description of mass transport and mineral reactivity in porous media. American Journal of Science 318, 921–948.

Churakov, S.V., Labbez, C., Pegado, L. and Sulpizi, M. (2014) Intrinsic acidity of surface sites in calcium-silicate-hydrates and its implication to their electrokinetic properties. Journal of Physical Chemistry C 118, 11752−11762.

Claret, F., Marty, N., Tournassat, C. (2018). Modeling the long-term stability of multibarrier systems for nuclear waste disposal in geological clay formations. In: Xiao, Y., Whitaker, F., Xu, T., Steefel, C. (eds.) Reactive Transport Modeling: Applications in Subsurface Energy and Environmental Problems, Wiley, 395-436.

Coussy, O., Dangla, P., Lassabat`ere, T., and Baroghel-Bouny, V. (2004). The equivalent pore pressure and the swelling and shrinkage of cement-based materials. Materials and structures, 37(1):15–20.

Dauzères A., P. Le Bescop, C. Cau-Dit-Coumes, F. Brunet, X. Bourbon, et al.. On the physico-chemical evolution of low-pH and CEM I cement pastes interacting with Callovo-Oxfordian pore water under its in situ CO2 partial pressure. Cement and Concrete Research, Elsevier, 2014, 58, pp.76-88.

Dauzères, A. (2016). Geochemical and physical evolution of cementitious materials in an aggressive environment. In: Vehmas, T., Holt, E. (eds.) CEBAMA Deliverable D 1.03 - WP1 Experimental studies – State of the art literature review, 136-174 (www.cebama.eu).

Dauzères, A., Achiedo, G., Nied, D., Bernard, E., Alahrache, S., Lothenbach, B. (2016). Magnesium perturbation in low-pH concretes placed in clayey environment - solid characterizations and modelling. Cement and Concrete Research 79, 137-150.

Dauzères, A., Le Bescop, P., Cau-Dit-Coumes, C., Brunet, F., Bourbon, X., Timonen, J., Voutilainen, M., Chomat, L., Sardini, P. (2014). On the physico-chemical evolution of low-pH and CEM I cement pastes interacting with Callovo-Oxfordian pore water under its in situ CO2 partial pressure. Cement and Concrete Research 58, 76-88.

Dauzères, A., Le Bescop, P., Sardini, P., Cau Dit Coumes, C. (2010). Physico-chemical investigation of clayey/cement-based materials interaction in the context of geological waste disposal: Experimental approach and results. Cement and Concrete Research 40, 1327-1340.

De Craen, M., I. Wemaere, S. Labat and M. Van Geet (Nov. 2006). Geochemical analyses of Boom Clay pore water and underlying aquifers in the Essen-1 borehole, External Report ER-19. Mol, Belgium: SCK·CEN.

Dehoux, A., Bouchelaghem, F., Berthaud, Y. (2015) Micromechanical and microstructural investigation of steel corrosion layers of variable age developed under impressed current method, atmospheric or saline conditions. Corrosion Science, Elsevier, 97, pp.49-61.

De Windt, L., Spycher, N.F.(2019) Reactive Transport Modeling: A Key Performance Assessment Tool for the Geologic Disposal of Nuclear Waste, Elements, 15 (2) 99-102.

De Windt L, Pellegrini D, van der Lee J. (2004) Coupled modeling of cement/claystone interactions and radionuclide migration. Journal of Contaminant Hydrology. 68, 3–4, 165-182.

De Windt, F. Marsal, E. Tinseau, D. Pellegrini. 2008. Reactive transport modeling of geochemical interactions at a concrete/argillite interface, Tournemire site (France) Phys. Chem. Earth, 33 (2008), pp. S295-S305

De Windt, L. and Devillers, P. (2010). Modeling the degradation of portland cement pastes by biogenic organic acids. Cement and Concrete Research, 40(8):1165–1174.

Deissmann, G., Ait Mouheb, N. (2021). Interface "cement/concrete – clay". Chapter 4 in: Deissmann, G., Ait Mouheb, N., Martin, C., Turrero, M. J., Torres, E., Kursten, B., Weetjens, E., Jacques, D., Cuevas, J., Samper, J., Montenegro, H., Leivo, M., Somervuori, M., Carpen, L. (2021). Experiments and numerical model studies on interfaces. Final version as of 12.05.2021 of deliverable D2.5 of the HORIZON 2020 project EURAD. EC Grant agreement no: 847593.

Dridi, W. and Lacour, J.-L. (2014). Experimental investigation of solute transport in unsaturated cement pastes. Cement and concrete research, 63:46–53.

Drouet, E., Poyet, S., Le Bescop, P., Torrenti, J.-M., and Bourbon, X. (2019). Carbonation of hardened cement pastes: Influence of temperature. Cement and Concrete Research, 115:445–459.

Dutzer, V., Dridi, W., Poyet, S., Le Bescop, P., and Bourbon, X. (2019). The link between gas diffusion and carbonation in hardened cement pastes. Cement and Concrete Research, 123:105795.

Eglinton, M. (1998). Resistance of concrete to destructive agencies. In: Hewlett, P.C. (Ed.): Lea's chemistry of cement and concrete. Arnold, London, 299-342.

Fernández, R., Mäder, U., Sánchez, L., Vigil de la Villa Mencía, R., Cuevas, J. (2007) Alkaline diffusion in compacted bentonite: Experiments and modeling. Water-Rock Interaction - Proceedings of the 12th International Symposium on Water-Rock Interaction, WRI-12. 1. 305-308. 10.1201/NOE0415451369.ch63.

Fernández, R., Mäder, U.K., Rodríguez, M., Vigil De La Villa, R., Cuevas J. (2009) Alteration of compacted bentonite by diffusion of highly alkaline solutions, European Journal of Mineralogy 21 (4) 725–735.

Fernández, R., Ruiz A.I., Cuevas, J. (2016). Formation of C-A-S-H phases from the interaction between concrete or cement and bentonite. Clay Minerals 51, 223-235.

Fernández, R., Torres, E., Ruiz, A.I., Cuevas, J., Alonso, M.C., García Calvo, J.L., Rodríguez, E., Turrero, M.J. (2017). Interaction processes at the concrete-bentonite interface after 13 years of FEBEX-Plug operation. Part II: Bentonite contact. Physics and Chemistry of the Earth, Parts A/B/C 99, 49-63.

Gaboreau S., Lerouge C., Dewonck S., Linard Y., Bourbon X., Fialips C.I., Mazurier A., Pret D., Borschneck D., Montouillout V., Gaucher E.C. & Claret F. (2012) In situ interaction of cement paste and shotcrete with claystones in a deep disposal context. Am. J. Sci., 312, 314-356.

Gaboreau, S., Prêt, D., Tinseau, E., Claret, F., Pellegrini, D., Stammose, D. 2011 : 15 years of in situ cement-argillite interaction from Tournemire URL: Characterisation oft he multi-scale spatial heterogeneities of pore space evolution. Applied Geochemistry, Vol. 25, pp 2159 - 2171

Galan, I., Glasser, F. P., Baza, D., and Andrade, C. (2015). Assessment of the protective effect of carbonation on portlandite crystals. Cement and concrete research, 74:68–77.

Galíndez, J.M. Molinero J. (2010) Assessment of the long-term stability of cementitious barriers of radioactive waste repositories by using digital-image-based microstructure generation and reactive transport modelling, Cement and Concrete Research, 40 (8), 1278-1289.

Garcia-Lodeiro, I., Goracci, G., Dolado, J., and Blanco-Varela, M. (2021). Mineralogical and microstructural alterations in a portland cement paste after an accelerated decalcification process. Cement and Concrete Research, 140:106312.

Gaucher, E.C., Blanc, P. (2006). Cement/clay interactions - A review: Experiments, natural analogues, and modeling. Waste Management 26, 776-788.

Genty, A. and Pot, V. (2014) Numerical Calculation of Effective Diffusion in Unsaturated Porous Media by the TRT Lattice Boltzmann Method. Transport Porous Med 105, 391-410.

Georget, F., Pr´evost, J. H., and Huet, B. (2018). Impact of the microstructure model on coupled simulation of drying and accelerated carbonation. Cement and concrete research, 104:1–12.

Ghantous, R. M., Poyet, S., l'Hostis, V., Tran, N.-C., and Franc¸ois, R. (2017). Effect of crack openings on carbonation-induced corrosion. Cement and Concrete Research, 95:257–269.

Giffaut, E., Grivé, M., Blanc, Ph., Vieillard , Ph., Colàs, E., Gailhanou, H., Gaboreau, S., Marty, N., Madé, N., Duro, L. (2014) Andra thermodynamic database for performance assessment: ThermoChimie, Applied Geochemistry, 49 225–236

González-Santamaría, D.E., Fernández, R., Ruiz, A. I., Ortega, A., Cuevas, J. (2020) High-pH/low pH ordinary Portland cement mortars impacts on compacted bentonite surfaces: Application to clay barriers performance, Applied Clay Science, 193, 105672,

Groves, G. W., Brough, A., Richardson, I., Dobson, G., Christopher, M. (1991) Progressive Changes in the Structure of Hardened C3S Cement Pastes due to Carbonation, Journal of the American Ceramic Society, 74 (11), 2891 - 2896

Gu, Y., Martin, R.-P., Metalssi, O. O., Fen-Chong, T., and Dangla, P. (2019). Pore size analyses of cement paste exposed to external sulfate attack and delayed ettringite formation. Cement and Concrete Research, 123:105766.

Guérillot, D. & Bruyelle, J. (2020): Geochemical equilibrium determination using an artificial neural network in compositional reservoir flow simulation. Computational Geosciences 24, 697–707. https://doi.org/10.1007/s10596-019-09861-4

Hagemann, S., Xie, M. and Herbert, H.-J. Unsicherheits- und Sensitivitätsanalyse zur Korrosion von Salzbeton durch salinare Lösungen. GRS-Bericht, A (3458), 2009.

Han, J., Sun, W., Pan, G., and Caihui, W. (2013). Monitoring the evolution of accelerated carbonation of hardened cement pastes by x-ray computed tomography. Journal of materials in civil engineering, 25(3):347–354.

Harris, A.W., Brodersen, K.E., Cole, G.B., Nickerson, A.K., Nilsson, K., Smith, A.C., 1998. The performance of cementitious barriers in repositories. Report EUR 17643.

Haworth, A., Sharland, S.M., Tasker, P.W. and Tweed, C.J., 1987. Evolution of the groundwater chemistry around a nuclear waste repository. Materials Research Society Symposium Proceedings 112, 425-434.

Hax Damiani, L., Kosakowski, G., Glaus, M.A. and Churakov, S.V. (2020) A framework for reactive transport modeling using FEniCS–Reaktoro: governing equations and benchmarking results. Computational Geosciences 24, 1071–1085.

Hernandez, N., Lizarazo-Marriaga, J., and Rivas, M. A. (2018). Petrographic characterization of portlandite crystal sizes in cement pastes affected by different hydration environments. Construction and Building Materials, 182:541–549.

Herold, P., Simo, E., Räuschel, H., Engelhardt, H-J., te Kook, J., Pflüger, B., Scior, C., Studeny, A. 2020: Ausbau von Grubenbauen für ein HAW-Endlager in Tonstein, BGE TECHNOLOGY GmbH, BGE TEC 2020-26

Hiemstra, T. and Riemsduk, W.H.v. (1996) A Surface Structural Approach to Ion Adsorption: The Charge Distribution (CD) Model. Journal of Colloid and Intarface Science 179, 488-508.

Ho, D. and Lewis, R. (1987). Carbonation of concrete and its prediction. Cement and Concrete Research, 17(3):489–504.

HODGKINSON, E.S., COLIN, R. H. (1999) The mineralogy and geochemistry of cement/rock reactions: high-resolution studies of experimental and analogue materials, Geological Society London Special Publications, 157(1) 195-211.

Hofmann, S., Voitchovsky, K., Spijker, P., Schmidt, M. and Stumpf, T. (2016) Visualising the molecular alteration of the calcite (104) - water interface by sodium nitrate. Scientific Reports 6.

Holz, M., Heil, S.R. and Sacco, A. (2000) Temperature-dependent self-diffusion coefficients of water and six selected molecular liquids for calibration in accurate H-1 NMR PFG measurements. Physical Chemistry Chemical Physics 2, 4740-4742.

Houst, Y. F. (1993). Diffusion de gaz, carbonatation et retrait de la pâte de ciment durcie. Ph.D. thesis, EPFL, Lausanne.

Huang, Y., Shao, H., Wieland, E., Kolditz, O., and Kosakowski, G. (2018). A new approach to coupled two-phase reactive transport simulation for long-term degradation of concrete. Construction and Building Materials, 190:805–829.

Huet, B. (2005). Comportement à la corrosion des armatures dans un béton carbonaté. Influence de la chimie de la solution interstitielle et d'une barrière de transport. Matériaux. INSA Lyon.

Hyvert, N. (2009). Application de l'approche probabiliste à la durabilité des produits préfabriqués en béton. Ph.D. thesis, Université Toulouse III Paul Sabatier.

Hummel, W., Berner, U., Curti, E., Pearson, F.J., Thoenen, T. (2002) Nagra / PSI Chemical Thermodynamic Data Base 01/01, TECHNICAL REPORT 02-16.

Hyvert, N., Sellier, A., Duprat, F., Rougeau, P., & Francisco, P. (2010). Dependency of C–S–H carbonation rate on CO2 pressure to explain transition from accelerated tests to natural carbonation. Cement and Concrete Research, 40(11), 1582-1589. https://doi.org/10.1016/j.cemconres.2010.06.010

Idiart, A., Laviña, M., Kosakowski, G., Cochepin, B., Meeussen, J.C.L., Samper, J., Mon, A., Montoya, V., Munier, I., Poonoosamy, J., Montenegro, L., Deissmann, G., Rohmen, S., Hax Damiani, L., Coene, E., Nieves, A. (2020). Reactive transport modelling of a low-pH concrete / clay interface. Applied Geochemistry 115, 104562.

Idiart, A., Coene E., Bagaria F., Román-Ross G., Birgersson M. (2019) Reactive transport modelling considering transport in interlayer water. SKB Technical Report TR-18-07

Idiart, A., Laviña M., Cochepin B., Pasteau A (2020b) Hydro-chemo-mechanical modelling of long-term evolution of bentonite swelling. Applied Clay Science, 195, 105717

Idiart, A., Laviña, M., Grandia, F., Pont A. (2020a) Reactive transport modelling of montmorillonite dissolution. SKB report R-19-15.

Jacquemet, N., Pironon, J., Lagneau, V., and Saint-Marc, J. (2012). Armouring of well cement in h2s–co2 saturated brine by calcite coating–experiments and numerical modelling. Applied geochemistry, 27(3):782–795.

Jain, A.K., Mao, J. & Mohiuddin, K.M. (1996): Artificial neural networks: A tutorial. Computer. https://doi.org/10.1109/2.485891

Jantschik, K., Czaikowski, O., Hertes, U., Meyer, T., Moog, H.C. und Zehle, B.: Development of Chemical-hydraulic Models for the Prediction of Long-term Sealing Capacity of concrete based Sealing Materials in Rock Salt. Gesellschaft für Anlagen- und Reaktorsicherheit (GRS) gGmbH, GRS-493, BMWi-FKZ 02 E 11324, ISBN 978-3-946607-78-6, Technischer Bericht, Köln, 2018.

Jatnieks, J., De Lucia, M., Dransch, D. & Sips, M. (2016): Data-driven surrogate model approach for improving the performance of reactive transport simulations. European Geosciences Union General Assembly 2016 97, 447–453. https://doi.org/10.1016/j.egypro.2016.10.047

Jenni, A. and Mäder, U., 2021. Reactive Transport Simulation of Low-pH Cement Interacting with Opalinus Clay Using a Dual Porosity Electrostatic Model. Minerals, 11(7), p.664.

Jenni, A., Gimmi, T., Alt-Epping, A., Mader, U, Cloet, V., 2017. Interaction of ordinary Portland cement and Opalinus Clay: Dual porosity modelling compared to experimental data. Physics and Chemistry of the Earth, Parts A/B/C 99, 22-37

Jenni, A., Mäder, U., Lerouge, C., Gaboreau, S., Schwyn, B. (2014). In situ interaction between different concretes and Opalinus Clay. Physics and Chemistry of the Earth, Parts A/B/C 70, 71–83.

Jerga J., Physico-mechanical properties of carbonated concrete, Constr. Build. Mater. 18 (2004) 645–652. https://doi.org/10.1016/j.conbuildmat.2004.04.029.

Jonsson, B., Nonat, A., Labbez, C., Cabane, B. and Wennerstrom, H. (2005) Controlling the cohesion of cement paste. Langmuir 21, 9211-9221.

Kamali, S., Moranville, M. Leclercq, S. (2008) Material and environmental parameter effects on the leaching of cement pastes: experiments and modelling, Cement and Concrete Research 38 575–585.

Kangni-Foli, E. (2019). Apport de mat´eriaux cimentaires mod`eles `a la description des cin´etiques de carbonatation de b´etons bas-pH: cons´equences sur la microstructure le transport de gaz et les d´eformations. PhD thesis, Paris Sciences et Lettres.

Kangni-Foli, E., Poyet, S., Le Bescop, P., Charpentier, T., Bernachy-Barb´e, F., Dauz`eres, A., L'Hˆopital, E., and de Lacaillerie, J.-B. d. (2021). Carbonation of model cement pastes: The mineralogical origin of microstructural changes and shrinkage. Cement and Concrete Research, 144:106446.

Kari, O.-P., Puttonen, J., and Skantz, E. (2014). Reactive transport modelling of long-term carbonation. Cement and Concrete Composites, 52:42–53.

Knight (2003) Scawt Hill – natural analogue, Available at http://www.natural-analogues.com/nawg-library/na-overviews/analogue reviews/235-Scawt-hill/file.

Kosakowski, G., Berner, U.R 2013. The evolution of clay rock/cement interfaces in a cementitious repository for low and intermediate level radioactive waste Phys. Chem. Earth A/B/C, 64, 65-86

Kosakowski, G., Blum, P., Kulik, D.A., Pfingsten, W., Shao, H., Singh, A., 2009. Evolution of a generic clay/cement interface: first reactive transport calculations utilizing a Gibbs energy minimization based approach for geochemical calculations. Journal of Environmental Science for Sustainable Society 3, 41-49.

Kosakowski, G., Watanabe, N., 2014. OpenGeoSys-GEM: A numerical tool for calculating geochemical and porosity changes in saturated and partially saturated media. Physics and Chemistry of the Earth Part A/B/C 70-71, 138-149.

Koskinen, K. (2014). Effects of cementitious leachates on the EBS. Posiva Report 2013-04, Posiva, Olkiluoto, Finland.

Kulik, D.A. (2009) Thermodynamic Concepts in Modeling Sorption at the Mineral-Water Interface, in: Oelkers, E.H., Schott, J. (Eds.), Thermodynamics and Kinetics of Water-Rock Interaction, pp. 125-+.

Kulik, D.A., Wagner, T., Dmytrieva, S. V., Kosakowski, G., Hingerl, F.F., Chudnenko, K. V. & Berner, U.R. (2012): GEM-Selektor geochemical modeling package: revised algorithm and GEMS3K numerical kernel for coupled simulation codes. Computational Geosciences 17, 1–24. https://doi.org/10.1007/s10596-012-9310-6

Kunther, W. Lothenbach, B., Scrivener, K.L. (2013) On the relevance of volume increase for the length changes of mortar bars in sulfate solutions, Cement and Concrete Research, 46, 23-29.

Labbez, C., Jonsson, B., Skarba, M. and Borkovec, M. (2009) Ion−Ion Correlation and Charge Reversal at Titrating Solid Interfaces. Langmuir 25, 7209–7213.

Lalan, P. , Dauzères, A., De Windt, L., Sammaljärvi, J., Bartier, D. (2019) Mineralogical and microstructural evolution of Portland cement paste/argillite interfaces at 70 °C – Considerations for diffusion and porosity properties. Cement and Concrete Research, Elsevier, 115, 414-425.

Lalan, P., Dauzères, A., De Windt, L., Bartier, D., Sammaljärvi, J., Barnichon, J.-D., Techer, I., Detilleux, V. (2016). Impact of a 70 °C temperature on an ordinary Portland cement paste/claystone interface: An in situ experiment. Cement and Concrete Research 83, 164-178.

Lanyon, G.W. (2015). Modellers Summary of LCS Experiment 2 (F16) Tracer Testing. Nagra Aktennotiz AN 15-025-Rev.1. Nagra, Wettingen, Switzerland.

Lasaga, A. C. (1981). Transition state theory. Rev. Mineral.;(United States), 8.

Leemann, Andreas, and Fabrizio Moro. 2017. "Carbonation of concrete: the role of CO2 concentration, relative humidity and CO2 buffer capacity." Materials and Structures 50 (1): 30. https://doi.org/10.1617/s11527-016-0917-2.

Leivo, M. (2021). Interface "cement/mortar – granite". Chapter 3 in: Deissmann, G., Ait Mouheb, N., Martin, C., Turrero, M. J., Torres, E., Kursten, B., Weetjens, E., Jacques, D., Cuevas, J., Samper, J., Montenegro, H., Leivo, M., Somervuori, M., Carpen, L. (2021). Experiments and numerical model studies on interfaces. Final version as of 12.05.2021 of deliverable D2.5 of the HORIZON 2020 project EURAD. EC Grant agreement no: 847593.

Lerouge C., Gaboreau S., Grangeon S., Claret F., Warmont F., Jenni A, Cloet V, Mäder. (2017). In situ interactions between Opalinus Clay and Low Alkali Concrete. Physics and Chemistry of the Earth, Parts A/B/C 99, 3-21.

Li, K., Xu, L., Stroeven, P., and Shi, C. (2021). Water permeability of unsaturated cementitious materials: A review. Construction and Building Materials, 302:124168.

Li, Y.H. and Gregory, S. (1974) Diffusion of Ions in Sea-Water and in Deep-Sea Sediments Geochimica Et Cosmochimica Acta 38, 703-714.

Lichtner, P. C. (1996). Continuum formulation of multicomponent-multiphase reactive transport. Reviews in mineralogy, 34:1–82.

Liteanu, E. and Spiers, C. (2011). Fracture healing and transport properties of wellbore cement in the presence of supercritical co2. Chemical Geology, 281(3-4):195–210.

Liu, C., Baudet, B. and Zhang, M.Z. (2022) Lattice Boltzmann modelling of ionic diffusivity in non-saturated limestone blended cement paste. Construction and Building Materials 316.

Liu, C., Qian, R.S., Wang, Y.C., Liu, Z.Y. and Zhang, Y.S. (2021) Microscopic Modelling of Permeability in Cementitious Materials: Effects of Mechanical Damage and Moisture Conditions. Journal of Advanced Concrete Technology 19, 1120-1132.

Liu, S., Jacques, D., Govaerts, J., Wang L. (2014) Conceptual model analysis of interaction at a concrete-Boom Clay interface. Phys. Chem. Earth, Parts A/B/C, 70–71, 150-159

Liu, S., Jacques, D. (2017) Coupled reactive transport model study of pore size effects on solubility during cement-bicarbonate water interaction, Chemical Geology, 466, 588-599.

Lothenbach, B., Kulik, D.A., Matschei, T., Balonis, M., Baquerizo, L., Dilnesa, B., Miron, G.D., Myers, R.J. (2019) Cemdata18: A chemical thermodynamic database for hydrated Portland cements and alkali-activated materials, Cement and Concrete Research, 115, 472-506

Lothenbach, B., Xu, B., Winnefeld, F. (2019) Thermodynamic data for magnesium (potassium) phosphates, Applied Geochemistry, 111, 104450.

Lothenbach, B., Matschei, T., M¨oschner, G., and Glasser, F. P. (2008). Thermodynamic modelling of the effect of temperature on the hydration and porosity of portland cement. Cement and Concrete Research, 38(1):1–18.

Lothenbach, B., Winnefeld, F. (2006) Thermodynamic modelling of the hydration of Portland cement, Cement and Concrete Research, 36 (2), 209-226

Lutzenkirchen, J. (2002) Surface complexation models of adsorption. Encyclopedia of Surface and Colloid Science, 5028-5046.

Lyklema, J. (1995) Fundamentals of Interface and Colloid Science

Ma, B., Lothenbach, B. (2020) Synthesis, characterization, and thermodynamic study of selected Na-based zeolites. Cement and Concrete Research, 135, 106111

Mäder, U., Jenni, A., Lerouge, C., Gaboreau, S., Miyoshi, S., Kimura, Y., Cloet, V., Fukaya, M., Claret, F., Otake, T., Shibata, M., Lothenbach, B. 2017: 5-year chemico-physical evolution of concrete-claystone interfaces, Mont Terri rock laboratory (Switzerland), Swiss Journal of Geosciences, Vol. 110, pp 307-327

Mäder, U.K., Fierz, T., Frieg, B., Eikenberg, J., Rüthi, M., Albinsson, Y., Möri, A., Ekberg, S., Stille, P. (2006). Interaction of hyperalkaline fluid with fractured rock: Field and laboratory experiments of the HPF project (Grimsel Test Site, Switzerland). Journal of Geochemical Exploration 90, 68-94.

Marty, N. C., Grangeon, S., Warmont, F., and Lerouge, C. (2015). Alteration of nanocrystalline calcium silicate hydrate (CSH) at ph 9.2 and room temperature: a combined mineralogical and chemical study. Mineralogical Magazine, 79(2):437–458.

Marty, N. C., Tournassat, C., Burnol, A., Giffaut, E., and Gaucher, E. C. (2009). Influence of reaction kinetics and mesh refinement on the numerical modelling of concrete/clay interactions. Journal of Hydrology, 364(1-2):58–72.

Marty, N., Bildstein, O., Blanc, P., Claret, F., Cochepin, B., Gaucher, E., Jacques, D., Lartigue, J.L., Liu, S., Mayer, K.U., Meeussen, J., Munier, I., Pointeau, I., Su, D., Steefel, C. 2015 Benchmarks for multicomponent reactive transport across a cement/clay interface. Comput. Geosci., 19, 635-653

Marty, N., Munier, I., Gaucher, E., Tournassat, C., Gaboreau, S., Vong, C.Q., Giffaut, E., Cochepin, B., Claret, f., 2014. Simulation of cement/clay interactions: feedback on the increasing complexity of modelling strategies. Transport Porous Media, 104 (2), 385-405

Matsushita, F., Aono, Y., and Shibata, S. (2004). Calcium silicate structure and carbonation shrinkage of a tobermorite-based material. Cement and concrete research, 34(7):1251–1257.

Mazurek, M., de Haller, A., 2017. Pore-water evolution and solute-transport mechanisms in Opalinus Clay at Mont Terri and Mont Russelin (Canton Jura, Switzerland). Swiss J. Geosci., 110.

Meeussen, J.C.L., 2003. ORCHESTRA: An object-oriented framework for implementing chemical equilibrium models. Environmental Science and Technology 37, 1175-1182.

Meier, S. A., M. A. Peter, A. Muntean, and M. Böhm. 2007. “Dynamics of the Internal Reaction Layer Arising during Carbonation of Concrete.” Chemical Engineering Science 62 (4): 1125–37.

Merah A., B. Krobba, Effect of the carbonatation and the type of cement (CEM I, CEM II) on the ductility and the compressive strength of concrete, Constr. Build. Mater. 148 (2017) 874–886. https://doi.org/10.1016/j.conbuildmat.2017.05.098.

Metcalfe, R., Walker, C. (2004). Proceedings of the International Workshop on Bentonite-Cement Interaction in Repository Environments, Tokyo. Posiva Working Report WR2004-25, Posiva, Olkiluoto, Finland.

Michau, N. (2005). ECOCLAY II: Effects of cement on clay barrier performance. Andra Report C.RP.ASCM.04.0009, Andra, Paris, France.

Millard, A., & L’Hostis, V. (2012). Modelling the effects of steel corrosion in concrete, induced by carbon dioxide penetration. European Journal of Environmental and Civil Engineering, 16(3-4), 375-391. https://doi.org/10.1080/19648189.2012.667976

Molins, S. (2015) Reactive Interfaces in Direct Numerical Simulation of Pore-Scale Processes, in: Steefel, C.I., Emmanuel, S., Anovitz, L.M. (Eds.), Pore-Scale Geochemical Processes, pp. 461-481.

Molins, S., Soulaine, C., Prasianakis, N.I., Abbasi, A., Poncet, P., Ladd, A.J.C., Starchenko, V., Roman, S., Trebotich, D., Tchelepi, H.A. & Steefel, C.I. (2020): Simulation of mineral dissolution at the pore scale with evolving fluid-solid interfaces: review of approaches and benchmark problem set. Computational Geosciences. https://doi.org/10.1007/s10596-019-09903-x

Mon, A., Samper, J., Montenegro, L., Naves, A., Fernández,J. (2017) Long-term non-isothermal reactive transport model of compacted bentonite, concrete and corrosion products in a HLW repository in clay, Journal of Contaminant Hydrology, 197, 1-16,

Montoya, V., Garibay-Rodriguez, J, Kolditz, O. 2021: Hydro-geochemical processes in the emplacement cavern of a low and intermediate-level waste repository in an indurated clay-rock, EGU General Assembly 2021, online, 19–30 Apr 2021, EGU21-12226, https://doi.org/10.5194/egusphere-egu21-12226, 2021.

Morandeau, A., M. Thiéry, and P. Dangla. 2014. “Investigation of the Carbonation Mechanism of CH and C-S-H in Terms of Kinetics, Microstructure Changes and Moisture Properties.” Cement and Concrete Research 56 (February): 153–70.

Morrow, N. R. (1970). Physics and thermodynamics of capillary action in porous media. Industrial & Engineering Chemistry, 62(6):32–56.

Moyce, E.B.A., Rochelle, C., Morris, K., Milodowski, A.E., Chen, X., Thornton, S., Small, J.S., Shaw, S. (2014). Rock alteration in alkaline cement waters over 15 years and its relevance to the geological disposal of nuclear waste. Applied Geochemistry 50, 91-105.

Muntean, A., M. Böhm, and J. Kropp. 2011. “Moving Carbonation Fronts in Concrete: A Moving-Sharp-Interface Approach.” Chemical Engineering Science 66 (3): 538–47. https://doi.org/10.1016/j.ces.2010.11.011.

Nardi, A., Idiart, A., Trinchero, P., de Vries, L.M., Molinero, J., 2014. Interface COMSOL-PHREEQC (iCP), an efficient numerical framework for the solution of coupled multiphysics and geochemistry. Computers & Geosciences 69: 10-21

NDA (2016). Geological disposal - Geosphere status report. NDA Report no. DSSC/453/01, Nuclear Decommissioning Authority, Harwell, Didcot, United Kingdom.

NEA (2012). Cementitious Materials in Safety Cases for Geological Repositories for Radioactive Waste: Role, Evolution and Interactions. NEA/RWM/R(2012)3/REV.

Neeft E., Jacques D., Deissmann G., (2022): Initial State of the Art on the assessment of the chemical evolution of ILW and HLW disposal cells. D 2.1 of the HORIZON 2020 project EURAD. EC Grant agreement no: 847593.

Neeft, E., Weetjens, E., Vokal, A., Leivo, M., Cochepin, B., Martin, C., Munier, I., Deissmann, G., Montoya, V., Poskas, P., Grigaliuniene, D., Narkuniene, A., García, E., Samper, J., Montenegro, L., Mon, A. (2020). Treatment of chemical evolution in National Programmes, D 2.4 of the HORIZON 2020 project EURAD. EC Grant agreement no: 847593.

Neji, M., Dauzères, A., Grellier, A., Sammaljärvi, J. Tikkanen, O., Siitari-Kauppi, M. (2022) Comparison of the chemo-mechanical behavior of low-pH cement exposed to calcareous water and to argillite pore water, Applied Geochemistry, 144, 105392,

Neretnieks, I., 2014. Development of a simple model for the simultaneous degradation of concrete and clay in contact. Applied Geochemistry 43, 101-113.

NF EN 206/CN. (2014) AFNOR, Concrete - Specification, performance, production and conformity - National addition to the standard NF EN 206.

Ngala, V., & Page, C. (1997). Effects of carbonation on pore structure and diffusional properties of hydrated cement pastes. Cement and Concrete Research, 27(7), 995-1007.

Oda, C., Honda, A., Savage, D. (2004) An analysis of cement–bentonite interaction and evolution of pore water chemistry. International Workshop on Bentonite–Cement Interaction in the Repository Environment, Nuclear Waste Management Organisation of Japan (NUMO), NUMO Report TR-04-05.

Omosebi, O., Sharma, M., Ahmed, R., Shah, S., Saasen, A., and Osisanya, S. (2017). Cement degradation in co2-h2s environment under high pressure-high temperature conditions. In SPE Bergen one day seminar. OnePetro.

Papadakis, V. G., Vayenas, C. G., and Fardis, M. N. (1991). Experimental investigation and mathematical modeling of the concrete carbonation problem. Chemical Engineering Science, 46(5-6):1333– 1338.

Parkhurst, D.L. (1995): User's guide to PHREEQC: A computer program for speciation, reaction-path, advective-transport, and inverse geochemical calculations. US Department of the Interior, US Geological Survey.

Parkhurst, D.L., Appelo, C. 1999. User's guide to PHREEQC (Version 2): A computer program for speciation, batch reaction, one-dimensional transport, and inverse geochemical calculations. USGS Water-Resources Investigations Report 99-4259, US Geological Survey, Denver, Colorado, USA.

Parrott, L.J., and D.C. Killoh. 1989. "Carbonation in a 36 Year Old, in-Situ Concrete." Cement and Concrete Research 19 (4): 649–56.

Pastina, B., Lehikoinen, J., Puigdomenech, I. (2012). Safety case approach for a KBS-3 type repository in crystalline rock. In: NEA, 2012. Cementitious materials in safety cases for geological repositories for radioactive waste: Role, evolution and interactions, NEA/RWM/R(2012)3/REV, 120-124.

Patel, R.A., Churakov, S.V. and Prasianakis, N.I. (2021) A multi-level pore scale reactive transport model for the investigation of combined leaching and carbonation of cement paste. Cement & Concrete Composites 115.

Patel, R.A., Perko, J., Jacques, D., De Schutter, G., Ye, G. and Van Breugel, K. (2018) A three-dimensional lattice Boltzmann method based reactive transport model to simulate changes in cement paste microstructure due to calcium leaching. Construction and Building Materials 166, 158-170.

Pfingsten, W., Paris, B., Soler, J.M., Mäder, U.K. (2006). Tracer and reactive transport modelling of the interaction between high-pH fluid and fractured rock: field and laboratory experiments. Journal of Geochemical Exploration 90, 95-113.

Phung, Q. T., Gaboreau, S., Claret, F., & Maes, N. (2018). Degradation of concrete in a clay environment. In 4th International Conference on Service Life Design for Infrastructures.

Pivonka, P., Narsilio, G.A., Li, R.N., Smith, D.W. and Gardiner, B. (2009) Electrodiffusive Transport in Charged Porous Media: From the Particle-Level Scale to the Macroscopic Scale Using Volume Averaging. Journal of Porous Media 12, 101-118.

Planel, D. & Sercombe, J. & Le Bescop, Patrick & Adenot, Frédéric & Torrenti, jean michel. (2006). Long-term performance of cement paste during combined calcium leaching-sulfate attack: Kinetics and size effect. Cement and Concrete Research. 36. 137-143.

Poonoosamy, J., Mahrous, M., Curti, E., Bosbach, D., Deissmann, G., Churakov, S.V., Geisler, T. and Prasianakis, N. (2021) A lab-on-a-chip approach integrating in-situ characterization and reactive transport modelling diagnostics to unravel (Ba,Sr)SO4 oscillatory zoning. Scientific Reports 11.

Poonoosamy, J., Wanner, C., Epping, P. A., Aguila, J., Samper, J., Montenegro, L., Xie, M., Su, D.,´ Mayer, U., M¨ader, U., et al. (2018). Benchmarking of reactive transport codes for a 2d setup with mineral dissolution/precipitation reactions and feedback on transport parameters. Comput. Geosci.

Poonoosamy, J., Westerwalbesloh, C., Deissmann, G., Mahrous, M., Curti, E., Churakov, S.V., Klinkenberg, M., Kohlheyer, D., Eric von Lieresb, Bosbach, D. and Prasianakisc, N.I. (2019) A microfluidic experiment and pore scale modelling diagnostics for assessing mineral precipitation and dissolution in confined spaces. Chemical Geology 528, 119264-119216.

Poupard, O., L'Hostis, V., Catinaud, S., Petre-Lazar, I. (2006) Corrosion damage diagnosis of a reinforced concrete beam after 40 years natural exposure in marine environment. Cement and Concrete Research, 36, 504- 520.

Pourbaix, M. (1963). Atlas d'équilibres électrochimiques. Gauthiers-Villars & Cie. Paris.

Poyet, S. (2016). Describing the influence of temperature on water retention using van genuchten equation. Cement and Concrete Research, 84:41–47.

Prasianakis, N.I., Curti, E., Kosakowski, G., Poonoosamy, J. and Churakov, S.V. (2017) Deciphering pore-level precipitation mechanisms. Scientific Reports 7, 13765.

Prasianakis, N.I., Gatschet, M., Abbasi, A. & Churakov, S.V. (2018): Upscaling strategies of porosity-permeability correlations in reacting environments from pore-scale simulations. Geofluids 2018. https://doi.org/10.1155/2018/9260603

Prasianakis, N.I., Haller, R., Mahrous, M., Poonoosamy, J., Pfingsten, W. & Churakov, S. V (2020): Neural network based process coupling and parameter upscaling in reactive transport simulations. Geochimica et Cosmochimica Acta 291, 126–143.

Prieto, M. (2014): Nucleation and supersaturation in porous media (revisited). Mineralogical Magazine 78, 1437–1447. https://doi.org/10.1180/minmag.2014.078.6.11

Quintessa (2012) QPAC: Quintessa's general-purpose modelling software. Quintessa Report QRS-QPAC-11, Quintessa, Henley-on-Thames, United Kingdom.

Read, D., Glasser, F.P., Ayora, C., Guardiola, M.T., Sneyers, A. (2001). Mineralogical and microstructural changes accompanying the interaction of Boom Clay with ordinary Portland cement. Advances in Cement Research 13, 175-183.

Regnault, O., Lagneau, V., and Schneider, H. (2009). Experimental measurement of portlandite carbonation kinetics with supercritical co2. Chemical Geology, 265(1-2):113–121.

Reinhold, K., Jahn, S., Kühnlenz, T., Ptock, L., Sönnke, J. 2013: Endlagerstandortmodell Nord (AnSichT) – Teil I: Beschreibung des geologischen Endlagerstandortmodells – Zwischenbericht, Hannover (BGR)

Revertégat E., Adenot F., Richet C., Wu L., Glasser F.P., Damidot D. & Stronach S.A. (1997) Theoretical and experimental study of degradation mechanisms of cement in the repository environment. Nucl. Sci. Tech., Final report FI2W-CT90-0035, EUR 17642 EN, 267p.

Richardson, I.G., Groves, G.W., Brought, A.R. and Dobsont, C.M. (1993) The carbonation of OPC and OPC/silica fume hardened cement pastes in air under conditions of fixed humidity, Advances in Cement Research, 5, 81-86.

Richet C., Le Bescop P., Gallé C., Peycelon H., Béjaoui S., Pointeau I., L'Hostis V. & Bary B. (2004) Dossier de synthèse sur le comportement à long terme des colis : dossier de référence phénoménologique « colis béton ». Rapport CEA RT-DPC/SCCME/04-679-A.

Roosz, C. Vieillard, Ph., Blanc, Ph., Gaboreau, S., Gailhanou, H., Braithwaite, D. Montouillout, V., Denoyel, R., Henocq, P., Madé, B. (2018) Thermodynamic properties of C-S-H, C-A-S-H and M-S-H phases: Results from direct measurements and predictive modelling, Applied Geochemistry, 92, 140-156

Rougeau P, Apport de l'étude de matériaux analogues anciens à la modélisation du comportement des barrières ouvragées en ciment vis-à-vis de la migration des radioéléments (1994), Thèse de l'Université de Poitiers.

Ruiz-Agudo, E., Kudl acz, K., Putnis, C. V., Putnis, A., and Rodriguez-Navarro, C. (2013). Dissolution and carbonation of portlandite [ca (oh) 2] single crystals. Environmental science & technology, 47(19):11342–11349.

Russell, D., P. A. M. Basheer, G. I. B. Rankin, and A. E. Long. 2001. "Effect of Relative Humidity and Air Permeability on Prediction of the Rate of Carbonation of Concrete." Proceedings of the Institution of Civil Engineers - Structures and Buildings 146 (3): 319–26.

Saaltink, M.W., Ayora, C., Carrera, J.A., 1998. A mathematical formulation for reactive transport that eliminates mineral concentrations. Water Resources Research 34, 1649-1656.

Sahai, N. and Sverjensky, D.A. (1997) Evaluation of internally consistent parameters for the triple-layer model by the systematic analysis of oxide surface titration data. Geochimica et Cosmochimica Acta 61, 2801-2826.

Samper, J., Yang, C., Montenegro, L., 2003. User's manual of CORE2D Version 4: A code for ground-water flow and reactive solute transport. Universidad de A Coruña, La Coruña, Spain.

Samper, J., Mon, A., Montenegro, L., Cuevas, J., Turrero, M.J., Naves, A., Fernández, R., Torres, E. (2018) Coupled THCM model of a heating and hydration concrete-bentonite column test, Applied Geochemistry, 94, 67-81

Sandl, E., Cahill, A., Welch, L., and Beckie, R. (2021). Characterizing oil and gas wells with fugitive gas migration through bayesian multilevel logistic regression. Science of The Total Environment, 769:144678.

Savage, D. (2009). A review of experimental evidence for the development and properties of cement bentonite interfaces with implications for gas transport. Nagra Report NAB 09-30, Nagra, Wettingen, Switzerland.

Savage, D. (2011). A review of analogues of alkaline alteration with regard to long-term barrier performance. Mineralogical Magazine 75, 2401-2418.

Savage, D. (2014). An assessment of the impact of the long term evolution of engineered structures on the safety-relevant functions of the bentonite buffer in a HLW repository. Nagra Technical Report TR 13-02, Nagra, Wettingen, Switzerland.

Savage, D., Benbow, S., 2007. Low-pH cements. SKI Report.

Savage, D., Cloet, V. (2018). A review of cement-clay modelling. Nagra Report NAB 18-24, Nagra, Wettingen, Switzerland.

Savage, D., Rochelle, C., 1993. Modelling reactions between cement pore fluids and rock: Implications for porosity change. Journal of Contaminant Hydrology 13, 365-378.

Savage, D., Walker, C., Arthur, R.C., Rochelle, C.A., Oda, C., Takase, H. (2007). Alteration of bentonite by hyperalkaline fluids: a review of the role of secondary minerals. Physics and Chemistry of the Earth 32, 287-297.

Savage, D., Wilson, J., Benbow, S., Sasamoto, H., Oda, C., Walker, C., Kawama, D., Tachi, Y. (2020) Using natural systems evidence to test models of transformation of montmorillonite, Applied Clay Science, 195, 105741.

Schmidt, T. (2007) Sulfate attack and the role of internal carbonate on the formation of thaumasite. No. THESIS. EPFL.

Seigneur, N., De Windt, L., Poyet, S., and Dauzèeres (2022). Modelling of the evolving contributions of gas transport, cracks and chemical kinetics during atmospheric carbonation of hydrated c_3s and c-s-h pastes. Cement and Concrete Research, 130:105966. In review.

Seigneur, N., Lagneau, V., Corvisier, J., and Dauzères, A. (2018). Recoupling flow and chemistry in variably saturated reactive transport modelling-an algorithm to accurately couple the feedback of

chemistry on water consumption, variable porosity and flow. Advances in water resources, 122:355–366.

Seigneur, N., Mayer, K. U., and Steefel, C. I. (2019). Reactive transport in evolving porous media. Reviews in Mineralogy and Geochemistry, 85(1):197–238.

Sellier, A. and Multon, S. (2018). Chemical modelling of delayed ettringite formation for assessment of affected concrete structures. Cement and Concrete Research, 108:72–86.

Sellier, A., Buffo-Lacarrière, L., Gonnouni, M.E., Bourbon, X. Behaviour of HPC nuclear waste disposal structures in leaching environment. Nuclear Engineering and Design (2011). Vol 241, N°1, pp.402–14.

Shen, J., Dangla, P., and Thiery, M. (2013). Reactive transport modeling of co2 through cementitious materials under co2 geological storage conditions. International Journal of Greenhouse Gas Control, 18:75–87.

Shiotani, T., Bisschop, J., and Van Mier, J. (2003). Temporal and spatial development of drying shrinkage cracking in cement-based materials. Engineering Fracture Mechanics, 70(12):1509–1525.

Sidborn, M., Marsic, N., Crawford, J., Joyce, S., Hartley, L., Idiart, A., de Vries, L.M., Maia, F., Molinero, J., Svensson, U., Vidstrand, P., Alexander, R. (2014). Potential alkaline conditions for deposition holes of a repository in Forsmark as a consequence of OPC grouting. SKB Report R-12-17, SKB, Stockholm, Sweden.

Simunek, J., Jacques, D., Langergraber, G., Bradford, S.A., Sejna, M., van Genuchten, M.T., 2013 Numerical modeling of contaminant transport using HYDRUS and its specialized modules, 93, 265–284. ISSN: 0970-4140 Coden-JIISAD

Sin, I. and Corvisier, J. (2019). Multiphase multicomponent reactive transport and flow modeling. Reviews in Mineralogy and Geochemistry, 85(1):143–195.

Soja, W., Georget, F., Maraghechi, H., and Scrivener, K. (2020). Evolution of microstructural changes in cement paste during environmental drying. Cement and Concrete Research, 134:106093.

Soler, J.M. (2012). High-pH plume from low-alkali-cement fracture grouting: reactive transport modeling and comparison with pH monitoring at ONKALO (Finland). Applied Geochemistry 27, 2096-2106.

Soler, J.M. 2013. Reactive transport modelling of concrete-clay interaction during 15 years at the Tournemire underground rock laboratory. Eur. J. Mineral, 25, 639-654

Soler, J.M., Mäder, U.K. (2007). Mineralogical alteration and associated permeability changes induced by a high-pH plume: modeling of a granite core infiltration experiment. Applied Geochemistry 22, 17-29.

Soler, J.M., Mäder, U.K. (2010). Cement-rock interaction: infiltration of a high-pH solution into a fractured granite core. Geol. Acta 8, 221–233.

Soler, J.M., Pfingsten, W., Paris, B., Mäder, U.K., Frieg, B., Neall, F., Källvenius, G., Yui, M., Yoshida, Y., Shi, P., Rochelle, C.H.A. (2006). HPF-Experiment: modelling report. Nagra Technical Report NTB--05-01, Nagra, Wettingen, Switzerland.

Soler, J.M., Vuorio, M., Hautojärvi, A. (2011). Reactive transport modeling of the interaction between water and a cementitious grout in a fractured rock. Application to ONKALO (Finland). Applied Geochemistry 26, 1115-1129.

Steefel, C.I., Appelo, C.A.J., Arora, B., Jacques, D., Kalbacher, T., Kolditz, O., Lagneau, V., Lichtner, P.C., Mayer, K.U., Meeussen, J.C.L., Molins, S., Moulton, D., Shao, H., Simunek, J., Spycher, N., Yabusaki, S.B. and Yeh, G.T. (2015) Reactive transport codes for subsurface environmental simulation. Computational Geosciences 19, 445-478.

Steefel, C.I. CrunchFlow: Software for Modeling Multicomponent Reactive Flow and Transport. 2009. Available online: https://bitbucket.org/crunchflow/crunchtope-dev/wiki/Home.

Steefel, C.I., Lichtner, P.C. (1994) Diffusion and reaction in rock matrix bordering a hyperalkaline fluid-filled fracture, Geochimica et Cosmochimica Acta, 58 (17), 3595-3612.

Steiner, Sarah, Barbara Lothenbach, Tilo Proske, Andreas Borgschulte, and Frank Winnefeld. 2020. "Effect of Relative Humidity on the Carbonation Rate of Portlandite, Calcium Silicate Hydrates and Ettringite." Cement and Concrete Research 135 (January): 106116.

Succi, S. (2001): The lattice Boltzmann equation: for fluid dynamics and beyond. Oxford university press.

Suda Y., J. Tomiyama, T. Saito, T. Saeki, Effect of relative humidity on carbonation shrinkage and hydration product of cement paste (in japanese), Cem. Sci. Concr. Technol. 73 (2019) 71–78. https://doi.org/10.14250/cement.73.71.

Sverjensky, D.A. (2001) Interpretation and prediction of triple-layer model capacitances and the structure of the oxide– electrolyte–water interface. Geochim. Cosmochim. Acta 65, 3643–3655,.

Sverjensky, D.A. (2005) Prediction of surface charge on oxides in salt solutions: Revisions for 1 : 1 (M+L-) electrolytes. Geochimica Et Cosmochimica Acta 69, 225-257.

Sverjensky, D.A. (2006) Prediction of the speciation of alkaline earths adsorbed on mineral surfaces in salt solutions. Geochimica Et Cosmochimica Acta 70, 2427-2453.

Swenson E.G., P.J. Sereda, Mechanism of the carbonation shrinkage of lime and hydrated cement, J. Appl. Chem. 18 (1968) 111–117.

Szabó-Krausz, Z., Aradi, L.E., Király, C., Kónya, P., Török, P., Szabó, C., Falus, G., (2021) Signs of in-situ geochemical interactions at the granite–concrete interface of a radioactive waste disposal, Applied Geochemistry, 126, 104881.

Taylor, H.F.W. (1997). Cement chemistry (2nd edition). Thomas Telford Publishing, London.

Techer, I., Bartier, D., Boulvais, P., Tinseau, E., Suchorski, K., Cabrera, J., Dauzères, A. (2012a). Tracing interactions between natural argillites and hyper-alkaline fluids from engineered cement paste and concrete: Chemical and isotopic monitoring of a 15-years old deep-disposal analogue. Applied Geochemistry 27, 1384-1402.

Techer, I., Michel. P., Bartier, D., Tinseau, E., Devol-Brown, I., Boulvais, P., Suchorski, K. (2012b). Engineered analogues of cement/clay interactions in the Tournemire experimental platform (France): A couple mineralogical and geochemical approach to track tiny disturbances. In: NEA, 2012. Cementitious materials in safety cases for geological repositories for radioactive waste: Role, evolution and interactions, NEA/RWM/R(2012)3/REV, 182-185.

Thiery, M. (2005). Modelling of atmospheric carbonation of cement based materials considering the kinetic effects and modifications of the microstructure and the hydric state. Engineering Sciences [physics]. Ecole des Ponts ParisTech, 2005. Phd thesis in frensh. ffpastel-00001517.

Thiery, Mickaël, G. Villain, P. Dangla, and G. Platret. 2007. "Investigation of the Carbonation Front Shape on Cementitious Materials: Effects of the Chemical Kinetics." Cement and Concrete Research 37 (7): 1047–58. https://doi.org/10.1016/j.cemconres.2007.04.002.

Thoenen, T., Hummel, W., Berner, U., Curti, E. (2014) The PSI/Nagra Chemical Thermodynamic Database 12/07 Nuclear Energy and Safety Research Department Laboratory for Waste Management (LES), ISSN 1019-0643

Thouvenot, P., Bildstein, O., Munier, I., Cochepin, B., Poyet, S., et al. Modeling of concrete carbonation in deep geological disposal of intermediate level waste (2013) EPJ Web of Conferences, EDP Sciences, International Workshop NUCPERF 2012: Long-Term Performance of Cementitious Barriers and Reinforced Concrete in Nuclear Power Plant and Radioactive Waste Storage and Disposal (RILEM Event TC 226-CNM and EFC Event 351), 56, pp.05004.

Tinseau, E., Bartier, D., Hassouta, L., Devol-Brown, I., Stammose, D. (2006). Mineralogical characterization of the Tournemire argillite after in situ reaction with concretes. Waste Management 26, 789-800.

Thomassin, J. H., & Rassineux, F. (1992) Ancient analogues of cement-base materials: stability of calcium silicate hydrates. Applied Geochemistry, Supplementary Issue, 1, 137–142.

Tran, V. Q., Soive, A., Bonnet, S., and Khelidj, A. (2018). A numerical model including thermodynamic equilibrium, kinetic control and surface complexation in order to explain cation type effect on chloride binding capability of concrete. Construction and Building Materials, 191:608–618.

Trapote-Barreira, A., Cama, J., and Soler, J. M. (2014). Dissolution kinetics of C–S–H gel: Flowthrough experiments. Physics and Chemistry of the Earth, Parts A/B/C, 70:17–31.

Trapote-Barreira, A., Cama, J., Soler, J.M. Lothenbach, B. (2016) Degradation of mortar under advective flow: Column experiments and reactive transport modeling, Cement and Concrete Research, 81, 81-93,

Trinchero, P., Nardi A., Silva O., Bruch, B. (2022) Simulating electrochemical migration and anion exclusion in porous and fractured media using PFLOTRAN. Computers & Geosciences, 166, 105166

Trotignon, L, Devallois, D., Peycelon, H., Tiffreau, C., Bourbon, X. 2007, Predicting the long term durability of concrete engineered barriers in a geological repository for radioactive waste Phys. Chem. Earth, 32, 259-274

Trotignon L., P. Thouvenot, I. Munier, B. Cochepin, E. Piault, E. Treille, X. Bourbon and S. Mimid. Numerical simulation of atmospheric carbonation of concrete components in a deep geological radwaste disposal site during operating period. Nuclear Technology (June 2011). Vol 174.

Trotignon, L., Peycelon, H., Bourbon, X. (2006) Comparison of performance of concrete barriers in a clayey geological medium, Physics and Chemistry of the Earth, Parts A/B/C, 31, (10–14), 610-617,

Trotignon, L., Devallois, V., Tiffreau, C., Peyeelon, H., & Bourbon, X. (2005). Predicting the long term durability of concrete engineered barriers in a geologicalwaste disposal. Clays in natural and engineered barriers for radioactive waste confinement, (p. 723). France

Tschegg E.K., E. Bohner, J. Tritthart, H.S. Müller, Investigations into fracture of carbonated concrete, Mag. Concr. Res. 63 (2011) 21–30. https://doi.org/10.1680/macr.2011.63.1.21.

Turrero, M.J., Cloet, V., 2017. FeBEX-DP concrete ageing, concrete/bentonite and concrete/rock interaction analysis. Nagra Report NAB 16-18, Nagra, Wettingen, Switzerland.

Van Breugel, K. (1995a) Numerical-simulation of hydration and microstructural development in hardening cement-based materials .1. Theory. Cement and Concrete Research 25, 319-331.

Van Breugel, K. (1995b) Numerical-simulation of hydration and microstructural development in hardening cement-based materials .2. Applications. Cement and Concrete Research 25, 522-530.

Van Der Lee, J., De Windt, L., Lagneau, V., and Goblet, P. (2002). Presentation and application of the reactive transport code hytec. In Developments in Water Science, volume 47, 599–606.

Van Der Lee, J., De Windt, L., Lagneau, V., and Goblet, P. (2003). Module-oriented modeling of reactive transport with hytec. Computers & Geosciences, 29(3):265–275.

Varzina, A., Cizer, O., Yu, L., Liu, S., Jacques, D., and Perko, J. (2020). A new concept for pore-scale¨ precipitation-dissolution modelling in a lattice boltzmann framework–application to portlandite carbonation. Applied Geochemistry, 123:104786.

Vehmas, T., Holt, E. (2016) WP1 Experimental studies – State of the art literature review, CEBAMA EC project, CEBAMA: Cement-based materials, properties, evolution, barrier functions - IGD-TP | Safe Solutions for Radioactive Waste (igdtp.eu) ,235p.

Vehmas T., V. Montoya, M. Cruz Alonso, R. Vasicek, E. Rastrick, S. Gaboreau, P. Vecernik, M. Leivo, E. Holt, N. Fink, N.A. Mouhebb, J. Svoboda, D. Read, R. Cervinka, R.Vasconcelos, and C. Corkhillh "Characterization of Cebama Low-pH Reference Concrete and Assessment of its Alteration with Representative Waters in Radioactive Waste Repositories", Appl. Geochem., 121, 104703 (2020).

Verbeck G.J., Carbonation of Hydrated Portland Cement, ASTM Spec. Tech. Publ. 205 (1958) 17–36.

Vinsot A., S. Mettler, S. Wechner. In situ characterization of the Callovo-Oxfordian pore water composition Physics and Chemistry of the Earth, 33 (2008), pp. S75-S86.

Wan, K., Xu, Q., Wang, Y., and Pan, G. (2014). 3d spatial distribution of the calcium carbonate caused by carbonation of cement paste. Cement and Concrete Composites, 45:255–263.

Watson, C., D. Savage, J. Wilson, S. Benbow, C. Walker, S. Norris. 2013. The Tournemire industrial analogue: reactive-transport modelling of a cement-clay interface Clay Miner., 48, 167-184

Watson, C., Savage, D., Wilson, J. (2017). Geochemical modelling of the LCS experiment. Quintessa Report QRS-1523D-2, Quintessa, Henley-on-Thames, United Kingdom.

Wigand, M., Kaszuba, J. P., Carey, J. W., and Hollis, W. K. (2009). Geochemical effects of co2 sequestration on fractured wellbore cement at the cement/caprock interface. Chemical Geology, 265(1):122 – 133. CO2 geological storage: Integrating geochemical, hydrodynamical, mechanical and biological processes from the pore to the reservoir scale.

Wilson, J., Bateman, K. Tachi, Y. (2021) The impact of cement on argillaceous rocks in radioactive waste disposal systems: A review focusing on key processes and remaining issues, Applied Geochemistry, 130, 2021, 104979.

Winter, Nicholas B. 2009. Understanding Cement: An Introduction to Cement Production, Cement Hydration and Deleterious Processes in Concrete. Woodbridge, UK: WHD Microanalysis Consultants.

Wolery, T.J. (1979) Calculation of Chemical Equilibrium Between Aqueous Solutions and Minerals, Lawrence Livermore Laboratory, UCRL-52658.

Xiao J., J. Li, B. Zhu, Z. Fan, Experimental study on strength and ductility of carbonated concrete elements, Constr. Build. Mater. 16 (2002) 187–192. https://doi.org/10.1016/S0950-0618(01)00034-4.

Xie, M., Dangla, P., and Li, K. (2021). Reactive transport modelling of concurrent chloride ingress and carbonation in concrete. Materials and Structures, 54(5):1–19.

Xie, M., Mayer, K. U., Claret, F., Alt-Epping, P., Jacques, D., Steefel, C., Chiaberge, C., and Simunek, J. (2015). Implementation and evaluation of permeability-porosity and tortuosity-porosity relationships linked to mineral dissolution-precipitation. Computational Geosciences, 19(3):655–671.

Xu, T., Sonnenthal, E., Spycher, N., Zhang, G., Zheng, L. & Pruess, K. (2012): Toughreact: A simulation program for subsurface reactive chemical transport under non-isothermal multiphase flow conditions, in: Groundwater Reactive Transport Models. pp. 74–95. https://doi.org/10.2174/978160805306311201010074

Yamaguchi, T., Kataoka, M., Sawaguchi, T., Mukai, M., Hoshino, S., Tanaka, T., Marsal, F., Pellegrini, D. (2013) Development of a reactive transport code MC CEMENT ver. 2 and its verification using 15-year in situ concrete/clay interactions at the Tournemire URL Clay Minerals, 48 (2) 185–197.

Yang, Y., Patel, R.A., Churakov, S.V., Prasianakis, N.I., Kosakowski, G. and Wang, M. (2019) Multiscale modeling of ion diffusion in cement paste: Electrical double layer effects. Cement and Concrete Composites 96, 55–65.

Yuan, H., Dangla, P., Chatellier, P., Chaussadent, T. (2013) Degradation modelling of concrete submitted to sulfuric acid attack, Cement and Concrete Research, 53, 267-277,

Ye, H., Radlin´ska, A., and Neves, J. (2017). Drying and carbonation shrinkage of cement paste containing alkalis. Materials and structures, 50(2):1–13.

Zajac, M., Skibsted, J., Durdzinski, P., Bullerjahn, F., Skocek, J., and Haha, M. B. (2020). Kinetics of enforced carbonation of cement paste. Cement and Concrete Research, 131:106013.

Zalzale, M., McDonald, P.J. and Scrivener, K.L. (2013) A 3D lattice Boltzmann effective media study: understanding the role of C-S-H and water saturation on the permeability of cement paste. Modelling and Simulation in Materials Science and Engineering 21.

Zhang H., C.R. Rodriguez, H. Dong, Y. Gan, E. Schlangen, B. Šavija, Elucidating the effect of accelerated carbonation on porosity and mechanical properties of hydrated Portland cement paste using X-ray tomography and advanced micromechanical testing, Micromachines. 11 (2020). https://doi.org/10.3390/MI11050471.

Zhang, M.Z. (2017) Pore-scale modelling of relative permeability of cementitious materials using X-ray computed microtomography images. Cement and Concrete Research 95, 18-29.

Zhang, M.Z., Xu, K.M., He, Y.J. and Jivkov, A.P. (2014) Pore-scale modelling of 3D moisture distribution and critical saturation in cementitious materials. Construction and Building Materials 64, 222-230.

Zhang, M.Z., Ye, G. and van Breugel, K. (2012) Modeling of ionic diffusivity in non-saturated cement-based materials using lattice Boltzmann method. Cement and Concrete Research 42, 1524-1533.

Zhen-Wu, B. Y, Prentice, D. P., Ryan, J.V., Ellison, K., Bauchy, M., Sant G. (2020) zeo19: A thermodynamic database for assessing zeolite stability during the corrosion of nuclear waste immobilization glasses. npj Materials Degradation, 4, 2.

ZHU, W., Francois, R., Zhang, C., Zhang, D. (2017) Propagation of corrosion-induced cracks of the RC beam exposed to marine environment under sustained load for a period of 26 years. Cement and Concrete Research, 103, 66-76.

ZHU, Wenjun & Francois, Raoul & Cheng-ping, Zhang & Zhang, Dingli. (2018). Propagation of corrosion-induced cracks of the RC beam exposed to marine environment under sustained load for a period of 26 years. Cement and Concrete Research, 103, 66-76.

2. Multiscale mechanical behaviour related to the disturbances imposed in geological disposal environments

Andra

After a brief description of mechanical constraints applied to cementitious materials in geological disposal environments (part 2.1), part 2.2 focuses on the existing data relative to concrete mechanical behaviour exposed to these types of environment at the nano and microscale, while part 2.3 is devoted to the meso and macroscale. The general objectives are to identify the current knowledge in terms of mechanics and to identify the gaps remaining, especially in representative chemical conditions.

2.1 Mechanical constraints applied to concrete in a geological disposal

Task 2 board

The mechanical behaviour of underground cementitious structures is influenced by various parameters, boundary conditions, and construction methods.

The first key parameter is the host rock response to the excavation of drifts. Excavation and/or construction generally disturb firstly the natural initial physical state of the host rock. It generates interaction of various rock mass parameters and boundary conditions possibly causing further changes of other rock parameters (Hudson, 1991). The strength of the rock mass is reduced in a plastic zone around the underground structure. Morrison and Coates (1955) were the first to describe it. That disturbance induces stresses/strains modification evolving or not with time, guided by the host rock hydromechanical characteristics and geological context. Therefore, various mechanical processes could be activated, for instance cracks induced by excavation (damaged zone), convergence, water pressure evolution, or creep. For instance, in indurated rock like Callovo-Oxfordian claystone or poorly indurated clay like Boom Clay, the excavation of drifts induces damages zones, convergence and creep (Armand et al., 2015; Blumling et al., 2007). Due to the high strength of hard rock compared to the in-situ stress state, mainly the vertical stress, the damage induced by excavation is often limited to the wall and does not lead to significant deferred strain (Martin et al., 1997; Martin and Chandler, 1994, Aoyagi et al., 2017).

The underground cementitious structure mechanical characteristics and their evolution is the second key factor. The underground disposal structures such as linings, plugs, or buffers can be loaded (directly/indirectly, with or without timelapse) by the host rock. This is particularly in the case of indurated or soft rocks. The loading is a result of the rock/structure interaction. As the structure stops the convergence of rocks, it becomes mechanically loaded, with stresses and strains generated as a function of its stiffness. In addition, the equivalent rigidity of the structure can also evolve in time. This evolution is due to different potential reasons:

- the level of loading (directly/indirectly) from the host rock, that can affect the stress/strains relation and increase the mechanical damage,

- the decrease in mechanical characteristics due to the chemical/microbial perturbation, and

- the concrete formulation, in particular with respect to the influence on shrinkage and creep behaviour. For example, shrinkage can influence the initial interface characteristics of the plug, leading to radial deformation in concurrence with the rock convergence.

The construction process (method and sequence) has an important impact concerning the delay of the loading activation (Zghondi et al., 2017) and the hydromechanical characteristics of the interface. It has also an effect on the mechanical characteristics of the structure and can have an influence on the rock damaged zone. For instance, the time delay to load a segment lining on a tunneling boring machine excavation is different from a poured in place lining following a traditional excavation method. The same applies to plugs and buffers, where the interaction with the rock (direct or indirect) will take place several

years after excavation, according to rock convergence (when present), which may have a different kinetics regarding the initial state. The rock/structure interfaces quality and characteristics are connected to the structural boundary conditions, in relation with the construction process. It is the case for example of setting up the concrete lining: shotcrete, pouring, or precast elements. Adding also the question of the progress of the construction that can be different in each method.

Different methods of prediction of the mechanical interaction have been proposed. They permit to describe at structure scale the mechanical behaviour with time, taking into account various boundary conditions regarding the building methods: analytical (Panet, 1976; Corbetta et al., 1991) and engineering top-down method. The engineering objective is first established and then appropriate models are developed (Hudson, 1991), such as a numerical model based on a rock and structure adapted behaviour law (Brown et al., 1989; Carter and Booker, 1990), or with a neural network approach (Cai et al., 2000).

2.2 Mechanical behaviour of concrete at the nano/microscale exposed to geological disposal environments

2.2.1 Experimental developments and key results

PSI, Empa, CEA, IRSN

Experimental methods such as micro-/nano-indentation and distinct types of Scanning Probe Microscopy (SPM), e.g., Atomic Force Microscopy (AFM), allow probing some mechanical properties locally and within a very broad range of length scales, in the micro- and nano-domains. Such length-scale versatility and the intrinsic local probing nature of such methods offer, several advantages for such heterogeneous composites as cement-based ones, including cement paste itself. The latter is the key component of concrete, a composite material by definition, mostly participating in the set of chemo-mechanical processes triggered in geological disposal environments and described in Sections 1.1 and 1.2.

One key advantage of particular relevance for the development and validation of computational models at the nano- and micro-scales consists of the possibility of probing selectively distinct cement hydrates. The latter allows estimating mechanical properties of single cement paste constituents, each with a distinct role in the degradation processes mentioned in Section 1. The local and highly selective mechanical probing is typically enabled and/or enhanced by the simultaneous use of chemical probes, e.g., Energy Dispersive X-ray Spectroscopy (EDX). The combination of the mechanical probe, e.g., a micro- or nano-indenter, with a chemical one, e.g., the electron beam of a Scanning Electron Microscope (SEM) plus an X-ray detector, already enabled nano- and micro-scale, fully chemo-mechanical characterizations of cement hydrates and their assemblages (Chen et al., 2010). One investigation example dealt with the assessment of the correlations between the elemental composition of C-S-H clusters and their mechanical properties (Krakowiak et al., 2015).

2.2.1.1 Resonant Ultrasound Spectroscopy for cement application

Resonant Ultrasound Spectroscopy (RUS) is a fully non-destructive technique, which can partly complement indentation-based methods in measuring mechanical properties of cement-based composites and of their single components.

RUS was originally developed in the condensed matter and mineral physics fields for estimating quantitatively, by a single measurement, the full tensor of linear elastic constants, independently of the material's elastic anisotropy class (Migliori and Sarrao, 1997; Zadler et al., 2004; Leisure, 2017). RUS relies on solving the inverse problem of finding the linear elastic constants, which, together with known density, specimen size and shape, determine the specimen's mechanical resonance frequencies, under free stress boundary conditions. The inverse problem is formulated and solved with numerical, iterative techniques. This leads to an optimal guess of the elastic anisotropy model and optimal estimates of the linear elastic constants (Zadler et al., 2004).

The measurement part of RUS, i.e., the measurement of the elastic resonance spectra, is fully non-destructive, thus enabling truly time-lapse investigations. For the MAGIC purposes, especially for supporting the formulation and validation of computational chemo-mechanical models, this is a unique advantage over micro- and nano-indentation techniques, which can be applied only to distinct specimens at distinct time points.

RUS can be practically implemented for specimens with a broad size range, namely from the cm scale, of interest in Section 2.3, down to the sub-mm scale. However, it is essentially not implementable at smaller scales due to technological limitations. Since RUS allows estimating only the bulk elastic moduli of the measured specimen, the specimen size determines the length scale at which such properties are quantified. This means that RUS can be used to estimate such mechanical properties starting from concrete's macroscopic and mesoscopic scales (ASTM C09 Committee, 2014; Payan et al., 2014; Di Bella et al., 2016) down to a length scale bridging the mesoscopic and microscopic ones, where, e.g., cement paste or mortars with fine aggregates can be investigated (Wu et al., 2010; Haecker et al., 2005). While RUS (in a simplified form) for the characterization of cement-based composites at the macro- and mesoscopic scales is already standardized since many decades (ASTM C09 Committee, 2014), its application for the same materials at the mm-scale and sub-mm scale has been more limited (Wu et al., 2010), mainly because of the need of producing cement paste specimens with size at such scales. Unless for basic research purposes, specimens at such scales are typically of less practical interest in concrete technology. Table 2-1 summarizes which RUS results at which length scales, for cement-based materials, have been reported in the literature.

Table 2-1*: Examples from the literature of estimates of linear elastic moduli of cement-based composites, obtained with Resonant Ultrasound Spectroscopy, with indications of specimen scale/size, composite type and study target*

Reference	Elastic moduli measured	Specimen scale/size and composite type	Study target
Haecker et al., 2005	Young's and shear moduli	Cement pastes	Validation of micromechanical models of cement pastes as composites
Wu et al., 2010	Young's and shear moduli	13.78×11.96×9.64 mm^3, cement paste	Validation of micromechanical models of cement pastes as composites
Chen et al., 2011	Bending modulus	25×25×275 mm^3, mortars	Alkali-silica reaction induced damage
Payan et al., 2014	Young's and shear moduli	100×100×60 mm^3, mortars and concretes	Damage due to thermal shocks
Di Bella et al., 2016	Young's modulus	40×40×160 mm^3, mortars	Early-age mechanical properties evolution due to drying shrinkage and cracking
Génoves et al., 2017	Young's modulus	40×40×160 mm^3, mortars	Damage due to sulfate attack

An extension of RUS, called Nonlinear RUS (NRUS), allows quantifying nonlinear elastic constants. From a computational modelling viewpoint, the latter parameters are of relevance only in deformation processes involving large (finite, e.g., > 10−4) strains. However, in the last three decades, it has been shown extensively and for a broad range of materials that nonlinear elastic constants are order of magnitudes more sensitive to microstructural changes, e.g., micro-cracking or local porosity changes, than linear ones. Thus, they have been exploited as damage proxy variables. The exploitation of NRUS

measurements for damage detection in concrete has occurred mainly at its macroscopic and mesoscopic scales and for a large variety of durability problems, such as carbonation (Bouchaala et al., 2011; Eiras et al., 2015) and sulphate attack (Genovés et al., 2015; 2017). However, NRUS measurements can be implemented also at the mm and sub-mm scales, where they would allow tracking, in a fully non-destructive and time-lapse way, the microstructural evolution of model cement pastes subjected to geological repository-relevant boundary conditions.

2.2.1.2 Nano-micro indentation measurements for cement application

Indentation (micro and nano) is an experimental technique commonly used for decades to extract the local elastic properties of materials (Oliver and Pharr, 2004). Basically, nano-micro indentation consists of making a contact between a sample and an indenter tip of known geometry and mechanical properties, followed by a continuously applied and recorded change in load, P, and depth, h. The analysis of the P-h curve proceeds by applying a continuum scale model to condense the indentation response into two indentation properties; indentation modulus, M and the indentation hardness H (Pharr and Oliver, 1992).

The high heterogeneity of cementitious materials implies that large grids of indentations are needed to estimate properly the mechanical properties of each inclusion (cement hydrates + other phases). The nano-indentation measurements have been mainly carried out on hardened cement paste to determine the elastic properties of hydrates and anhydrous phases (Ulm et al., 2007; Constantinides et al., 2006). At this scale, the response of the material corresponds to the compounds located at the surface in the indented zone. Thus, the indentation depth should be in adequation with the average size of the elementary components (Ulm et al., 2007; Constantinides et al., 2006; Luo et al., 2018). Most nanoindentation studies on hardened cement paste considered an indentation depth of between 200 and 300 nm (Brown et al., 2018; Kim et al., 2013; Hu and Li, 2015; Constantinides and Ulm, 2004; Chen et al., 2010; Zhu et al., 2007). Research has shown that the actual indenter-material interaction volume of a nanoindentation test is larger than the volume of the indenter that has penetrated into the tested material, and the interaction volume may be up to 1 μm^3 (Lura et al., 2011) requiring to have a careful post treatment analyse.

Besides the theory of nanoindentation testing is based on the assumption of an infinite half-space model, it furthermore assumes that the surface is perfectly flat and smooth (Miller et al., 2008). The sample preparation has significant effects on the nanomechanical properties obtained from nano-indentation tests. Miller et al. (2008), for instance, proposed a three-step sample preparation procedure to make the surface of a sample as flat as possible and limit the surface roughness.

A statistical analysis coupled with deconvolution methods is carried out with the grid nanoindentation data. The deconvolution steps are based on the experimental cumulative density function CDF (Brown et al., 2018; Randall et al., 2009) or probability PDF (Ulm et al., 2007; Lura et al., 2011; Constantinides and Ulm, 2007). The statistical analysis allows an estimation of the volume fraction of each constituent of the indented zone, provided the mechanical properties of the cement constituents are known, as detailed in the Table 2-2 (Ulm et al., 2007; Constantinides et al., 2006; Randall et al., 2009; Constantinides and Ulm, 2007, Bernachy-Barbe, 2019; Sasmal and Anoop, 2019). The robustness of this approach is controlled by the approximation made by chemical or mineralogical analyses allowing to cross chemical and mechanical data.

Table 2-2: Elastic moduli of individual cement and cement paste phases, taken from several sources in the literature

	Young Modulus (GPa)	Error Young Modulus (GPa)	Hardness (GPa)	Error Hardness (GPa)	References
C3S	135	7	8.7	0.5	(Velez et al., 2001)

C2S	130	20	8	1	(Velez et al., 2001)
C3A	145	10	10.8	0.7	(Velez et al., 2001)
C4AF	125	25	9.5	1.4	(Velez et al., 2001)
CH	40.3	4.2	1.31	0.23	(Constantinides and Ulm, 2007)
CSH_LD*	23.03	4.48	0.561	0.121	(Vandamme and Ulm, 2013)
CSH_HD*	31.35	3.84	0.812	0.131	(Vandamme and Ulm, 2013)
Aft	20.27	1	0.206	0.003	(Yang and Guo, 2014)
Afm	40.3	4.2	1.31	0.23	(Haecker et al., 2005)

*A difference is made between C-S-H LD (low density) and HD (high density) in agreement with the work of Tennis and Jennings (2000).

In micro-indentation testing, the load is always up to 10 mN to highlight the macroscopic behaviour of the indented zone (Oliver and Pharr, 2004). Recently, Xu et al. (2020) developed a model to determine the fracture properties based on micro-indentation techniques. The model was initiated by the fracture energy generated additionally that is assumed to be averagely distributed during indentation, and only involves the load–displacement curves that follow power functions. An explicit equation for estimating the plastic energy considering the effect of holding procedure that has not been considered before was established, which, together with the principle of energy balance, allows us to assess the fracture energy, energy release rate and fracture toughness of the HCP. The accuracy, reliability and robustness of the model were validated by the experimental data with changing the maximum load, loading speed and holding time. Overall, the micro fracture testing method developed here provides an efficient way to assess the fracture properties of cement-based materials in micro scale.

2.2.1.3 Nano-micro indentation measurements on degraded cementitious materials

Currently, no study exists on the micro-mechanical consequences of groundwater on cementitious materials. Therefore, several authors have investigated the impact of chemical degradation, such as leaching (Brown et al., 2018; Constantinides and Ulm, 2004; Gaitero et al., 2009), nitric acid (Muthu and Santhanam, 2018), or carbonation (Han et al., 2012) on the micro-mechanical behaviour of cementitious materials. These works highlight a non-negligible evolution of elastic mechanical properties of the cement matrix subjected to an aggressive solution. A significant decrease of the Young modulus is observed in the leached zone of a Portland cement paste due to the dissolution of portlandite combined with decalcification of C-S-H (Brown et al., 2018; Gaitero et al., 2009) (Figure 2-1).

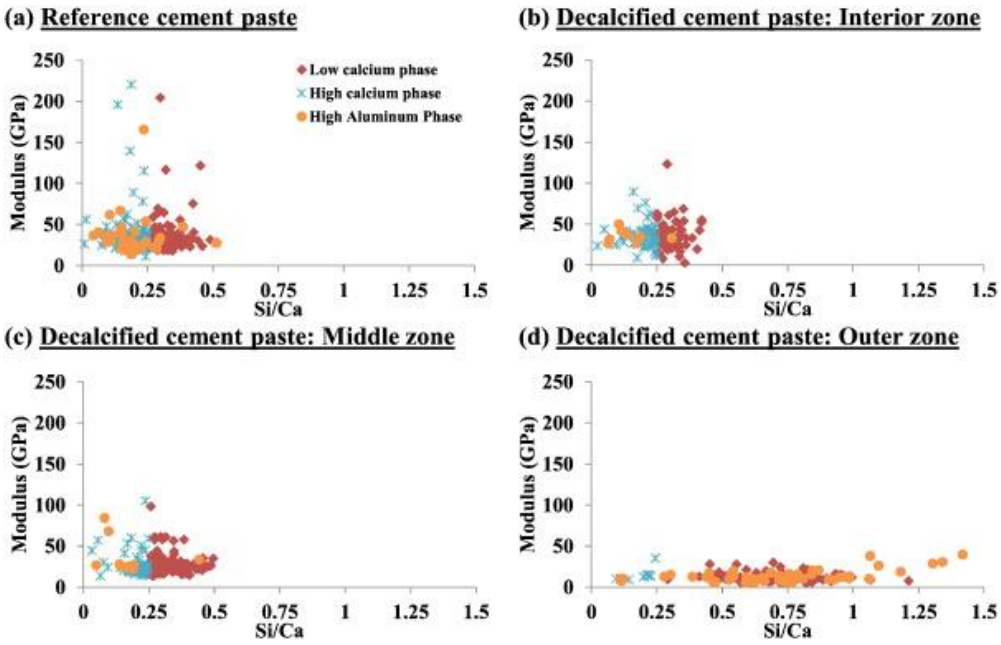

Figure 2-1: Indentation modulus vs. silicon to calcium (Si/Ca) ratio for the hydrates of the (a) the reference cement paste and the (b) interior, (c) middle, and (d) outer zone of the decalcified cement paste (Brown et al., 2018).

Indeed, as illustrated by the Figure 2-1, portlandite has a Young modulus equal to 40.3 GPa, its dissolution decreases necessarily the mechanical properties of the indented zone. In parallel, as demonstrated by Constantinides and Ulm (2004), high decalcified C-S-H has very low Young modulus, close to 2-3 GPa.

Previous works on the chemical impact of the groundwaters studied in MAGIC highlight decalcification of C-S-H and portlandite dissolution in the cement matrix (Dauzères et al., 2014; Dauzères et al., 2016; Lalan et al., 2019). Then, the decrease of mechanical properties due to the leaching would occur in combination with other unknow mechanisms.

The main challenge of this kind of study concerns the difficulty to obtain an acceptable surface roughness in the degraded zone (Constantinides et al., 2006). The significant change of mechanical properties between the sound and degraded zones further complicate the polishing steps for sample preparation (Miller et al., 2008).

Micro- and nano-indentation methods are on the other side limited in the number of mechanical properties which can be quantified (typically a single elastic modulus). They are also strongly affected, in the estimates they can provide, by viscoelastic processes, e.g., creep, in addition to be fully destructive methods, thus not allowing for time-lapse investigations.

As example of application, very useful results about chemo-mechanical effects were studied on smaller scale for C-(A)-S-H carbonation (Hay et al., 2022). Authors show that nanoindentation, high-pressure XRD, and atomic force microscopy can be used to probe the micro and nanomechanical properties of C-(A-)S-H, whose nanostructure can be described as colloids of globules containing solid C-(A-)S-H, pores and water. Moreover, nanoindentation is able to capture the aggregate effects of the solid C-(A-)S-H and pores.

2.2.2 Modelling approaches and key results

LaMcube

For the work developed by LaMcube on multi-scale modelling, analytical homogenization techniques are used to formulate the macroscopic strength criteria by considering different scales. For the sake of consistency, a single synthesis is presented below (section 2.3.2).

CEA

Regarding the modelling and simulation aspects, many studies have been devoted to the analysis and description of the evolution of the microstructure and mechanical properties of cementitious materials when subjected to the contact of groundwater and argillite (Heukamp et al., 2001; Dauzeres et al., 2010; Sarkar et al., 2010). At the nano-microscale, the different minerals (phase assemblage) composing the hydrated cement paste should in principle be considered. Indeed, they have different mechanical properties and react differently depending on the ionic species that migrate within the porosity. From this viewpoint, while mechanical properties of most mineral phases can be considered as relatively well known, the description of C-S-H phase and modelling of its associated properties and evolution upon exposure to solution containing different species remains challenging. At the nanoscale, the use of approaches based on molecular dynamics is widely accepted to this aim, see e.g. (Pellenq et al., 2009; Fan and Yang, 2018); however, the corresponding simulations require generally a huge computation time. These approaches allow in particular estimating the Young's modulus, strength and fracture energy of C-S-H, and predicting the effects of water on C-S-H behaviour and its related volume changes, see e.g. (Abdolhosseini Qomi et al., 2021).

At the microscale, as an alternative to macroscopic empirical laws fitted on experimental data to describe the impact on the mechanical properties of degradation phenomena related to the geological disposal environment, as for instance calcium leaching, e.g. (Gérard et al., 1998; Le Bellégo et al., 2003), more advanced and versatile methods have been developed to estimate these properties. Analytically, the application of micromechanics and upscaling techniques turns out to be particularly well adapted in this context to estimate the mechanical and diffusive properties, based on more or less simplified representations of the microstructure. Classical schemes such as the Mori-Tanaka method provide good estimations of mechanical properties, though the microstructure of cement paste and mortar, whose morphology is of the matrix/inclusion type, contains an important volume fraction of particulate phase (greater than 50 %). Thus, many studies have been devoted to investigate the evolution of mechanical properties of cementitious materials by means of micromechanical approaches in different contexts including hydration, viscoelasticity (creep) and chemical attack, see e.g. (Bernard et al., 2003; Constantinides and Ulm, 2004; Pichler et al., 2007; Bary, 2008; Scheiner and Hellmich, 2009; Esposito and Hendriks, 2016). More recently, such approaches have been extended to the estimation of strength, see for instance (Königsberger et al., 2014; Königsberger et al., 2018). Note that in addition to mechanical properties, diffusive properties may also be estimated by applying similar upscaling techniques, see e.g. (Stora et al., 2008; Stora et al., 2009; Gu at al., 2022). The homogenization schemes that reveal more adapted to the diffusive properties are in general different from the ones applied for mechanical properties. This is mainly due to the fact that (1) the key characteristics of the pore phase responsible for the diffusive phenomena are its connectivity and associated tortuosity, and (2) the properties contrast between this pore phase and the solid ones is infinite since the hydrated products are non-diffusive (diffusivity of the C-S-H phase is related to its nanoporosity).

On the other hand, the recourse of numerical approaches to determine the mechanical behaviour of cementitious materials has gained growing interests in recent years, due to the continuous increase of computational power. Different numerical methods have been applied to investigate the mechanical response of samples representative of the studied materials. The most popular ones are the finite element method (FEM), the discrete element method (DEM) and the fast Fourier transform (FFT), see e.g. (Camborde et al., 2000; Principallo et al., 2003; Sun et al., 2007; Dunant and Scrivener, 2010; Escoda et al., 2011; Bernard and Kamali-Bernard, 2015). These methods rely on numerical samples constructed from an appropriate representation of the microstructure, which can be either generated numerically or obtained from the real microstructure characterized e.g. by image analysis from X-CT scans (Bernachy-Barbe and Bary, 2019). The behaviour of the material is then computed by imposing classical boundary conditions on the sample borders. The advantages of the numerical methods over

analytical ones based on micromechanical approaches are that there are generally much less limitations regarding the shapes and sizes of the different particle phases. Besides, various aspects as the mechanical interactions between the inclusions, the effect of respective arrangement of phases (multicomponent phases) and of interfaces between some inclusions and the matrix (ITZ – interfacial transition zone) are much better captured than with purely analytical procedures. The description of the initiation and propagation of microcracks and their impact on the effective properties are also deemed to be much more accurate with 3D simulations, although this aspect remains computationally challenging. This is related to the inherent complexity of modelling and numerically representing microcracks satisfactorily (different approaches have been developed to this aim; their description is beyond the scope of this section, see e.g. (Nguyen et al., 2015; Naderi et al., 2021 for several illustrations). The main drawback of 3D numerical determination of properties compared to analytical estimations is the much larger computational resources and simulation time required. Note that recently several methods relying on machine learning techniques, whose basic idea is to replace the initial problem by a simplified one, have been deployed to limit the computation time, see e.g. (Bock et al., 2019).

Whether analytically or numerically, the characterisation of the mechanical properties of cementitious materials necessitates the knowledge of the evolution of the microstructure and corresponding phase assemblage of the cement paste in the context of disposal environment. This means that to investigate accurately the mechanical response, a coupled approach with a chemical model describing the hydration product changes should be developed. Again, several methods and models have been proposed in the literature for this purpose. The most simple ones consider only a limited set of ionic species for defining the chemical state of the system, together with simplified chemical reactions, see (Tixier and Mobasher, 2003; Bary, 2008; Idiart et al., 2011; Cefis and Comi, 2017) for illustrative examples regarding the modelling of sulphate attack in cementitious materials. More sophisticated approaches are based on a direct coupling between a reactive transport code and a code dedicated to solve the mechanical problem (Stora et al., 2009; Bary et al., 2014; Nardi et al., 2014; Deng et al., 2016; Socié et al., 2021). Such methods allow describing accurately the time evolution of (1) the microstructure considering the appropriate chemical reactions and related diffusion of species, (2) the effects of the microstructure changes including microcracking development on the mechanical (and diffusive) properties, and (3) the impact of possible expansion or shrinkage phenomena, as for instance in the case of differed ettringite formation, desiccation and carbonation shrinkage of C-S-H, etc. Besides, using a reactive transport code extends significantly the application domains of the coupled approaches. Indeed, as the phase assemblage composing the hardened cement paste and the related chemical reactions and diffusion of species in pore solution are described realistically, it makes it possible to simulate the behaviour of the materials upon various chemical exposures and configurations. However, an important limitation of these numerical methods is the computation resources and time required. Moreover, the formulation of the mechanical and reactive transport problems generally necessitate the development of specific algorithms to solve them, independently of the coupled problem. For instance, nonlinear mechanical problems are commonly solved by the finite element methods with iterative procedures based on Newton methods, while the well-known Picard or 'fixed point' method is usual for solving the system of mass conservation equations describing the transport. Note that the modelling and simulation of cracking at the microscale face the same numerical difficulties as at the meso or macroscale, and similar approaches may be applied depending on the adopted numerical methods for calculating the mechanical behaviour. Whatever the scale considered, an accurate description of the microcracking and its repercussions on both mechanical and diffusive properties is essential to the simulation of the coupled response of cementitious materials. This topic is beyond the scope of the present subsection, and should be addressed specifically as many methods and approaches exist to model its initiation, propagation etc.

2.3 Mechanical behaviour of concrete at the meso/macroscale exposed to geological disposal environments

2.3.1 Experimental developments and key results

Based on the D16.3: LMDC (Th. Vidal), ANDRA (O. Helson) COVRA (E. NEEFT)

2.3.1.1 Leaching and reinforcement corrosion and their consequences on mechanical properties

Many authors have studied the influence of chemical degradation on the mechanical behaviour of cementitious materials (Carde and François, 1996; Gérard, 1996; Gerard et al., 1998; Le Bellégo et al., 2001; Ulm et al., 2002). The overlying principle of these studies was to evaluate the mechanical behaviour of samples that had previously been subjected to chemical attacks. In order to identify this influence, it is necessary to carry out tests establishing the behaviour of cementitious materials that have undergone quantifiable chemical degradation. For instance, the kinetics of leaching with pure water is relatively slow, so it is necessary to accelerate the process by using an ammonium nitrate solution. The accelerated leaching test amplifies the kinetics of decalcification without modifying general form of the portlandite profile. Only the depth of decalcification is higher with ammonium nitrate solution at a same date. The results will remain analogous to those obtained in decalcification condition with pure water, which allows studying the consequences of decalcification on mechanical behaviour and physical properties. This type of test is thus used to characterise the influence of the chemical alteration factor and the chemical degradation time on the mechanical behaviour and physical properties of concretes.

Goncalves and Rodrigues (1991) examined the influence of chemical attack with ammonium nitrate (NH_4NO_3) solution for different concentrations (0, 0.0625, 0.625 and 6.25 mol/l) on the mechanical strength of mortar-based samples (W/C = 0.5). After many years of study, the authors have shown that a higher concentration of the aggressive solution reduces more the residual strength of the sample in compression or bending. They also showed that Portland cement-based mortar had lost about 90% of its compressive and tensile strength after fourteen years of leaching with a concentration 6.25 mol/l of ammonium nitrate solution.

Gérard (1996) analysed the influence of leaching of the cement type by using microhardness measurements. The microhardness loss of a previously leached material is related to the loss of calcium in the solid phase. Then, the relationship between Young's modulus of the material and the calcium concentration in solution is established through the evolution of the microhardness as a function of the calcium concentration in solution (Figure 2-2).

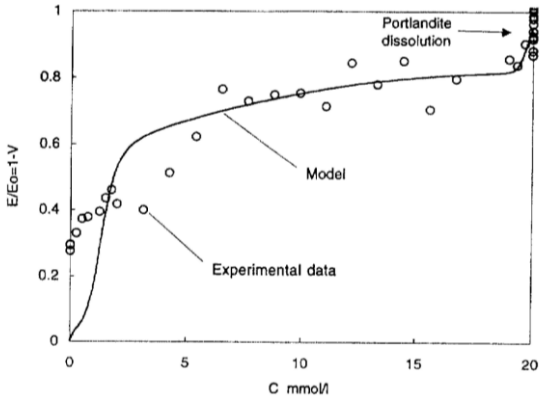

Figure 2-2: Evolution of Young's modulus as a function of the calcium concentration in the liquid phase (Gérard, 1996)

This result shows that the dissolution of portlandite causes a drop in Young's modulus. When all portlandite is dissolved, Young's modulus continues to decrease with the progressive dissolution (and decalcification) of the other hydrates. Thus, contrary to carbonation, leaching mechanically damages concrete.

Nguyen (2005) determined the evolution of compression strength as a function of degradation rate for hollow cylinders attacked on the outer and inner surfaces (Figure 2-3a) and solid cylinders attacked on the outer surfaces (Figure 2-3b).

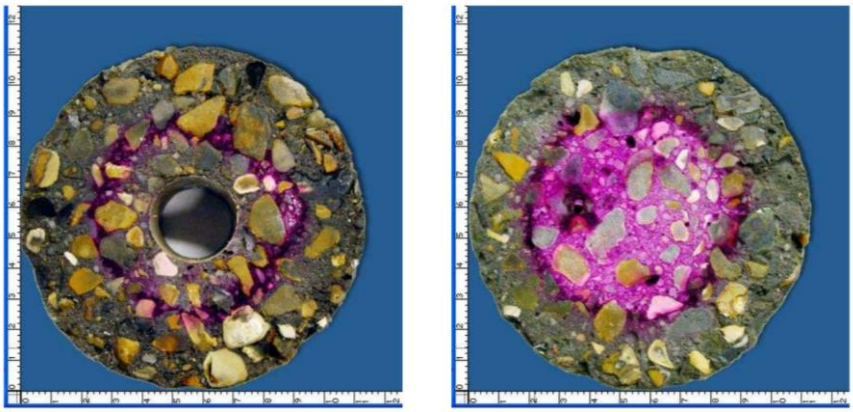

(a) Hollow cylinder (b) Solid cylinder

Figure 2-3: Degradation depth after 153 days of accelerated leaching with NH_4NO_3 solution 6M (Nguyen, 2005).

A strong decrease in compressive strength can be observed at the beginning of chemical degradation. This decrease then stabilizes as the concrete degrades (Figure 2-4). The compressive strength of the degraded concrete is equal to 24% of the strength of the sound concrete.

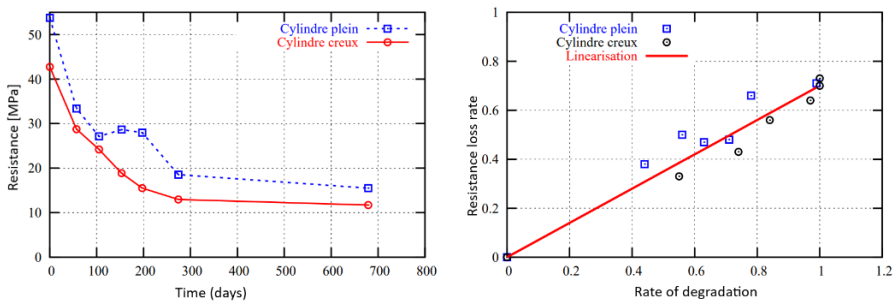

Figure 2-4: Evolution of compressive strength as a function of degradation (Nguyen, 2005).

The results achieved by Nguyen (2005) show that the increase in the rate of chemical degradation leads not only to a decrease in the compressive strength and in elastic modulus, but also to an increase in ductility characterized by a higher ultimate deformation (Figure 2-5). The behaviour of concrete becomes more and more ductile as it degrades. Babaahmadi et al (2015) investigated the effects of leaching on concrete mechanical behaviour using an accelerated method based on electrical migration to faster transport of calcium ions. Two types of concretes with W/C of 0.48 and 0.62 were tested. Splitting tensile strength were reduced by up to approximately 70 % and 55 % for W/C of 0.48 and 0.62 respectively. The effect on compressive strength was rather similar with a decrease of 70 % and 59 % for W/C of 0.48 and 0.62 respectively. The Young's modulus decreased by 40% for both concretes.

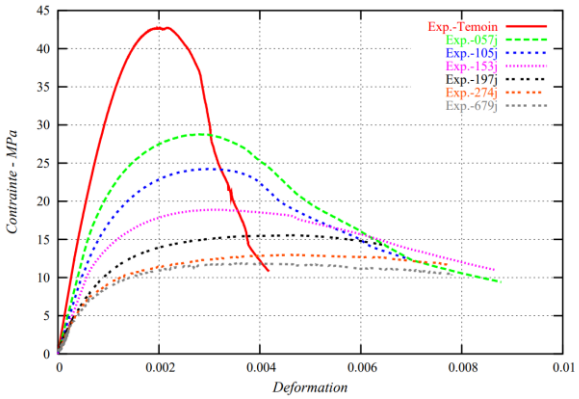

Figure 2-5: The stress-strain curves of the compression test at different chemical degradation stages (Nguyen, 2005).

Some studies have also investigated the behaviour of concrete under creep test in compression coupled with accelerated leaching (Nguyen et al., 2007; Torrenti et al., 2008; Sellier et al., 2011). Figure 2-6 presents the results of the compression creep test during leaching obtained by Sellier et al. (2011). It was shown that the creep kinetics increases in the leached concrete. There is, therefore, a strong coupling between chemical degradation and creep.

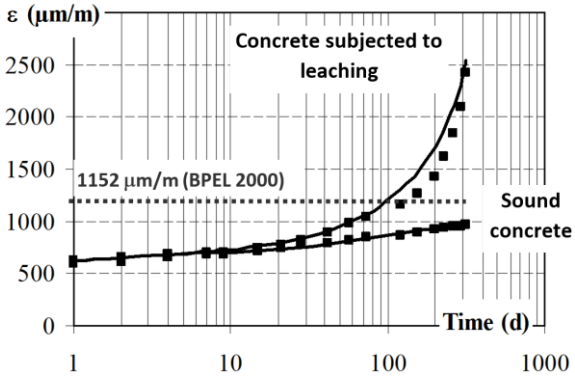

Figure 2-6: Evolution of creep curves for the sound concretes and leached ones (Sellier et al., 2011).

When the concrete is leached, the dissolution of portlandite and the other hydrates modifies the microstructure of the cement paste. Camps (2008) studied the evolution of physical properties for concrete specimens with different types of cement attacked with NH_4NO_3 solution to accelerate the leaching process. The evolution of the leached calcium for the different types of cement is shown in Figure 2-7. CEM IF and CEM VF refer respectively to fibre-reinforced concrete containing silica fume for CEM I-based concrete and for CEM V-based concrete. The W/C ratio of these concretes mixes equal to 0.40.

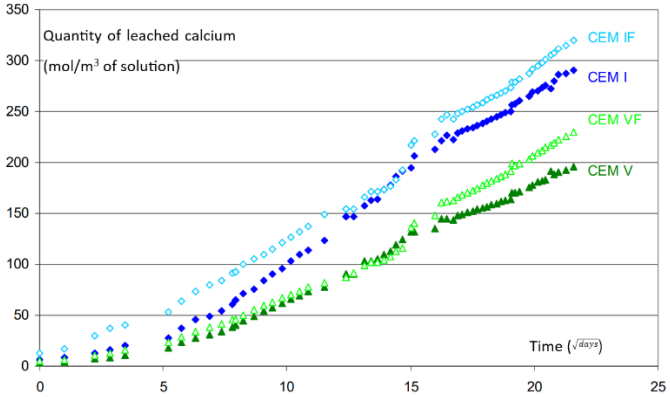

Figure 2-7: Evolution of leached calcium quantity as a function of square root of time (Camps, 2008).

The values of porosity and permeability measured by Camps (2008) are shown in Table 2-3, with T_0 corresponding to the date of immersion (around 80 days after casting). The average porosity accessible to water increases by about 30% during the first nine months of accelerated leaching. This increase is due to consumption of portlandite and the partial decalcification of C-S-H. In the case of CEM I, the portlandite content available for degradation is larger, leading to a greater increase in porosity between 9 and 18 months. For CEM V the porosity increases by about 10% between 9 and 18 months. For CEM IF and CEM VF, the increase between 9 and 18 months is therefore due to the progressive decalcification of C-S-H.

Table 2-3: Evolution of physical properties in sound specimen at T_0 and after 9 and 18 months of decalcification

	T_0			T_0+9 months			T_0+18 months		
	Porosity %	**Permeability ($x10^{-17}$ m²)**	**D_{Cl-} ($x10^{-12}$ m²/s)**	**Porosity %**	**Permeability ($x10^{-17}$ m²)**	**D_{Cl-} ($x10^{-12}$ m²/s)**	**Porosity %**	**Permeability ($x10^{-17}$ m²)**	**D_{Cl-} ($x10^{-12}$ m²/s)**
CEM I	12.3 ± 0.3	4.0	8.5 ± 1.9	16.1 ± 0.3	-	95 ± 6	20.4 ± 0.3	21.0	96 ± 20
CEM IF	12.8 ± 0.2	5.0	2.2 ± 1.2	17.4 ± 0.4	-	50 ± 10	19.2 ± 0.2	21.0	85 ± 6
CEM V	14.4 ± 0.3	5.5	2.0 ± 0.3	18.2 ± 0.1	-	57 ± 15	19.5 ± 0.2	17.2	132 ± 6
CEM VF	12.5 ± 0.2	5.0	2.0 ± 1.1	-	-	54 ± 16	19.9 ± 0.1	16.8	116 ± 17

As the modification of the microstructure by leaching leads to an increase in porosity and pore size, the permeability is also higher in the degraded zone (T_0+18 months). The influence of fibres on permeability has not been quantified in these concrete specimens due to the presence of silica fume. Either the fibres have no influence, or the influence is compensated by the silica fume. The diffusion coefficients have been measured and are shown in the Table 2-3. Diffusivity is related to the pore network, tortuosity and connectivity of pores. These different characteristics are influenced by the cement and the pozzolanic additives it contains. After nine months, the diffusivity of CEM I is about 11 times higher, while for the other three compositions the value is about 25 times higher. Indeed, the measured diffusion coefficient between 9 and 18 months are identical for CEM I, while for the other compositions, the diffusion coefficients have continued to increase.

2.3.1.2 Corrosion of steel reinforcements

In reinforced concrete, corrosion causes mechanical damage to the concrete under the combined effect of the corrosion-induced expansion (generating internal mechanical stresses) and the loss of cross-sectional area and bonding of the steel, which causes the structure to lose its load-bearing capacity.

In "classical" civil engineering, when the diffusion front of the aggressive agents (typically CO_2 and/or Cl) reaches the reinforcement, the steel is considered depassivated and the corrosion starts in a so-called "active" mode. For the reinforced concrete components of Cigéo, the scenario envisaged is mechanical damage to the concrete due to the growth of the oxide layer in the passive state.

In a cementitious environment, the steel is maintained in a passive state thanks to the high pH of the the porewater. Corrosion rates are then less than 1 µm.yr^{-1} (Tuutti, 1982). However, the impact of

corrosion is not negligible because of the multi-millennial time scales involved. Even at a particularly low speed, which is of no consequence on the scale of a few tens to hundreds of years, the growth on multi secular to multi millennial time scales could cause mechanical damage (cracking).

The microstructure and elastic properties of corrosion products in cement (micro-indentation, Raman spectroscopy, optical microscopy) were determined under accelerated conditions in the laboratory and on samples from monuments aged between 50 and 660 (in an ancient ferrous artefact) years (Dehoux et al., 2015). The results highlighted the heterogeneity of the corrosion product layers and the evolution of the mechanical properties of the layers with time and ageing conditions. A realistic modelling scenario should consider a modulus of elasticity close to 1 GPa for corrosion products as in conventional civil engineering (considered between 0.5 and 1 GPa). However, given the time scales considered for Cigéo, an increase in the modulus of elasticity up to 30 GPa in the very long term should be considered.

2.3.2 Modelling approaches and key results

LaMcube (J. Shao, W. Shen)

Cement-based materials are characterized by complex and multiscale micro-structures. Their macroscopic mechanical behaviour is intimately influenced by the micro-structural composition and evolution. When subjected to chemical degradation processes, for instance leaching and carbonation, the macroscopic mechanical properties, in particular elastic modulus and strength, can be significantly modified. In classical phenomenological approaches, different types of empirical relations are determined based on extensive laboratory data. Such models do not provide explicit relationships between the macroscopic properties and micro-structural changes. Therefore, they are not predictive models. Therefore, their predictive capacity is limited.

During the last decades, significant efforts have been devoted to the development of multi-scale models based on various upscaling techniques for modelling the basic mechanical behaviour of cement-based materials and the consequences of chemical degradation. The main objective here is to first establish explicit (analytical) relations between the key micro-structural parameters and mechanical properties (elastic tensor, strength criterion) and then to interpret the effects of chemical degradation in terms of evolution of such micro-structural parameters.

There are a high number of works reported on the multi-scale modeling of concrete materials by using different upscaling approaches including analytical and numerical homogenization techniques. Without intending to give an exhaustive review, we summarize only some recent representative works. Considering the CO2 ingression, the effects of damage on concrete carbonation were investigated in a number of works (Jiang et al., 2015; Pan et al., 2018; Jiang et al. 2018; Metalssi et al., 2002) by taking the residual strain as an indicator to evaluate damage evolution. The coupled carbonation-porosity-moisture transfer of concrete is investigated in (Metalssi et al., 2002). A system of mass conservation equations representative of coupled phenomena has been developed. A three-dimensional lattice type model was developed in (Pan et al., 2018) to simulate the concrete carbonation at the meso-scale. To construct the meso-scale concrete model, the 3D reconstruction technique was applied to obtain the shape of real coarse aggregates. In the work (Bao et al., 2019), a novel mathematical model was proposed to simulate random distribution of coarse aggregates in concrete and a new supercritical carbonation model was developed to study the effect of randomly distributed coarse aggregates and porosity on the irregularities of carbonation depth of concrete. A mathematical model describing the diffusion of carbon-dioxide in concrete with considering the effect of concrete carbonation was presented in (Li et al. 2020). The effect of concrete carbonation on carbon-dioxide diffusion was considered by using a sink term added in the diffusion equation. The influence of high temperature heating for carbonation was studied in (Iwama et al., 2022). And a multi-scale thermo-chemo-physics model has been proposed for the description of carbonation, decarbonation and re-carbonation processes during and after high-temperature heating.

For the sake of illustration, we shall present below some examples of multiscale modeling performed by the LaMcube team by using the analytical homogenization method. Indeed, these previous works will serve as the starting point of the works to be done in the present project.

In this synthesis, the emphasis is put on two widely encountered chemical processes in cement-based materials, calcium leaching (or lixiviation) and carbonation. Based on extensive laboratory studies, the main consequences of calcium leaching and carbonation can be summarized as follows.

As mentioned in Section 1.1, the main chemical process of carbonation is the production of solid calcite. Among others, the key significant and easily measurable micro-structural change is the reduction of porosity. At the same time, there is also a decrease of pore size, as illustrated in 1-4. As a consequence of carbonation on macroscopic mechanical properties, it is widely observed that there is a significant increase of elastic modulus and failure strength. In Figure 2-8, on can see the evolution of peak strength in triaxial compression tests with different values of confining stress. Based on the classical Mohr-Coulomb criterion, it is found that both the cohesion and friction angle of concrete are enhanced by the carbonation process (Takla, 2010; Takla et al., 2011). At the same time, the mechanical behaviour of carbonated material is generally more brittle than the sound one.

Due to material heterogeneity, micro-cracking is sometimes another important consequence of carbonation. There is a competition between hardening and cracking due to carbonation on macroscopic mechanical properties (micro-cracking leads to a decrease of elastic modulus and failure strength). (Takla, 2010; Takla et al., 2011; Cheng et al., 2016; Auroy et al., 2018; Al-Ameeri et al., 2021).

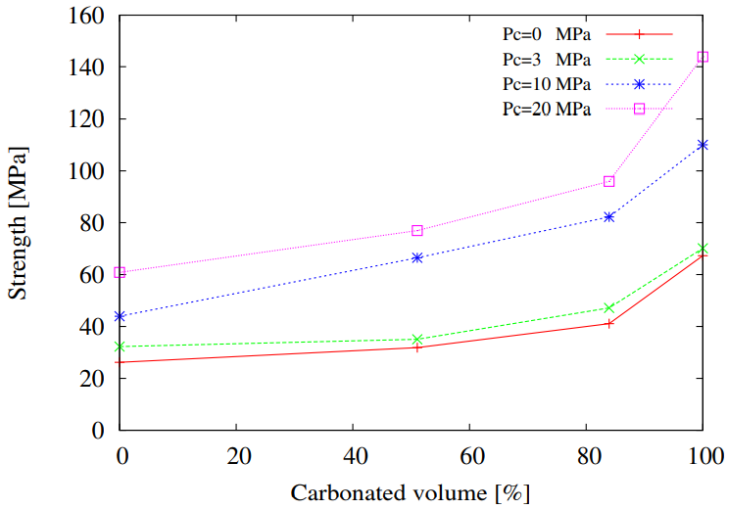

Figure 2-8: Evolution of deviatoric failure stress with carbonation ratio during triaxial compression tests of concrete (Takla, 2010; Takla et al., 2011)

About the chemical calcium leaching, the main micro-structural change is the increase of porosity due to the dissolution of solid portlandite. As a consequence, there is a significant decrease of elastic modulus and failure strength, as shown in Figure 2-9 and Figure 2-10, respectively. The leaching process decreases both the cohesion (related to the strength under uniaxial compression) and friction angle of material (related to the slope of strength line).

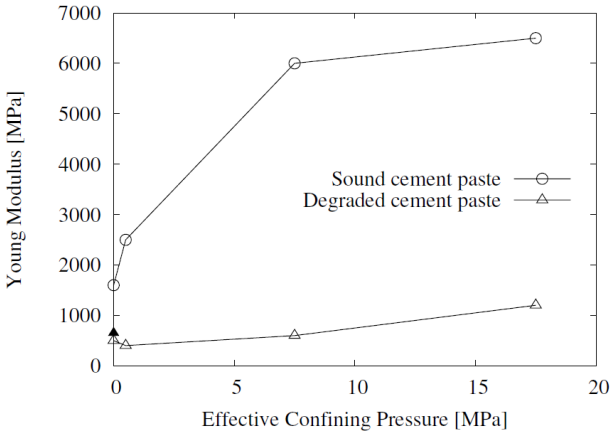

Figure 2-9: Diminution of elastic modulus of cement paste due to chemical leaching in triaxial compression tests (Yurtdas et al., 2011)

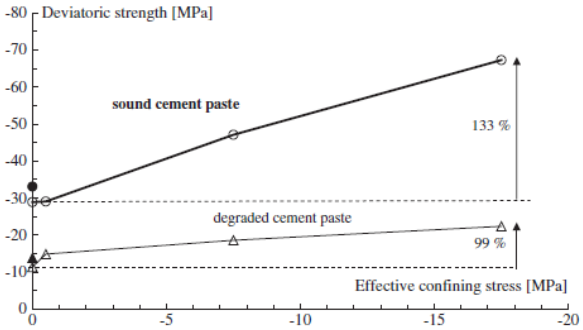

Figure 2-10: Diminution of deviatoric failure stress of cement paste due to chemical leaching in triaxial compression tests (Yurtdas et al., 2011)

Analytical homogenization-based multi-scale modelling

The main objective is to develop analytical models which are able to provide explicit relations between micro-structural compositions and macroscopic mechanical properties and then to describe their evolution due to chemical degradation. For this purpose, some significations on micro-structural representation and description are necessary.

In general, three representative scales are selected: nano-micro, micro-meso and meso-macro. Depending on the related sizes of pores (mainly capillary pores) and calcite grains, two different representations can be adopted, as shown in Figure 2-11. In the first case, it is assumed that the capillary pores are larger than the calcite particles, while the second case considers the opposite situation.

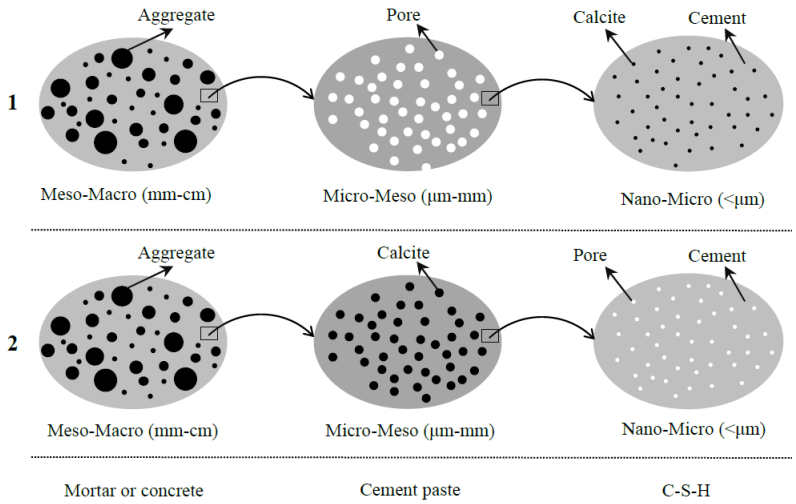

Figure 2-11: Two typical micro-structural representations of concrete materials (Ghorbanbeigi, 2014)

On the other hand, the choice of micro-structural parameters used in the description of chemical degradation process is also simplified. Only two basic parameters are retained, namely the porosity and volume fraction of solid calcite particles. Therefore, the consequence of carbonation is characterized by the increase of calcite volume fraction and the decrease of porosity. On the contrary, the micro-structural change due to leaching is simply described by the increase of porosity.

The methodology adopted here is as follows. We shall first establish the analytical expressions of macroscopic elastic properties and strength criterion of concrete explicitly as functions of calcite fraction, porosity and aggregate volume fraction. Then, the consequences of chemical processes are naturally described by the variations of porosity and calcite volume fraction.

This is done by performing three steps of homogenization. Consider the micro-structural representation 1 (Figure 2-11). The first step of homogenization is completed by considering the effect of calcite particles at the nano-micro scale. The influence of pores is taken into account in the second step of homogenization at the micro-meso scale. Finally, at the third step, the effect of large aggregates is included at the meso-macro scale. These steps of homogenization are illustrated in Figure 2-12. The porosity (f) and volume fractions of calcite (ρ_c) and aggregates (ρ_a) are defined as follows (Ghorbanbiegi et al., 2016):

$$\rho_c = \frac{\Omega_c}{\Omega_s + \Omega_c}, \quad f = \frac{\Omega_p}{\Omega_s + \Omega_c + \Omega_p}, \quad f = \frac{\Omega_a}{\Omega_s + \Omega_c + \Omega_p + \Omega_a} \tag{2-1}$$

$\Omega_s$is the volume of solid cement paste, $\Omega_c$the volume of calcite particles, $\Omega_p$the volume of pores and $\Omega_a$the volume of aggregates.

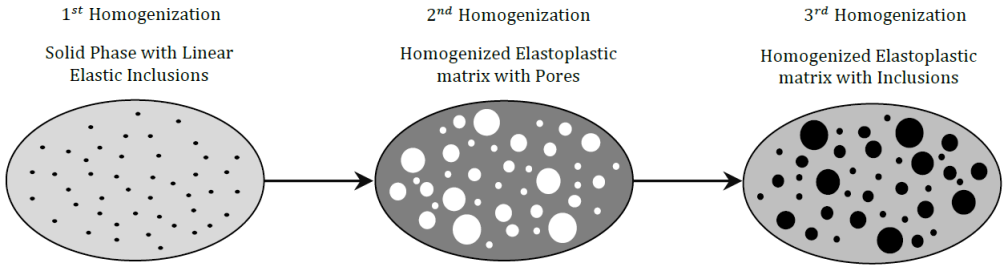

Figure 2-12: Illustration of three steps of analytical homogenization

Due to the matrix-inclusion morphology, the classical Mori-Tanaka (1973) scheme is used for the homogenization of elastic properties. By assuming an isotropic behaviour, the effective elastic properties obtained respectively from the three steps of homogenization are summarized below.

First step:

At this step, the effective elastic bulk and shear moduli κ_{mi}, μ_{mi} of the calcite reinforced cement paste is determined and given as follows.

$$\kappa_{mi} = \frac{\frac{\rho_c \kappa_c}{3\kappa_c + 4\mu_s} + \frac{(1-\rho_c)\kappa_s}{3\kappa_s + 4\mu_s}}{\frac{\rho_c}{3\kappa_c + 4\mu_s} + \frac{(1-\rho_c)}{3\kappa_s + 4\mu_s}}$$

$$\mu_{mi} = \frac{\frac{\rho_c \mu_c}{\mu_s(9\kappa_s + 8\mu_s) + 6\mu_c(\kappa_s + 2\mu_s)} + \frac{(1-\rho_c)\mu_s}{\mu_s(9\kappa_s + 8\mu_s) + 6\mu_s(\kappa_s + 2\mu_s)}}{\frac{\rho_c}{\mu_s(9\kappa_s + 8\mu_s) + 6\mu_c(\kappa_s + 2\mu_s)} + \frac{(1-\rho_c)}{\mu_s(9\kappa_s + 8\mu_s) + 6\mu_s(\kappa_s + 2\mu_s)}} \tag{2-2}$$

κ_s, μ_s are the bulk and shear moduli of solid cement paste, and κ_c, μ_c are those of calcites particles.

Second step:

The second step is devoted to determine the effective elastic moduli of porous cement paste κ_{mp}, μ_{mp}, by taking into account the effect of porosity f. One gets:

$$\kappa_{mp} = \frac{4(1-f)\kappa_{mi}\,\mu_{mi}}{4\mu_{mi} + 3f\,\kappa_{mi}}; \quad \mu_{mp} = \frac{(1-f)\mu_{mi}}{1 + 6f\,\dfrac{\kappa_{mi} + 2\mu_{mi}}{9\kappa_{mi} + 8\mu_{mi}}} \qquad 2\text{-}3$$

The values of κ_{mi}, μ_{mi} are determined at the first step.

Third step:

Finally, the macroscopic elastic moduli of homogenized equivalent material, $\kappa^{\hom}, \mu^{\hom}$ are determined at this step by considering the effect of aggregate at the mesoscopic scale. And one obtains:

$$\kappa^{\hom} = \frac{\dfrac{\rho_a \kappa_a}{3\kappa_a + 4\mu_{mp}} + \dfrac{(1-\rho_a)\kappa_{mp}}{3\kappa_{mp} + 4\mu_{mp}}}{\dfrac{\rho_a}{3\kappa_a + 4\mu_{mp}} + \dfrac{(1-\rho_a)}{3\kappa_{mp} + 4\mu_{mp}}}$$

$$\mu^{\hom} = \frac{\dfrac{\rho_a \mu_a}{\mu_{mp}(9\kappa_{mp} + 8\mu_{mp}) + 6\mu_a(\kappa_{mp} + 2\mu_{mp})} + \dfrac{(1-\rho_a)\mu_{mp}}{\mu_{mp}(9\kappa_{mp} + 8\mu_{mp}) + 6\mu_{mp}(\kappa_{mp} + 2\mu_{mp})}}{\dfrac{\rho_a}{\mu_{mp}(9\kappa_{mp} + 8\mu_{mp}) + 6\mu_a(\kappa_{mp} + 2\mu_{mp})} + \dfrac{1-\rho_a}{\mu_{mp}(9\kappa_{mp} + 8\mu_{mp}) + 6\mu_{mp}(\kappa_{mp} + 2\mu_{mp})}} \qquad 2\text{-}4$$

κ_a, μ_a are the bulk and shear moduli of aggregates.

The macroscopic strength criterion of concrete is also established by three steps of nonlinear homogenization. The so-called modified secant method (or equivalently variational approach) is here adopted (Maghous et al., 2009; Shen et al., 2013). For this purpose, both the calcite particles and aggregates are assumed to exhibit a linear elastic behaviour. The solid cement paste has an elastic-plastic one. The plastic behaviour of cement paste is described by a Drucker-Prager type linear criterion. After the first homogenization step, one gets the following plastic criterion of the reinforced cement paste by the calcite particles:

$$\varphi^{si} = \tilde{\sigma}_d + \tilde{T}(\tilde{\sigma}_m - h) = 0; \quad \tilde{T} = T\sqrt{\frac{1 + \dfrac{3}{2}\rho_c}{1 - \dfrac{2}{3}\rho_c T^2}} \qquad 2\text{-}5 \quad 2\text{-}6$$

$\tilde{\sigma}_m, \tilde{\sigma}_d$ are respectively the mean and deviatoric stresses in the reinforced cement paste at the nano-micro scale. T is the frictional coefficient of sound (not reinforced) cement paste and h its hydrostatic tensile strength.

After the second homogenization step, the effective strength criterion of porous cement paste is obtained and given in the following form:

$$\varphi^{mp} = \frac{1+\frac{2}{3}f}{\tilde{T}^2}\tilde{\Sigma}_d^2 + \left(\frac{3f}{2\tilde{T}^2}-1\right)\tilde{\Sigma}_m^2 + 2(1-f)h\tilde{\Sigma}_m - (1-f)^2h^2 = 0 \qquad 2\text{-}7$$

$\tilde{\Sigma}_m, \tilde{\Sigma}_d$ are the mean and deviatoric stresses of the homogenized porous cement paste at the micro-meso scale.

Finally, after completing the third homogenization step, one gets the following macroscopic strength criterion of concrete materials (Ghorbanbeigi et al., 2016; 2017):

$$F = \frac{\frac{1+\frac{2}{3}f}{\tilde{T}^2} + \frac{2}{3}\rho_a\left(\frac{3f}{2\tilde{T}^2}-1\right)}{\frac{4\tilde{T}^2-12f-9}{6\tilde{T}^2-13f-6}\rho_a+1}\Sigma_d^2 + \left(\frac{3f}{2\tilde{T}^2}-1\right)\Sigma_m^2 + 2(1-f)h\Sigma_m - \left(\frac{3f\rho_a}{3+2f}+1\right)(1-f)^2h^2 = 0$$

2-8

Σ_m, Σ_d are the macroscopic mean and deviatoric stresses on the equivalent homogenized medium (EHM). It is clear that the macroscopic strength of concrete is explicitly dependent of the calcite particles, porosity and aggregates.

Main results:

Based on the homogenized macroscopic strength criterion above and taking into account the evolution of porosity and calcite particle fraction, the macroscopic strength envelops of concrete samples subjected to different ratios of carbonation are predicted and compared with experimental measurements. An example of results is presented in Figure 2-13 (Ghorbanbeigi et al., 2016; 2017; Takla et al., 2011). It is also possible to evaluate the evolution of strength with carbonation time. In Figure 2-14, one can see the evolution of uniaxiale compression strength with carbonation time (Chang et Chen., 2005; Ghorbanbeigi et al., 2016; 2017). There is a very good agreement between analytical predictions and experimental data.

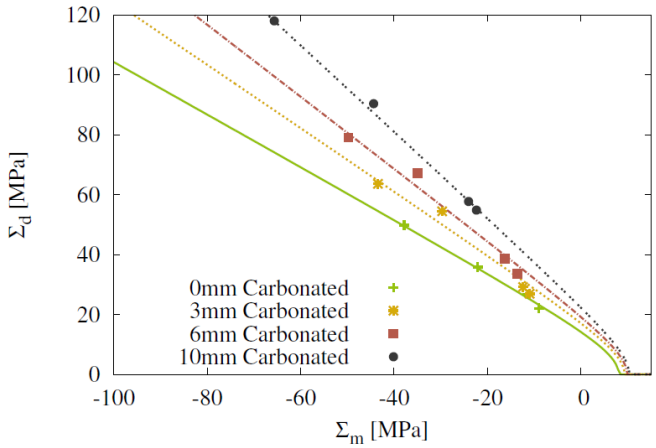

Figure 2-13: Failure envelops of cement paste samples with different carbonation ratios (experimental data from Takla, 2010; Takla et al., 2011)

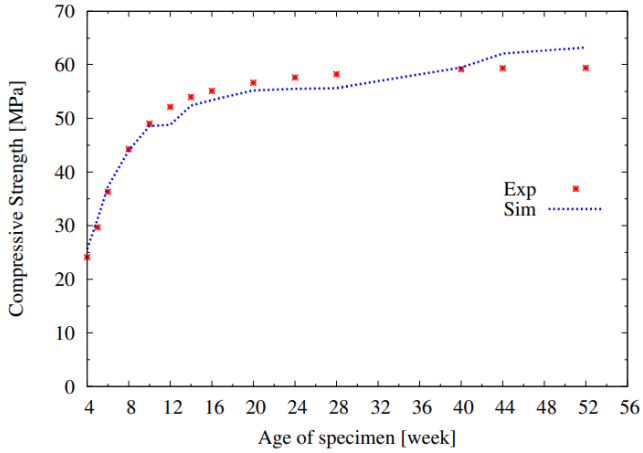

Figure 2-14: Evolution of uniaxial compression strength with carbonation time (experimental data from Chang and Chen (2005)

On the other hand, incorporating a suitable plastic hardening law and a plastic flow rule, one can predict fully stress-strain curves under different loading paths. In Figure 2-15, one shows the stress-strain curves in uniaxial compression tests of concrete samples with different carbonation ratios. There is still a possibility to improve the model in order to describe well the transition from volumetric compressibility to dilatancy.

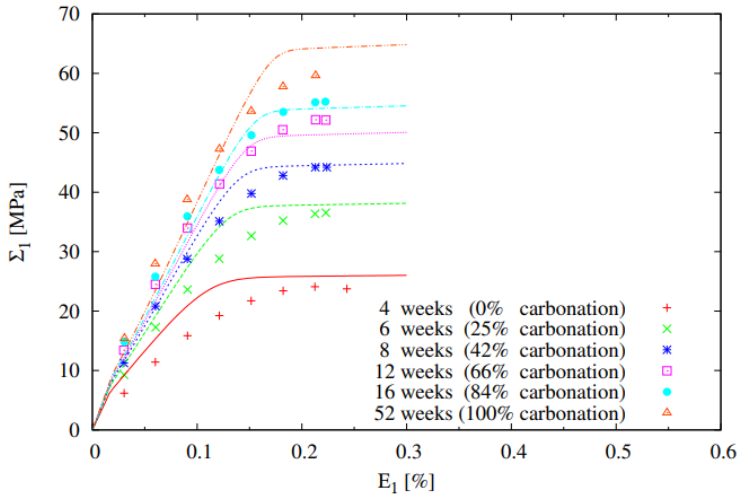

Figure 2-15: Stress-strain curves in uniaxial compression tests of concrete samples with different carbonation ratios (experimental data from Chang and Chen (2005))

The efficiency of micromechanics-based model for the description of chemical leaching effects is also assessed. By determining the increase of porosity due to cement paste dissolution, the evolution of strength envelops are predicted with degradation ratio, as shown in Figure 2-16. It is seen that the chemical leaching induces the diminution of both tensile and shear strength and the increase of failure surface curvature (or non-linearity). In Figure 2-17, the stress-strain curves in uniaxial compression tests of samples subjected to different leaching ratios are presented. Again, there is a good agreement between model's predictions and experimental data.

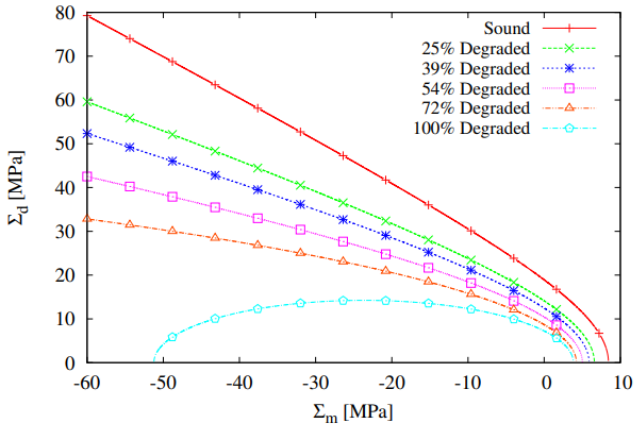

Figure 2-16: Failure envelops of concrete samples with different chemical leaching ratios

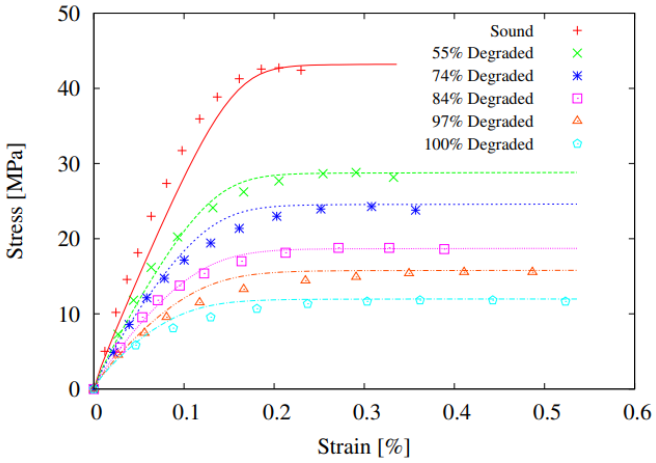

Figure 2-17: Stress-strain curves in uniaxial compression tests of concrete samples with different chemical leaching ratios (experimental data from Nguyen, 2005)

2.4 Synthesis and identified gaps

The mechanical behaviour of underground cementitious structures depends of various parameters: boundary conditions and construction methods. One needs to take into account the host rock loading and the evolution of the rigidity of the structure. This evolution is depending to the chemical and microbial perturbations, the level of loading and also the concrete formulation.

In the case of reinforced concrete, corrosion causes mechanical damage to the concrete under the combined effect of the corrosion-induced expansion (generating internal mechanical stresses) and the loss of cross-sectional area and bonding of the steel, which causes the structure to lose its load-bearing capacity. Previous experimental results highlighted the heterogeneity of the corrosion product layers and the evolution of the mechanical properties of the layers with time and ageing conditions.

The multiscale characterization and especially the coupled approach at nano/microscale with RUS, nano/micro indentation, SEM/EDX allows to obtain key data allowing to feed numerical chemo-mechanical modelling. Currently, studies of the micro-mechanical consequences of groundwater interaction with cementitious materials are very scarce (mainly in pure water, nitric solution or sulphated water). These works highlight a non-negligible evolution of elastic mechanical properties of the cement matrix subjected to an aggressive solution.

The recourse of numerical approaches to determine the mechanical behaviour of cementitious materials has gained growing interests in recent years, due to the continuous increase of computational power. The characterisation of the mechanical properties of cementitious materials necessitates the knowledge of the evolution of the microstructure and corresponding phase assemblage of the cement paste in the context of disposal environment.

Regarding the modelling and simulation aspects, many studies have been devoted to the analysis and description of the evolution of the microstructure and mechanical properties of cementitious materials when subjected to the contact of groundwater and argillite. At the nano-microscale, the different minerals (phase assemblage) composing the hydrated cement paste should in principle be considered. At the nanoscale, the use of approaches based on molecular dynamics is widely accepted. At the microscale, more advanced and versatile methods (micromechanics and upscaling, Mori-Tanaka method, homogenization scheme…) have been developed to estimate the properties evolutions.

carbonation and leaching have antagonistic effects on porosity and some mechanical parameters. Both processes are integrated in the multi-scale model but treated separately experimentally. This raises several questions:

- Will one process dominate the other? If so, over what period of the concrete's life?
- Would one process dominate in the short term and the other in the longer term?
- Has their superposition been treated experimentally?

Whatever the scale considered, an accurate description of the microcracking and its repercussions on both mechanical and diffusive properties is essential to the simulation of the coupled response of cementitious materials in the disposal environment.

2.5 References for part 2

Abdolhosseini Qomi, M.J., Brochard, L., Honorio, T., Maruyama, I., Vandamme, M., 2021. Advances in atomistic modeling and understanding of drying shrinkage in cementitious materials. Cement and Concrete Research 148, 106536.

Al-Ameeri A, Rafiq MI, Tsioulou O (2021), Combined impact of carbonation and crack width on the Chloride Penetration and Corrosion Resistance of Concrete Structures, Cement and Concrete Composite 115(2021), 103819

Aoyagi K, Ishii E, Ishida T (2017a) Field Observations and Failure Analysis of an Excavation Damaged Zone in the Horonobe Underground Research Laboratory, Journal of MMIJ 133: 25–33

Armand, G., Plas, F., Bosgiraud, J-B., 2015, L'apport du Laboratoire souterrain de l'Andra pour le choix et la mise au point des techniques de creusement des ouvrages souterrains du projet de stockage de déchets radioactifs Cigéo, Tunnel et Ouvrages Souterrain (AFTES), n°250, p.251-268

ASTM C09 Committee. 2014. "Test Method for Fundamental Transverse, Longitudinal, and Torsional Resonant Frequencies of Concrete Specimens." Standard ASTM C215-14. ASTM International. https://doi.org/10.1520/C0215-14.

Auroy M, Poyet S, Le Bescop P, Torreti JM, Charpentier T, Moskura M, Bourbon X (2018), Comparison between natural and accelerated carbonation (3% CO2): Impact on mineralogy, microstructure, water retention and cracking, Cement and Concrete Research 109(2018), 64-80

Babaahmadi, A., Tang, L., Abbas, Z., Mårtensson, P. 2015. "Physical and Mechanical Properties of Cementitious Specimens Exposed to an Electrochemically Derived Accelerated Leaching of Calcium", 9, 295-306. DOI: 10.1007/s40069-015-0108-5.

Bao H, Yu M, Xu L, Saafi M, Ye J, Experimental study and multi-physics modelling of concrete under supercritical carbonation, Construction and Building materials 227(2019), 116680.

Barsoum, M. W., M. Radovic, T. Zhen, P. Finkel, and S. R. Kalidindi. 2005. "Dynamic Elastic Hysteretic Solids and Dislocations." *Physical Review Letters* 94 (8): 085501. https://doi.org/10.1103/PhysRevLett.94.085501.

Bary, B., 2008. Simplified coupled chemo-mechanical modeling of cement pastes behavior subjected to combined leaching and external sulfate attack. Int. J. Numer. Anal. Meth. Geomech. 32, 1791–1816.

Bary, B., Leterrier, N., Deville, E., Le Bescop, P., 2014. Coupled chemo-transport-mechanical modelling and numerical simulation of external sulfate attack in mortar. Cement and Concrete Composites 49, 70–83.

Bernachy-Barbe F., A data analysis procedure for phase identification in nanoindentation results of cementitious materials, Materials and Structures. 52 (2019). https://doi.org/10.1617/s11527-019-1397-y.

Bernachy-Barbe, F., Bary, B., 2019. Effect of aggregate shapes on local fields in 3D mesoscale simulations of the concrete creep behavior. Finite Elements in Analysis and Design 156, 13–23.

Bernard, O., Ulm, F.J., Lemarchand, E., 2003. A multiscale micromechanics-hydration model for the early-age elastic properties of cement-based materials. Cement and Concrete Research 33, 1293–1309.

Bernard, F., Kamali-Bernard, S., 2015. Numerical study of ITZ contribution on mechanical behavior and diffusivity of mortars. Computational Materials Science 102, 250–257.

Blumling P, Bernier F, Lebon P, Martin CD (2007) The excavation damaged zone in clay formations time-dependent behaviour and influence on performance assessment. Phys Chem Earth 32:588–599

Bock, F.E., Aydin, R.C., Cyron, C.J., Huber, N., Kalidindi, S.R., Klusemann, B., 2019. A review of the application of machine learning and data mining approaches in continuum materials mechanics. Front. Mater. 6.

Bouchaala, F., C. Payan, V. Garnier, and J.P. Balayssac. 2011. "Carbonation Assessment in Concrete by Nonlinear Ultrasound." *Cement and Concrete Research* 41 (5): 557–59. https://doi.org/10.1016/j.cemconres.2011.02.006.

Brown L., P.G. Allison, F. Sanchez, Use of nanoindentation phase characterization and homogenization to estimate the elastic modulus of heterogeneously decalcified cement pastes, Materials & Design. 142 (2018) 308–318. https://doi.org/10.1016/j.matdes.2018.01.030.

Brown, E.T., Bray, J.W. and Santarelli, F.J. (1989). Influence of stress-dependent elastic moduli on stress and strains around axisymmetric boreholes, Rock Mechanics and Rock Engineering, Vol. 22, pp 189-203.

Cai, Bian, Zhao (2000), Tunnels and Undrground Structures, Zhao, Shrilaw &Krishnana, Taylor & Francis ISBN0° 5809 171 6

Camborde, F., Mariotti, C., Donzé, F.V., 2000. Numerical study of rock and concrete behaviour by discrete element modelling. Computers and Geotechnics 27, 225–247.

Camps, G. (2008). Etude des interactions chemo-mécaniques pour la simulation du cycle de vie d'un élément de stockage en béton. Ph.D. thesis, Université Toulouse III - Paul Sabatier.

Carde C, R Francois, JM Torrenti (1996), Leaching of both calcium hydroxide and c-s-h from cement paste: Modeling the mechanical behaviour, Cement and Concrete Research, 26:1257-1268

Carter, J.P. and Booker, J.R. (1990). Sudden excavation of a long circular tunnel in elastic ground, Int. Jnl. of Rock Mechanics and Mining Sciences, Vol. 27, No. 2, pp 129-132.

Cefis, N., Comi, C., 2017. Chemo-mechanical modelling of the external sulfate attack in concrete. Cement and Concrete Research 93, 57–70.

Chang CF and JW Chen (2005), Strength and elastic modulus of carbonated concrete, ACI Materials Journal, 102:315-321

Chen J.J., L. Sorelli, M. Vandamme, F.-J. Ulm, G. Chanvillard, A Coupled Nanoindentation/SEM-EDS Study on Low Water/Cement Ratio Portland Cement Paste: Evidence for C-S-H/Ca(OH) $_2$ Nanocomposites, Journal of the American Ceramic Society. (2010). https://doi.org/10.1111/j.1551-2916.2009.03599.x.

Chen, J., Kim, J.-Y., Kurtis, K.E., Jacobs, L.J. (2011) Theoretical and experimental study of the nonlinear resonance vibration of cementitious materials with an application to damage characterization, J. Acoust. Soc. Amer., 130, 2728–2737.

Cheng YC, Zhang YW, Jiao YB, Yang JS (2016), Quantitative analysis of concrete property under effects of crack, freeze-thaw and carbonation, Construction and Building Materials 129(2016), 106-115

Constantinides G., F.-J. Ulm, The effect of two types of C-S-H on the elasticity of cement-based materials: Results from nanoindentation and micromechanical modeling, Cement and Concrete Research. 34 (2004) 67–80. https://doi.org/10.1016/S0008-8846(03)00230-8.

Constantinides G., F.-J. Ulm, The nanogranular nature of C–S–H, Journal of the Mechanics and Physics of Solids. 55 (2007) 64–90. https://doi.org/10.1016/j.jmps.2006.06.003.

Constantinides G., K.R. Chandran, F.-J. Ulm, K.J. Van Vliet, Grid indentation analysis of composite microstructure and mechanics: Principles and validation, Materials Science and Engineering: A. 430 (2006) 189–202.

Corbetta, F., Bernaud, D. and Minh, D.N. (1991). Contribution to the convergenceconfinement method by the principle of simlitude (In French), Rev. Fr Geotech. No. 54, pp 5-11.

Dauzeres A., G. Achiedo, D. Nied, E. Bernard, S. Alahrache, B. Lothenbach, Magnesium perturbation in low-pH concretes placed in clayey environment—solid characterizations and modeling, Cement and Concrete Research. 79 (2016) 137–150. https://doi.org/10.1016/j.cemconres.2015.09.002.

Dauzères A., P. Le Bescop, C. Cau-Dit-Coumes, F. Brunet, X. Bourbon, J. Timonen, M. Voutilainen, L. Chomat, P. Sardini, On the physico-chemical evolution of low-pH and CEM I cement pastes interacting with Callovo-Oxfordian pore water under its in situ CO2 partial pressure, Cement and Concrete Research. 58 (2014) 76–88.

Dauzeres, A., Le Bescop, P., Sardini, P., Cau Dit Coumes, C., 2010. Physico-chemical investigation of clayey/cement-based materials interaction in the context of geological waste disposal: Experimental approach and results. Cement and Concrete Research 40, 1327–1340.

Dehoux A., Fatiha Bouchelaghem, Y Berthaud. Micromechanical and microstructural investigation of steel corrosion layers of variable age developed under impressed current method, atmospheric or saline conditions. Corrosion Science, Elsevier, 2015, 97, pp.49-61.

Deng, H., Molins, S., Steefel, C., DePaolo, D., Voltolini, M., Yang, L., Ajo-Franklin, J., 2016. A 2.5D reactive transport model for fracture alteration simulation. Environ. Sci. Technol. 50, 7564–7571.

Di Bella, Carmelo, Michele Griffa, T.J. Ulrich, and Pietro Lura. 2016. "Early-Age Elastic Properties of Cement-Based Materials as a Function of Decreasing Moisture Content." *Cement and Concrete Research* 89 (November): 87–96. https://doi.org/10.1016/j.cemconres.2016.08.001.

Eiras, Jesus N., Tribikram Kundu, John S. Popovics, José Monzó, María V. Borrachero, and Jordi Payá. 2015. "Effect of Carbonation on the Linear and Nonlinear Dynamic Properties of Cement-Based Materials." *Optical Engineering* 55 (1): 011004. https://doi.org/10.1117/1.OE.55.1.011004.

Escoda, J., Willot, F., Jeulin, D., Sanahuja, J., Toulemonde, C., 2011. Estimation of local stresses and elastic properties of a mortar sample by FFT computation of fields on a 3D image. Cem. Concr. Res. 41, 542–556.

Esposito, R., Hendriks, M.A.N., 2016. A multiscale micromechanical approach to model the deteriorating impact of alkali-silica reaction on concrete. Cement and Concrete Composites 70, 139–152.

Fan, D., Yang, S., 2018. Mechanical properties of C-S-H globules and interfaces by molecular dynamics simulation. Construction and Building Materials 176, 573–582.

Finkel, P., A. G. Zhou, S. Basu, O. Yeheskel, and M. W. Barsoum. 2009. "Direct Observation of Nonlinear Acoustoelastic Hysteresis in Kinking Nonlinear Elastic Solids." *Applied Physics Letters* 94 (24): 241904. https://doi.org/10.1063/1.3155201.

Gaitero J.J., W. Zhu, I. Campillo, Multi-scale study of calcium leaching in cement pastes with silica nanoparticles, in: Nanotechnology in Construction 3, Springer, 2009: pp. 193–198.

Genovés, V., F. Vargas, J. Gosálbez, A. Carrión, M.V. Borrachero, and J. Payá. 2017. "Ultrasonic and Impact Spectroscopy Monitoring on Internal Sulphate Attack of Cement-Based Materials." *Materials & Design* 125 (July): 46–54. https://doi.org/10.1016/j.matdes.2017.03.068.

Genovés, V., L. Soriano, M.V. Borrachero, J. Eiras, and J. Payá. 2015. "Preliminary Study on Short-Term Sulphate Attack Evaluation by Non-Linear Impact Resonance Acoustic Spectroscopy Technique." *Construction and Building Materials* 78 (March): 295–302. https://doi.org/10.1016/j.conbuildmat.2015.01.016.

Gérard, B. (1996). Contribution of the mechanical, chemical, and transport couplings in the long-term behaviour of radioactive waste repository structures',. Ph.D. Thesis, Civil Engineering Department, Laval University, Quebec City, Canada / ENS Ca&an, France, (in French).

Gérard, B., Pijaudier-Cabot, G., & Laborderie, C. (1998). Coupled diffusion-damage modelling and the implications on failure due to strain localisation. International Journal of Solids and Structures, 35(31-32), 4107-4120. https://doi.org/10.1016/s0020-7683(97)00304-1

Ghorbanbeigi H, Shen WQ, Yurtdas I, Shao JF (2016), A micro-mechanics based model for concrete materials subjected to carbonation, International Journal for Numerical and Analytical Methods in Geomechanics 40: 1203-1218

Ghorbanbeigi H (2014), Multi-scale modeling of mechanical behavior of cementitious materials subjected to carbonation and leaching, Doctoral thesis, University of Lille, France

Ghorbanbeigi H, Shen WQ, Yurtdas I, Shao JF (2016), A micromechanical model for porous materials with a reinforced matrix, Mechanics Research Communications 72: 81-86

Ghorbanbeigi H, Yurtdas I, Shen WQ, Shao JF (2017), Influences of chemical leaching on elastic and plastic properties of cement-based materials, European Journal of Environmental and Civil Engineering 21(6): 696-711

Ghosh, Sayak, Michael Matty, Ryan Baumbach, Eric D. Bauer, K. A. Modic, Arkady Shekhter, J. A. Mydosh, Eun-Ah Kim, and B. J. Ramshaw. 2020. "One-Component Order Parameter in URu $_2$ Si $_2$ Uncovered by Resonant Ultrasound Spectroscopy and Machine Learning." *Science Advances* 6 (10): eaaz4074. https://doi.org/10.1126/sciadv.aaz4074.

Goncalves, A., & Rodrigues, X. (1991). The resistance of cements to ammonium nitrate attack. Proceedings of 2nd CANMET/ACI International conference on Durability on concrete, Montréal, Canada, 2, pp. 1093–1118.

Gu, Y., Bary, B., Machner, A., De Weerdt, K., Bolte, G., Ben Haha, M., 2022. Multi-scale strategy to estimate the mechanical and diffusive properties of cementitious materials prepared with CEM II/C-M. Cement and Concrete Composites 131, 104537.

Haecker C.-J., E.J. Garboczi, J.W. Bullard, R.B. Bohn, Z. Sun, S.P. Shah, T. Voigt, Modeling the linear elastic properties of Portland cement paste, Cement and Concrete Research. 35 (2005) 1948–1960. https://doi.org/10.1016/j.cemconres.2005.05.001.

Han J., G. Pan, W. Sun, C. Wang, D. Cui, Application of nanoindentation to investigate chemomechanical properties change of cement paste in the carbonation reaction, Science China Technological Sciences. 55 (2012) 616–622.

Hay, R., Li, J., & Celik, K. (2022). Phase evolution, micromechanical properties, and morphology of calcium (alumino)silicate hydrates C-(A-)S-H under carbonation. Cement and Concrete Research, 152, 106683.

Heukamp, F.H., Ulm, F.-J., Germaine, J.T., 2001. Mechanical properties of calcium-leached cement pastes: Triaxial stress states and the influence of the pore pressures. Cement and Concrete Research 31, 767–774.

Hu C., Z. Li, Property investigation of individual phases in cementitious composites containing silica fume and fly ash, Cement and Concrete Composites. 57 (2015) 17–26. https://doi.org/10.1016/j.cemconcomp.2014.11.011.

Hudson J.A., (1991) Atlas of rock engineering mechanism: underground excavations. Int. J.Rock Mech. Min. Sci. and Geomech. Abstr. 28:523-526.

Idiart, A.E., Lopez, C.M., Carol, I., 2011. Chemo-mechanical analysis of concrete cracking and degradation due to external sulfate attack: A meso-scale model. Cement and Concrete Composites 33, 411–423.

Iwama K, Maekawa K, Modeling of carbonation, decarbonation and re-carbonation processes of structural concrete subjected to high temperature heating, Cement and Concrete Composites, 129(2022), 104493.

Jiang C, Gu X, Zhang W, Zou W, Modeling of carbonation in tensile zone of plain concrete beams damaged by cyclic loading, Construction and Building Materials, 77(2015), 479-488

Jiang C, Huang QH, Gu XL, Zhang WP, Modeling the effects of fatigue damage on concrete carbonation, Construction and Building Materials 191(2018), 942-962

Krakowiak, J., Konrad, William Wilson, Simon James, Simone Musso, and Franz-Josef Ulm. 2015. "Inference of the Phase-to-Mechanical Property Link via Coupled X-Ray Spectrometry and Indentation Analysis: Application to Cement-Based Materials." *Cement and Concrete Research* 67 (January): 271–85. https://doi.org/10.1016/j.cemconres.2014.09.001.

Kim J.J., E.M. Foley, M.M. Reda Taha, Nano-mechanical characterization of synthetic calcium–silicate–hydrate (C–S–H) with varying CaO/SiO2 mixture ratios, Cement and Concrete Composites. 36 (2013) 65–70. https://doi.org/10.1016/j.cemconcomp.2012.10.001.

Königsberger, M., Pichler, B., Hellmich, C., 2014. Micromechanics of ITZ-aggregate interaction in concrete Part II: strength upscaling. Journal of the American Ceramic Society 97, 543–551.

Königsberger, M., Hlobil, M., Delsaute, B., Staquet, S., Hellmich, C., Pichler, B., 2018. Hydrate failure in ITZ governs concrete strength: A micro-to-macro validated engineering mechanics model. Cement and Concrete Research 103, 77–94.

Lalan P., A. Dauzères, L. De Windt, J. Sammaljärvi, D. Bartier, I. Techer, V. Detilleux, M. Siitari-Kauppi, Mineralogical and microstructural evolution of Portland cement paste/argillite interfaces at 70 °C – Considerations for diffusion and porosity properties, Cement and Concrete Research. 115 (2019) 414–425. https://doi.org/10.1016/j.cemconres.2018.09.018.

Le Bellégo C., Gérard B., Pijaudier Cabot G., (2001), "Mechanical analysis of concrete structure submitted to an aggressive water attack", Fracture of Concrete Structure, de Borst et al.(eds) Swets &Zeilinger, Lisse ISBN 902651 825 0.

Leisure, Robert G. 2017. *Ultrasonic Spectroscopy. Applications in Condensed Matter Physics and Materials Science*. Cambridge University Press.

Li D, Li LY, Wang X, Mathematical modelling of concrete carbonation with moving boundary, International Communications in Heat and Mass Transfer, 117(2020), 104809

Luo Z., W. Li, K. Wang, S.P. Shah, Research progress in advanced nanomechanical characterization of cement-based materials, Cement and Concrete Composites. 94 (2018) 277–295. https://doi.org/10.1016/j.cemconcomp.2018.09.016.

Lura P., P. Trtik, B. Münch, Validity of recent approaches for statistical nanoindentation of cement pastes, Cement and Concrete Composites. 33 (2011) 457–465. https://doi.org/10.1016/j.cemconcomp.2011.01.006.

Maghous S, L Dormieux, JF Barthelemy (2009), Micromechanical approach to the strength properties of frictional geomaterials. European Journal of Mechanics - A/Solids, 28(1):179-188

Martin C.D., N. Chandler, The progressive fracture of Lac du Bonnet granite, Int J Rock Mech Min Sci 31 (1994) 643–659.

Martin C.D., Read R.S., and Martino J.B. 1997. Observations of brittle failure around a circular test tunnel. International Journal of Rock Mechanics and Mining Sciences, 34(7): 1065–1073.

Metalssi OO, Aït-Mokhtar A, Turcry P, A proposed modelling of coupling carbonation-porosity-moisture transfer in concrete based on mass balance equilibrium, Construction and Building materials 230(2020),116997

Migliori, Albert, and John L Sarrao. 1997. *Resonant Ultrasound Spectroscopy. Applications to Physics, Materials Measurements, and Nondestructive Evaluation*. New York, NY, USA: John Wiley & Sons, Ltd.

Miller M., C. Bobko, M. Vandamme, F.-J. Ulm, Surface roughness criteria for cement paste nanoindentation, Cement and Concrete Research. 38 (2008) 467–476. https://doi.org/10.1016/j.cemconres.2007.11.014.

Miller, W., Alexander, R., Chapman, N., McKinley, I., Smellie, J. (2000) Geologic disposal of radioactive wastes and natural analogues – lessons from nature and archaeology. Waste Management Series, New York, Pergamon, 2, 316 p.

Mori T and K Tanaka (1973), Average stress in matrix and average elastic energy of materials with misfitting inclusions, Acta Metallurgica 21(5):571-574

Morrison, R.G.K. and Coates, D.F. (1955). Soil mechanics applied to rock failure in mines, The Canadian Mining and Metallurgical Bulletin, Vol. 48, No. 523, Montreal, Canada, pp. 701-711

Muthu M., M. Santhanam, Effect of reduced graphene oxide, alumina and silica nanoparticles on the deterioration characteristics of Portland cement paste exposed to acidic environment, Cement and Concrete Composites. 91 (2018) 118–137.

Naderi, S., Tu, W., Zhang, M., 2021. Meso-scale modelling of compressive fracture in concrete with irregularly shaped aggregates. Cement and Concrete Research 140, 106317.

Nardi, A., Idiart, A., Trinchero, P., de Vries, L.M., Molinero, J., 2014. Interface COMSOL-PHREEQC (iCP), an efficient numerical framework for the solution of coupled multiphysics and geochemistry. Computers & Geosciences 69, 10–21.

Ngala VT and CL Page (1997), Effects of carbonation on pore structure and diffusional properties of hydrated cement pastes. Cement and Concrete Research, 27:995-1007

Nguyen VH (2005), Couplage degradation chimique - comportement en compression du beton. PhD thesis, Ecole des Ponts ParisTech

Nguyen VH, H Colina, JM Torrenti, C Boulay, B Nedjar (2007), Chemomechanical coupling behaviour of leached concrete: Part I: Experimental results, Nuclear Engineering and Design, 237:2083-2089

Nguyen, V. H. (2005). Couplage dégradation chimique - comportement en compression du béton. Thèse de Doctorat, Ecole Nationale des Ponts et Chaussées, Paris, France, 200p.

Nguyen, V.H., Nedjar, B., & Torrenti, J. (2007). Chemo-mechanical coupling behaviour of leached concrete. Nuclear Engineering and Design, 237(20-21), 2090-2097. https://doi.org/10.1016/j.nucengdes.2007.02.012

Nguyen, T.T., Yvonnet, J., Zhu, Q.-Z., Bornert, M., Chateau, C., 2015. A phase field method to simulate crack nucleation and propagation in strongly heterogeneous materials from direct imaging of their microstructure. Engineering Fracture Mechanics 139, 18–39.

Oliver W.C., G.M. Pharr, Measurement of hardness and elastic modulus by instrumented indentation: Advances in understanding and refinements to methodology, Journal of Materials Research. 19 (2004) 3–20. https://doi.org/10.1557/jmr.2004.19.1.3.

Pan Z, Chen A, Ma R, Wang D, Tian H, Three-dimensional lattice modeling of concrete carbonation at meso-scale based on reconstructed coarse aggregates, Construction and Building materials 192(2018), 253-271

Panet, M. (1976). Analysis de la Stabilite d'un Tunnel Creuse dans un Massif Rocheux en Tenant Compte du Cmportement apres la Rupture Rock Mechanics, Vienna, Austria, Vol. 8, No. 4, pp. 209-233.

Payan, C., T. J. Ulrich, P. Y. Le Bas, T. Saleh, and M. Guimaraes. 2014. "Quantitative Linear and Nonlinear Resonance Inspection Techniques and Analysis for Material Characterization: Application to Concrete Thermal Damage." *The Journal of the Acoustical Society of America* 136 (2): 537–46. https://doi.org/10.1121/1.4887451.

Pellenq, R.J.-M., Kushima, A., Shahsavari, R., Vliet, K.J.V., Buehler, M.J., Yip, S., Ulm, F.-J., 2009. A realistic molecular model of cement hydrates. Proceedings of the National Academy of Sciences 106, 16102–16107.

Pharr G.M., W.C. Oliver, Measurement of Thin Film Mechanical Properties Using Nanoindentation, MRS Bulletin. 17 (1992) 28–33. https://doi.org/10.1557/S0883769400041634.

Pichler, C., Lackner, R., Mang, H.A., 2007. A multiscale micromechanics model for the autogenous-shrinkage deformation of early-age cement-based materials. Engineering Fracture Mechanics 74, 34–58.

Planel, D. & Sercombe, J. & Le Bescop, Patrick & Adenot, Frédéric & Torrenti, jean michel. (2006). Long-term performance of cement paste during combined calcium leaching-sulfate attack: Kinetics and size effect. Cement and Concrete Research. 36. 137-143.

Principigallo, A., Lura, P., van Breugel, K., Levita, G., 2003. Early development of properties in a cement paste: A numerical and experimental study. Cement and Concrete Research 33, 1013–1020.

Randall N.X., M. Vandamme, F.-J. Ulm, Nanoindentation analysis as a two-dimensional tool for mapping the mechanical properties of complex surfaces, Journal of Materials Research. 24 (2009) 679–690. https://doi.org/10.1557/jmr.2009.0149.

Sarkar, S., Mahadevan, S., Meeussen, J.C.L., Van der Sloot, H., Kosson, D., 2010. Numerical simulation of cementitious materials degradation under external sulfate attack. Cement and Concrete Composites 32, 241–252.

Sasmal S., M.B. Anoop, 7 - Nanoindentation for evaluation of properties of cement hydration products, in: F. Pacheco-Torgal, M.V. Diamanti, A. Nazari, C.G. Granqvist, A. Pruna, S. Amirkhanian (Eds.), Nanotechnology in Eco-Efficient Construction (Second Edition), Woodhead Publishing, 2019: pp. 141–161. https://doi.org/10.1016/B978-0-08-102641-0.00007-4.

Scheiner, S., Hellmich, C., 2009. Continuum microviscoelasticity model for aging basic creep of early-age concrete. J. Eng. Mech.-ASCE 135, 307–323.

Sellier, A., Buffo-Lacarrière, L., Gonnouni, M. E., & Bourbon, X. (2011). Behaviour of HPC nuclear waste disposal structures in leaching environment. Nuclear Engineering and Design, *241*(1), 402-414. https://doi.org/10.1016/j.nucengdes.2010.11.002

Shen WQ, Cao YJ, Shao JF, Liu ZB (2020), Prediction of plastic yield surface for porous materials by a machine learning approach, Materials Today Communications 25, (2020), 101477

Shen WQ, D Kondo, L Dormieux, JF Shao (2013), A closed-form three scale model for ductile rocks with a plastically compressible porous matrix. Mechanics of Materials, 59:73-86

Shen WQ, Shao JF, Burlion N, Liu ZB (2020), A microstructure-based constitutive model for cement paste with chemical leaching effect, Mechanics of Materials 150, (2020), 103571

Socié, A., Dubois, F., Monerie, Y., Perales, F., 2021. Multibody approach for reactive transport modeling in discontinuous-heterogeneous porous media. Computational Geosciences 1–19.

Stora, E., Bary, B., He, Q.-C., Deville, E., Montarnal, P., 2009. Modelling and simulations of the chemo–mechanical behaviour of leached cement-based materials: Leaching process and induced loss of stiffness. Cement and Concrete Research 39, 763–772.

Stora, E., Bary, B., He, Q.-C., 2008. On estimating the effective diffusive properties of hardened cement pastes. Transp Porous Med 73, 279–295.

Sun, Z., Garboczi, E.J., Shah, S.P., 2007. Modeling the elastic properties of concrete composites: Experiment, differential effective medium theory, and numerical simulation. Cement and Concrete Composites 29, 22–38.

Takla I (2010), Thermo-hydromechanical behaviour of oil cement under effect of CO2, PhD thesis, University of Sciences and Technologies of Lille, 2010.

Takla, I., Burlion, N., Shao, J.F., Saint-Marc, J., Garnier, A. (2011). Effects of the storage of CO2 on multiaxial mechanical and hydraulic behaviours of oil-well cement, Journal of Materials in Civil Engineering, 23(6):741-746

Tennis P.D., Jennings H.M. (2000) A model for two types of calcium silicate hydrate in the microstructure of Portland cement pastes, Cement and Concrete Research, Volume 30, Issue 6, 855-863.

Tixier, R., Mobasher, B., 2003. Modeling of damage in cement-based materials subjected to external sulfate attack. I: Formulation. Journal of Materials in Civil Engineering 15, 305.

Torrenti J.M., Nguyen V.H., Colina H., Le Maou F., Benboudjema F., Deleruyelle F., (2008), "Coupling between leaching and creep of concrete", Cement and Concrete Research, Volume 38, Issue 6, 816-821.

Tuutti, K. (1982). Corrosion of steel in concrete. Swedish Cement and Concrete Research Institute, Stockholm. http://www.cbi.se/viewNavMenu.do?menuID=317&oid=857

Ulm F.-J., M. Vandamme, C. Bobko, J. Alberto Ortega, K. Tai, C. Ortiz, Statistical Indentation Techniques for Hydrated Nanocomposites: Concrete, Bone, and Shale, Journal of the American Ceramic Society. 90 (2007) 2677–2692. https://doi.org/10.1111/j.1551-2916.2007.02012.x.

Ulm, F.-J., Heukamp, F.H., Germaine, J.T., (2002), "Residual design strength of cement-based materials for nuclear waste storage systems", Nuclear Engineering and Design, 211 (1), p.51-60

Vandamme M., F.-J. Ulm, Nanoindentation investigation of creep properties of calcium silicate hydrates, Cement and Concrete Research. 52 (2013) 38–52. https://doi.org/10.1016/j.cemconres.2013.05.006.

Velez K., S. Maximilien, D. Damidot, G. Fantozzi, F. Sorrentino, Determination by nanoindentation of elastic modulus and hardness of pure constituents of Portland cement clinker, Cement and Concrete Research. 31 (2001) 555–561. https://doi.org/10.1016/S0008-8846(00)00505-6.

Wu, W., A. Al-Ostaz, J. Gladden, A. H.-D. Cheng, and G. Li. 2010. “Measurement of Mechanical Properties of Hydrated Cement Paste Using Resonant Ultrasound Spectroscopy.” *Journal of ASTM International* 7 (5): 102657. https://doi.org/10.1520/JAI102657.

Xu S., Y. Feng, J. Liu, Q. Zeng, Micro indentation fracture of cement paste assessed by energy-based method: The method improvement and affecting factors, Construction and Building Materials. 231 (2020) 117136. https://doi.org/10.1016/j.conbuildmat.2019.117136.

Xue J, Shao JF, Burlion N, Estimation of constituent properties of concrete materials with an artificial neural network based method, Cement and Concrete Research 150 (2021) 106614

Yang D.Y., R. Guo, Experimental study on modulus and hardness of ettringite, Exp Tech. 38 (2014) 6–12. https://doi.org/10.1111/j.1747-1567.2011.00744.x.

Yurtdas I, SY Xie, N Burlion, JF Shao, J Saint-Marc, A Garnier (2011), Influence of chemical degradation on mechanical behaviour of a petroleum cement paste, Cement and Concrete Research, 41(4):412-421

Zadler, Brian J., Jérôme H. L. Le Rousseau, John A. Scales, and Martin L. Smith. 2004. “Resonant Ultrasound Spectroscopy: Theory and Application.” *Geophysical Journal International* 156 (1): 154–69. https://doi.org/10.1111/j.1365-246X.2004.02093.x.

Zghondi.J, M.N.Vu, G.Armand, Mechanical behaviour of different concrete lining supports in the Callovo Oxfordian claystone. Clayconference, Davos 2017

Zhu W., J.J. Hughes, N. Bicanic, C.J. Pearce, Nanoindentation mapping of mechanical properties of cement paste and natural rocks, Materials Characterization. 58 (2007) 1189–1198. https://doi.org/10.1016/j.matchar.2007.05.018.

3. Existing knowledge on the chemo-mechanical (C/M) modelling of concrete including parallel applications

Part 3 is directly linked to the approach developed by MAGIC to make the link between the chemical evolutions and the mechanical behaviours. As this effort was not highly supported in the past as part of the geological disposal context, the next development takes into account modelling carried out beyond the boundaries of the disposal context, at the pore/microstructure scales (part 3.1) and the meso/macroscale (part 3.2). A last part (3.3) has for objective to identify what are the key limits and gaps remaining to obtain representative chemo-mechanical models of concrete in geological disposal context.

3.1 C/M modelling at the pore scale/microstructure scale in saturated and unsaturated environment

SCK-CEN / CSIC

The term pore scale defines spatial scales that take into account separate phases and pore structure of cement paste. In other words, the pore scale builds on the understanding of material and processes below representative elementary volume (REV) of continuum scale. Pore scale models aim at reducing the use of constitutive models to the minimum and focusing on the use of physical parameters that can be measured.

Knowledge of the evolving cement pore water and solid phase composition during hydration and ageing processes of cementitious materials is a key aspect for the understanding of dissolution-precipitation mechanisms. Hence, pore scale modelling became an important approach in the modern research and engineering studies related to porous material (Blunt et al., 2013). The heterogeneity and complexity of cement makes the use of the pore scale study even more necessary. In the framework of MAGIC project (at least) three main physics are involved, namely bio-geochemical reactions, ion transport and mechanical behaviour of material. This overview covers all three fields. First part relates to the coupling of geochemistry and ion transport. The focus is on the processes of leaching and carbonation of cement paste. The second part includes an overview of mechanical processes and chemo-mechanical processes although the literature on coupled processes at pore scale is very scarce.

3.1.1 Reactive transport at pore scale

Pore-scale models increase the detail of micro-scale heterogeneity such as the explicit representation of the pore structure or mineral structure (Li et al., 2006; Raoof et al., 2012; Prasianakis et al., 2018; Molins and Knabner, 2019). Several reactive transport models are already developed to study dissolution-precipitation reactions at micro- and mesoscales: finite-volume methods (Deng et al., 2016; Li and Jun, 2017; Molins et al., 2017; Seigneur et al., 2017), smoothed particle hydrodynamics (Tartakovsky et al., 2007), pore-network models (Li et al., 2006; Raoof et al., 2012), and lattice Boltzmann methods (Kang et al., 2007; Kang et al., 2010; Yoon et al., 2012; Prasianakis et al., 2018; Patel et al., 2014; Poonoosamy et al., 2019). Most numerical studies for carbonation of cementitious materials deal with CO_2-rich environments for the application in fields such as CO_2 sequestration. The process and the evolution of carbonation are different when concrete structures are exposed to CO_2 concentrations close to atmospheric conditions or to high CO_2 concentration conditions. Furthermore, some case studies for dissolution-precipitation considered only constant boundary dissolved CO_2 concentrations (Raoof et al., 2012; Seigneur et al., 2017). However, for structures exposed to atmospheric conditions, a fixed partial pressure of CO_2 at air-liquid boundary interface would be an appropriate choice.

In cementitious materials, the rate of chemical evolution is often controlled by ion transport. This is because cementitious materials are characterized by very fine pores, majority below the scale of a few micrometers. Moreover, cementitious materials also have heterogeneous distribution of solid phases. Similar to pore sizes, also the sizes of solid phases are mostly below the scale of a few micrometers.

Hence, the study of processes needs to be done at least on the spatial scale of micrometers (Shih et al., 1999; Thomas et al., 1996). Cement paste microstructure is described by a complex network of different phases, either being physical phases (solid/liquid) or distinct minerals at different scales. Each transition between phases or minerals requires an interface with mostly a very sharp transition of physical, chemical and mechanical properties. The numerical description of such system requires numerical approaches that can cope with many boundaries, sharp transitions and are computationally cheap. In addition to the traditional numerical methods (finite difference, finite element and finite volume methods), the lattice Boltzmann method is often used in recent years (Molins et al., 2021). The lattice Boltzmann method stems from particle methods and solves a simplified form of the discrete Boltzmann equation, which describes the evolution of a particle distribution function $f_i(\boldsymbol{x},t)$ at position $\boldsymbol{x}$ in time t and direction i. The particle distribution function $f_i(\boldsymbol{x},t)$ in the lattice Boltzmann method does not represent discrete particles, but the probability of finding a particle with speed e_i at position $\boldsymbol{x}$ in time t. Because the method is based on particles, the definition of particle translation and collision in the lattice are quick operations and boundary conditions can be very easily defined (e.g. particle bounce-back for no-flow condition). Moreover, the behaviour of particles at position $\boldsymbol{x}$ is only defined by the particles at the neighbouring nodes in the lattice. Hence, there is no need to solve systems of equations, which makes the method very attractive for parallelization. Moreover, because of the particle nature of the method and inherent link between spatial and temporal scales, von Neumann criteria are always respected.

Although the description of the system at pore scale assumes different discrete phases, some phases and processes cannot be represented explicitly in the model. The pore size distribution of a typical microstructure of a hardened cement paste (Phung et al., 2017) shows pore sizes ranging from a few nano-meter scale to micrometers. Such large range of scales (10^2-10^3) obviously cannot be represented in a single model. Many pore-scale dissolution-precipitation models assume that the voxels contain either pore space or a single solid phase (Kang et al., 2004; Kang et al., 2010; Yoon et al., 2012). However, the regions with mixtures of very small pores and solids are often more homogeneous (e.g. C-S-H amorphous phase in hardened cement pastes).

For such “multiscale” materials it has been proposed to upscale the properties for these phases and use them as effective properties in the pore-scale model (Patel et al., 2021). When we have a combination of discrete phases and phases with effective properties in the same model, we refer to this approach as multi-level approach (Patel et al., 2021; Varzina et al., 2020).

Multi-level models have been used to examine the role of gel porosity in the diffusivity of cement paste (Patel et al., 2018), to study the evolution of leaching from cement paste (Perko et al., 2020) and carbonation of portlandite (Varzina et al., 2020). An example of 3D dissolution at pore scale is shown in Figure 3-1.

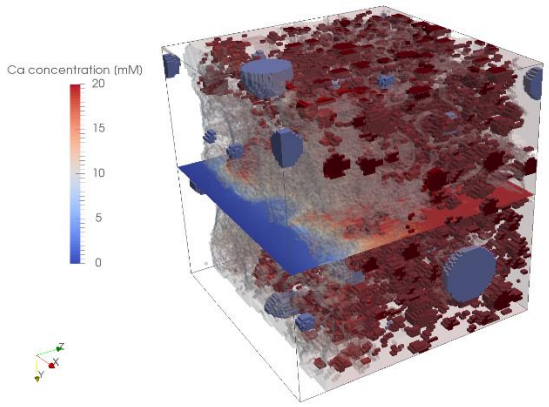

Figure 3-1: Modelling of leaching of cement paste with de-ionised water (left boundary condition). Portlandite is marked with red colour, C-S-H phases with grey and clinkers with blue. The cross-section represents dissolved Ca concentration (Perko et al., 2020).

One of the open questions to date with multi-level approach with several primary and secondary phases is simultaneous dissolution and precipitation reactions in the same voxel containing one or more phases. For example, dissolving portlandite in a voxel provides space for calcite precipitation and additional pores. These processes can only occur in adjacent voxels when single phase voxels are assumed. To overcome the discussed limitations in most available pore-scale models that deal with combined precipitation-dissolution processes in general, and with carbonation of cement-based materials in particular, a new pore-scale modelling concept is introduced in (Varzina et al., 2020) to account for simultaneous dissolution and precipitation reactions within a voxel and the development of residual porosity. The pore-scale coupled reactive transport process is solved with a lattice Boltzmann method using the multilevel approach that allows representation of voxels with mixed phases. A specific framework is added to handle sub-grid dissolution and precipitation patterns and effects of limitation of the precipitation in confined spaces with extreme small pore radii (Emmanuel and Berkowitz, 2007) also termed as pore-size dependent solubility (Ghosh et al., 2001; Liu and Jacques, 2017). Taking a pore-size dependent solubility into account may prevent the pore space to be completely occupied by solid phases during carbonation. Consequently, a so-called residual porosity remains in a carbonated layer allowing for diffusive transport of aqueous species.

Recently, a lot of attention has been devoted in the nucleation principles in pore-scale models. Most models until now assume heterogeneous nucleation that initiates at the boundary of dissolving mineral. This assumption is based on the classical nucleation theory (CNT) where it is shown that the energy barriers and formation of critical nuclei is higher for homogeneous reaction (Prasianakis et al., 2017).

Several studies touched upon the effect of nucleation to the precipitation process. For example, Nooraiepour et al. (2021) investigates the precipitation of calcium carbonate crystals on a heterogeneous sandstone substrate as a function of chemical supersaturation, temperature, and time. The goal of the study is to delineate the amount and location of nucleation and precipitation events in the spatio-temporal domain. The results showed that probabilistic nucleation contributes to broad stochastic distributions in both amounts and locations of crystals in temporal and spatial domains. The influence of the use of CNT on heterogeneous nucleation has been studied in (Starchenko, 2022). This study coupled the pore-scale reactive transport modelling with the Arbitrary Lagrangian-Eulerian approach which allowed for tracking evolution of explicit solid interface during mineral precipitation.

Pore scale models can be time consuming. The reason is that in order to capture the critical features at the pore scale, such as the presence of capillary pores or heterogeneity in mineral phases, geometrical information with high resolution is needed. Often the purpose of a microstructural model is to upscale the information obtained at the pore to the continuum scale. In practice this entails respecting representative elementary volume (REV) which, in heterogeneous materials, can be large. Thus, detailed spatial information for a sufficiently large simulation domain requires a fine and large computational discretization resulting in a large number of unknowns and huge memory and computational costs, especially for three-dimensional domains.

The time step is constrained by numerical stability criteria, for example by Neumann criteria for diffusion, or Courant-Friedrichs-Lewy (CFL) stability criterion for advection/diffusion transport conditions. These criteria are linked to the spatial discretization and smaller time steps are needed for finer spatial discretization. Usually the size of the numerical domain and its discretization are defined by the experimental settings and characterization methods. Consequently, when more complex and larger models are imposed, the most straightforward approach is to computationally optimize the solution, either by parallelization of processes or by increasing of computational resources e.g. solve the problem on a supercomputer. Groen et al. (2013) have shown that lattice Boltzmann method can be well scalable up to 32.000 cores with only 11% slowdown. However, even for a parallelized framework, the number of time steps is fixed as it is defined by stability criteria enforced by the migration conditions, either being diffusion or advection/diffusion (fixed by physics) and spatial discretization (fixed by the model). This issue has also been recognised in (Blunt et al., 2013) for flow simulations on pore-scale. Another way of reducing computational time in a coupled reactive transport model is by making the computationally demanding geochemical calculations less demanding by e.g. look up tables (Huang et al., 2018), first-

order estimations (Leal et al., 2014, 2016a, 2016b, Allan et al., 2017) or surrogate modelling (De Lucia et al., 2017).

For chemically buffered materials, a very efficient approach is to reduce the number of geochemical time steps by scaling of solid amount. The conditions under which the scaling is possible and the extent to which they could be scaled is described in (Perko and Jacques, 2019).

3.1.2 Mechanical pore-scale models

Mechanical evolution at pore scale can be simulated with different approaches. One of the most used approaches are lattice (or spring network) models (Ostoja-Starzewski, 2002). The Lattice model is a type of discrete element model in which the continuum is discretized by a set of simple beam or truss elements. These models have shown excellent capabilities for simulating deformation and fracture processes in quasi-brittle materials like cement paste and/or concrete (Zhang et al., 2018; Schlangen et al., 2007; Man and Van Mier, 2008).

One example is the Delft lattice model (Schlangen and Vanmier, 1992; Schlangen and Garboczi, 1997), the solid material is discretized as a set of Timoshenko beam elements, which can transfer normal forces, shear forces, and bending and torsional moments. An example of an overlay procedure for the cement paste is proposed in Figure 3-2.

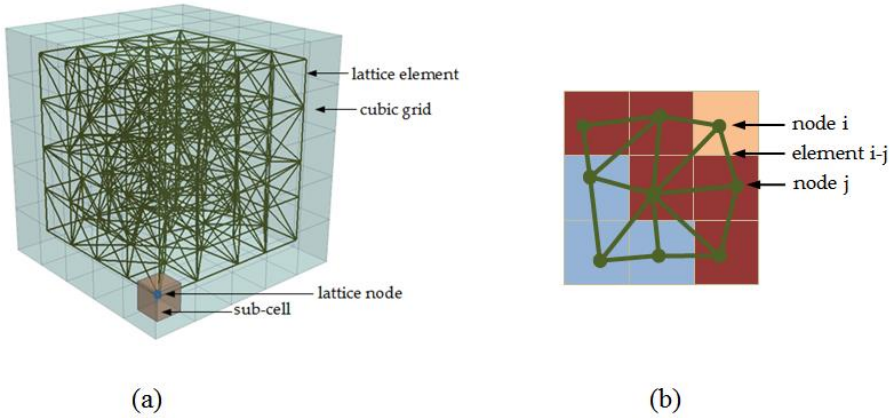

Figure 3-2: (a) Node and mesh generation procedure; (b) an example of the overlay procedure for cement paste, shown in 2D for simplicity (pink – outer product, red – inner product, light blue – unhydrated cement), adapted from (Šavija et al., 2019).

Typically, each element is assigned with a linear ideal elastic brittle behaviour. Loading is stepwise applied to the global mesh, and once an element becomes critical, meaning the element has reached the highest stress-to-strength ratio, it is identified and removed from the mesh. This procedure is then repeated until a certain force or displacement criterion has been reached. This is commonly referred to as a sequentially linear solution procedure (Rots and Invernizzi, 2004). As this approach closely mimics the process that obviously occurs during fracturing of quasi-brittle materials, very realistic global and softening behaviour of crack propagation paths can be simulated. The downside of the lattice model is that they are computationally expensive when dealing with heterogeneous materials, such as cement paste.

A computational framework based on analytical and numerical homogenization for estimating elastic properties at the cement paste scales already exists. The following review focusses on numerical homogenization. Smilauer et al., 2006, studied a microstructure-based model in order to predict mechanical properties of hydrating cement paste. They utilized CEMHYD3D (Bentz, 2000) for microstructural modelling and finite element (FE) and fast Fourier transform (FFT) techniques for computation of Young's modulus. Mazaheripour et al., 2018 used micromechanical modelling for estimation of Young's modulus using a lattice model. Their lattice model was verified with the results from FEM. They used HYMOSTRUC3D (Ye, 2003) to generate a synthetic microstructure, which formed a basis for the micromechanical analysis. More recently, Babaei (2021) presented a combined

CEMHYD3D and CAST3M (FEM code) (Cast3M, 2019) framework to determine not only elastic properties but also thermal and drying shrinkage coefficients, including interpretation of complex stress distribution at the pore scale. Essentially, all these approaches first produce a synthetic microstructure from the hydration models and assign mechanical properties for individual phases of hardened cement paste. By solving a boundary value problem, average thermo-mechanical properties of hardened cement paste are estimated. This framework can be easily extended to chemo-mechanical coupling within the MAGIC project, via tracking the chemical evolution of each phase in the cement paste due to leaching and/or carbonation.

3.1.3 Hydro-(thermo)-mechanical pore-scale models

Traditionally, THM models are set up through continuum approaches based on mathematical frameworks combining sets of equations to describe thermodynamics, solid mechanics and hydraulics principles. However, continuum modelling approaches based on FEM or the finite difference method (FDM) would suffer critical computational and continuity limitations when applied to discontinuous and highly deformable media. As an alternative, the discrete approaches like, for instance, the discrete element method (DEM) (Cundall and Strack, 1979), have proven successful at modelling the behaviour of these discrete systems. Several studies have proposed hydraulic (Catalano et al., 2014) or thermal (Caulk et al., 2020) (Figure 3-3), (Feng et al., 2008) couplings with DEM.

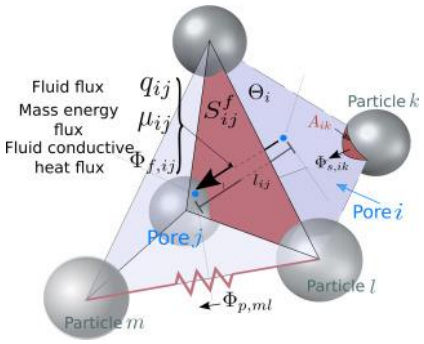

Figure 3-3: Heat transfer model notations and geometric considerations for fluid flow, advection, and conduction models. The figure is taken from (Caulk et al., 2020).

3.1.4 Chemo-mechanical pore-scale models

The Chemo-Mechanical pore scale models are very scarce. The model based on micromechanics has been published by (Stora et al., 2010) related to the process of leaching from the cement paste. In this paper the multi-scale homogenization has been used to evaluating the evolution of the mineral composition, diffusive and elastic properties inside a concrete material subjected to leaching. Hence it does not deal with the pore scale itself, but the model takes into account separate solid phases on the geochemical level that are homogenised before performing the mechanical modelling. The basic idea used by this micromechanical model for dealing with damage consists in representing the microcracks as voids in which the length of its revolution axis is reduced to zero. Damage variables that characterize material microdefects are the crack density parameters characterizing a family of cracks having the same normal vector associated with the driving forces. The damaged material is then viewed as a homogeneous matrix of cement-based material in which the microcracks are distributed.

The microstructural changes presumably affect the concrete porosity, diffusion, and permeability, detrimentally modifying the concrete mechanical properties (Stora et al., 2010; Kuhl et al., 2004; Mahadevan et al., 2014; Ulm et al., 1998). Understanding the link between these reactions and the mechanical response of concrete relies on the perception of the heterogeneous nature of concrete (i.e., multiscale heterogeneity), characterized by underlying mineralogy and microstructure. Accurate transfer of this lower-scale information towards the macroscales is a requisite for simulating the impact of chemo-mechanical degradations on concrete durability, which can be accomplished only by combined multiscale and multiphysics approaches (Ulm et al., 1998; Bosco et al., 2020).

The continuum hypothesis holds separately from pore scale to macro/structural scales. Thus, continuum conservation equations (mass/energy) and thermodynamic expressions can be written for every single point at every location of the concrete domain. Nevertheless, the domains of many problems of interest are too large, and phase contributions are too complex to be modelled at the pore scale. The most miniature scale addressed in microstructural models has the characteristic length of 10^{-9}-10^{-7} meters, where the C-S-H matrix forms (Heukamp, 2003). Indeed, this scale is the smallest material length that is at present accessible by the nanoindentation test, where it is established that C-S-H exists in two forms with two different volume fractions and mechanical properties (Ulm, 2003; Stora et al., 2010; Kuhl et al., 2004).

Numerical models accounting for coupled chemo-mechanical processes at the microscale for concrete are rare (Dunant and Scrivener, 2010; Sciume et al., 2013). Analytical models, however, can be formulated from either phenomenological or mechanistic points of view. Nevertheless, the lack of consensus about the origin of the degradation mechanism and the difficulty of measuring the advance of chemical reactions rather than their consequences make the formulation of experimentally based mechanistic models burdensome. That is why we focus on analytical phenomenological-based models from this point on. These models rely on the underlying hypotheses about degradation mechanisms and are categorized based on the primary chemical reactions they are focused on.

Calcium leaching is the paramount degradation reaction covered in microscale modelling, as the most critical and sluggish reaction that deteriorates concrete. Some developed models, though, account for alkali-silica reaction or sulfate penetration in which concrete encounters internal expansion forces due to gel or ettringite forming reactions (Dunant and Scrivener, 2010; Chen et al., 2016; Wu et al., 2011). In a general sense, chemo-mechanical models work based on the definition of two damage variables (if they are based on mechanics damage). One accounts for mechanical loads (d^m), and the second elucidates chemical aging (d^c). The damage constitutive equation then reads broadly as follow

$$\sigma_{ij} = (1 - d^m).(1 - d^c).E_{ijkl}.\varepsilon_{kl} \,, \qquad 3\text{-}1$$

where σ, E, and ε are the stress, initial stiffness, and strain tensors, respectively. The chemical damage variable is a non-dimensional scalar varying between 0 and 1 and is considered independent of the mechanical one. Isotropic damage is typically considered in these models. Several models define d^c as a function of ion concentration in the pore fluid solution, e.g., calcium in leaching reactions (Gerard, 1996). It may also be described through a variable named chemical porosity ϕc depending exclusively on the reaction extent (Pignatelli et al., 2013). Ulm (2003) described ϕc as volume changes related to calcium leaching reaction occurring at the solid phase boundary. Pignatelli et al. (2013) have used the same concept to describe the chemical damage variable for the alkali-silica reaction.

The mechanical damage variable d^m also varies between 0 and 1. Diverse models are proposed in the literature differing in the way they calculate this parameter. The most widely used, though, is the one proposed by Mazars (1986) due to its simplicity. This model defines an isotropic damage variable with tensile and compressive strength contributions, depending on the stress state (Mazars, 1986).

The concept of continuum damage modelling outlined above is mainly concerned with homogenous single-phase materials. Thus, a rigorous model is needed to build a homogenous material over the complex heterogeneous concrete structures at different scales. The underlying idea of this approach is that it is possible to separate the heterogeneous concrete into phases with, on average, constant material properties. Such models involve three main steps:

- **Representation** deals with the geometrical description of the considered heterogeneous material. This step includes the identification of different mechanical phases of the microstructures in a REV and their mechanical and geometrical characteristics. In the sense of continuum micromechanics, a phase is a material domain that can be identified with a homogeneous deformation state at a given scale, with constant material properties. Geometrical representations at a given scale are commonly generated from statistical information about the size, location, and orientation of the concrete constituents or microscale imaging data (Bosco et al., 2020; Dunant et al., 2013). However,

mechanical properties are measured from mechanical testing, e.g., nanoindentation, at the microscales (Ulm, 2003; Ulm et al., 2004).

- **Localization** is concerned with the mechanical modelling of the interactions between different phases. This step also accounts for the link between the local stress and strain fields within the REV and the macroscopic stress and strain quantities.
- **Homogenization** delivers the effective macroscopic properties of the REV as a function of the microscopic phase properties, their volume fractions, and their specific geometries. Homogenization schemes aim to replace an actual heterogeneous complex body with a fictitious homogeneous one that behaves globally in the same way.

A rough breakdown of the concrete domain into three elementary levels is shown in Figure 3-4.

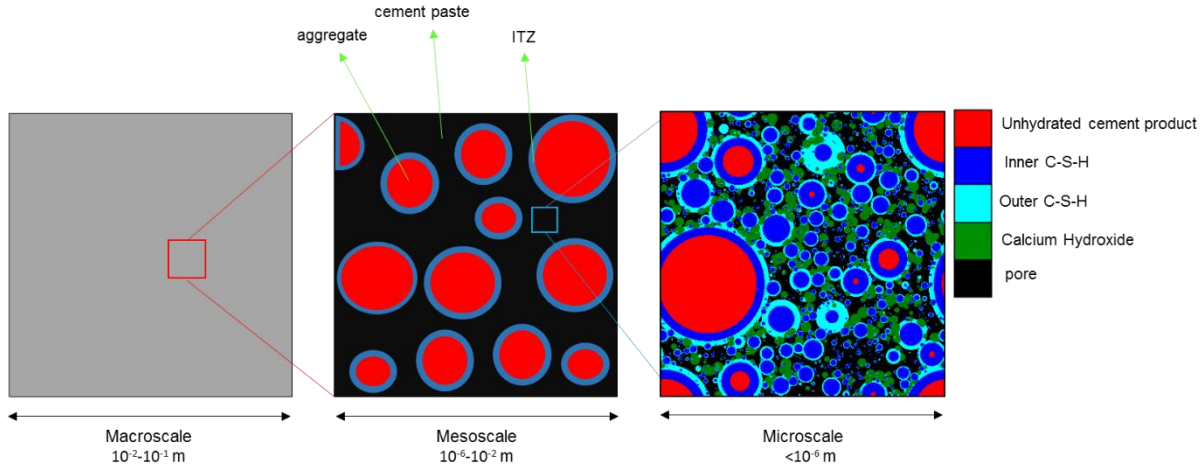

Figure 3-4: Idealized concrete representation involves three different length scales: the macroscale, the mesoscale, and the microscale. ITZ stands for interfacial transition zone.

Concrete is assumed to be a homogenous material characterized with effective material properties at the macroscale. It is then idealized as a two-phase material composed of particle aggregates embedded in the (porous) cement paste at the mesoscale. The presence of an interfacial transition zone (ITZ) at the interface between aggregates and cement paste is also reported for this scale, which is characterized by a higher porosity than the adjacent cement paste. The porous cement paste finally represents the microscale of concrete. This paste comprises a solid phase and capillary pores filled or not filled with water for saturated and unsaturated concrete, respectively. The solid phase typically consists of amorphous hydrate-S-H, portlandite, and unhydrated cement products. Due to the difficulty of identifying material properties for each of these individual components, the cement paste is commonly treated as an isotropic and homogeneous medium (Bosco et al., 2020; Ulm et al., 2004). Yet, homogenization approaches can be extended in a straightforward manner to account for different solid phases at the microscale by modelling them as separate components. Note that these models allow for incorporating even smaller length scales, for instance, to explore the influence of heterogeneities in the hydrate-S-H phase on the effective material properties (Ulm, 2003, Ulm et al., 2004). After this scale separation, the general problem of obtaining apparent or homogenized properties of the concrete at each scale can be approached by employing proper homogenization schemes. As the well-known Mori-Takana, self-consistent and asymptotic schemes have reportedly given reasonable estimates of the time-evolving effective properties of the concrete at different scales (Stora et al., 2010; Wu et al., 2011; Dunant et al., 2013). In homogenization processes, concrete aggregates and pores are generally modelled as sphere-shaped phases for simplicity and regarding the difficulty in characterizing their actual shape. This approximation works quite well for concrete. However, it should be noted that studies on modelling the chemo-mechanical behaviour of sedimentary rocks as analogue cementitious materials have used more generalized prolate or oblate sphere shapes for inclusion phase/pores with different aspect ratios to better capture the rock behaviour (Arson and Vanario, 2015). It is worth mentioning that homogenization schemes may fall short if the phase contrasts at each scale are too

high or the geometrical characteristics are too complex. These limitations, however, are not commonly involved in the case of concrete (Dunant et al., 2013).

3.2 C/M modelling at the macroscale (in saturated and unsaturated environment)

LMDC

3.2.1 Saturated environment

Underground disposal concrete structures are exposed to chemical degradation combined with mechanical loadings due to the host rock convergence and the nuclear waste heating. The saturated environment leads to the concrete leaching. The leaching of calcium can be a matter concerning their service life caused by long-term contact with low pH water, which decreases the performance of concrete (Figure 3-5).

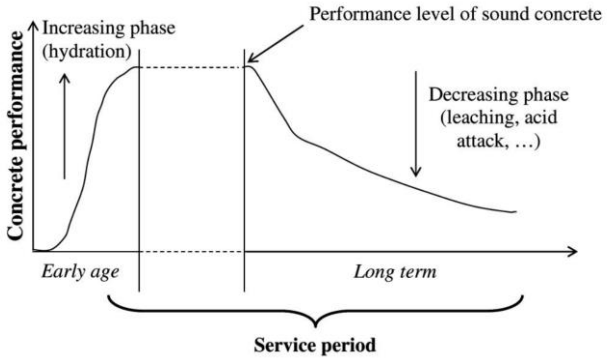

Figure 3-5: Life cycle of concrete in aggressive solution (Buffo-Lacarrière and Sellier, 2011)

3.2.1.1 Modelling of calcium leaching

Calcium is the main element of hydrated cement. It can be used as an indicator to describe the chemical degradation of a cement-based material. Therefore, a simplified approach based on the mass conservation of calcium has been used by some authors to model the chemical degradation of cementitious material, then to reflect these phenomena on mechanical properties (Adenot, 1992; Berner, 1992; Gérard, 1996; Gérard et al., 1998; Torrenti et al., 1999; Gérard, 2002).

The mass balance equation allows to determine the kinetics of calcium leaching where the calcium of the interstitial water can be chosen as a state variable:

$$\frac{\partial(\varphi Ca^{2+})}{\partial t} + \frac{\partial Ca_{solid}}{\partial t} = div\left[D(Ca^{2+}).\overrightarrow{grad}\,Ca^{2+}\right] \qquad 3\text{-}2$$

Where Ca^{2+} is the calcium ionic concentration in interstitial water,φ is the concrete porosity, D is the effective diffusion coefficient of calcium, a function of porosity and the calcium concentration.

The principle of modelling is based on the thermodynamic equilibrium between the pore solution and the surrounding hydrates element of cement (Figure 3-6). Therefore, the dissolution of cement hydrates is controlled by the global equilibrium curve of solid calcium represented by the evolution of the CaO/SiO2 ratio as a function of the calcium concentration in interstitial water (Adenot, 1992; Berner, 1992; Buil, 1992; Gérard et al., 1998).

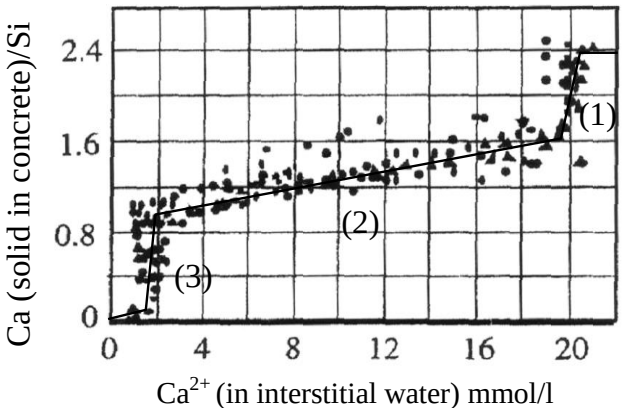

Figure 3-6: Thermodynamic equilibrium curve of solid/liquid calcium (Gérard et al., 1998)

The conservation of mass equation is solved by different methods such as finite difference method, finite element method, finite volume method. The non-linearity of the equation is due to the diffusivity term and the relationship between calcium in solution and solid calcium (the equilibrium curve of Figure 3-6).

The study carried out by Yokozeki et al. (2004) apply the mass conservation equation in the pore solution and the degradation depth of concrete is estimated by the first-order finite difference method. This model is verified with measured experimental data. Yokozeki et al. (2004) studied the effect of bentonite in contact with the concrete on the degradation depth. They showed that the maximum degradation depth of cementitious hydrates is 100 mm in 100 years. This depth decreases in the case of presence of bentonite in contact with concrete to only 70 mm Figure 3-7.

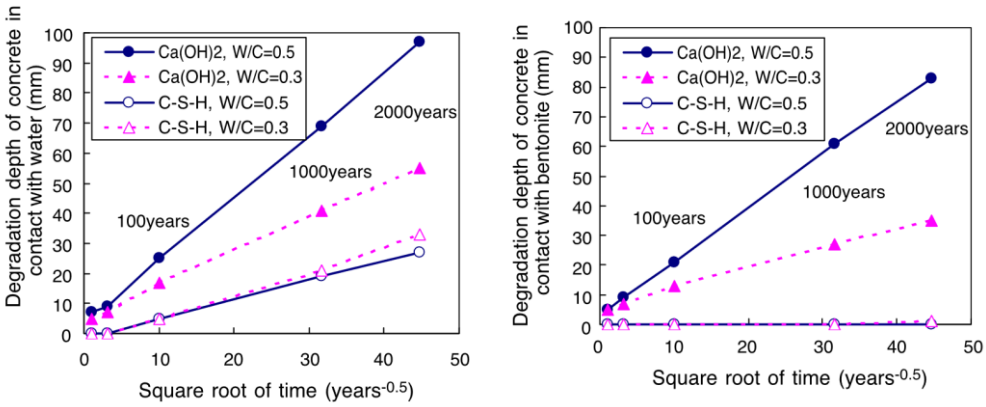

Figure 3-7 : Degradation depth of concrete in contact with water and in the case in presence of bentonite (Yokozeki et al., 2004)

Another study in the scale of the structure based on the mass conservation equation to simulate the degradation depth using the non-linear FE code Cast3m. The geometry of the tunnel is shown in Figure 3-8. Two types of cement are tested, the CEM I have an effective diffusion coefficient $2.5 \times 10^{-12}\ m^2/s$ and for CEMV this value is $0.65 \times 10^{-12}\ m^2/s$. The initial concentration of calcium in the concrete is $22\ mol/m^3$ and the surrounding soil has a value of $10\ mol/m^3$ of calcium concentration. The results of the simulation over 10^6 years of leaching is shown in Figure 3-8. The leaching depth for CEM I is more critical, reaching first the internal corner of the tunnel. The CEM V has high chemical stability and a smaller diffusion coefficient; hence, the leaching process is less important.

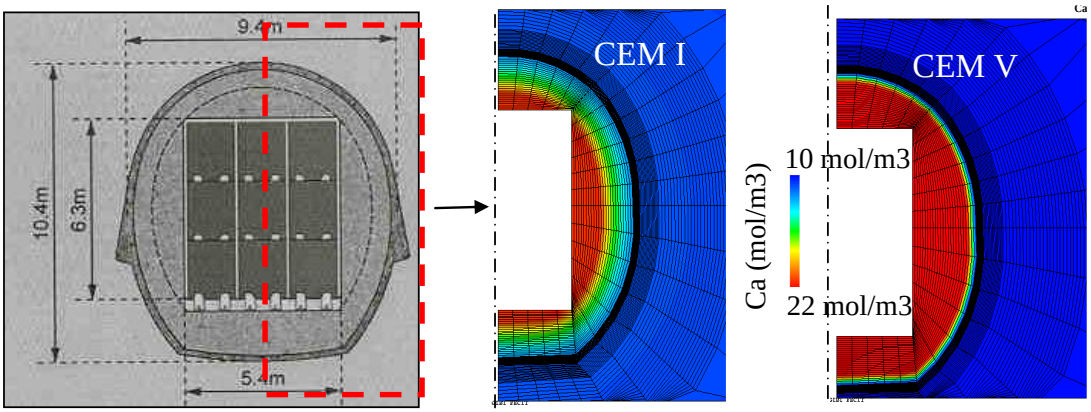

Figure 3-8: The concentration of calcium in interstitial water after 10^6 years of leaching (Sellier et al., 2011)

3.2.1.1 Chemo-mechanical coupling:

The chemo-mechanical coupling models explained previously at pores scale are applicable at macro scale. These models were based on damage theory by defining two variables, the first variable describing the mechanical damage due to cracking and the second to account for chemical degradation(Gerard, 1996; Ulm et al., 1999; Bernard et al., 2003; Heukamp et al., 2003; Kuhl et al., 2004).

Bangert et al. (2003) proposed a chemo mechanical analysis of a concrete panel based on the continuum damage theory of Kanchanov. An isotropic damage parameter *dm* is used this model. The leaching of calcium is modeled by a transient non-linear diffusion equation where *s* is the amount of calcium in the skelton and *c* is the calium in the pore solution. The coupling between calcium leaching and mechanical damage was achieved by defining the total porosity. The damage parameter increases in the leached area (Figure 3-9) wich illustrate the influence of chemical degradation on the materials properties.

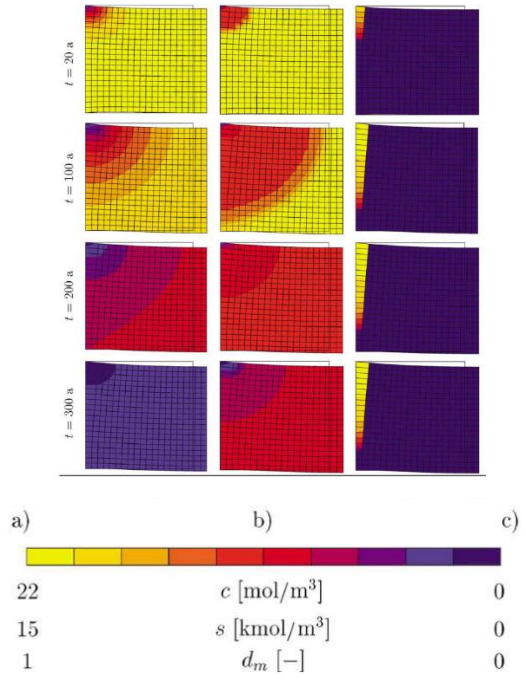

Figure 3-9: Distribution of the (a) calcium concentration c in the pore solution, (b) concentration of calcium in the skelton s, (c) scalar damage parameter *dm* in a concrete pane (Bangert et al.,2003)

The model proposed by Choi et al. (2018), based on an experimental study of a reinforced concrete beam (Figure 3-10), considers a 20-60% reduction in the strength of the sound concrete specimen to simulate the damage associated with leaching. They used the finite element code Abaqus and a model of concrete damage plasticity provided by this code. This model has shown a good agreement to the tests results (Figure 3-11). It was shown that the propagation of leaching degradation increases the compressive block in the beam and the concrete behaviour becomes ductile (Figure 3-12).

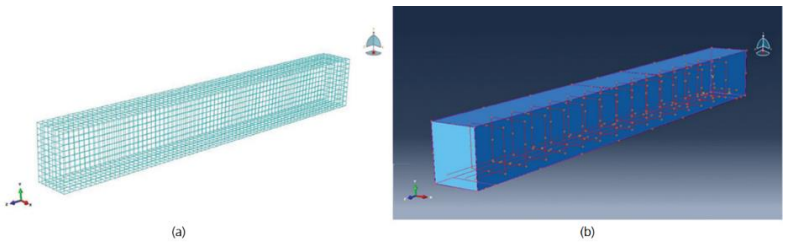

Figure 3-10:The finite element mesh (a) for the concrete, (b) for the reinforcements ans stirrups in the concrete member. (Choi et al.,2018)

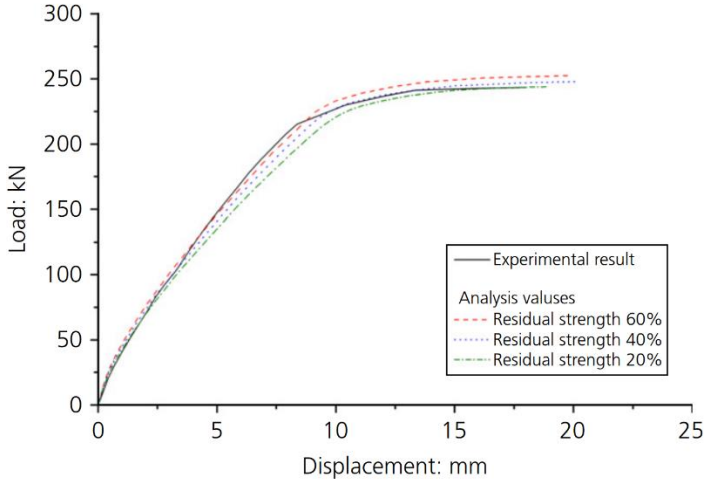

Figure 3-11 :Load-displacement curve (w/c = 0.5) of test results and calculated curves considering a partial reduction of the flexural compressive strengh due to the leaching effect. (Choi et al., 2018)

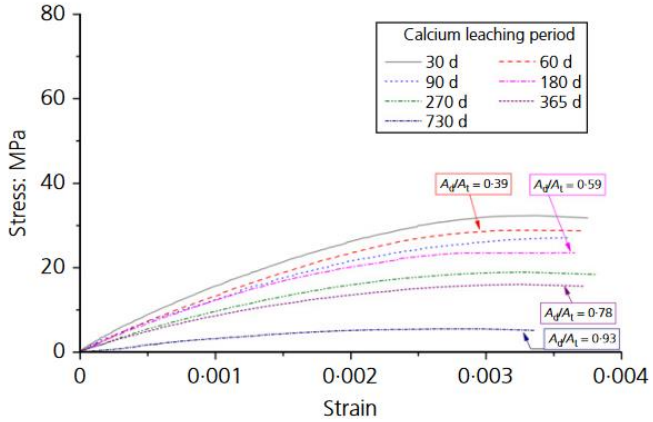

Figure 3-12: Stress-strain curve (w/c=0.5) of the damaged members for different ration of degradation (A_d/A_t) (Choi et al.,2018)

Danèse (1997) proposed a law (Equation 3-4), based on experimental results, allows following the evolution of the microhardness of cement paste as a function of the calcium concentration.

$$H = H_0 \left\{ 0.2 + \left((0.8 - CH_0) \left(\frac{Ca}{Ca_0} \right)^2 + CH \right) \right\} \qquad 3\text{-}3$$

Where: - H_0 is the microhardness of the sound material,

-Ca_0 is the initial calcium concentration,

-Ca is the calcium concentration during leaching process,

-CH_0 is the initial volume fraction of portlandite in the sound fully hydrated paste,

-CH is the volume fraction of portlandite during leaching process.

In order to simulate the mechanical behaviour of concrete specimen. This law has been generalised by Lacarrière et al. (2006) and Sellier (2006) to examine the evolution of different mechanical properties during the leaching process.

$$X = X_0 \left\{ \alpha + \left((1 - \alpha) \left(1 - \frac{CH_0}{\beta} \right) \left(\frac{Ca}{Ca_0} \right)^2 + \frac{CH}{\beta} \right) \right\} \qquad 3\text{-}4$$

The mechanical property of the sound material is represented by X_0, and X is the same property during the leaching process. The coefficient α has been calibrated for each mechanical parameter by an inverse analysis technique based on an experimental. β (equal to 0.8) is a parameter fitted on experimental micro-hardness profile.

Simulations of tensile and compressive tests were performed using the attenuation laws of the mechanical model parameters as a function of the decalcification rate (Lacarrière et al., 2006). The uniaxial behaviour laws of the sound and decalcified materials are compared in Figure 3-13 and Figure 3-14, where the loss of strength and stiffness and the increase in ductility of the decalcified material can be seen.

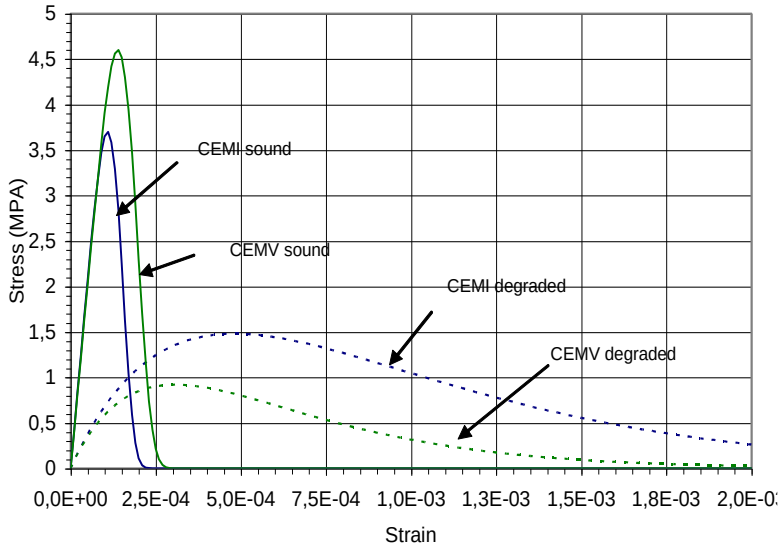

Figure 3-13: The simulation of tensile behaviour for sound and leached concrete (Lacarrière et al., 2006)

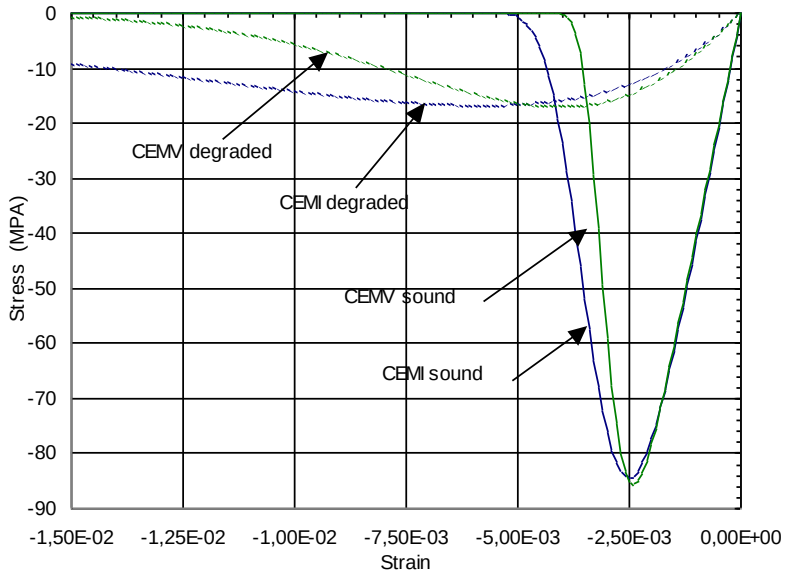

Figure 3-14: The simulation of compressive behaviour for sound and leached concrete (Lacarrière et al., 2006)

A structural scale simulation for a leached tunnel was performed by Sellier et al. (2011) (shown in the part 2.3.1). The equation 3-4 has been implemented in a FE code to simulate the mechanical behaviour of the tunnel. The CEM I was chosen for the simulation over 10^6 years. The chemo-mechanical coupling is treated using a "weak" formulation, where the chemistry and mechanics equations are solved separately. Once the mass equation of calcium is applied to the tunnel mesh and the calcium content has been calculated, the mechanical simulation starts. The deformed mesh shown in Figure 3-15 represents the change of the volume due to the creep in the CEM I based concrete at different times. During the first period, the evolution of volume is due to the interstitial water pressure. After 1300 years, water resaturation is expected to be complete, and decalcification of concrete is calculated to occur, leading to a decrease in its mechanical properties. Creep and leaching of concrete cause localisation of compressive stress in the sound core in the very long term and the occurrence of damage at the tunnel corners (Figure 3-15). At the end of the simulation (1 million years), the radial convergence calculated is about 10 cm between the ceiling and floor of the gallery.

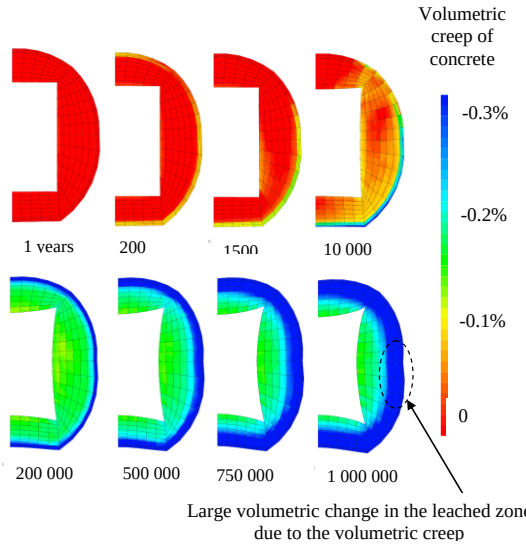

Figure 3-15: Volumetric change after 1 million years due to creep in CEMI based concrete (Sellier et al., 2011)

A hydro-chemo-mechanical model was also developed and implemented in iCP, starting from the previous reactive transport models (Idiart et al., 2019). The HCM model is used to analyse the effect of calcium leaching on the mechanical stability of the BHK vault (SKB concept for geological disposal), studied with 2D models of a cross-section. A range of sensitivity cases is used to evaluate the influence of mechanical boundary conditions and material parameters on the results.

3.2.2 Unsaturated environment

In an unsaturated environment, the durability of reinforced concrete structures is affected by atmospheric carbonation. The modelling of the carbonation process in unsaturated environment is based on the mass conservation equation of the carbon dioxide diffused into the pores (Saetta, Schrefler and Vitaliani, 1993; Ishida and Maekawa, 2000; Ishida, Maekawa and Soltani, 2004; Bary and Mügler, 2006; Phung *et al.*, 2016). The carbonation process can be briefly described as follows: atmospheric carbon dioxide diffuses into the concrete in gaseous form, dissolves in the solution, and reacts with the hydrates in the cement paste, especially the portlandite, to form calcium carbonates $CaCO_3$ (calcite). The simplified equation of carbon dioxide mass conservation is:

$$\frac{\partial\left[\varphi\left((1-S_l)CO_2^g + S_l CO_2^l\right)\right]}{\partial t} + div\left[-(D_{CO2}^l.\nabla CO_2^l + D_{CO2}^g.\nabla CO_2^g\right] = \frac{\partial CaCO_3}{\partial t} \qquad 3\text{-}5$$

Where: - CO_2^g is the carbon dioxide concentration in gaseous form,

- CO_2^l is the carbon dioxide concentration in aqueous form,

-φ is the concrete porosity,

-S_l is the concrete saturation degree,

- D_{CO2}^l is the effective diffusion coefficient of aqueous carbon dioxide,

- D_{CO2}^g is the effective diffusion coefficient of gaseous carbon dioxide.

Henry's law allows to express the equilibrium between the CO_2 concentration in the water in the pores and the atmosphere. Thus, using the law of ideal gases, the concentration of carbon dioxide can be written as follows at a constant temperature, and it's proportional to the partial pressure of CO_2.

$$[CO_2] = n_{CO2}\frac{P_{atm}}{RT} \qquad 3\text{-}6$$

Where $[CO_2]$ is the concentration of carbon dioxide in the atmosphere, n_{CO2} its molar fraction in air, P_{atm} the atmospheric pressure, R= 8.32 J.mol^{-1}.K^{-1} the constant of ideal gases and T the temperature.

Henry's law then allows us to write:

$$[CO_2]_{aq} = H \times P_{CO2} = H \times n_{CO2}P_{atm} \qquad 3\text{-}7$$

Where H is Henry constant equal to $3{,}4\times10^{-2}$ [mol.L^{-1}.atm^{-1}] in pure water at 25°C, this constant depends on the electrolyte studied and on the temperature (Zawisza and Malesinska, 1981); $[CO_2]_{aq}$ in [mol.L^{-1}] is the concentration of carbon dioxide in the aqueous solution, P_{CO2} is the partial pressure of CO_2.

The Ca ionic species is supplied to the pore water by the decalcification of hydrates, while the CO_3 results from the dissolution of carbon dioxide present in the gas phase.

This phenomenon progressively modifies the chemical composition and the internal microstructure of the concrete by acting on the products resulting from the hydration of the cement. The calcite formation equation is represented in Equation 3-8, and the thermodynamic equilibrium of calcite in water at a temperature 20°C is reached according to Equation 3-9 (Plummer and Busenberg, 1982). Ishida et al., (2000) express the rate of this reaction as follow in Equation 3-10 which is the source term in the mass conservation equation.

$$CO_3^{2-} + Ca^{2+} \rightarrow CaCO_3 \quad \text{(calcium carbonate)} \qquad 3\text{-}8$$

$$[CO_3^{2-}]\,[Ca^{2+}] = Kc = 10^{-8,35} \qquad 3\text{-}9$$

$$\frac{\partial CaCO_3}{\partial t} = k[CO_3^{2-}]\,[Ca^{2+}] \qquad 3\text{-}10$$

The resolution of the mass conservation equation is based on finite element simulations. The modelling of the carbonation process must be able to manage the transfer phenomena that occur in a partially saturated environment; the coupling of all the equations that govern these transports in a porous medium and then resolution of different equation in parallel.

Saetta et al. (1993) propose a model based on the consideration of carbon dioxide diffusion carbon dioxide diffusion, water transfer coupled with heat transport and the formation of calcium carbonate crystals and the evolution of porosity as a function of the rate of carbonation.

Ishida et al. (2004) show the importance of the water saturation rate of the material on the evolution of the carbonation depth. The reduction of porosity is driven by the W/C ratio. The authors conclude that the most important factor influencing the depth of carbonation is the diffusion of carbon dioxide. The model is enhanced by Ishida and Li (2008) to integrate a detailed description of the evolution of the microstructure of C-S-H. The model achieves a better accuracy in predicting the evolution of the carbonation depth. Figure 3-16 below shows the progress of carbonation depth in accelerated condition, however this model is limited for CEMI.

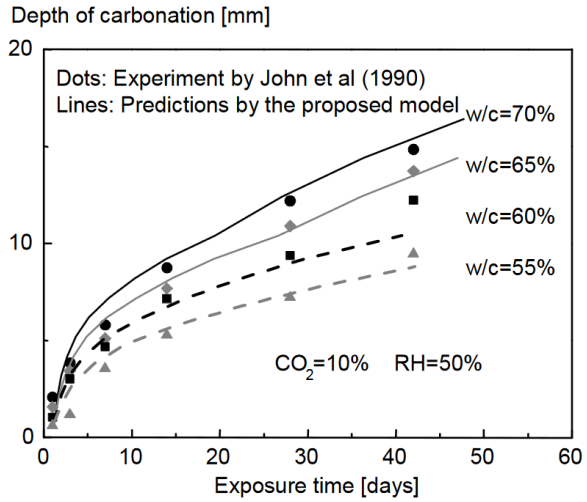

Figure 3-16 : Progress of carbonation depth for different w/c ratio (Ishida and Li, 2008)

The model proposed by Bary and Sellier (2004) couples the transfer of CO_2 in the gas phase with those of liquid water and the calcium ions Ca^{2+} in interstitial solution. The model is based on three mass conservation equations: the mass of water, the mass of calcium and the mass of carbon dioxide.

The model provides the carbonation profiles during decalcification and drying of the material. This model was applied to a CEM I concrete, and the experimental results of accelerated carbonation allowed the parameters calibration and the validation of the model.

The simulation results of accelerated testing are shown in terms of calcium concentration profiles in Figure 3-17 and 3-18 and porosity profiles in Figure 3-18 Bary and Sellier observe that the transport of Ca^{2+} ions, by diffusion and by convection, occurs from the non-carbonated zone (rich in Ca^{2+}) to the carbonation front (where the concentration of calcium is closed to zero), inducing from there the beginning of decalcification and thus an increase in porosity downstream of the carbonation front. After 70 days, the profile of calcium concentration is modified due to calcite formation.

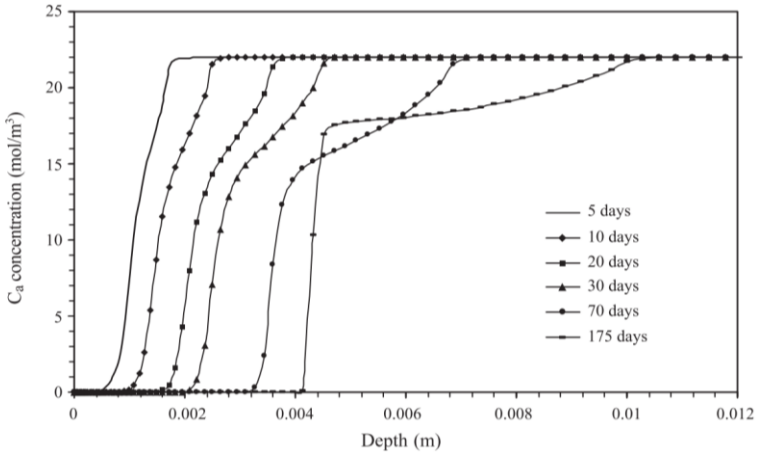

Figure 3-17: Profiles of calcium concentration in interstitial water for different stage of degradation (Bary and Sellier, 2004)

Therefore, the filling of pores by the calcite increases with the progression of the carbonation front, simultaneously, an increase in porosity occurs just before the carbonation front (Figure 3-18).

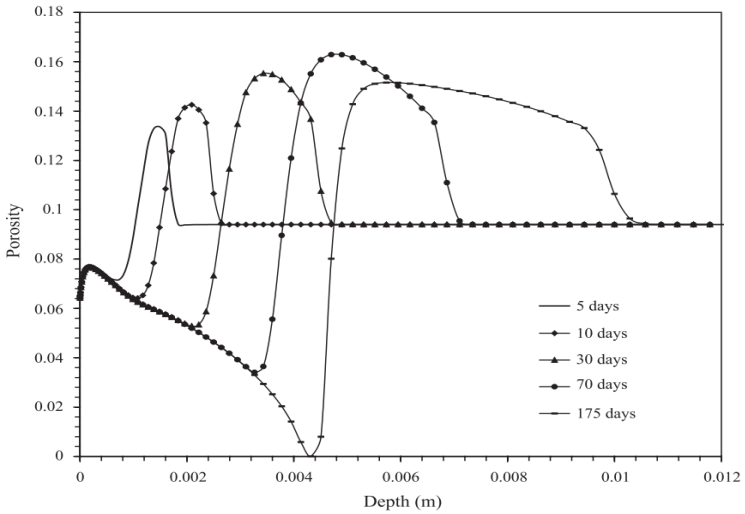

Figure 3-18: Profiles of porosity for different stage of degradation (Bary and Sellier, 2004)

Analytical models of carbonation have been proposed in the case of unidirectional carbonation. These models characterise the carbonation of concrete by calculating the depth of carbonation and its kinetics (Papadakis et al., 1991; Rafaï et al., 2002; Hyvret et al., 2010). The evolution of the carbonation depth is often expressed as follows (Equation 3-11):

$$x_c = A\sqrt{t} \qquad 3\text{-}11$$

x_c Is the depth of carbonation, t is the exposure time, and A is a coefficient that depends on many preponderant parameters in the carbonation mechanism and is related to the accessibility of carbon dioxide, to the quantities of carbonatable calcium, and also depends on the CO_2 partial pressure.

Papadakis et al. propose a modelling of the physico-chemical processes of concrete carbonation which the coefficient A of the above equation takes into account : the diffusion of CO2 in the aqueous phase in the pores of the concrete ; the dissolution of portlandite, its diffusion in the pore solution and its reaction with the dissolved carbon dioxide ; the carbonation of C-S-H and residual C2S and C3S compounds in the anhydrous state; the porosity of the concrete decrease during hydration and carbonation and an equilibrium between the condensation of water vapour on the pore walls of the concrete and the relative humidity.

The elementary model proposed by Hyvert et al. (2010) considers different parameters influencing the carbonation depth evolution (Equation 3-12):

$$x_c = \sqrt{\frac{2.D_0^{co2}.P_0.t}{R.T.Q}} \qquad 3\text{-}12$$

D_0^{co2} is the diffusion coefficient on carbon dioxide, which depends on moisture and porosity filling by calcium carbonates, P_0 the partial pressure of carbon dioxide, T the temperature, R the constant of ideal gases and t the exposure time. The parameter Q in the denominator depends on the quantities of C-S-H as a function of partial pressure of carbon dioxide, as well as the quantities of carbonatable calcium contained in the other hydrates of the cement matrix. This approach shows the dependency of carbonation on partial pressure of carbon dioxide for different types of cement validated with experiment results (Figure 3-19).

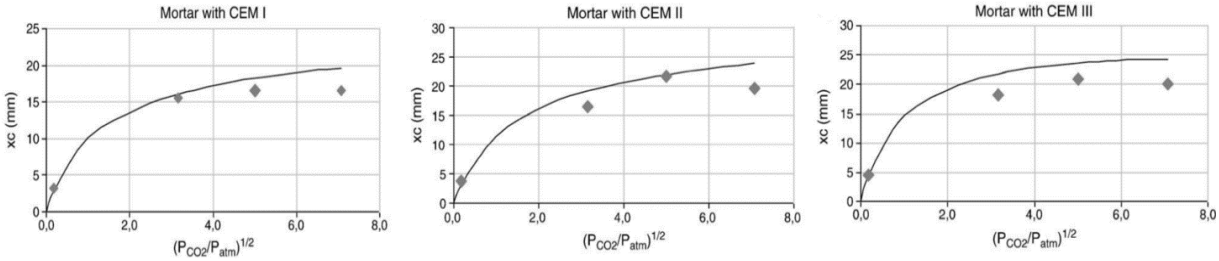

Figure 3-19: Evolution of carbonation depth as a function of carbon dioxide content for different types of cement (Hyvret et al., 2010)

3.3 Synthesis and identified gaps

3.3.1 Pore-scale models

Since the field of pore-scale modelling is relatively young, there are many limits and gaps. The pore scale follows below the continuum REV scales and thus require new conceptualisations that might be different from more established continuum approaches. This is true for both, chemical and mechanical processes. Typically, pore scale models have discrete phases, but they also might include sub-scale elements (for example amorphous phases) that are treated differently. Because of the heterogeneity of cement paste microstructure, the number of voxels/elements of pore-scale models is large. The need for computationally efficient approaches is paramount. The most obvious approach is to use parallelization and more powerful computers, but the physical limit of small time steps at lower spatial scales results in huge amount of iterations and requires broader solution. One mitigation strategy is an effective geochemistry calculation. The solution time of non-linear equations for the geochemical system can be reduced by the use of tabulated values or abstracted chemical systems. On the other hand, the number of time steps can be reduced by adjusting the chemical systems.

Another field that needs attention is the validation of pore-scale models. Most experiments provide continuum or effective values (e.g. mass of a specific solid phase) or information without spatial information, for example pore size distribution. It is very difficult to obtain spatial information of a property at precisely the same location in an evolving material, for example after the geochemical alteration reaction. For this reason, pore scale models are usually validated using averaged values. However, it is important to stress that this is an indirect validation where a part of the important information is lost during averaging. In the future, more efforts need to be devoted to the experimental techniques that can directly support validation of pore scale models.

Coupling between chemistry and mechanics is very recent on the pore scale. This coupling can result in the complex spatial-temporal evolution of composition, microstructure and morphology in materials. The relationships are interconnected as for example not only the formation of the secondary phases cause stresses, but also the stresses influence the conditions of the formation of secondary phases. Reliable chemo-mechanical models are not very common, especially not in a multiscale framework.

Appropriate upscaling is another challenge. The purpose of pore-scale models is to support the choice of parameter values and constitutive laws on larger scales. The upscaling in this sense usually stretches beyond pure mathematical principles and includes the development of conceptual models and concepts that are appropriate to use on larger scales.

3.3.2 Up-scaling of mechanical properties versus cement alteration

Previous structural chemo-mechanical models (Sellier et al., 2011; Buffo-Lacarrière and Sellier, 2011; Nguyen et al., 2007a; Nguyen et al., 2007b) decoupled the macroscopic modelling from the mesoscopic phenomena; however, in order to compare concrete made of the different matrices, a non-linear analytical homogenisation model for the chemical-mechanical behaviour of concrete is required to be implemented. This model must be able to manage the solid phases of cement paste versus the chemical state of concrete, and this must be reflected in the mechanical properties (Young's modulus, compressive and tensile strength, creep rate of concrete, anchorage of steels). Furthermore, during the chemical damage processes (leaching, carbonation, NaCl ingress…in the hydrated cement paste), this model should also consider the amount and nature of aggregates on macroscopic residual mechanical properties.

3.3.3 Impact of chemo-mechanics damages on transfer properties

Another phenomenon to be considered and incorporated into this model is the cracking of reinforced concrete, along with predicting its impact on the transport properties (permeability, diffusion coefficient, water retention curve…) of the concrete.

3.3.4 Reinforcement chemo-mechanical damage

In the case of reinforced concrete, until now, the phenomenon of reinforcement corrosion was decoupled from the chemical state of the concrete (Chalhoub et al., 2020; Millard and L'Hostis, 2012); hence the lock to be lifted in this chemo-mechanical model will consist in predicting the progress of steels corrosion as a function of the chemical state of the concrete at the interface and in localised cracks, and deducing its effect in terms of steel anchorage and their contribution on reinforced concrete mechanical performances.

3.3.5 Implementation of the improvements in finite element codes

The filling of these gaps must be carried out together with the implementation in a Thermo-Hydro-Chemo-Mechanical finite element code able to compute the evolution of a tunnel during several thousand years. Once implemented, it will allow a more accurate prediction of the lifetime of radioactive waste disposal structures, but also the simulation of their very long-term behaviour under mechanical loading (induced by host rock convergence) and physicochemical degradation caused by host rock water (carbonation, leaching, corrosion of the reinforcement bars...). Different chemistry of binders could be considered to perform comparative studies of envisioned solutions.

3.4 References for part 3

Adenot, F. (1992). Durabilité du béton : Caractérisation et modélisation des processus physiques et chimiques de dégradation du ciment. *Ph.D. thesis, Univ. of Orléans, Orléans, France (in French).*

Allan, M., Leal, M., Kulik, D. A., & Saar, M. O. (2017). Ultra-Fast Reactive Transport Simulations When Chemical Reactions Meet Machine Learning: Chemical Equilibrium. *arXiv:1708.04825*.

Arson C., T. Vanario, Chemomechanical evolution of pore space in carbonate microstructures upon dissolution: linking pore geometry to bulk elasticity, Journal of Geophysical Research: Solid Earth 120 (2015) 6878-6894.

Babaei, S. (2021). *A Multiscale Approach to Model Thermo-Hydro-Mechanical Behaviour of non-reinforced Concrete.* PhD Thesis, 1 Apr 2021, UA - Universiteit Antwerpen. 212 p.

Bangert, F. et al. (2003) 'Environmentally induced deterioration of concrete: physical motivation and numerical modeling', Engineering Fracture Mechanics, 70(7–8), pp. 891–910. Available at: https://doi.org/10.1016/S0013-7944(02)00156-X.

Bary, B. and Mügler, C. (2006) 'Simplified modelling and numerical simulations of concrete carbonation in unsaturated conditions', p. 23.

Bary, B., & Sellier, A. (2004). Coupled moisture—carbon dioxide–calcium transfer model for carbonation of concrete. Cement and Concrete Research, 34(10), 1859-1872. https://doi.org/10.1016/j.cemconres.2004.01.025

Bentz, D. (2000). *CEMHYD3D: A Three-Dimensional Cement Hydration and Microstructure Development Modelling Package. Version 2.0.* National Institute of Standards and Technology, Gaithersburg (2000).

Bernard, O., Ulm, F. J., & Germaine, J. T. (2003). Volume and deviator creep of calcium-leached cement-based materials. *Cement and Concrete Research*, *33*(8), 1127-1136.

Berner, U. (1992). Evolution of pore water chemistry during degradation of cement in a radioactive waste repository environment. *Waste Management*, *12*(2-3), 201-219. https://doi.org/10.1016/0956-053x(92)90049-o

Blunt, M., Bijeljic, B. D., Gharbi, O., Iglauer, S., Mostaghimi, P., Paluszny, A., & Pentland, C. (2013). Pore-scale imaging and modelling. *Advances in Water Resources , 5*, 197-216.

Bosco E., R, J.M.A. Classens, A.S.J. Suiker, Multiscale prediction of chemomechanical properties of concrete materials through asymptotic homogenization, Cement and Concrete Research 128 (2020) 105929.

Buffo-Lacarrière, L., & Sellier, A. (2011). Chemo-Mechanical Modeling Requirements for the Assessment of Concrete Structure Service Life. *Journal of Engineering Mechanics*, *137*(9), 625-633. https://doi.org/10.1061/(asce)em.1943-7889.0000261

Carde, C., François, R., & Torrenti, J. M. (1996). Leaching of both calcium hydroxide and C-S-H from cement paste : Modeling the mechanical behaviour. *Cement and Concrete Research*, *26*(8), 1257-1268. https://doi.org/10.1016/0008-8846(96)00095-6

Cast3M. (2019). http://www-cast3m.cea.fr/.

Catalano, E., Chareyre, B., & Barthelemy, E. (2014). Pore-scale modeling of fluid-particles interaction and emerging poromechanical effects. *Int. J. Numer. Anal. Methods Geomech., 38*(1), 51-71.

Caulk, R., Scholtès, L., Krzaczek, M., & Chareyre, B. (2020). A pore-scale thermo–hydro-mechanical model for particulate systems. Computer Methods in Applied Mechanics and Engineering, 372, 113292.

Chalhoub, C., François, R., Garcia, D., Laurens, S., & Carcasses, M. (2020). Macrocell corrosion of steel in concrete: Characterization of anodic behaviour in relation to the chloride content. Materials and Corrosion, 71(9), 1424-1441. https://doi.org/10.1002/maco.201911398

Chen J. K., C. Qian, H. Song, A new chemomechanical model of damage in concrete under sulfate attack, Construction and Building Materials 115 20160 536-543.

Choi, Y. et al. (2018) 'Experimental study on the structural behaviour of calcium-leaching damaged concrete members', Magazine of Concrete Research 70(21): 1102–1117,. Available at: https://doi.org/10.1680/jmacr.17.00297.

Cundall, P., & Strack, O. (1979). A discrete numerical model for granular assemblies. Géotechnique, 2(1), 47-65.

Danèse, S. (1997). Etude du couplage fissuration dégradation chimique des bétons : fissure modèle sur pâte de ciment. End-of-Studies Project, Ecole Nationale Supérieure des Arts et Industries de Strasbourg.

Deby, F., Carcassès, M., & Sellier, A. (2009). Probabilistic approach for durability design of reinforced concrete in marine environment. Cement and Concrete Research, 39(5), 466-471. https://doi.org/10.1016/j.cemconres.2009.03.003

De Lucia, M., Kempka, T., Jatnieks, J., & Kühn, M. (2017). Integrating surrogate models into subsurface simulation framework allows computation of complex reactive transport scenarios. Energy Procedia, 125, 580 – 587;

Deng, H., Molins, S., Steefel, C., DePaolo, D., Voltolini, M., Yang, L., & Ajo-Franklin, J. (2016). A 2.5 d reactive transport model for fracture alteration simulation. Environmental science & technology, 50(14), 7564–7571.

Dorange, G., Marchand, A., & le Guyader, M. (1990). Produit de solubilité de la calcite et constantes de dissociation de CaHCO3+ et CaCO30 entre 5 et 75 °C. Revue des sciences de l'eau / Journal of Water Science, 3(3), 261–275..

Dunant C. F., B. Bary, A. B. Gliorla, C. Peniguel, J. Sanahuja, C. Toulemonde, A.B. Tran, F. Willot, J. Yvonnet, A critical comparison of several numerical methods for computing effective properties of highly heterogeneous materials, Advances in Engineering Software 58 (2013) 1-12.

Dunant C. F., K.L Scrivener, Micro-mechanical modeling of alkali-silica-reaction-induced degradation using AMIE framework, Cement and Concrete Research 40 (2010) 517-525.

Emmanuel, S., & Berkowitz, B. (2007). Effects of pore-size controlled solubility on reactive transport in heterogeneous rock. Geophysical Research Letters, 34(6).

Feng, Y., Han, K., Li, C., & Owen, D. (2008). Discrete thermal element modelling of heat conduction in particle systems: Basic formulations. Journal of Computational Physics, 227(10), 5072-5089.

Ishida, T. and Li, C.-H. (2008) 'Modeling of Carbonation based on Thermo-Hygro Physics with Strong Coupling of Mass Transport and Equilibrium in Micro-pore Structure of Concrete', Journal of Advanced Concrete Technology, 6(2), pp. 303–316. Available at: https://doi.org/10.3151/jact.6.303.

Ishida, T. and Maekawa, K. (2000) 'MODELING OF PH PROFILE IN PORE WATER BASED ON MASS TRANSPORT AND CHEMICAL EQUILIBRIUM THEORY', Doboku Gakkai Ronbunshu, 2000(648), pp. 203–215. Available at: https://doi.org/10.2208/jscej.2000.648_203.

Ishida, T., Maekawa, K. and Soltani, M. (2004) 'Theoretically Identified Strong Coupling of Carbonation Rate and Thermodynamic Moisture States in Micropores of Concrete', Journal of Advanced Concrete Technology, 2(2), pp. 213–222. Available at: https://doi.org/10.3151/jact.2.213.

Gerard B., Contribution of the mechanical, chemical and transport couplings in long term behaviour of radioactive waste repository structures, Ph.D. thesis, Dept. de Genie Civil, Univ. Laval, Quebec, Canda, Ecole Normale Superieure de Cachan, France (1996).

Gérard, B. (2002). Simplified modelling of calcium leaching of concrete in various environments. Materials and Structures, 35(254), 632-640. https://doi.org/10.1617/13937

Gérard, B., Pijaudier-Cabot, G., & Laborderie, C. (1998). Coupled diffusion-damage modelling and the implications on failure due to strain localisation. International Journal of Solids and Structures, 35(31-32), 4107-4120. https://doi.org/10.1016/s0020-7683(97)00304-1

Ghosh, S., Lee, K., & Raghavan, P. (2001). A multi-level computational model for multi-scale damage analysis in composite and porous materials. International Journal of Solids and Structures, 38(14), 2335–2385.

Groen, D., Hetherington, J., Carver, H. B., Nash, R. W., Bernabeu, M. O., & Coveney, P. V. (2013). Analysing and modelling the performance of the HemeLB lattice-Boltzmann simulation environment. Journal of Computational Science, 4(5), 412-422.

Heukamp F. H., Chemomechanics of Calcium Leaching of Cement-Based Materials at Different Scales: The Role of CH-Dissolution and C-S-H-Degradation on Strength and Durability Performance of Materials and Structures, Ph.D. thesis, Massachusetts Institute of Technology, U.S.A. (2003).

Heukamp, F., Ulm, F. J., & Germaine, J. (2001). Mechanical properties of calcium-leached cement pastes. Cement and Concrete Research, 31(5), 767-774. https://doi.org/10.1016/s0008-8846(01)00472-0

HEWLETT, P.C. (1998). Lea's Chemistry of Cement and Concrete. 4th Edition, Arnold, London, England.

Huang, Y., Shao, H., Wieland, E., Kolditz, O., & Kosakowski, G. (2018). A new approach to coupled two-phase reactive transport simulation for long-term degradation of concrete. Construction and Building Materials, 190, 805-829.

Hyvert, N., Sellier, A., Duprat, F., Rougeau, P., & Francisco, P. (2010). Dependency of C–S–H carbonation rate on CO2 pressure to explain transition from accelerated tests to natural carbonation. Cement and Concrete Research, 40(11), 1582-1589. https://doi.org/10.1016/j.cemconres.2010.06.010

Idiart, A., Laviña, M., Coene, E. (2019) Modelling of concrete degradation – Hydro-chemo-mechanical processes Report for the safety evaluation SE-SFL, ISSN 1402-3091 SKB R-19-12 ID 1590478.

Kang, Q., Lichtner, P. C., & Zhang, D. (2007). An improved lattice Boltzmann model for multicomponent reactive transport in porous media at the pore scale. Water Resources Research, 43(12).

Kang, Q., Lichtner, P. C., Viswanathan, H. S., & Abdel-Fattah, A. I. (2010). Pore scale modeling of reactive transport involved in geologic CO2 sequestration. Transport in porous media, 82(1), 197–213.

Kang, Q., Zhang, D., Lichtner, P. C., & Tsimpanogiannis, I. N. (2004). Lattice boltzmann model for crystal growth from supersaturated solution. Geophysical Research Letters, 31(21).

Kuhl D., F. Bangert, G. Meschke, Coupled chemomechanical deterioration of cementitious materials part II: numerical methods and simulations, International Journal of Solid and Structures 41 (2004) 41-67.

Lacarrière, L., Sellier, A., & Bourbon, X. (2006). Concrete mechanical behaviour and calcium leaching weak coupling. Revue Européenne de Génie Civil, 10(9), 1147-1175.

Leal, A. M., Blunt, M. J., and LaForce, T. C. (2014). Efficient chemical equilibrium calculations for geochemical speciation and reactive transport modelling. Geochimica et Cosmochimica Acta, 131:301–322.

Leal, A. M., Kulik, D. A., and Kosakowski, G. (2016a). Computational methods for reactive transport modeling: A Gibbs energy minimization approach for multiphase equilibrium calculations. Advances in Water Resources, 88:231–240.

Leal, A. M., Kulik, D. A., Kosakowski, G., and Saar, M. O. (2016b). Computational methods for reactive transport modeling: An extended law of mass-action, xLMA, method for multiphase equilibrium calculations. Advances in Water Resources, 96:405–422.

Le Bellégo, C. L., Gérard, B., & Pijaudier-Cabot, G. (2000). Chemo-Mechanical Effects in Mortar Beams Subjected to Water Hydrolysis. Journal of Engineering Mechanics, 126(3), 266-272. https://doi.org/10.1061/(asce)0733-9399(2000)126:3(266)

Le Bellégo, C., Pijaudier-Cabot, G., Gérard, B., Dubé, J. F., & Molez, L. (2003). Coupled Mechanical and Chemical Damage in Calcium Leached Cementitious Structures. Journal of Engineering Mechanics, 129(3), 333-341. https://doi.org/10.1061/(asce)0733-9399(2003)129:3(333)

Li, L., Peters, C. A., & Celia, M. A. (2006). Upscaling geochemical reaction rates using pore-scale network modeling. Advances in Water Resources, 29(9), 1351–1370.

Li, Q. S., & Jun, Y.-S. (2017). Incorporating nanoscale effects into a continuum-scale reactive transport model for co2-deteriorated cement. Environmental science & technology, 51(18), 10861–10871.

Liu, S., & Jacques, D. (2017). Coupled reactive transport model study of pore size effects on solubility during cement-bicarbonate water interaction. Chemical Geology, 466, 588–599.

Mahadevan S., V. Agarwal, K. Neal, D. Kosson, D. Adams, Interim report on concrete degradation mechanism and online monitoring techniques, U.S. Department of Energy Office of Nuclear Energy (2014).

Man, H., & van Mier, J. (2008). Influence of particle density on 3D size effects in the fracture of (numerical) concrete. Mech. Mater., 40, 470–486;

Mazars J., A description of micro- and macroscale damage of concrete structures, Engineering Fracture Mechanics 25 (1986) 729-737.

Mazaheripour, H., Faria, R., Ye, G., Schlangen, E., Granja, J., Azenha, M. (2018) Microstructure-based prediction of the elastic behaviour of hydrating cement pastes, Applied Sciences Volume 8 (3) 442.

Millard, A., & L'Hostis, V. (2012). Modelling the effects of steel corrosion in concrete, induced by carbon dioxide penetration. European Journal of Environmental and Civil Engineering, 16(3-4), 375-391. https://doi.org/10.1080/19648189.2012.667976

Molins, S., & Knabner, P. (2019). Multiscale approaches in reactive transport modeling. Reviews in Mineralogy and Geochemistry, 85(1), 27–48.

Molins, S., Soulaine, C., Prasianakis, N., Abbasi, A., Poncet, P., Ladd, A., . . . Steefel, C. (2021). Simulation of mineral dissolution at the pore scale with evolving fluid-solid interfaces: review of approaches and benchmark problem set. Computational Geosciences, 25, 1285–1318.

Molins, S., Trebotich, D., Miller, G. H., & Steefel, C. I. (2017). Mineralogical and transport controls on the evolution of porous media. Water Resources Research, 53(5), 3645–3661.

Nguyen, V., Colina, H., Torrenti, J., Boulay, C., & Nedjar, B. (2007a). Chemo-mechanical coupling behaviour of leached concrete. Nuclear Engineering and Design, 237(20-21), 2083-2089. https://doi.org/10.1016/j.nucengdes.2007.02.013

Nguyen, V., Nedjar, B., & Torrenti, J. (2007b). Chemo-mechanical coupling behaviour of leached concrete. Nuclear Engineering and Design, 237(20-21), 2090-2097. https://doi.org/10.1016/j.nucengdes.2007.02.012

Nooraiepour, M., Masoudi, M., Shokri, N., & Hellevang, H. (2021). Probabilistic Nucleation and Crystal Growth in Porous Medium: New Insights from Calcium Carbonate Precipitation on Primary and Secondary Substrates. ACS Omega, 6, 28072−28083.

Ostoja-Starzewski, M. (2002). Lattice models in micromechanics. Appl Mech Rev, 55, 35-60.

Papadakis V.G., Vayenas C.G., and Fardis M.N. (1991). Physical and Chemical Characteristics Affecting the Durability of Concrete. ACI Materials Journal, 88(2). https://doi.org/10.14359/1993

Patel, R. A., Perko, J., Jacques, D., De Schutter, G., Van Breugel, K., & Ye, G. (2014). A versatile pore-scale multicomponent reactive transport approach based on lattice boltzmann method: Application to portlandite dissolution. Physics and Chemistry of the Earth, Parts A/B/C, 70, 127–137.

Patel, R. A., Perko, J., Jacques, D., De Schutter, G., Ye, G., & Van Bruegel, K. (2018). Effective diffusivity of cement pastes from virtual microstructures : role of gel porosity and capillary pore percolation. CONSTRUCTION AND BUILDING MATERIALS, 165.

Patel, R., Churakov, S., & Prasianakis, N. (2021). A multi-level pore scale reactive transport model for the investigation of combined leaching and carbonation of cement paste. Cement and Concrete Composites, 115, 103831.

Perko, J., & Jacques, D. (2019). Numerically accelerated pore-scale equilibrium dissolution. Journal of contaminant hydrology, 220, 119-127.

Perko, J., Ukrainczyk, N., Šavija, B., Phung, Q. T., & Koenders, E. A. (2020). Influence of Micro-Pore Connectivity and Micro-Fractures on Calcium Leaching of Cement Pastes—A Coupled Simulation Approach. Materials, 13(12), 2697.

Phung, Q. T., Maes, N., & Jacques, D. (2017). Application of Multiple Techniques to Quantify Pore Structure of Degraded Cementitious Materials. . XIV DBMC 14th International Conference on Durability of Building Materials and Components. Ghent.

Phung, Q.T. et al. (2016) 'Modelling the carbonation of cement pastes under a CO2 pressure gradient considering both diffusive and convective transport', Construction and Building Materials, 114, pp. 333–351. Available at: https://doi.org/10.1016/j.conbuildmat.2016.03.191.

Pignatelli R., C. Comi, P. J. M. Monteiro, A coupled chemomechanical model for concrete affected by alkali-silica reaction, Cement and Concrete Research 53 (2013) 196-210.

Plummer, L., & Busenberg, E. (1982). The solubilities of calcite, aragonite and vaterite in CO2-H2O solutions between 0 and 90°C, and an evaluation of the aqueous model for the system CaCO3-CO2-H2O. Geochimica et Cosmochimica Acta, 46(6), 1011-1040. https://doi.org/10.1016/0016-7037(82)90056-4

Poonoosamy, J., Westerwalbesloh, C., Deissmann, G., Mahrous, M., Curti, E., Churakov, S. V., . . . Bosbach, D. (2019). A microfluidic experiment and pore scale modelling diagnostics for assessing mineral precipitation and dissolution in confined spaces. Chemical Geology, 528, 119264.

Prasianakis, N. I., Curti, E., Kosakowski, G., Poonoosamy, J., & Churakov, S. V. (2017). Deciphering pore-level precipitation mechanisms. Nature Scientific Reports, 7, 13765.

Prasianakis, N. I., Gatschet, M., Abbasi, A., & and Churakov, S. (2018). Upscaling strategies of porosity-permeability correlations in reacting environments from pore-scale simulations. Geofluids.

Rafaï, N., Hornain, H., Villain, G., Bouny, V. B., Platret, G., & Chaussadent, T. (2002). Comparaison et validité des méthodes de mesure de la carbonatation. Revue Française de Génie Civil, 6(2), 251-274. https://doi.org/10.1080/12795119.2002.9692364

Rahal, S., & Sellier, A. (2019). Influence of crack reclosure on concrete permeability. Theoretical and Applied Fracture Mechanics, 100, 65-77. https://doi.org/10.1016/j.tafmec.2018.11.010

Rahal, S., Sellier, A., & Verdier, J. (2016). Modelling of change in permeability induced by dilatancy for brittle geomaterials. Construction and Building Materials, 125, 613-624. https://doi.org/10.1016/j.conbuildmat.2016.08.002

Raoof, A., Nick, H., Wolterbeek, T., & and Spiers, C. (2012). Pore-scale modeling of reactive transport in wellbore cement under co2 storage conditions. International Journal of Greenhouse Gas Control, 11, S67–S77.

Rots, J., & Invernizzi, S. (2004). Regularized sequentially linear saw-tooth softening model. Int. J. Numer. Anal. Met., 28, 821–856.

Saetta, A.V., Schrefler, B.A. and Vitaliani, R.V. (1993) 'The carbonation of concrete and the mechanism of moisture, heat and carbon dioxide flow through porous materials', Cement and Concrete Research, 23(4), pp. 761–772. Available at: https://doi.org/10.1016/0008-8846(93)90030-D.

Šavija, B., Zhang, H., & Schlangen, E. (2019). Assessing Hydrated Cement Paste Properties Using Experimentally Informed Discrete Models. J. Mater. Civil. Eng., 31, 04019169.

Schlangen, E., & Garboczi, E. (1997). Fracture simulations of concrete using lattice models: Computational aspects. Eng. Fract. Mech., 57, 319–332.

Schlangen, E., & Vanmier, J. (1992). Simple Lattice Model for Numerical-Simulation of Fracture of Concrete Materials and Structures. Mater. Struct., 25, 534–542.

Schlangen, E., Koenders, E., & Van Breugel, K. (2007). Influence of internal dilation on the fracture behaviour of multi-phase materials. Eng. Fract. Mech., 74, 18–33.

Sciume G., F. Benboudjema, C. D. Sa, F. Pesavento, Y. Berthaud, B. A. Schrefler, A multiphysics model for concrete at early age applied to repairs problems, Engineering Structures 57 (2013) 374-387.

Seigneur, N., L'Hôpital, E., Dauzères, A., Sammaljärvi, J., Voutilainen, M., Labeau, P., . . . Detilleux, V. (2017). Transport properties evolution of cement model system under degradation-incorporation of a

pore-scale approach into reactive transport modelling. Physics and Chemistry of the Earth, Parts A/B/C, 99, 95–109.

Sellier, A. (2006). Modélisation numérique pour la durabilité des ouvrages de génie civil. Dissertation for Habilitation à Diriger des Recherches, Université Paul Sabatier, Toulouse.

Sellier, A., & Millard, A. (2019). A homogenized formulation to account for sliding of non-meshed reinforcements during the cracking of brittle matrix composites: Application to reinforced concrete. Engineering Fracture Mechanics, 213, 182-196. https://doi.org/10.1016/j.engfracmech.2019.04.008

Sellier, A., Buffo-Lacarrière, L., Gonnouni, M. E., & Bourbon, X. (2011). Behaviour of HPC nuclear waste disposal structures in leaching environment. Nuclear Engineering and Design, 241(1), 402-414. https://doi.org/10.1016/j.nucengdes.2010.11.002

Shih, S.-M., Ho, C.-S., Song, Y.-S., & Lin, J.-P. (1999). Kinetics of the reaction of Ca(OH)2 with CO2 at low temperature. Industrial & engineering chemistry research, 38(4), 1316–1322.

Smilauer, V., Bittnar, Z. (2006) Microstructure-based micromechanical prediction of elastic properties in hydrating cement paste, Cement and Concrete Research, 36 (9) 1708-1718.

Starchenko, V. (2022). Pore-Scale Modeling of Mineral Growth and Nucleation in Reactive Flow. Frontiers in Water, 3.

Stora, E. B., He, Q.-C., Deville, E., & Montarnal, P. (2010). Modelling and simulations of the chemo-mechanical behaviour of leached cement-based materials: Interactions between damage and leaching. Cement and Concrete Research, 40(8), 1226-1236.

Tartakovsky, A. M., Meakin, P., Scheibe, T. D., & Wood, B. (2007). A smoothed particle hydrodynamics model for reactive transport and mineral precipitation in porous and fractured porous media. Water resources research, 43(5).

Thiery, M. (2005). Modelling of atmospheric carbonation of cement based materials considering the kinetic effects and modifications of the microstructure and the hydric state. Engineering Sciences [physics]. Ecole des Ponts ParisTech, 2005. Ph.D. thesis in frensh. ffpastel-00001517.

Thomas, J. J., Hsieh, J., & Jennings, H. M. (1996). Effect of carbonation on the nitrogen bet surface area of hardened portland cement paste. Advanced cement based materials, 3(2), 76–80.

Torrenti, J. M., Didry, O., Ollivier, J. P., & Has, F. (1999). The degradation of concrete: couplings between cracking and chemical degradation. Hermes Science Press, Paris, Paris, (in French)., 128-130.

Ulm F. J., Chemomechanics of concrete at finer scales, Materials and Structures 36 (2003) 426-438.

Ulm F.J, O. Coussy, Couplings in early-age concrete: from material modeling to structural design, International Journal of Solid Structures 35 (1998) 4295-4311.

Ulm F.J., G. Constantinides, F.H. Heukamp, Is concrete a poromechanics material? - A multiscale investigation of poroelastic properties, Concrete Science and Engineering 37 (2004) 43-58.

Ulm, F. J., Torrenti, J. M., & Adenot, F. (1999). Chemoporoplasticity of Calcium Leaching in Concrete. Journal of Engineering Mechanics, 125(10), 1200-1211. https://doi.org/10.1061/(asce)0733-9399(1999)125:10(1200)

Varzina, A., Cizer, Ö., Yu, L., Liu, S., Jacques, D., & Perko, J. (2020). A new concept for pore-scale precipitation-dissolution modelling in a lattice Boltzmann framework – Application to portlandite carbonation. Applied Geochemistry, 123, 104786.

Wu T., I. Temizer, P Wriggers, A method of two-scale chemo-thermo-mechanical coupling for concrete, XI Conference on computational plasticity, fundamentals, and applications (2011) 1637-1648.

Ye, G. (2003). Experimental Study and Numerical Simulation of the Development of the Microstructure and Permeability of Cementitious Materials. Ph.D. Thesis, TU Delft, Delft University of Technology, Delft, The Netherlands.

Yokozeki, K. et al. (2004) 'Modeling of leaching from cementitious materials used in underground environment', Applied Clay Science, 26(1–4), pp. 293–308. Available at: https://doi.org/10.1016/j.clay.2003.12.027.

Yoon, H., Valocchi, A. J., Werth, C. J., & Dewers, T. (2012). Pore-scale simulation of mixing-induced calcium carbonate precipitation and dissolution in a microfluidic pore network. Water Resources Research, 48(2).

Zawisza, A., & Malesinska, B. (1981). Solubility of carbon dioxide in liquid water and of water in gaseous carbon dioxide in the range 0.2-5 MPa and at temperatures up to 473 K. Journal of Chemical & Engineering Data, 26(4), 388-391. https://doi.org/10.1021/je00026a012

Zhang, H., Šavija, B., & Schlangen, E. (2018). Towards understanding stochastic fracture performance of cement paste at micro length scale based on numerical simulation. Construction and building Materials, 183, 189–201.

4. Microbial activity influence on the chemo-mechanical behaviour of concrete

Microorganisms are highly adaptable and versatile single-cell living organisms inhabiting diverse environments including highly alkaline ones. Microbes utilize nutrients and energy sources from the living environment for their growth. As a result, they secrete metabolic by-products that are either harmful (causing bio-deterioration) or beneficial (healing of the concrete cracks by calcium carbonate precipitation) to surrounding environments. However, the extent of both processes in the frame of geological disposal are not yet clarified. Studies carried out in the past in this type of context are very limited. However, several experimental programs were conducted in other environments like sewage pipes and structures exposed to marine conditions (Part 4.1). A second part (Part 4.2) will focus more on the assessment of microbial population likely to be encountered in geological disposal and likely to alter the chemo-mechanical properties of concretes. A synthesis is also proposed about the preliminary studies existing in the field of geological disposal (Part 4.3) before a synthesis (Part 4.4) identifying the remaining gaps and justifying the studies proposed in the MAGIC WP.

4.1 Knowledge synthesis of microbial impact on cementitious materials in various contexts (sewage pipes, marine structures)

TUL (T.D. Le, V. Hlavackova), SCK-CEN (K. Mijnendonckx)

Microbial degradation of cementitious materials has been shown in various environments such as sewage pipes, marine structures and wastewater treatment systems (reviewed in Wei et al. 2013). Generally, immediately after its construction, the highly alkaline environment imposed by the cement inhibits microbial activity. However, several processes affect the chemical evolution of cementitious materials, resulting in a local decrease in pH, which enables microbial activity. Furthermore, concrete is a quasi-brittle material, leading to the formation of (micro)cracks through which microorganisms are able to migrate. Microbes generally form biofilms, clusters of dead and alive cells embedded in extracellular polymeric substances (EPS) to protect themselves from harsh conditions. Biofilms contract and swell due to physical tension and continue weakening minerals underneath the surface crust and disintegrating binding material of the outer surface. This process increases the moisture content in the pores. EPS and metabolic products can dissolve and bind salts from the concrete. This can favour microbial growth and degradation of cement (De Graef et al., 2005). Moreover, biofilms facilitate generation of locally high concentrations of harmful metabolites (Magniont et al., 2011) leading to dramatic changes in concrete material properties such as loss of alkalinity, corrosion of rebars, erosion, and finally collapse (De Belie et al., 2000; Bertron et al., 2005).

Microbial influenced degradation of concrete is caused due to excretion of the metabolic intermediates or end products and exoenzyme (De Graef et al., 2005). In general, the metabolic by-products can react with the cement, resulting in the formation of soluble calcium salts. Leaching of calcium from the cement can result in an increased porosity and a decreased pH value at the surface layer. Subsequently, degradation proceeds gradually to the interior concrete matrix, affecting the whole structure. The rate and degree of concrete biodegradation depend on physical and geochemical parameters that control microbial growth and activity. Some parameters are carbon flow, H2, availability and abundance of energy sources like compounds involved in sulphur, iron, and nitrogen oxidation, and bioavailability of microbes (Turick and Berry, 2016). The main microbiological actors of biodeterioration in concrete are bacteria and fungi, both being major components of an acidic or neutral biofilm. Fungi are able to disrupt chemically and mechanically the surface by growing fungal fibres (Warscheid and Braams, 2000; Mahapatra and Banerjee, 2013) and also produce an extracellular matrix that helps to maintain biofilm cohesion. Three different genera of bacteria are primarily responsible for cement degradation: organic acid-producing heterotrophic bacteria, nitrifying bacteria, and sulphur-oxidizing bacteria. Heterotrophic bacteria can produce organic acids by assimilating organic carbon compounds such as lactic, citric, gluconic, malic, and some other acids that are by-products of their metabolism. Nitrifying bacteria are commonly found in soil and are chemoautotrophs. They obtain energy through the oxidation of inorganic

nitrogen compounds and produce nitric acid, which can dissolve the concrete and break it down into calcium nitrate. Their growth is not sequential; instead, they are found as mixed cultures of different nitrifying bacteria. Sulphur-oxidizing bacteria (SOB) are most often associated with the biological degradation of concrete. They corrode the cement by producing sulphuric acid (Rogers et al., 1996). The biodegradation process of cement in the natural environment is slow, which makes it difficult to study its kinetics. Nevertheless, the mechanism of biodeterioration is known in several environments.

4.1.1 Biodeterioration of sewage systems

Wastewater collection and its transportation occurs through sewer systems, which are mainly constructed of reinforced concrete. Since the 1940's it is clear that the most important cause of sewer concrete corrosion has a biological origin (Parker 1945). Concrete corrosion is a considerable problem with a serious economic impact with the catastrophic biogenic sulphuric-acid attack of the Hamburg sewer system reported by Sand and Bock in 1988 as an example. A newly completed sewage system with its high alkalinity provides an antimicrobial environment. However, processes such as carbonation and the production of hydrogen sulphide (H_2S) lower the pH, providing a more favourable environment for microbial activity (Figure 4-1). Hydrogen sulphide is ubiquitously present in sewer systems and is produced by SRB mostly in the pumped sections of the sewer network. On its turn, H_2S is transported to the gravity flow sections of the sewer network and is released to the gas phase and absorbed in the condensation layer of the pipe surface. There, H_2S is oxidized to H_2SO_4 by sulphide oxidizing bacteria (SOB) that disrupts the concrete surface and further lowers the pH (Okabe et al., 2007). Furthermore, H_2SO_4 can diffuse through a biofilm layer to the concrete surface up to 2 mm deep (Okabe et al., 2007). The interaction of H_2SO_4 with calcium silicate results in the formation of gypsum ($CaSO_4 \cdot 2H_2O$). Further watering of cement leads to the reaction of gypsum with calcium aluminate and the formation of ettringite ($((CaO)_3 \cdot Al_2O_3 \cdot (CaSO_4)_3 \cdot 32H_2O)$). Both gypsum and ettringite are expansive minerals and cause internal cracking and spalling. This provides a large surface area for chemical reactions to occur, hence increases the corrosion progress (Parande et al., 2006).

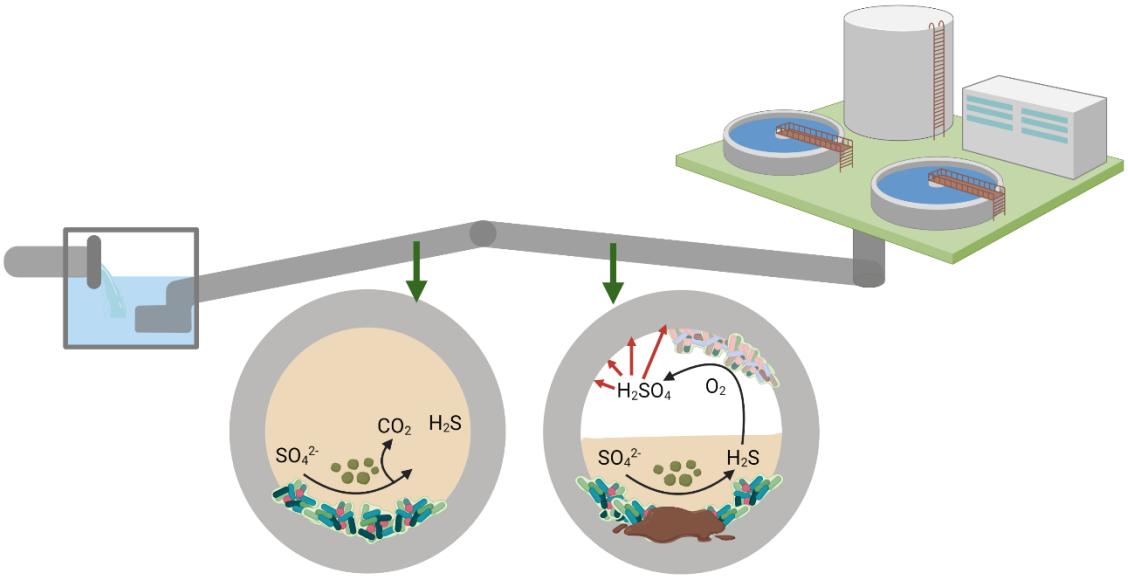

Figure 4-1: Part of the sewer network and cross-sections of a pumped section and a gravity pipe with the main biological reactions that result in concrete deterioration. Figure adapted from (Li et al. 2017) and created with BioRender.com.

However, the negative impacts are not just only exerted by sulphur bacteria but also by the whole microbial community colonizing on the surface of the concrete (Satoh et al., 2009; Wei et al., 2013). In some cases, acidophilic iron oxidizing bacteria also play a role as these bacteria can be involved in the formation of magnetite, which can cause local changes in the structure of concrete (Yamanaka et al., 2002, Jiang et al., 2014). Moreover, in environments with a low concentration of H_2S, locally microbially

produced acids, whether inorganic (HNO_3, H_2CO_3) or organic (lactic, acetic etc.) can cause the deterioration (Turick and Berry, 2016).

4.1.2 Deterioration and biofouling of marine structures

Chloride ingress and magnesium attack are considered as the most important degradation processes for concrete structures in marine environments. However, microbial induced corrosion can also be significant. Deterioration of the marine constructions depends on the level of irrigation. A marine environment can be classified into four zones with their own effects: atmospheric, tidal, splash, and submerged zones (Islam et al., 2010; Ting et al., 2021). Structures that are repeatedly watered and splashed are prone to higher rate of corrosion (high concentration of oxygen and chlorides) whereas those steadily submerged or atmospheric places with low oxygen exposure and low chloride content respectively, are less affected (Ting et al., 2021).

Once the concrete structure is submerged, seawater with high concentration of chloride (up to 17087 ppm) penetrating into the structure via pores initiates the corrosion in the absence of oxygen and carbon dioxide (Mohammed et al., 2004). Furthermore, increasing hydrostatic pressure with depth and other penetrated harmful ions can intensify the deterioration. However, the main corrosive cause in marine environments is not in the submerged zone, but the tidal and splash zones. The variation of tidal current levels causes the different wetting and drying cycles initiating the electrochemical process of corrosion, and building up harmful ions at the rebar level (Browne et al., 1977; Ting et al., 2021). Moreover, the availability of oxygen and carbon dioxide can speed up the deterioration.

Recently, it has been shown that a biofilm on submerged concrete constructions can have a protective effect by a process called biofouling (Chlayon et al., 2018; Georges et al., 2021; Lv et al., 2021) (Figure 4-2). After being immersed underwater, the structure surfaces absorb organic and inorganic compounds with a mechanism known as “surface conditioning” adsorption. This modifies the physicochemical properties of the structure surfaces and makes them favourable to the adhesion of marine bacteria (Siboni et al., 2007; Grzegorczyk et al., 2018). The biofilm facilitates the colonization of other organisms (e.g. cyanobacteria, fungi, algae and protozoa) on the concrete surfaces and eventually form the macrofouling (Chambers et al., 2006; Mieszkin et al., 2013; Grzegorczyk et al., 2018). The characteristics of each biofouling depend on the thickness and adhesive strengths of the macrofouling (Bixler and Bhushan 2012). The biofouling functions as a barrier against physical and chemical attack by reducing surface permeability and accessibility of aggressive ions (Cl^-, Mg^{2+}, and OH^-), which in turn leads to an increase of durability of concrete structure underwater (Coombes et al., 2017; Chlayon et al., 2018). On the contrary, other studies show detrimental effect of biofouling on mechanical properties of concrete marine structures (Hughes et al., 2013; Georges et al., 2021). For example, at the microscale, colonization and growth of algal filaments between fine aggregates and cement proves how filamentous microorganisms may contribute to loss of mechanical strength (Hughes et al., 2013).

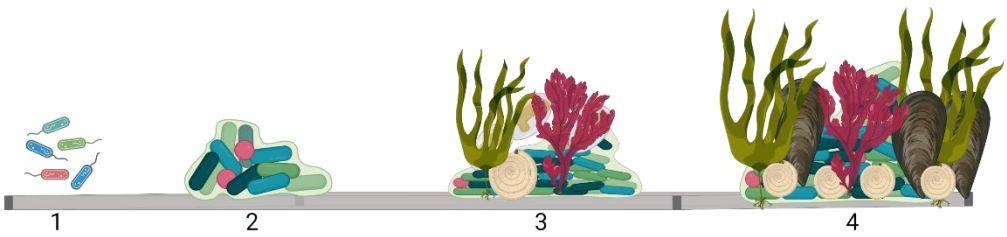

Figure 4-2: Principle of biofouling. (1-2) microbial film formation allows (3-4) the growth of diatoms, algae, invertebrates and other eukaryotes. Figure adapted from (Hayek et al. 2021) and created with Biorender.com.

4.1.3 Microbial induced calcite precipitation

Early studies reported that almost all bacteria are capable of $CaCO_3$ precipitation, which occurs as a by-product of their metabolic processes such as sulphate reduction and urea hydrolysis and are beneficial

for healing of cracks in cement-based materials (Siddique et al., 2011). These bacteria species are found in various natural environments like soil, geological formations, freshwater biofilms, oceans, and saline lakes. Some of the most common bacteria used in crack healing of concrete that produce carbonate are *Bacillus pasteurii*, *Pseudomonas aeruginosa*, *Bacillus sphaericus*, and *Shewanella* spp. (Alshalif et al., 2016).

Calcium carbonate precipitation can occur by two different mechanisms: controlled or induced by microbes (Lowenstam and Weiner, 1989). First, the controlled mechanism in bacteria has several steps i.e. nucleating and maturely growing mineral particles, which are independent of environmental conditions and specific for a certain species (De Muynck et al., 2010). However, the second mechanism, microbial-induced mineral deposition, is considered to be the most dominant pathway. This calcite production pathway is heavily dependent on the environmental conditions and can involve various microbial species (Boquet et al., 1973; Rivadeneyra et al., 1994; Douglas and Beveridge, 1998).

Microbial-induced calcite precipitation (MICP) is a chemical process with four key factors: the concentration of calcium and inorganic carbon, pH, and the availability of nucleation sites (Hammes and Verstraete, 2002). Two broad metabolic pathways are involved in bacteria: the autotrophic– and heterotrophic-mediated pathway. In brief, the autotrophic-mediated pathway occurs when calcium ions and CO_2 are available in the environment. In the heterotrophic-mediated pathway, MICP occurs through two different cycles: sulphur and nitrogen cycles with the urea degradation pathway belonging to the nitrogen cycle widely used in various applications (Castanier et al., 1999). The urea hydrolysis pathway is induced when urea is available in the environment where bacteria comprising a urease enzyme are present. The urea is hydrolysed into carbonates, ammonia, and hydroxide ions. The amount of ammonia increases the pH level creating an alkaline environment around the bacterial cell. The negatively charged components of the bacterial cell wall attract positively charged cations e.g. Ca^{2+} and Mg^{2+} from the surroundings and as such enable formation of the favourable nucleating sites. The formation of carbonate together with the availability of calcium ions precipitates calcium carbonate at the bacterial surface (Joshi et al., 2017).

The intrinsic characteristic of the MICP in cementitious materials have been intensively investigated. MICP has been approached as a promising eco-solution to reduce the permeability and mechanical properties of the concrete structure. It can support the refinement of pores and enable healing of external cracks up to 1 mm (Wang et al., 2014; Luo et al., 2015; Kaur et al., 2016). Ramachandran et al. (2001) suggested the use of MICP in cracked mortar with an improvement of compressive strength. However, using MICP to heal deeper cracks is less effective than to heal shallow ones. An improvement in strength and leakage preventing properties was observed when treating the fly ash-amended mortar and concrete specimens with *Bacillus megaterium* (Achal et al., 2011). Kim et al. reported the forming of denser calcium carbonate crystals and lower weight increment when using *Bacillus sphaericus* in comparison with *Sporosarcina pasteurii* (Kim et al., 2013). Two other studies report an increase in compressive strength of 49% with treatment using *B. cohnii* (Kumari et al., 2017) and of 30% for treatment using *B. subtilis* (Kalhori and Bagherpour, 2017) showing promising advantages of ureolytic organisms in this field. However, optimizations are still needed. Bacteria actively growing in oxygen conditions better perform calcium carbonate precipitation (Nielsen et al., 2020). To enhance the effectiveness of calcium carbonate precipitation, a technology using polyurethane-immobilized *S. pasteurii* cells in the treatment of cement matrices could be used (Bang et al., 2001). Luo et al. (2015) found a decrease in the healing effect of 60-day-old cracks due to the reduction of viable bacteria in such an environment of aged cement mortar. Jonkers (2011) also investigated and confirmed a higher healing effect in *B. pseudormus* spores than vegetative cells in proper conditions and enough nutrients. Moreover, a dramatic decrease in bacterial survival rate shows the unstable self-healing efficiency.

Some investigators address the putative negative aspects of the ammonia production in the ureolytic cycle by using alternative energy sources or alternative microorganisms. To challenge this, the usage of carbon dioxide instead of urea as an energy source in *B. megaterium* SS3 has been proposed (Kaur et al., 2016). The treatment of CO_2 resulted in a higher compressive strength (117 %) in comparison to urea (49 %) showing the improvement of this replacement. Another way to overcome the problem is

using alternative genera with different mechanisms of MICP. For instance, cyanobacteria *Synechococcus* PCC8806 can form a thick layer of calcite-cell aggregation attaching to the concrete and leading to a decrease of water permeability (Zhu et al., 2015). Byrd et al. (2021) studied the degradation of citric acid in anaerobic conditions with initial pH of 11.2. The degradation of citrate CO_3^{2-} /HCO_3^- species. These species could react with Ca^{2+}(aq), derived from cement, to form sparingly-soluble minerals such as calcite. There was a decrease in pH to a value of 9 and a decrease in Ca^{2+}. Data from SEM, EDS, and 3D XCT revealed precipitation of calcite coating on the cement sample.

4.2 Assessment of microbial populations likely to be encountered in geological disposals and to create problems for concrete structures.

ANDRA, Uni. Manchester

Microbes are exceedingly adaptable, and they are successful in colonizing new environments. In fact, environments provide the conditions necessary for the selection and adaptation of the organisms (Chapelle, 2001; Onstott et al., 2009). The relative importance of various microbial processes in a specific repository greatly depends on the ambient environment of the repository, and the materials to be emplaced. Free space/open volumes (porosity, cracks…), moisture, energy sources and supply of nutriments are limiting factors with respect to microbial life (Stroes-Gascoyne et al. 2002; Masurat et al., 2010a,b). In addition to this, several environmental parameters like pH, temperature, or pressure could influence the microbial activity. Waste disposal concepts considered by a large majority of the waste management agencies around the world include various environments that we have to distinguish in order to assess the microbial populations able to affect the concrete structures (Meike and Stroes-Gascoyne, 2000).

4.2.1 Physiochemical factors that influence microbial activity

Successful approaches to assess microbial population associated to concrete biodegradation will likely be most successful if they take concrete composition, present materials and specific environmental parameters into account at each location and each life-phase of a disposal. For instance, some specific localizations and time conditions are known to reduce the microbial potential:

- Localization (sedimentary or crystalline host rock; EDZ; interface or inside materials) and present materials (reworked clay materials; steel re-bars; metallic overpack) to constrain space availability and nutriment flux;
- Before (short-term) / after closure (medium-long-term) to constrain the moisture and the redox conditions;
- Inside / outside waste cells to constrain the carbon sources availability.

By taking in account these space and time conditions and considering the vast diversity of microorganisms and their capacity to grow in harsh environments, the following parameters provide some guidance as to potential occurrence of microbial activity susceptible to change the mechanical properties of concrete.

4.2.1.1 Free space and porosity

The Bacteria and Archaea are exclusively microorganisms and are usually in the range 0.2 - 2 µm in diameter (Ultramicrobacteria could be smaller with less than 0.1 μm^3 in volume) , whereas unicellular eukaryotes (i.e., protozoa, fungi, primitive animals) may be as large as 1 mm in size. Due to their small size and simple, often specialized, metabolism, many microbial representatives have the potential to survive within the small matrices of subsurface environments, as evidenced by numerous reports of various members of Bacteria and Archaea having been recovered from subsurface samples (Urios et al., 2012 ; Mayeux et al., 2013 ; Bagnould, 2015 ; Gam et al., 2016 ; Leupin et al., 2017).

Whatever is the cement considered, the porous network limits the penetration of microorganisms because the access to the network in hardened cement paste is made by pore diameters that are lower

than the size of many bacteria. The presence of aggregates in mortars/concretes produces a second family of porosity, at the interface of cement matrix and aggregates. Their thresholds of access can reach few µm and could authorize the penetration of the microorganisms (Bur et al., 2010). By characterizing the porous network and its evolution on several samples of mortars, Bur et al. (2010) revealed a "skin phenomenon". This zone of 8 to 12 mm thickness, depending on the cement grades studied, controls the penetration of water with the chemical and biological elements present in it. This skin can therefore be colonized by bacteria. This study also shows the effect of the formulation on the microstructure of the material by increasing the macroporosity and the skin phenomenon. In particular, the accessible porosity increases with the proportion of blast furnace slag in the cement and is accessible at an increasing average threshold: 0.4 µm for CEM I, 0.9 µm for CEM III/A and 1.3 µm for CEM III/C. Interfaces between concrete structures and other materials are privileged places for microorganisms to develop and to be active. At these interfaces, the bacteria have generally more space and moisture and sufficient nutrients could be accumulated or be transited (Krumholz et al., 1997). In opposite, in the concrete material itself, if the open porosity and the pore interconnectivity is not sufficiently developed, microfauna or microflora will only be able to develop on the external surfaces. On the other hand, the local environment, at the concrete pore scale, should be enough evolved to impose a bacteria life-adapted pH and an ionic strength of the pore water solution (see below).

4.2.1.2 Moisture

Water is essential for microbial growth. The hydric conditions of a disposal settled in a sedimentary rock could be considerably modified by the closure of the repository and then the resaturation of around the galleries and ILW disposal cells. Before, during and after the thermal transient, the hydric conditions are also going to change.

Water availability can be expressed as water activity (a_w), a ratio of air vapor pressure in equilibrium with a solution to the vapor pressure of pure water. Water activity values are from 0 to 1, with most agricultural soils between 0.9 and 1. In general, microbial growth occurs at aw values from 1 to 0.75 (Pedersen and Karlsson, 1995; Brown, 1976), with fungi usually more tolerant of low moisture conditions (Turick and Berry, 2016). Many bacteria are not able to grow below approximately 0.90 and most of them perish, sporulate, or become dormant when water activity falls below 0.6 (Lin et al., 2007 ; Leupin et al. 2017).

In a full-scale test conducted at Atomic Energy Canada Ltd. (Stroes-Gascoyne, 1996), a simulated waste container was buried for 2.5 years, surrounded by compacted buffer materials. Extensive microbial analysis of this test has shown that most viable organisms in the buffer material disappear around a moisture content of 15 percent (corresponding to a relative humidity 95 to 96 percent).

4.2.1.3 Energy and carbon sources

The metabolic pathway that a given microorganism will use depends on the energy source (light or chemical); thus, a microorganism is described as either a phototroph or chemotroph, respectively. In a deep geological repository after closure, the activity of phototrophs can be excluded because of the lack of a light source.

If a chemotroph uses organic carbon as its source of carbon, it is referred to as a heterotroph; if it derives energy from the oxidation of inorganic compounds and derives cell carbon from CO_2, it is called an autotroph. Because of their different nutritional requirements, the activities of these two types of microorganisms in a deep geological disposal are limited in different ways, depending on the ambient chemical environment.

CO_2 is a common inorganic carbon source used for growth by organisms like eukaryotic algae, cyanobacteria, iron oxidizing bacteria (IOB) and sulphur oxidizing bacteria (SOB). Autotrophic microbes play a potentially important role in concrete biodegradation (as discussed below). Because CO_2 is only a carbon source and not an energy source, energy must be supplied from photons or reduced inorganics like H_2S and FeS. Since CO_2 is present in most systems, autotrophic activity is expected to persist and

the availability of reduced inorganic species (e.g., H_2) is expected to be a major limiting factor for autotrophs.

The overall activity of heterotrophs is limited by the supply of organic carbon; the relative importance of individual reaction pathways depends on the availability of electron acceptors. The interior of a low and intermediate level nuclear waste contain a large portion of organic materials (e.g., cellulose) and a significant amount of inorganic nutrients (e.g., NO_3^-) whereas, outside, the organic carbon supply is relatively limited (MO of host rocks and the introduced materials). Cellular biomass and waste products produced by autotrophs will also contribute to organic carbon content to some degree.

Concrete mixes used for repository applications typically include 0.5 to 1% of a superplasticizer (SP) (i.e., sulphonated naphthalene condensates, co-polymer ether-polycarboxylate…) to reduce the w/c and to improve the workability and strength of the cement. These plasticizers are carbon-containing compounds and thus they may be subject to microbial breakdown as a possible carbon source. The study of plasticizer leaching from concrete still remains incomplete, and despite the small quantities of SP added, there is evidence to suggest that some microorganisms use these compounds as a carbon source (reviewed in García et al. 2018).

4.2.1.4 Redox conditions

The redox potential of a specific environment relates to the balance between oxidizing and reducing conditions in the considered environment and can be controlled by chemicals present in this environment. For instance, oxygenated soils demonstrate more oxidizing conditions compared to anaerobic soils. Regarding microbial activity, aerobic microbial growth and respiration is generally favoured in soils with oxidizing redox conditions while anoxic soils favour anaerobic growth and fermentation. The range of redox conditions can favour specific metabolic functions of microorganisms and hence, specific physiological types of microbes.

Microbial groups are known to use many redox pairs to derive their energy. Metabolic activities involve coupling the oxidation of an energy source to the reduction of a terminal electron acceptor (TEA), resulting in the conservation of energy used for cellular activities (Albrecht et al., 2013). Microorganisms tend to accumulate at redox interfaces, where both metabolic electron donors and electron acceptors are available. As discussed previously, heterotrophs derive their energy from the oxidative breakdown of external organic substrates; hence, microbial ecologies are frequently classified in terms of dominant pathways. The principal pathways are aerobic respiration, denitrification, manganese reduction, iron reduction, sulphate reduction, fermentation, and methanogenesis (Albrecht et al., 2013). From a biochemical point of view, the energy-yielding metabolic processes involve complex electron transfer chains. From a geochemical perspective, the significant reaction is the final electron transfer to an external electron acceptor. The common electron acceptors in subsurface environments are O_2, NO_3^-, MnO_2, $Fe(OH)_3$, SO_4^{2-}, and CO_2. Fermentation does not rely on an external electron acceptor; instead, it partially oxidizes and reduces an organic substrate. The final fermentation products include CO_2, H_2, alcohols, and organic acids.

A repository in unsaturated igneous rock formations is generally expected to be oxidizing in its chemical environment longer than a repository in a hydrologically saturated zone, particularly in sedimentary rocks, which could be reducing. Sedimentary rocks contain a certain amount of organic matter, which may stimulate significant microbial activities and, thus, maintain the repository and its surrounding areas in a reducing condition.

With time, the redox conditions could evolve. After closure, and the stop of the ventilation, O_2 may become depleted, thereby allowing the emergence of anaerobic metabolic pathways. In opposite, during the exploitation time, aerobic respiration is the most energetically favourable reaction, aerobic bacteria have a competitive advantage over anaerobic microorganisms when a certain level of O_2 is present. Anaerobic chemotrophic organisms can utilize various chemicals as sources of energy and therefore, depending on the chemistry of the system, have the potential for being highly active.

Sustainable autotrophic microbial activity requires the accumulation of a certain amount of reduced inorganic species in the repository, implying that a reducing environment is a prerequisite to possible autotrophic microbial activity within a geologic repository. Reduced inorganic species may be brought in by groundwater or gas flows from the surrounding areas. The anaerobic oxidation of organic compounds by heterotrophic bacteria can serve as the primary source of both the reduced inorganic substrates and the inorganic carbon for autotrophic metabolisms. For instance, fermentation produces H_2 and CO_2, both of which are needed by autotrophic methanogens for synthesizing methane.

Evidence from surface (e.g., roads, bridges) and underground cement structures (e.g., sewer pipes) has shown that the integrity of concrete over extended timescales can indeed be influenced by microorganisms, particularly the well-known sulphur-oxidizing bacteria such as *Acidithiobacillus thiooxidans* (previously *Thiobacillus thiooxidans*), which produces sulphuric acid under aerobic conditions through the oxidation of reduced sulphur, sulphide, and thiosulphate compounds. The oxidation product, sulphuric acid, contributes to the degradation of concrete by dissolving the calcium silicate hydrate and calcium hydroxide cement matrix constituents (Spor et al., 1992 ; Aviam et al., 2004; Okabe et al., 2007). Nitric acid, produced by ammonia and nitrite oxidizing bacteria, may similarly lead to acid-mediated concrete deterioration. It is noteworthy that within a deep geological repository, oxygen would be in finite supply in sharp contrast to the situation of roads and bridges. Thus, once utilized during corrosion, mineral dissolution and microbial redox reactions, oxygen would no longer be able to contribute to the formation of sulphuric acid.

4.2.1.5 pH conditions

Regarding the pH, most of the microorganisms have an optimum of growth around the neutrality (pH ~ 7), and thus are classified as neutralophiles. Microorganisms that have their optimum of growth in slightly alkaline conditions (pH ~ 11) are named as alkalophiles, and the ones which tolerate acidic conditions (pH < 5.5) are classified acidophiles. Among neutralophiles, a significative part can be alkalo- or acido-tolerant. In this case, bacteria will be able to survive a higher or lower pH than their optimum of growth but their growth will be zero or limited. Indeed, the energy used to growth in neutral conditions are redirect to establish pH gradients over their membranes when the surrounding pH is more or less alkaline than the intracellular pH.

Several geochemical processes can affect the chemical evolution of concrete buffer such as chloride ingress, sulphate attack, alkali-silica reactions, carbonation and Ca^{2+} leaching, which are mostly followed by alteration of the microstructure what might change the physical properties (e.g.transport and mechanical properties) of the concrete. Moreover, these processes can result in a local decrease in pH, leading to niches where growth of microorganisms can be possible.

In addition, when the alkaline plume reaches the interface of the clay host rock with the disposal gallery, chemical reactions are likely to occur. For instance, some primary minerals are unstable at high pH and tend to dissolve, forming new secondary minerals. Possibly this will lead to the consumption of OH^- ions. Moreover, the CO_2 will diffuse, driven by the relatively high partial pressure within the clay rock, towards the cementitious repository and react with the high concentration of calcium from concrete to form calcite at the interface of the repository and the clay host rock.

The combination of chemical reactions results in lowering of pH to maximally 10.5 This pH of 10.5 is not expected to be limited for microbial activity (Bertron et al., 2013; Horikoshi , 1999; Pedersen et al., 2004), thus, microbial activity might be present at the clay rock - disposal gallery interface of the repository. Furthermore, concrete has a low capacity for deformation under tensile stress, leading to the formation of (micro)cracks through which microorganisms are able to migrate and at the surfaces of cracks, they are able to form a biofilm. Microbial degradation of cementitious materials in a wide variety of conditions is commonly known, and might result in a loss of alkalinity, erosion, spalling of the concrete skin, corrosion of reinforcing bars, loss of water- or airtightness, and collapse. In addition, microorganisms can produce organic and inorganic acids, which can be corrosive towards cementitious materials and can lead to a decrease in pH. On the other hand, microbial metabolic activity can lead to the formation

of calcium carbonate, which can result in partially clogging of the fractures, as the molar volume of calcite is larger than that of portlandite.

4.2.2 Physiology of relevant types of microorganisms

Wide varieties of microorganisms are capable of contributing to the degradation of concrete surfaces. Potential bio-reactions on concrete surfaces are multiples and complexes. These reactions range from those occurring on concrete exposed to air and light as well as those after the disposal closure without oxygen and fully saturated.

4.2.2.1 Autotroph

Autotrophic microorganisms can utilize CO_2 (atmospheric or from carbonates) as a carbon source for growth. Energy for growth of these organisms is from a variety of sources such as light (phototrophic autotrophic microorganisms), or reduced chemicals like H_2S, Fe(II), etc. (chemotrophic autotrophic microorganisms).

In presence of air, light and moisture, evolved concrete surface (pH<11) can become colonized by photosynthetic microorganisms like algae and cyanobacteria (Gorbushina, 2007). Biofilms made up predominantly of algae and cyanobacteria are resistant and are able to survive under some relatively harsh conditions. Damage to concrete could occur as a result of adsorption of chemicals necessary for microbial growth, like calcium and magnesium, from the concrete (Javaherdashti et al., 2009). This process can lead to drying and cracking of the concrete. However, the occurrence of air, light and moisture on evolved concrete structures at the same time is not expected in a repository in sedimentary host rock. Alcalinophilic (pH>11) chemo- (without light) autotrophic (CO_2 as carbon source) microorganisms, like *Alkaliphilus metalliredigens* (Ye et al., 2004), could yet colonized concrete structures in case of sufficient relative humidity. If these microorganisms form biofilms, a variety of other physiological types can be encountered (as described below) taking benefit of the increasing complexity of physico-chemical conditions and of the microbial community in the biofilm organization.

4.2.2.2 Sulphur-oxidizing and sulphate-reducing bacteria

Sulphur oxidizing bacteria (SOB) play a key role in the overall biogeochemical cycling of sulphur. The sulphur cycle is complex, but the portions most pertinent to concrete degradation include sulphur oxidation and sulphate reduction. SOBs are well documented in degradation of concrete structures associated with nuclear waste containment (Aviam et al., 2004; Spor et al., 1992). In general, these bacteria grow at neutral to acidic pH; can utilize CO_2 as a carbon source (some SOB are also heterotrophic and use organic carbon), reduced sulphur compounds such as metal sulphides and H_2S as energy sources and oxygen as the TEA. For repositories in sedimentary host rock, the concomitance of aerobic conditions, a sufficient moisture and an efficient atmospheric carbonation to reduce the pH as lower as 9 in concrete niche to allow SOB to colonize is unlikely except, maybe, after the closure phase and the beginning of the saturation process in the near field, during the transient period until the complete O_2 consumption by rock oxidation, steel corrosion and bioactivities.

Exceptions do exist however, for instance, an alkaliphilic concrete degrading SOB was isolated and was shown to be capable of using NO_3^- as a TEA (Maeda et al., 1998).

During the course of growth of SOB, reduced S is oxidized ultimately to H_2SO_4. The process of SOB growth on concrete has been defined in three steps (Okabe et al., 2007). In step 1, prior to concrete degradation by SOB, the pH of the concrete surface is reduced by atmospheric CO_2 to around 9, which can facilitate growth of neutrophilic SOB. Based on XRD and SEM observations the surface at the end of step 1 is covered with calcium carbonate, resembling limestone more than concrete (Wiktor et al., 2011). Growth continues in step 2 until a pH of about 4 is reached. At step 3, the population shifts to acidophilic SOB, which continue to drop in pH to around 1.0 (Knight et al., 2002; Aviam et al., 2004).

Growth rates of the common acidophilic SOB Acidithiobacillus thiooxidans were reported to range from 0.342 to 2.874 d^{-1} between pH 0.9-4.3, with optimum growth demonstrated in the pH range of 1.0-3.5

(Jensen et al., 2011). In these studies, oxygen, CO_2 and sulphide were not limited, so the growth rates are likely close to maximum growth rates. The lower pH results in dissolution of hydrated cement. In addition, the alkaline components of concrete, such as calcium, react with H_2SO_4 (from SOB activity) to form gypsum ($CaSO_4.2H_2O$). Due to the weak structural properties of gypsum, this process can lead to additional weakening of concrete (Jensen et al., 2011). The deposition of jarosite ($KFe_3(SO_4)_2(OH)_6$) and gypsum are stimulated by SOB activity during concrete biodegradation (Tazaki et al., 1992; Grengg et al., 2015). The gypsum formation process continues into the concrete and increases the rate and degree of degradation due to the large density difference between the reaction products and concrete (Aviam et al., 2004). When newly formed gypsum reacts with less acidic (pH > 3) calcium aluminate inside the concrete (Mori et al., 1992; Grengg et al., 2015), this leads to formation of ettringite ($3CaO.Al_2O_3.\ 3CaSO_4.32H_2O$). Ettringite is much more destructive because it increases the internal pressure leading to crack formation, which leads to increased surface area that is open to microbial activity and acid penetration.

In the environment, the source of H_2S is likely the ubiquitous sulphate reducing bacteria (SRB) that function in anaerobic zones and are associated with the cycling of numerous S compounds. Contrasted to SOB, SRB are strict anaerobes that can use a variety of carbon sources (autotroph and heterotroph) and typically do not tolerate pH values below 5.5 (Muyzer and Stams 2008, Sánchez-Andrea et al. 2015) . In this case, SO_4^- serves as the TEA with the resultant HS^- released into the environment. The reactive HS^- can react with metals in solution and form sulphide minerals or it can be used by SOB as an energy source.

4.2.2.3 Iron oxidizing and reducing bacteria

Iron exists naturally as ferrous (Fe^{2+}) and ferric (Fe^{3+}) oxidation states. Ferric iron reduction is common in clay materials with the ferric iron often serving as a TEA for dissimilatory iron reducing bacteria. This reaction can occur when ferric iron is in solution or if it is in solid form as a ferric oxide. The resulting ferrous iron can be assimilated biologically, react with other metals in solution or oxidize rapidly if it diffuses into aerobic zones. Ferrous iron can also be oxidized by iron oxidizing bacteria either in non-acidic, nutrient rich aerobic zones where ferrous iron is chelated to humics, or in acidic zones where ferrous iron is stable. Iron oxidizing bacteria (IOB) are similar to SOB except they utilize ferrous iron as an energy source and may accelerate the corrosion of steel rebar used as reinforcement in concrete structures.

Exposure of the rebar in the concrete to the environment can occur through microbial corrosion or abiotic corrosion. In any event the exposed steel is a likely energy source for IOB. In the presence of biofilms with SOB activity, the resulting low pH will increase Fe^{2+} solubility and IOB activity. IOB enhanced pitting corrosion as determined through electrochemical impedance spectroscopy and scanning electron microscopy in the presence of steel coupons, compared to sterile controls. Compared to IOB alone, steel exposure to IOB and SRB together resulted in a synergistic effect on the steel, demonstrating a greater degree of corrosion than IOB or SRBs alone (Xu et al., 2008).

4.2.2.4 Nitrifying bacteria

Nitrifying bacteria are similar to sulphur oxidizers as they can use CO_2 or carbonate as a carbon source. They differ from sulphur oxidizers based on their energy source for growth. Nitrifying bacteria obtain energy through the oxidation of NH_4^+ or NO_2^-, ultimately to NO_3^-, resulting in nitric acid production. Nitrifying bacteria have been detected in a wide variety of environments and are more tolerant to low water activity than sulphur oxidizers (Gu et al., 2011).

Microbial activity is responsible for catalysing a majority of redox reactions involving nitrogen. Similarly, nitrogen is a major requirement for microbial growth as a component of proteins and other cellular constituents but also as alternative terminal electron acceptors in a number of anaerobic respiratory reactions.

4.2.2.5 Heterotroph

Heterotrophic microorganisms require organic carbon as a source of carbon and energy for growth. In aerobic environments, and especially on concrete exposed to the air, growth with oxygen as TEA (aerobic respiration) could predominate. In this scenario, fungi may play a significant role in this process due to their rapid growth rates and greater tolerance of low water availability and pH ranges (Wiktor et al., 2011). In addition rock-inhabiting fungi demonstrate enough mechanical strength in their hyphae to penetrate into crevices for nutrients. Fungi in this case, especially those that produce melanin, which confers extra-mechanical strength, can rapidly penetrate millimeters to centimeters into concrete-like structures (Magniont et *al*., 2011; Gorbushina, 2007; Wiktor et *al*., 2011). Fungi can also produce peroxide, by the enzyme peroxidase. This is usually associated with their ability to breakdown complex organic molecules to serve as carbon and energy sources. These reactions in close association to concrete will likely have deleterious effects on the concrete structure (Gu et *al*., 2011).

For repositories in sedimentary host rock, the concomitance of aerobic conditions and a sufficient moisture to allow alkalinophilic fungi to colonize concrete surface exist only during the closure phase and the transient period until the complete O_2 consumption by rock oxidation, steel corrosion and bioactivities. In these periods, organic wastes would not be accessible to provide a source of carbon for fungi outside the concrete containers. The only organic carbon sources should be the carbon of the organic matter present in the host rock and backfill materials or the carbon of organic concrete adjuvants whose bioavailability is not fully demonstrated. These carbon sources have been sufficiently demonstrated to maintain a microbial activity but limited to allow microorganisms to take a large expansion. Nevertheless, in case of successful colonization during this period, these organisms can serve as primary colonizers that potentially condition the surface for other microorganisms, like fermenters or sulphur oxidizers.

Heterotrophic microorganisms comprise another large segment of environmental inhabitants capable of growth on concrete without oxygen: anaerobic fermenter microorganism using organic carbon as a carbon and energy source. ***However, the occurrence of these anaerobic fermenter microorganisms should be also limited by the low availability of carbon sources and high pH conditions as long as the carbon in organic wastes remains inaccessible.*** When fermentation is the primary type of growth, for the most part, acid production occurs during anaerobic growth (Spor et *al*., 1992). Fermentation conditions can occur as a result of increased microbial biomass and activity which can decrease dissolved oxygen levels. Fermentation rates will be linked to the availability of organic carbon and in turn, acid byproducts will be controlled by the type of organic carbon used for growth as well as the type(s) of microbes present. Since fermentation is an incomplete oxidation of organic carbon, many organic acids are produced as byproducts, hence fermenters could take part in concrete biodegradation processes. Their diverse physiologies provide a wide range of acid byproducts such as, lactic, citric, gluconic, malic and many others. A description of concrete biodegradation by a pure culture identified intense chemical zonation and decalcification in the concrete matrix due to the close proximity of fermenters to the concrete surface (Magniont et *al*., 2011).

Heterotroph bacteria that can undergo respiration without the need for oxygen must utilize other TEAs: SO_4^{2-}, Fe^{3+}, NO_3^-, NO_2^-, N_2O... ***In relation to concrete degradation SRB contribute significantly to this process both directly and indirectly but, as anaerobic fermenters, SRB activity should be limited by the low availability of carbon sources and high pH conditions as long as the carbon in organic wastes remains inaccessible.*** Indirectly, (as mentioned above), sulphate reduction is responsible for H_2S production, which can feed into sulphur oxidizing metabolism resulting in H_2SO_4 production and concrete degradation. In addition, H_2S can contribute directly to concrete structure degradation through penetration into concrete and contribute to both concrete and metal rebar corrosion (Gu et *al*., 2011). Because concrete structures are reinforced with steel rebar, structural degradation of these reinforcements over many years may contribute to significant corrosion and structural instability.

4.2.3 Natural analogous sites representing cement systems

There are several natural analogous to the cement system of a geological disposal facility (GDF), giving the opportunities to assess the impact of cementitious conditions on microbial communities over prolonged periods. De Putter and Charlet (1994) studied the thermally metamorphosed limestones and organic-rich marls at Maraqin, Jordon, cement-like materials. Leaching of minerals in this system increased the alkalinity of Maqarin natural spring to pH of max 12.9 (Pederson et al., 2004). A low abundance of microbial communities was found in the Maraqin sediment samples, but their origin is still a question (Butterworth et al., 2021). Serpentinization of the olivine rocks of Semail ophiolite Nappe of Oman also resulted in groundwater alkalinity and a reduced environment (Bath et al., 1987). From this alkaline groundwater, a range of minerals is precipitated like brucite, magnesium hydroxide, and portlandite, making it an excellent analogue to a late-phase cementitious repository of GDFs. A low abundance of SRB spores with high tolerance to extreme pressure, temperature, and ratio doses was identified in this site samples.

4.2.3.1 Studies on Harpur Hill, an analogue site in the UK

Another analogue is the lime (CaO) working site at Harpur Hill, Buxton, with a pH range of 6.5-12. Highly alkaline calcium hydroxide leachates (pH > 12) were produced by rainwater and groundwater percolation, and these leachates further reacted with local bicarbonate water and atmospheric carbon dioxide to precipitate calcium carbonate downstream (Milodowski et al. 2013). The Manchester group has made several studies using alkaliphilic microbial communities from this site, addressing the upper pH limit for microbial metabolism (including anaerobic respiratory processes), degradation pathways for cellulose and other organic substrates, and the potential for microbial reduction and precipitation for priority radionuclides. Anaerobic microorganisms have the potential to degrade organic matter through the fermentation process which can lead to enzymatic radionuclide reduction and resultant reductive immobilization. The formation of reduced iron and sulphide phases through biogeochemical reactions can provide new reactive biomineral surfaces for radionuclide reduction and sorption. The sample from Harpur Hill was incubated at a range of high pH (10, 11, 12) values and was supplemented with electron donors and a range of electron acceptors (nitrate, Fe(III), and sulphate) to explore the upper limits of alkali tolerant microbial communities. The general order of utilization of electron acceptors that are observed is nitrate> Fe (III)-citrate> Fe (III) oxyhydroxide> sulphate, which was calculated in accordance with free energy yield and Eh values over the pH range 10-12. This study suggested that a subsequent robust redox cascade would be expected at a pH value up to 11. (Rizoulis et al., 2012). The solubility of various redox-active metals and radionuclides is partially controlled by microbial metabolism under anaerobic conditions. Metal-reducing bacteria are diverse and have a complex respiratory network in the cell which gives them the advantage to utilize a wide range of electron acceptors which include redox-active metal and radionuclides like Fe(III), Co(III), V(V), Cr(VI), U(VI), Np(V), Tc(VIII), I (V), Te(VI), Se(IV) and Pu(IV) (Kuippers et al., 2021).

There is a wide range of anaerobic, alkaliphilic microbial communities in Harpur Hill sediments, capable of reducing metals and radionuclides. This can give an indication of the wide range of microbial activities that may be expected in cementitious GDF environments. This range of microorganisms and their activities is illustrated by the work of Williamson et al. (2013, 2014, 2015, 2021). In 2013 they reported the reduction of Fe(III) (as ferrihydrite) to magnetite. Magnetite behaved as a reducing agent of radionuclides with U(VI), Np(V), and Tc(VII). Microbial communities in the starting sediments were dominated by organisms mostly from the bacterial phylum *Bacteroidetes*. But after incubation in the presence of Fe(III) and a suitable electron donor (lactate), the community was dominated by Gram-positive bacteria of the genus *Clostridium*. In 2014, the group investigated the biogeochemical fate of radionuclide U(VI) in the presence and absence of Fe (III), which is a common element expected in waste and sub-surface facilities. In the first case, the removal of U(VI) from the solution and sorption to the Fe (III) mineral was reported, which formed a complex U(IV)-bearing phase with the uraninite present followed by bioreduction and biomagnetite formation. In the second case, U(VI) was reduced to U(IV)-bearing non-uraninite phase. Bacteria from the phyla *Firmicutes* and *Bacteroidetes* dominated in the post-reduction phases. In 2015, Williamson et al. studied the biogeochemistry of Np(V) reduction in the

presence and absence of Fe(III) again. Through X-ray absorption spectroscopy (XAS), they observed a partial reduction of Np(V) in the system with no Fe and a complete reduction of Np(V) in the system with Fe, with Fe (II)-a mediated pathway for Np(V) reduction in the same time. The pH also dropped from 10 to ~7, suggesting active microbial metabolism in these systems. Again, the role of alkali-tolerant, Gram-positive bacteria belonging to the phylum *Firmicutes* was suggested for Fe(III) reduction and Np immobilization. In their recent studies, Williamson et al. (2021) reported the reduction of Tc(VIII) mediated by high pH microbial community via reaction with biogenic Fe(II) at pH 10.

Cementitious ILW and LLW are a heterogeneous mixture of different substrates like nitrate, iron, metal oxides, radionuclides, and organic carbon. ILW and LLW also contain a substantial amount of cellulosic material in concrete. This cellulosic material undergoes chemical hydrolysis in alkaline conditions and forms a water-soluble low molecular-weight compound. ISA and VFA are the major product of alkaline cellulose hydrolysis. ISA can form soluble complexes with radionuclides and mobilize them in a period of time. Bacteria can degrade ISA and couple this with a reduction of electron acceptors like nitrate- and Fe (III) post-closure. That reduces the mobility of radionuclides from ILW-GDFs (Bassil et al., 2015). Kuippers et al. (2019) studied microbial degradation of ISA under the anaerobic conditions at pH 7 to 10 with Fe(III) oxyhydroxide (ferrihydrite) as a terminal electron acceptor. They found that the ISA degradation was constrained to pH not more than 9. Bacteria from the genera *Clostridium* and *Geobacter*, as well as *Rhodoferax ferrireducens* were catalysing this process. There was a microbial reduction of ferrihydrite into siderite and vivianite possibly as a result of chelation of ISA with Fe (III). This could potentially impact the reductive immobilization of U(VI), Np(V), and Tc(VII) when adsorbed on the surface of Fe(II)-bearing biominerals. This is reported in the recent experiments done by Kuippers et al. (2021) where they found that in a neutral pH system containing ISA as the sole carbon source with Fe(III)-reducing condition and high phosphate concentration, uranium was precipitated as reduced U(IV)-phosphate by enzymatic reduction of *Geobacter* spp. This study is of importance for the far-field geosphere that surrounds a GDF.

Other than this, the presence of other organic complexes, which can mobilize radionuclides via chelation, is also a challenge in waste disposal sites. Byrd et al. (2021) studied the fate of citric acid, a polycarboxylic organic decontaminants, in experiments using Harpur Hill sediment. This study showed that citrate is readily degraded at high pH under nitrate- and Fe-(III) reducing conditions, potentially reducing the mobility of citrate-complexed radionuclides It also developed a reducing condition and prevent mobility of metal and radionuclides further. Durban et al. (2018) investigated nitrate reduction abilities of microbial consortia in lime-rich Harpur Hill sediments, with a pH of 11-12 of pore water in a cementitious environment. Reduction of oxyanions such as nitrate promotes an oxidizing condition in the vicinity of the waste and thus promotes the mobility of redox-sensitive radionuclides. The consortium's maximum total oxidized nitrogen reduction rate was 0.124 mM/h in the bioreactor identified in this site samples.

Studies conducted at Huddersfield University also support the view that organic carbon sources present within the near-field of a GDF provide substrates for methanogenesis and sulphate reduction. Rout et al. (2015) observed ISA degradation under iron-reducing conditions at pH 10 considering fermentative and methanogenic processes are likely to play an important role in ILW-GDF post-closure. Methane was generated from the resultant H_2/CO_2 produced from fermentation processes. The dominating microbial community appeared to be *Clostridium* spp. with methanogenesis being attributed to *Methanobacterium* spp. and *Methanomassiliicoccus* spp. Incubation of cellulose facilitated a range of active microbial processes, including sulphate reduction by *Desulphobacter* spp. and hydrogenotrophic methanogenesis by members of the order *Methanomicrobiales*. Their survival in an extreme environment is facilitated by extracellular polymeric substances (EPS) and metabolic acid. At pH 10.0 for hydrogenotrophic metabolism, sub-cultures of the alkaline methanogenic microcosms show the ability to utilize precipitated calcium carbonates as a reported potential carbon source (Wormald, 2019).

4.2.3.2 Microbes from other cement systems

Apart from natural analogues, some other high alkaline cement systems have a range of bacteria thriving in that harsh condition. Kunal et al. (2014) treated alkaliphilic bacteria from rhizosphere soil with highly alkaline cement kiln dust (CKD), resulting in an increase in the strength of concrete with a reduction in water absorption and porosity. Bacterial treatment of CKD concrete also increased calcium silicate hydrate and formed non-expansive ettringite in pores, increasing the compressive strength. Tummalapalle Uranium mine, Andhra Pradesh, India is a rich source of Uranium. Vempalle carbonate rock formation is the host rock for U mineralization (Rana et al., 2015). Water samples collected from the area have a high quantity of U, Fe, Al, Mg, Mn, Na, and Ca. The reported pH is of groundwater varies from 7.28 to 8.61 (Kumar et al., 2020). Other alkalic sites where microbial diversity is studied are the salterns of Turkey and Peruvian Andes (Çınar & Mutlu, 2016; Maturrano et al., 2006).

Some anthropogenic activities also create an alkaline environment suitable for finding alkaliphilic bacteria. The Solvay soda process produces multistage sodium carbonate from limestone and sodium chloride in Poland. Alkaline soda lime is generated as a by-product of the third process stage. This alkaline soda-lime is deposited in a "white sea" repository pound. It has a high pH (~11) and is a potential habitat for haloalkaliphilic and haloalkalitolerate microbes. The upper surface layer was a highly alkaline and nutrient-poor environment and phyla *Proteobacteria* and *Firmicutes* were dominant there. In contrast, the more stable deeper zone was dominated by members of the genera *Phenylobacterium*, Chelativorans, Skermanella, and aerobic genus *Bacillus* (Kalwasińska et al., 2017). Leon and Silao cities have lots of leather industries and car manufacturing plants. The residue generated is alkaline with a high amount of Fe and Cr. Brito et al. (2013) investigated the microbiome of the area and found an abundant population of *Bacillus*, *Lysobacter*, and *Thiobacillus* and talked about Cr (VI) reducing bacteria.

Early studies also reported that almost all bacteria are capable of $CaCO_3$ precipitation, which occurs as a by-product of their metabolic processes such as sulphate reduction and urea hydrolysis and are beneficial for healing cement crack (Siddique et al., 2011). These bacteria species are found in various natural environments like soil, geological formation, freshwater biofilms, oceans, and saline lakes. Some most common bacteria used in crack healing of concrete that produce carbonate are *Bacillus pasteurii*, *Pseudomonas aeruginosa*, *Bacillus sphaericus*, and *Shewanella* spp. (Alshalif et al., 2016).

Overall, GDFs condition is very different from surface. In a geological timescale, conditions of GDFs will evolve. The pH of 10-11 is expected to dominate for low-pH cementitious materials (and highly altered Portland materials) over the period. So, there is considerable potential for alkaliphilic anaerobic microbes to colonize and influence the cementitious ILW and LLW. They can have a positive as well as negative impact on the properties of cement used as a backfill in LLW and ILW. But fewer studies about activities under GDF conditions at dilute porewater conditions with lower carbon levels and limited electron acceptor is reported to date. Quantitative work on the impact of microbial colonization and metabolism with GDF relevant porewater electron donors and acceptors on the structure and properties of cement in long-term experiments performed on the chemo-mechanical evolution of low pH cement will be done in this project through geochemistry, 3D X-ray CT microstructure analysis, XRD, ESEM, X-ray fluorescence, and 16S/18S rRNA analysis.

4.3 Preliminary studies on the degradation of concrete due to microbial activity in geological disposals.

SCK CEN

Cementitious geological waste repositories are typified by their high alkalinity. In general, alkaline conditions hamper microbial processes as the lack of hydrogen (H^+) ions likely impedes the proton motive force needed by most respiring microorganisms to synthesize adenosine triphosphate (ATP) and the need to maintain a circumneutral intracellular pH (Horikoshi and Akiba 1982) (see 4.1 and 4.2). Extreme alkali-tolerant microorganisms have been identified and microbial processes at high pH are studied using several sites analogue to a cementitious waste repository (Takai et al. 2001, Pedersen et al. 2004, Roadcap et al. 2006, Shapovalova et al. 2008, Smith et al. 2016). However, there is no

consensus regarding the upper limit for microbial life. Nevertheless, the high alkaline pH (up to 12.5) alone is probably not sufficient to eliminate microbial presence in a geological repository, but it can induce a significant shift in the microbial community and inhibit microbial activity (Mijnendonckx et al. 2019). Moreover, several geochemical processes can affect the chemical evolution of the cementitious material, resulting in a local decrease in the pH value, which enables microbial activity. Such a heterogeneity was also observed in the large-scale Finnish gas generation experiment, which illustrated a pH neutralization and homogenization after 10 years, while initially pH values ranged from neutral in the waste drums to 11 in the tank water buffered by the concrete (Small et al. 2008, Small et al. 2017). Heterogeneity in pH value or a decrease to values <11 could enable microbial processes. Furthermore, at the interface with the host rock, pH is not expected to be limiting for microbial activity (Mijnendonckx et al. 2019).

Although a multitude of studies is published investigating microbial metabolism at high pH, most of these studies do not include a solid fraction to examine microbial degradation of cementitious material (Rizoulis et al. 2012, Bassil et al. 2015, Wormald et al. 2020, Byrd et al. 2021). Nevertheless, accelerated biodegradation tests of low-level radioactive waste solidified in cement have been performed (Rogers et al. 1996, Rogers et al. 2003, Aviam et al. 2004). In a first set of tests, biomass and spent medium of different microbial species were exposed to different types of simulated cemented low-level waste forms for different time periods (Figure 4-3). Representative species of heterotrophic, nitrifying and sulphur-oxidizing bacteria were selected as these types of organisms were shown to be indigenous to soils from low-level waste repositories. It was demonstrated that the buffering capacity of the cement formulations was sufficient to resist the chemical attack from organic acids produced by heterotrophic organisms (*Pseudomonas cepacia*) for 60 days. It was not examined if biofilms were formed on the cement. Nitrifying bacteria (*Nitrosomonas europea*) were not active as long as the pH remained 11-12. Growth on fresh cement samples could only be initiated after a pH decrease (due to carbonation). This resulted in the observation of biofilm on the cement and microbial induced cement deterioration after 66 days. *Thiobacillus ferroxidans* and *Thiobacillus thiooxidans* were selected as representatives for sulphur oxidizing species. Total immersion of the spent medium of these species caused extensive damage (spalling, material loss and lightning of colour) to the cement matrix compared to immersion in sterile growth medium after 60 days. Material loss and lightning of colour was also observed after intermittent immersion of the spent medium. Intermittent immersion with *T. thiooxidans* lixiviant was also used to test degradation on actual radioactive waste forms from power reactors (ion exchange resin and filter sludge). Physical damage was observed for both waste forms after 60 days. The ion exchange resin samples crumbled with unattached resin beads and the filter sludge samples completely disintegrated. Moreover, waste forms exposed to the *Thiobacillus* lixiviant showed a greater loss of ^{60}Co, ^{14}C, ^{99}Tc, and ^{90}Sr compared to waste forms exposed to sterile medium. Biofilm formation on the cemented waste forms was not examined (Rogers et al. 1996).

In a follow-up study, the test procedure with *Thiobacillus* was modified as the spent medium immersed on the cemented waste forms has a pH of 1.5-2 (Figure 4-3). Consequently, no distinction between the acidic pH of the bulk solution and the acid generated by microbial metabolism near the surface of the waste form can be made. Moreover, with this test it is impossible to evaluate inhibitory effects of the waste components or from nutrient limitations on biofilm development and activity (Rogers et al. 2003). The main difference in the modified test procedure is that samples were pre-exposed to *T. thiooxidans* lixiviant or sterile growth medium for 12 days followed by an additional exposure to sterile growth medium for 18 days. This demonstrated the development of an active biofilm on the waste form, which did not protect the cement from additional degradation. Instead, the active biofilm amplified degradation rates as the same amount of calcium released in 46 days in the original test procedure was now released in 30 days (Rogers et al. 2003).

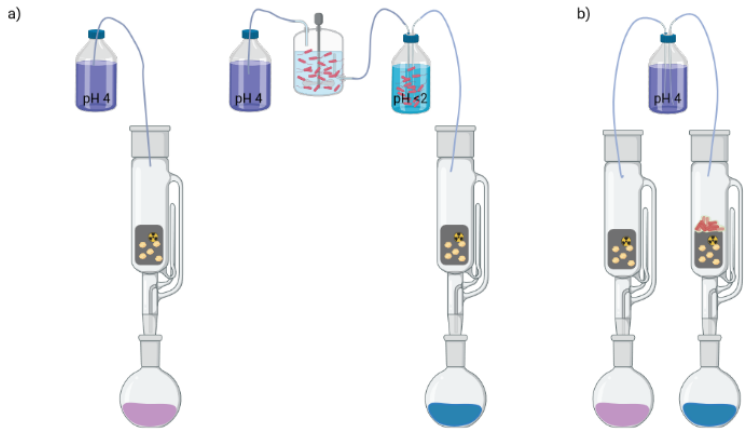

Figure 4-3: a) Original accelerated test where cemented waste is exposed to sterile growth medium are to a combination of biomass and spent medium; b) modified accelerated test were cemented waste pre-exposed to sterile medium or to microbial cells is further exposed to sterile medium (Rogers et al. 1996, Rogers et al. 2003).

Another study used semicontinuous cultures of *Halothiobacillus neapolitanus* and *Thiomonas intermedia* to study biodegradation of cement in frame of low-level radioactive waste disposal (Figure 4-4). To allow bacterial growth, the cement cubes were first exposed to atmospheric air to allow carbonation and consequently a pH decrease of the surface layer. However, when cementitious samples were exposed to a medium with initial pH 6.5, the pH rapidly increased up to pH 11 and no growth was observed after 4 days. Therefore, the initial pH of the exposure medium was reduced to pH 5.5, which resulted in a final pH of ~ 6.5. This allowed a rapid biodegradation of the cement. Up to 16% weight loss was observed after 40 days and clear cracks in the cement cubes were observed (Aviam et al. 2004).

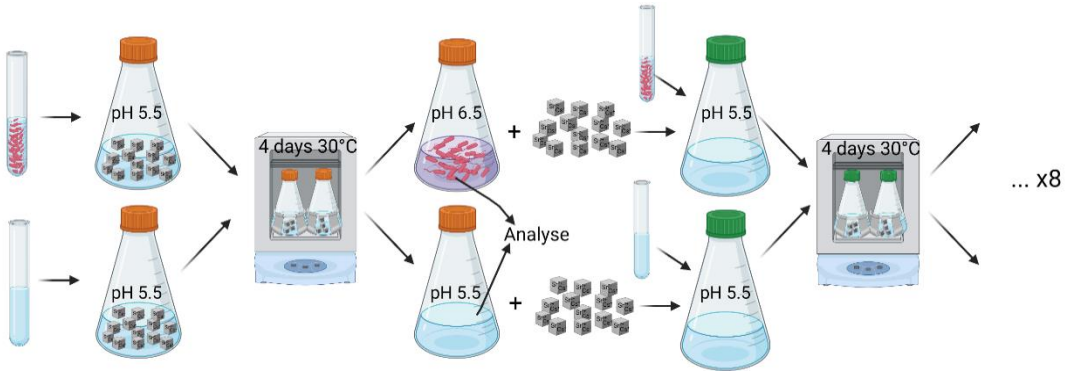

Figure 4-4: Accelerated cement biodegradation test with semicontinuous cultures. Cement cubes are exposed to a medium with (above) or without (below) $5x10^8$ cells. Samples are incubated 4 days at 30°C at 100 rpm. Afterwards, the spent medium is analysed and the cement cubes are transferred to fresh exposure medium with or without cells and the steps are repeated.

Although these studies demonstrate a rapid biodegradation of cemented waste, the pH conditions were decreased to favourable conditions for microbial growth, which is not representative for disposal conditions. A more representative study was performed where two cement cylinders were immersed in a mineral medium inoculated with either a mixture of fungi and heterotrophic organisms or with a mixed culture of *Thiobacillus* for 12 months. In the samples without bacteria, a rapid pH increase up to pH 12 was observed. This pH increase inhibited *Thiobacillus* up to 80 days but H_2SO_4 production started afterwards. This resulted in a pH decrease and an increase in acid production and calcium leaching. Notably, a pH increase was not observed in the exposure medium inoculated with fungi and heterotrophic microorganisms. These organisms are rapidly adapted to the alkaline conditions and immediately produced acid to lower the pH (Libert et al. 1992). These experiments showed that microorganisms can adapt to the high pH, however, oxygen was present throughout the entire experimental setup. To investigate microbial degradation of cement in anoxic conditions, Alquier et al. (2014) focused on the barrier between bituminized waste and the concrete overpack with the denitrifying

bacteria *Halomonas desiderata.* Batch experiments showed that the presence of a solid cement fraction enhanced the denitrification rates and enabled denitrification at pH 10-12. This was accompanied by biofilm formation on the cement paste. A follow-up study where a bioreactor was connected to an exposure chamber with the cement paste examined various scenarios likely to occur in a geological repository, i.e. a nutrient limited environment (Rafrafi et al. 2015). It was shown that planktonic cells in the bioreactor were not able to carry out denitrification at pH 12, while denitrification was still ongoing in the biofilms formed at the cement surface in the exposure chamber (Rafrafi et al. 2017). Putative biofilm structures were also observed in preliminary batch experiments with Ordinary Portlandite Cement in nitrate– and sulphate-reducing conditions and a decrease in the pH value from >12 to 10 was observed in some conditions. A pH decrease was also reported in experiments studying a cement-bentonite interface (Mijnendonckx et al., 2019b). As the focus of these studies was more on possible microbial activity in such extreme conditions, no detailed experiments were performed to investigate biodegradation of the cement.

4.4 Synthesis and identified gaps

Although much research has been performed to characterize microbial interactions with cementitious materials (see sections 4.1 and 4.2), studies in relation to disposal of nuclear waste remain scarce (see section 4.3). Microbial degradation of cementitious materials has been shown in various environments such as sewage pipes, marine structures and wastewater treatment systems (see section 4.1 and Wei et al., 2013). Cementitious materials impose a highly alkaline environment, which inhibits microbial activity. However, several processes affect the chemical evolution of cementitious materials, which can result in a local decrease in pH, enabling microbial activity. Furthermore, concrete is a quasi-brittle material so that (micro)cracks can give microorganisms space to migrate and attach along the surfaces. In such a case a biofilm can be formed. Microbial degradation of cementitious materials is mainly caused by the biological production of organic and inorganic acids, which can react with the cement, resulting in the formation of calcium salts. Leaching of calcium salts from the cement can result in an increased porosity and a decreased pH at the surface layer. Subsequently, degradation proceeds gradually to the interior concrete matrix, affecting the whole structure.

On the other hand, microbial-induced calcite precipitation is a well-known process and is studied extensively including different metabolic activities leading to calcium carbonate precipitation, their native environment, and potential applications (see section 4.1 and review from Zhu and Dittrich, 2016). Microbial carbonate precipitation can be induced by different metabolisms such as ureolysis, denitrification, sulphate reduction, iron reduction and methane oxidation. Microbial-induced calcite precipitation results in decreased concrete permeability and decreased penetration of corrosive substances, thus improving concrete durability (Wang et al., 2016). However, carbonation has a pH value-lowering effect and increases the corrosion rate of reinforcing bars (Phung et al., 2017).

Heterogeneity in pH or a decrease to values <11 (e.g. at the interface with the host rock) can promote microbial processes. Furthermore, low-pH cement is considered for the massive plugs and seals to close the disposal gallery. Specific research on this cementitious material is needed with respect to microbial activity and will be studied within MAGIC. Most studies have been performed in the frame of LLW and not deep geological disposal (see section 4.3). Therefore, the conditions for a deep geological repository will be considered for the planned experiments.

Otherwise, the durability of cementitious materials has so far been explored mainly with limited or no mechanical load, e.g., the Roman concretes and mortars. In geological disposal facilities, all cementitious materials are envisaged to be under a mechanical load. The generation of fractures within the chemically evolved zones of cementitious materials by mechanical loading is expected (creating space for potential bacterial activity development) to change the transport properties and thereby the chemical evolution is expected to take place at a faster rate than without or limited mechanical load. Microbial activity is limited by space restriction in so-called impermeable engineered concrete that is used for liners, plugs and buffers but can be increased by the generation of these fractures. This is another important gap that will be addressed within MAGIC.

The alteration processes in cementitious materials under complex coupled perturbation phenomena (i.e., pore saturation, chemical evolution of the barriers, loading and gas formation) including the microbial activity has not been yet studied. Therefore, the impact of microbially induced processes on the chemo-mechanical behaviour of cementitious materials will be studied in this project. Former studies that focused on deep geological disposal did not take into account cement degradation and focused mainly on microbial activity in such conditions (see section 4.3). The effect of microbial activity on the chemical evolution will be addressed as well.

4.5 References for part 4

Achal, V., Mukherjee, A., Reddy, M.S., 2011. Effect of calcifying bacteria on permeation properties of concrete structures. Journal of industrial microbiology & biotechnology 38, 1229–1234.

Albrecht, A., Bertron, A., Libert, M., 2013. Microbial Catalysis of Redox Reactions in Concrete Cells of Nuclear Waste Repositories: A Review and Introduction. NUWCEM-2011 Conference talks and posters, p. 825-841. France

Alquier, M., C. Kassim, A. Bertron, C. Sablayrolles, Y. Rafrafi, A. Albrecht and B. Erable (2014). Halomonas desiderata as a bacterial model to predict the possible biological nitrate reduction in concrete cells of nuclear waste disposals. Journal of Environmental Management 132: 32-41

Alshalif, A.F., Irwan, J.M., Othman, N. and Anneza, L.H., 2016. Isolation of sulphate reduction bacteria (SRB) to improve compress strength and water penetration of bio-concrete. In MATEC Web of Conferences (Vol. 47, p. 01016). EDP Sciences

Aviam, O., Bar-Nes, G., Zeiri, Y., Sivan, A., 2004. Accelerated biodegradation of cement by sulfur-oxidizing bacteria as a bioassay for evaluating immobilization of low-level radioactive waste. Appl. Environ. Microbiol. 70: 6031-6036

Bagnoud, A. Microbial metabolism in the deep subsurface: Case study of Opalinus Clay (2015). École polytechnique fédérale de Lausanne (EPFL). Thèse de doctorat, Spécialité Sciences. 190 p

Bang, S.S., Galinat, J.K., Ramakrishnan, V., 2001. Calcite precipitation induced by polyurethane-immobilized *Bacillus pasteurii*. Enzyme and Microbial Technology 28, 404–409. https://doi.org/10.1016/S0141-0229(00)00348-3

Bath, A.H., Christofi, N., Neal, C., Philp, J.C., Cave, M.R., McKinley, I.G. and Berner, U., 1987. Trace element and microbiological studies of alcaline groundwaters in Oman, Arabian Gulf: a natural analogue for cement pore-waters (No. NAGRA-NTB--87-16). Nationale Genossenschaft fuer die Lagerung Radioaktiver Abfaelle (NAGRA)

Bassil NM, Bryan N, Lloyd JR. Microbial degradation of isosaccharinic acid at high pH. ISME J. 2015;9(2):310-20.

Bassil, N.M., Bewsher, A.D., Thompson, O.R. and Lloyd, J.R. (2015) Microbial degradation of cellulosic material under intermediate-level waste simulated conditions. Mineralogical Magazine

Bertron, A., Duchesne, J., Escadeillas, G., 2005. Accelerated tests of hardened cement pastes alteration by organic acids: analysis of the pH effect. Cement and Concrete Research 35, 155–166. https://doi.org/10.1016/j.cemconres.2004.09.009

Bertron, A., B. Erable, M. Alquier, N. Jacquemet, C. Kassim, C. Sablayrolles, C. Albasi, R. Basseguy, P. Strehaiano, M. Vignoles, A. Albrecht, et G. Escadeillas, 2013. Catalyse biotique et abiotique de la réduction des nitrates en milieu alcalin dans le contexte du stockage profond des déchets radioactifs. Matériaux & Techniques, 101: p. 1-10

Bixler, G. D. and B. Bhushan (2012). Biofouling: lessons from nature. *Philosophical Transactions of the Royal Society A: Mathematical, Physical and Engineering Sciences* 370: 2381-2417

Boquet, E., Boronat, A., Ramos-Cormenzana, A., 1973. Production of Calcite (Calcium Carbonate) Crystals by Soil Bacteria is a General Phenomenon. Nature 246, 527–529. https://doi.org/10.1038/246527a0

Brito, E.M., Piñón-Castillo, H.A., Guyoneaud, R., Caretta, C.A., Gutiérrez-Corona, J.F., Duran, R., Reyna-López, G.E., Nevárez-Moorillón, G.V., Fahy, A. and Goñi-Urriza, M., 2013. Bacterial biodiversity from anthropogenic extreme environments: a hyper-alkaline and hyper-saline industrial residue contaminated by chromium and iron. Applied microbiology and biotechnology, 97(1), pp.369-378

Bur, N., S. Roux, L. Delmas, Y. Géraud and F. Feugeas, 2010. Porosité des mortiers et bioréceptivité. Matériaux & Techniques 98 : 31-40

Brown, A.D. 1976. Microbial Water Stress. Bacteriological Reviews 40: 803-846.

Browne, R.D., Domone, P. l., Geoghegan, M.P., 1977. 6. Deterioration of concrete structures under marine conditions and their inspection and repair, in: Maintenance of Maritime Structures. Thomas Telford Publishing, pp. 137–162. https://doi.org/10.1680/moms.00506.0009

Butterworth, S.J., Stroes-Gascoyne, S. and Lloyd, J.R., 2021. The microbiology of natural analogue sites. In The Microbiology of Nuclear Waste Disposal (pp. 21-39). Elsevier

Byrd, N., Lloyd, J.R., Small, J.S., Taylor, F., Bagshaw, H., Boothman, C. and Morris, K., 2021. Microbial Degradation of Citric Acid in Low Level Radioactive Waste Disposal: Impact on Biomineralization Reactions. Frontiers in Microbiology, 12, p.723.

Castanier, S., Le Métayer-Levrel, G., Perthuisot, J.-P., 1999. Ca-carbonates precipitation and limestone genesis — the microbiogeologist point of view. Sedimentary Geology 126, 9–23. https://doi.org/10.1016/S0037-0738(99)00028-7

Chambers, L.D., Stokes, K.R., Walsh, F.C., Wood, R.J.K., 2006. Modern approaches to marine antifouling coatings. Surface and Coatings Technology 201, 3642–3652. https://doi.org/10.1016/j.surfcoat.2006.08.129

Chapelle, F.H. 2001. Ground-Water Microbiology and Geochemistry. 2nd Edition. New York: John Wiley & Sons

Chlayon, T., Iwanami, M., Chijiwa, N., 2018. Combined protective action of barnacles and biofilm on concrete surface in intertidal areas. Construction and Building Materials 179, 477–487. https://doi.org/10.1016/j.conbuildmat.2018.05.223

Çınar, S. and Mutlu, M.B., 2016. Comparative analysis of prokaryotic diversity in solar salterns in eastern Anatolia (Turkey). Extremophiles, 20(5), pp.589-601

Coombes, M.A., Viles, H.A., Naylor, L.A., La Marca, E.C., 2017. Cool barnacles: Do common biogenic structures enhance or retard rates of deterioration of intertidal rocks and concrete? Science of The Total Environment 580, 1034–1045. https://doi.org/10.1016/j.scitotenv.2016.12.058

De Belie, N., Lenehan, J.J., Braam, C.R., Svennerstedt, B., Richardson, M., Sonck, B., 2000. Durability of Building Materials and Components in the Agricultural Environment, Part III: Concrete Structures. Journal of Agricultural Engineering Research 76, 3–16. https://doi.org/10.1006/jaer.1999.0520

De Graef, B., Cnudde, V., Dick, J., De Belie, N., Jacobs, P. and Verstraete, W., 2005. A sensitivity study for the visualization of bacterial weathering of concrete and stone with computerized X-ray microtomography. Science of the total environment, 341(1-3), pp.173-183

De Muynck, W., De Belie, N., Verstraete, W., 2010. Microbial carbonate precipitation in construction materials: A review. Ecological Engineering, Special Issue: BioGeoCivil Engineering 36, 118–136. https://doi.org/10.1016/j.ecoleng.2009.02.006

De Putter, T. and Charlet, J.M., 1994. Natuurlijke analogieën in klei: een bibliografische synthese. NIRAS

Douglas, S., Beveridge, T.J., 1998. Mineral formation by bacteria in natural microbial communities. FEMS Microbiology Ecology 26, 79–88. https://doi.org/10.1111/j.1574-6941.1998.tb00494.x

Durban, N, Y Rafrafi, A Rizoulis, A Albrecht, J-C Robient, JR. Lloyd, A Bertron, B Erable 2018 Nitrate and nitrite reduction at high pH in a cementitious environment by a microbial microcosm International Biodeterioration & Biodegradation 134 93–102

Gam, Z., Daumas, S., Casalot, L., Bartoli-Joseph, M., Necib, S., Linard, Y., Labat, M. Thermanaeromonas burensis sp. nov., a thermophilic anaerobe isolated from a subterranean clay environment. International journal of systematic and evolutionary microbiology (2016). Vol 66, N°1, pp.445–9

García, D., M. Grivé, L. Duro, S. Brassinnes and J. de Pablo (2018). The potential role of the degradation products of cement superplasticizers on the mobility of radionuclides. Applied Geochemistry 98: 1-9

Georges, M., Bourguiba, A., Chateigner, D., Sebaibi, N., Boutouil, M., 2021. The study of long-term durability and bio-colonization of concrete in marine environment. Environmental and Sustainability Indicators 10, 100120. https://doi.org/10.1016/j.indic.2021.100120

Gorbushina, A., 2007. Life on the rocks. Environ. Microbiol. 9: 1613-1631

Grengg, C., Mittermayr, F., Baldermann, A., Böttcher, M.E., Leis, A., Koraimann, G., Grunert, P., Dietzel, M., 2015. Microbiologically induced concrete corrosion: A case study from a combined sewer network. Cement and Concrete Research 77: 16-25

Grzegorczyk, M., Pogorzelski, S.J., Pospiech, A., Boniewicz-Szmyt, K., 2018. Monitoring of Marine Biofilm Formation Dynamics at Submerged Solid Surfaces With Multitechnique Sensors. Frontiers in Marine Science 5

Gu, J.D., Ford, T.E., Mitchell, R., 2011. Microbiological Corrosion of Concrete. In Uhlig's Corrosion Handbook, R.W. Revie (Ed.), pp. 451-460

Hammes, F., Verstraete, W., 2002. Key roles of pH and calcium metabolism in microbial carbonate precipitation. Reviews in Environmental Science and BioTechnology 1, 3–7. https://doi.org/10.1023/A:1015135629155

Hayek, M., M. Salgues, J.-C. Souche, E. Cunge, C. Giraudel and O. Paireau (2021). Influence of the Intrinsic Characteristics of Cementitious Materials on Biofouling in the Marine Environment. *Sustainability* 13: 2625

Horikoshi K, Akiba T. Alkalophilic Microorganisms: a New Microbial World. Japan Scientific Societies Press. 1982

Horikoshi, K., 1999. Alkaliphiles: Some Applications of Their Products for Biotechnology. Microbiology and Molecular Biology Reviews, 63: p. 735-750

Hughes, P., Fairhurst, D., Sherrington, I., Renevier, N., Morton, L.H.G., Robery, P.C., Cunningham, L., 2013. Microscopic study into biodeterioration of marine concrete. International Biodeterioration & Biodegradation 79, 14–19. https://doi.org/10.1016/j.ibiod.2013.01.007

Islam, M.S., Mondal, B.C., Islam, M.M., 2010. Effect of Sea Salts on Structural Concrete in a Tidal Environment. Australian Journal of Structural Engineering 10, 237–252. https://doi.org/10.1080/13287982.2010.11465048

Javaherdashti, R., 2009. A brief review of general patterns of MIC of carbon steel and biodegradation of concrete. IUFS J. Biol. 68: 65-73

Jensen, H.S., Lens, P.N.L., Nielsen, J.L., et al., 2011. Growth kinetics of hydrogen sulfide oxidizing bacteria in corroded concrete from sewers. J. Hazard. Mater. 189: 685-691

Jiang, G., Wightman, E., Donose, B.C., Yuan, Z., Bond, P.L., Keller, J., 2014. The role of iron in sulfide induced corrosion of sewer concrete. Water Research 49, 166–174. https://doi.org/10.1016/j.watres.2013.11.007

Jonkers, H.M., 2011. Bacteria-based self-healing concrete. Heron, 56 (1/2).

Joshi, S., Goyal, S., Mukherjee, A., Reddy, M.S., 2017. Microbial healing of cracks in concrete: a review. Journal of Industrial Microbiology and Biotechnology 44, 1511–1525. https://doi.org/10.1007/s10295-017-1978-0

Kalhori, H., Bagherpour, R., 2017. Application of carbonate precipitating bacteria for improving properties and repairing cracks of shotcrete. Construction and Building Materials 148, 249–260. https://doi.org/10.1016/j.conbuildmat.2017.05.074

Kalwasińska, A., Felföldi, T., Szabó, A., Deja-Sikora, E., Kosobucki, P. and Walczak, M., 2017. Microbial communities associated with the anthropogenic, highly alkaline environment of a saline soda lime, Poland. Antonie van Leeuwenhoek, 110(7), pp.945-962

Kaur, G., Dhami, N.K., Goyal, S., Mukherjee, A., Reddy, M.S., 2016. Utilization of carbon dioxide as an alternative to urea in biocementation. Construction and Building Materials 123, 527–533. https://doi.org/10.1016/j.conbuildmat.2016.07.036

Kim, H.K., Park, S.J., Han, J.I., Lee, H.K., 2013. Microbially mediated calcium carbonate precipitation on normal and lightweight concrete. Construction and Building Materials, 25th Anniversary Session for ACI 228 – Building on the Past for the Future of NDT of Concrete 38, 1073–1082. https://doi.org/10.1016/j.conbuildmat.2012.07.040

Knight, J., Cheeseman, C., Rogers, R., 2002. Microbial influenced degradation of solidified waste binder. Waste Manag. Oxf. U. K. 22: 187-193

Kuippers, G., Boothman, C., Bagshaw, H., Beard, R., Bryan, N.D. and Lloyd, J.R., 2019. Microbial reduction of Fe (III) coupled to the biodegradation of isosaccharinic acid (ISA). Applied Geochemistry, 109, p.104399

Kuippers, G., Morris, K., Townsend, L.T., Bots, P., Kvashnina, K., Bryan, N.D. and Lloyd, J.R., 2021. Biomineralization of uranium-phosphates fueled by microbial degradation of isosaccharinic acid (ISA). Environmental Science & Technology, 55(8), pp.4597-4606

Kumar, M.P., Nagalakshmi, K., Jayaraju, N., Prasad, T.L. and Lakshmanna, B., 2020. Deciphering water quality using WQI and GIS in Tummalapalle Uranium Mining area, Cuddapah Basin, India. Water Science, 34(1), pp.65-74

Kumari, C., Das, B., Jayabalan, R., Davis, R., Sarkar, P., 2017. Effect of Nonureolytic Bacteria on Engineering Properties of Cement Mortar. Journal of Materials in Civil Engineering 29, 06016024. https://doi.org/10.1061/(ASCE)MT.1943-5533.0001828

Kunal, Siddique, R., Rajor, A. and Singh, M., 2016. Influence of bacterial-treated cement kiln dust on strength and permeability of concrete. Journal of Materials in Civil Engineering, 28(10), p.04016088

Krumholz, L.R., J.P. McKinley, G.A. Ulrich, et J.M. Suflita, 1997. Confined subsurface microbial communities in Cretaceous rock. Nature 386: p. 64 - 66.

Leupin, O., Bernier-Latmani, R., Bagnoud, A., Moors, H., Leys, N., Wouters, K., Stroes-Gascoyne, S. Fifteen years of microbiological investigation in Opalinus Clay at the Mont Terri rock laboratory (Switzerland). Swiss Journal of Geosciences (2017). Vol 110, N°1, pp.343–54

Li, X., U. Kappler, G. Jiang and P. L. Bond (2017). The Ecology of Acidophilic Microorganisms in the Corroding Concrete Sewer Environment. *Frontiers in Microbiology* 8

Lin, L. C. and Beuchat, L. R., 2007. Survival of Enterobacter sakazakii in infant cereal as affected by composition, water activity, and temperature. Food Microbiology, 24, 767–777

Libert MF, Sellier R, Jouquet G, Trescinski M, Spor H. Effects of microorganisms growth on the long-term stability of cement and bitumen. MRS Online Proceedings Library (OPL). 1992;294

Lowenstam, H.A., Weiner, S., 1989. On Biomineralization. Oxford University Press, New York. https://doi.org/10.1093/oso/9780195049770.001.0001

Luo, M., Qian, C., Li, R., Rong, H., 2015. Efficiency of concrete crack-healing based on biological carbonate precipitation. J. Wuhan Univ. Technol.-Mat. Sci. Edit. 30, 1255–1259. https://doi.org/10.1007/s11595-015-1304-5

Lv, J., Cao, Z., Hu, X., 2021. Effect of biological coating (Crassostrea gigas) on marine concrete: Enhanced durability and mechanisms. Construction and Building Materials 285, 122914. https://doi.org/10.1016/j.conbuildmat.2021.122914

Madigan, M.T., Martinko, J., Parker, J., 2003. Metabolic Diversity, in Biology of Microorganisms. Pearson Education, London, pp. 151-165

Maeda, T., Oshima, Y., Nogami, Y., et al., 1998. Isolation of a sulfur-oxidizing bacterium, that can grow under alkaline pH, from corroded concrete. Biosci. Biotechnol. Biochem. 62: 1087-1092

Mahapatra, S., Banerjee, D., 2013. Optimization of a bioactive exopolysaccharide production from endophytic Fusarium solani SD5. Carbohydrate Polymers 97, 627–634. https://doi.org/10.1016/j.carbpol.2013.05.039

Magniont, C., Coutand, M., Bertron, A., Cameleyre, X., Lafforgue, C., Beaufort, S., Escadeillas, G., 2011. A new test method to assess the bacterial deterioration of cementitious materials. Cement and Concrete Research 41, 429–438. https://doi.org/10.1016/j.cemconres.2011.01.014

Masurat, P., S. Eriksson, et K. Pedersen, 2010a. Evidence for indigenous sulphate-reducing bacteria in commercial Wyoming bentonite MX-80. Applied Clay Science 47: p. 51-57

Masurat, P., S. Eriksson, et K. Pedersen, 2010b. Microbial sulphide production in compacted Wyoming bentonite MX-80 under in situ conditions relevant to a repository for high-level radioactive waste. Applied Clay Science 47: p. 58-57

Maturrano, L., Santos, F., Rosselló-Mora, R. and Antón, J., 2006. Microbial diversity in Maras salterns, a hypersaline environment in the Peruvian Andes. Applied and Environmental Microbiology, 72(6), pp.3887-3895

Mayeux, B., Fardeau, M.L., Bartoli-Joseph, M., Casalot, L., Vinsot, A., Labat, M. *Desulfosporosinus burensis* sp. nov., a spore-forming, mesophilic, sulfate-reducing bacterium isolated from a deep clay environment. International journal of systematic and evolutionary microbiology (2013). Vol 63, N°2, pp.593–8

Meike, A., Stroes-Gascoyne, S., 2000. Review of microbial responses to abiotic environmental factors in the context of the proposed Yucca Mountain repository (AECL--12101). Canada

Mieszkin, S., Callow, M.E., Callow, J.A., 2013. Interactions between microbial biofilms and marine fouling algae: a mini review. Biofouling 29, 1097–1113. https://doi.org/10.1080/08927014.2013.828712

Mijnendonckx K, Small J, Abrahamsen-Mills L, Pedersen K, Leys N. MIND Deliverable 3.7: Final Integration and Evaluation Report. European Commission; 2019b.

Mijnendonckx K, Van Gompel A, Coninx I, Bleyen N, Leys N. Radiation and Microbial Degradation of Bitumen. 2019a

Milodowski, A., R. Shaw and D. Stewart (2013). The Harpur Hill Site: its geology, evolutionary history and a catalogue of materials present. *British Geological Survey, Keyworth, Nottingham, UK*

Mohammed, T.U., Hamada, H., Yamaji, T., 2004. Performance of seawater-mixed concrete in the tidal environment. Cement and Concrete Research 34, 593–601. https://doi.org/10.1016/j.cemconres.2003.09.020

Mori, T., Nonaka, T., Tazaki, K., Koga, M., Hikosaka, Y., Noda, S., 1992. Interactions of nutrients, moisture and pH on microbial corrosion of concrete sewer pipes. Water Research 26, 29–37. https://doi.org/10.1016/0043-1354(92)90107-F

Muyzer, G. and A. J. Stams (2008). The ecology and biotechnology of sulphate-reducing bacteria. Nat Rev Microbiol 6: 441-454

Nielsen, S.D., Koren, K., Löbmann, K., Hinge, M., Scoma, A., Kjeldsen, K.U., Røy, H., 2020. Constraints on $CaCO_3$ precipitation in superabsorbent polymer by aerobic bacteria. Appl Microbiol Biotechnol 104, 365–375. https://doi.org/10.1007/s00253-019-10215-4

Okabe, S., Odagiri, M., Ito, T., Satoh, H., 2007. Succession of Sulfur-Oxidizing Bacteria in the Microbial Community on Corroding Concrete in Sewer Systems. Appl. Environ. Microbiol. 73, 971–980. https://doi.org/10.1128/AEM.02054-06

Onstott, T. C., Colwell, F. S., Kieft, T. L., Murdoch, L. and Phelps, T. J., 2009. New Horizons for Deep Subsurface Microbiology. Microbe 4: 499-505

Parande, A.K., Ramsamy, P.L., Ethirajan, S., Rao, C.R.K. and Palanisamy, N., 2006, March. Deterioration of reinforced concrete in sewer environments. In Proceedings of the Institution of Civil Engineers-Municipal Engineer (Vol. 159, No. 1, pp. 11-20). Thomas Telford Ltd

Parker, C. (1945). The corrosion of concrete 2. The function of Thiobacillus concretivorus (nov. spec.) in the corrosion of concrete exposed to atmospheres containing hydrogen sulphide. *Australian Journal of Experimental Biology & Medical Science* 23

Pedersen, K. and Karlsson, F. 1995. Investigations of Subterranean Microorganisms: Their Importance for Performance Assessment of Radioactive Waste Disposal. SKB 95-10. Stockholm, Sweden: Swedish Nuclear Fuel and Waste Management Company.

Pedersen, K., 1999. Subterranean microorganisms and radioactive waste disposal in Sweden. Engineering Geology 52, 163–176. https://doi.org/10.1016/S0013-7952(99)00004-6

Pedersen, K., Nilsson, E., Arlinger, J., Hallbeck, L. and O'Neill, A., 2004. Distribution, diversity and activity of microorganisms in the hyper-alkaline spring waters of Maqarin in Jordan. Extremophiles, 8(2), pp.151-164

Phung, Q.T., N. Maes, and D. Jacques, Current concerns on durability of concrete used in nuclear power plants and radioactive waste repositories, in CIGOS 2017: Proceedings of the 4th Congrès International de Géotechnique - Ouvrages -Structures. 2017, Springer

Rafrafi Y, Ranaivomanana H, Bertron A, Albrecht A, Erable B. Surface and bacterial reduction of nitrate at alkaline pH: Conditions comparable to a nuclear waste repository. Int Biodeter Biodegr. 2015;101:12-22

Rafrafi Y, Durban N, Bertron A, Albrecht A, Robinet J-C, Erable B. Use of a continuous-flow bioreactor to evaluate nitrate reduction rate of Halomonas desiderata in cementitious environment relevant to nuclear waste deep repository. Biochemical Engineering Journal. 2017;125:161-70

Ramachandran, S.K., Bang, S.S., Bang, S.S., 2001. Remediation of concrete using micro-organisms. ACI Materials Journal-American Concrete Institute 98, 3–9.

Rana, B.K., Dhumale, M.R., Lenka, P., Sahoo, S.K., Ravi, P.M. and Tripathi, R.M., 2016. A study of natural uranium content in groundwater around Tummalapalle uranium mining and processing facility, India. Journal of Radioanalytical and Nuclear Chemistry, 307(2), pp.1499-1506

Rivadeneyra, M.A., Delgado, R., del Moral, A., Ferrer, M.R., Ramos-Cormenzana, A., 1994. Precipatation of calcium carbonate by Vibrio spp. from an inland saltern. FEMS Microbiology Ecology 13, 197–204. https://doi.org/10.1111/j.1574-6941.1994.tb00066.x

Rizoulis, A., Steele, H.M., Morris, K. and Lloyd, J.R. 2012 The potential impact of anaerobic microbial metabolism during the geological disposal of intermediate-level waste. Mineralogical Magazine 76 397–406

Roadcap GS, Sanford RA, Jin QS, Pardinas JR, Bethke CM. Extremely alkaline (pH > 12) ground water hosts diverse microbial community. Ground Water. 2006;44(4):511-7

Rogers, R.D., Hamilton, M.A., Veeh, R.H. and McConnell Jr, J.W., 1996. Microbial degradation of low-level radioactive waste. Final report (No. NUREG/CR--6341). Idaho National Engineering Lab

Rogers RD, Knight JJ, Cheeseman CR, Wolfram JH, Idachaba M, Nyavor K, et al. Development of test methods for assessing microbial influenced degradation of cement-solidified radioactive and industrial waste. Cement Concrete Res. 2003;33(12):2069-76

Rout, S.P., Charles, C.J., Garratt, E.J., Laws, A.P., Gunn, J. and Humphreys, P.N., 2015. Evidence of the generation of isosaccharinic acids and their subsequent degradation by local microbial consortia within hyper-alkaline contaminated soils, with relevance to intermediate level radioactive waste disposal. PloS one, 10(3), p.e0119164

Sánchez-Andrea, I., A. J. M. Stams, S. Hedrich, I. Ňancucheo and D. B. Johnson (2015). Desulfosporosinus acididurans sp. nov.: an acidophilic sulfate-reducing bacterium isolated from acidic sediments. Extremophiles 19: 39-47

Sand, W. and E. Bock, 1988, "Biogenic Sulfuric Acid Attack in Sewage Systems," 7th International Biodeterioration Symposium: Cambridge England, D. R. Houghton, R. N. Smith, and H. O. W. Eggins (eds.), pp. 113-117

Satoh, H., Odagiri, M., Ito, T., Okabe, S., 2009. Microbial community structures and in situ sulfate-reducing and sulfur-oxidizing activities in biofilms developed on mortar specimens in a corroded sewer system. Water Research 43, 4729–4739. https://doi.org/10.1016/j.watres.2009.07.035

Siboni, N., Lidor, M., Kramarsky-Winter, E., Kushmaro, A., 2007. Conditioning film and initial biofilm formation on ceramics tiles in the marine environment. FEMS Microbiology Letters 274, 24–29. https://doi.org/10.1111/j.1574-6968.2007.00809.x

Shapovalova AA, Khijniak TV, Tourova TP, Muyzer G, Sorokin DY. Heterotrophic denitrification at extremely high salt and pH by haloalkaliphilic Gammaproteobacteria from hypersaline soda lakes. Extremophiles. 2008;12(5):619-25

Siddique, R. and Chahal, N.K., 2011. Effect of ureolytic bacteria on concrete properties. Construction and building materials, 25(10), pp.3791-3801

Small, J., M. Nykyri, M. Helin, U. Hovi, T. Sarlin and M. Itävaara (2008). Experimental and modelling investigations of the biogeochemistry of gas production from low and intermediate level radioactive waste. Applied Geochemistry 23: 1383-1418

Small, J. S., M. Nykyri, M. Vikman, M. Itävaara and L. Heikinheimo (2017). The biogeochemistry of gas generation from low-level nuclear waste: Modelling after 18 years study under in situ conditions. Applied Geochemistry 84: 360-372

Smith SL, Rizoulis A, West JM, Lloyd JR. The Microbial Ecology of a Hyper-Alkaline Spring, and Impacts of an Alkali-Tolerant Community During Sandstone Batch and Column Experiments Representative of a Geological Disposal Facility for Intermediate-Level Radioactive Waste. Geomicrobiol J. 2016;33(6):455-67

Spor, H., Trescinski, M., Libert, M., 1992. Microbial Effects on the Radionuclide Transport in a Deep Nuclear Waste Repository. MRS Proceedings 294: 771

Stroes-Gascoyne S. 1996. Microbial Studies in the Canadian Nuclear Fuel Waste Management Program. High Level Radioactive Waste Management, Proceedings of the Seventh Annual International Conference, Las Vegas, Nevada, April 29-May 3

Stroes-Gascoyne, S., C.J. Hamon, P. Vilks, et P. Gierszewski, 2002. Microbial, redox and organic characteristics of compacted clay-based buffer after 6.5 years of burial at AECL's underground research laboratory. Applied Geochem. 17: 1287-1303

Takai K, Moser DP, Onstott TC, Spoelstra N, Pfiffner SM, Dohnalkova A, et al. Alkaliphilus transvaalensis gen. nov., sp. nov., an extremely alkaliphilic bacterium isolated from a deep South African gold mine. International Journal of Systematic and Evolutionary Microbiology. 2001;51(4):1245-56

Tazaki, K., Mori, T., Nonaka, T., 1992. Microbial jarosite and gypsum from corrosion of portland cement concrete. Can. Mineral. 30: 431-434.

Ting, M.Z.Y., Wong, K.S., Rahman, M.E., Meheron, S.J., 2021. Deterioration of marine concrete exposed to wetting-drying action. Journal of Cleaner Production 278, 123383. https://doi.org/10.1016/j.jclepro.2020.123383

Turick, C.E., Berry, C.J., 2016. Review of concrete biodeterioration in relation to nuclear waste. Journal of Environmental Radioactivity 151, 12–21. https://doi.org/10.1016/j.jenvrad.2015.09.005

Urios, L., Marsal, F., Pellegrini, D., Magot, M. Microbial diversity of the 180 million-year-old Toarcian argillite from Tournemire, France. Applied geochemistry (2012). Vol 27, N°7, pp.1442–50

Xu, C., Zhang, Y., Cheng, G., et al., 2008. Pitting corrosion behavior of 316L stainless steel in the media of sulfate-reducing and iron-oxidizing bacteria. Mat. Character. 59: 245-255

Wang, J.Y., Soens, H., Verstraete, W., De Belie, N., 2014. Self-healing concrete by use of microencapsulated bacterial spores. Cement and Concrete Research 56, 139–152. https://doi.org/10.1016/j.cemconres.2013.11.009

Wang, J., Y.C. Ersan, N. Boon, and N. De Belie, Application of microorganisms in concrete: a promising sustainable strategy to improve concrete durability. Appl Microbiol Biotechnol, 2016. 100(7): p. 2993-3007

Warscheid, Th., Braams, J., 2000. Biodeterioration of stone: a review. International Biodeterioration & Biodegradation, Biodeteriation of Cultural Property 2, Part 2 46, 343–368. https://doi.org/10.1016/S0964-8305(00)00109-8

Wei, S., Z. Jiang, H. Liu, D. Zhou and M. Sanchez-Silva (2013). Microbiologically induced deterioration of concrete--a review. Braz J Microbiol 44: 1001-1007

Wiktor, V., Grosseau, P., Guyonnet, R., Garcia-Diaz , E., 2006. Biodétérioration d'une matrice cimentaire par les champignons : influence du vieillissement accéléré sur le développement fongique. Mater. Tech. 94: 507-515

Wiktor, V., Grosseau, P., Guyonnet, R., et al., 2011. Accelerated weathering of cementitious matrix for the development of an accelerated laboratory test of biodeterioration. Mater. Struct. 44: 623-640

Williamson, A.J., Lloyd, J.R., Boothman, C., Law, G.T., Shaw, S., Small, J.S., Vettese, G.F., Williams, H.A. and Morris, K., 2021. Biogeochemical Cycling of 99Tc in Alkaline Sediments. Environmental science & technology, 55(23), pp.15862-15872.

Williamson, A.J., Morris, K., Boothman, C., Dardenne, K., Law, G.T. and Lloyd, J.R., 2015. Microbially mediated Np (V) reduction by a consortium of alkaline tolerant Fe (III)-reducing bacteria. Mineralogical Magazine, 79(6), pp.1287-1295.

Williamson, A.J., Morris, K., Law, G.T., Rizoulis, A., Charnock, J.M. and Lloyd, J.R., 2014. Microbial reduction of U (VI) under alkaline conditions: implications for radioactive waste disposal. Environmental science & technology, 48(22), pp.13549-13556.

Williamson, A.J., Morris, K., Shaw, S., Byrne, J.M., Boothman, C. and Lloyd, J.R. 2013 Microbial reduction of Fe(III) under alkaline conditions relevant to geological disposal. Applied and Environmental Microbiology

Wormald, R., 2019. Environmental Limits of Methanogenesis and Sulphate Reduction (Doctoral dissertation, University of Huddersfield)

Wormald RM, Rout SP, Mayes W, Gomes H, Humphreys PN. Hydrogenotrophic Methanogenesis Under Alkaline Conditions. Frontiers in Microbiology. 2020;11

Yamanaka, T., Aso, I., Togashi, S., Tanigawa, M., Shoji, K., Watanabe, T., Watanabe, N., Maki, K., Suzuki, H., 2002. Corrosion by bacteria of concrete in sewerage systems and inhibitory effects of formates on their growth. Water Research 36, 2636–2642. https://doi.org/10.1016/S0043-1354(01)00473-0

Ye Q, Roh Y, Carroll SL, Blair B, Zhou J, Zhang CL, Fields MW., 2004. Alkaline anaerobic respiration: isolation and characterization of a novel alkaliphilic and metal-reducing bacterium. Appl Environ Microbiol. 70, pp.5595-602

Zhu, T., Paulo, C., Merroun, M.L., Dittrich, M., 2015. Potential application of biomineralization by Synechococcus PCC8806 for concrete restoration. Ecological Engineering 82, 459–468. https://doi.org/10.1016/j.ecoleng.2015.05.017

Zhu T and Dittrich M (2016) Carbonate precipitation through microbial activities in natural environment, and their potential in biotechnology: a review. Front. Bioeng. Biotechnol. 4:4

Conclusion

Three decades of extensive Research & Development (R&D) allow to identify the key reactive mechanisms, the alteration processes and consequences on the microstructure in cementitious materials emplaced in underground environment. However, the evolution under complex coupled perturbation phenomena are still not fully explored and understood. Moreover, recent innovations in terms of material formulations (low-pH cements notably) require dedicated R&D to better understand how their long-term performance is influenced by the host rock and the near-field conditions (i.e., pore degree saturation, chemical evolution of the barriers, microbial impact, loading and gas formation). Nowadays, most of the experimental data are limited to the short-term material evolution. Long-term mechanical integrity of the cementitious material remains largely unknown, despite data existing about ageing of Roman cement or natural analogue, providing evidence that the ageing of cementitious materials can be a very low process, if well manufactured in function to the environment.

Summary about the physico-chemical evolution

The main reactive processes controlling the chemical evolution of cementititous materials are globally well understood in interface with the host rock or directly with the natural water:

- In saturated conditions: leaching, carbonation, magnesium and sulfate attacks, sometimes chloride attack (in function to the envrionment and concentration in sulfate) are the main processes identified.
- In unsaturated conditions, carbonation is the main process.

If some studies focused on it, the impact of chemical changes on microstructure evolution and transport properties remains challenging. For example, the intensity of the pore clogging is influenced by the type and amount of salt and by the pore structure of the substract. Several continuum scale reactive transport models have been developed to simulate these coupled disturbances (especially leaching and carbonation process). Recent works focused on the Mg attack modeling due to the knowledge improvement in the field of Si-Mg phases precipitations. The predictive capability of such models depend on the accuracy of input parameters and their changes as the pore-structure evolves. If these essential parameters could be obtained from a pore-scale simulation able to resolve heterogeneities in cement paste microstructures, how to extract these essential parameters is still an open issue.

Proper coupled description of reactive transport in unsaturated systems, while accounting for multiphase transport, evaporation and porosity changes is only recent. This SOTA lists a few limitations to using reactive transport within cementitious materials in unsaturated conditions. The long-term processes impacting the cementitious materials exclude a simple approach and require multiscale modelling to take into account the relevant reactive pathways identified at the nano/micro and mesoscale, including the skeleton evolution. Indeed, the classical REV approach with a single porosity seems not relevant to reproduce complex materials like concrete composed by several porosity level (capillary, C-S-H…) at long term.

Summary about the microbial interactions with cement

Limited research has been performed to characterize microbial interactions with cementitious materials. Especially studies in relation to nuclear waste disposal remain scarce. Microbial degradation of cementitious materials has been shown in various environments such as sewage pipes, marine structures and wastewater treatment systems. Cementitious materials impose a highly alkaline environment, which inhibits microbial activity. However, several processes affect the chemical evolution of cementitious materials, which can result in a local decrease in pH, enabling microbial activity. Furthermore, concrete is a quasi-brittle material in which the formation of cracks gives microorganisms space to migrate and attach along the surfaces. In such a case, a biofilm can be formed. Microbial

degradation of cementitious materials is mainly caused by the biological production of organic and inorganic acids, which can react with the cement.

Summary about mechanical evolution

The main part of studies relative to cementitious materials in geological disposal environment focus in the chemistry and microstructure evolutions. But cementitious materials will play essentially a mechanical role in repositories and consequences of the chemical and microstructural changes on the mechanical properties were under-explored.

The mechanical behaviour of underground cementitious structures depends of various parameters: boundary conditions and construction methods. It requests to take into account the host rock loading and the rigidity evolution of the structure. This evolution is depending to the chemical and microbial perturbations, the level of loading and also the concrete formulation.

In the case of reinforced concrete, corrosion causes mechanical damage to the concrete under the combined effect of the corrosion-induced expansion (generating internal mechanical stresses) and the loss of cross-sectional area and bonding of the steel, which causes the structure to lose its load-bearing capacity. Previous experimental results highlighted the heterogeneity of the corrosion product layers and the evolution of the mechanical properties of the layers with time and ageing conditions. A specific effort has to be made on this point.

The multiscale characterization and especially the coupled approach at nano/microscale with RUS, nano/micro indentation, SEM/EDX is a key to recover key data to feed numerical chemo-mechanical modelling. Currently, studies on the micro-mechanical consequences of groundwater on cementitious materials are very scarce (mainly in pure water, nitric solution or sulphated water). These works highlight a non-negligible evolution of elastic mechanical properties of the cement matrix subjected to an aggressive solution.

The recourse of numerical approaches to determine the mechanical behaviour of cementitious materials has gained growing interests in recent years, due to the continuous increase of computational power. The characterisation of the mechanical properties of cementitious materials necessitates the knowledge of the evolution of the microstructure and corresponding phase assemblage of the cement paste in the context of disposal environment.

Many studies have been devoted to the analysis and description of the evolution of the microstructure

and mechanical properties of cementitious materials when subjected to the contact of groundwater and argillite. At the nano-microscale, the different minerals (phase assemblage) composing the hydrated cement paste should in principle be considered. At the nanoscale, the use of approaches based on molecular dynamics is widely accepted. At the microscale, more advanced and versatile methods (micromechanics and upscaling, Mori-Tanaka method, homogenization scheme…) have been developed to estimate the properties evolutions.

Concretely, carbonation and leaching have antagonistic effects on porosity and some mechanical parameters. Both processes are integrated in the multi-scale model but treated separately experimentally. This raises several questions:

- Will one process dominate the other? If so, over what period of the concrete's life?
- Would one process dominate in the short term and the other in the longer term?
- Has their superposition been treated experimentally?

Whatever the scale considered, an accurate description of the microcracking and its repercussions on both mechanical and diffusive properties is essential to the simulation of the coupled response of cementitious materials.

Summary about the chemo-mechanical coupling

The multiscale chemo-mechanical modelling was not sufficiently supported in the past as part of the geological disposal context. Two main reasons explain this situation: (i) logically the limitation (now outdated) of the power of the modelling tools, (ii) the isolation of themes and researchers between chemistry and mechanics with difficulties to communicate. In the SOTA, this part was considered beyond the boundaries of the disposal context, at the pore/microstructure scales, mesoscale and the macroscale A special attention was paid to identify what are the key limits and gaps remaining to obtain representative chemo-mechanical models of concrete in geological disposal context.

The pore scale modelling

The pore-scale modelling is relatively young, and then, there are many limits and gaps. The pore scale approach requires new conceptualizations that might be different from more established continuum approaches. This is true for both, chemical and mechanical processes. Typically, pore scale models have discrete phases, but they also might include sub-scale elements (for example amorphous phases) that are treated differently. Because of the heterogeneity of cement paste microstructure, the number of voxels/elements of pore-scale models is large. The need for computationally efficient approaches is paramount. The most obvious approach is to use parallelization and more powerful computers, but the physical limit of small time steps at lower spatial scales results in huge amount of iterations and requires broader solution. One mitigation strategy is an effective geochemistry calculation. The solution time of non-linear equations for the geochemical system can be reduced by the use of tabulated values or abstracted chemical systems. On the other hand, the number of time steps can be reduced by adjusting the chemical systems.

Another field that needs attention is the validation of pore-scale models. Most experiments provide continuum or effective values (e.g. mass of a specific solid phase) or information without spatial information, for example pore size distribution. It is very difficult to obtain spatial information of a property at precisely the same location in an evolving material, for example after the geochemical alteration reaction. For this reason, pore scale models are usually validated using averaged values. However, it is important to stress that this is an indirect validation where a part of the important information is lost during averaging. In the future, more efforts need to be devoted to the experimental techniques that can directly support validation of pore scale models.

As mentioned, coupling between chemistry and mechanics is very recent on the pore scale. This coupling can result in the complex spatial-temporal evolution of composition, microstructure and morphology in materials. The relationships are interconnected as for example not only the formation of the secondary phases cause stresses, but also the stresses influence the conditions of the formation of secondary phases. Reliable chemo-mechanical models are not very common, especially not in a multiscale framework.

The challenge of upscaling

Appropriate upscaling is another challenge. The purpose of pore-scale models is to support the choice of parameter values and constitutive laws on larger scales. The upscaling in this sense usually stretches beyond pure mathematical principles and includes the development of conceptual models and concepts that are appropriate to use on larger scales.

Previous structural chemo-mechanical models decoupled the macroscopic modelling from the mesoscopic phenomena; however, in order to compare concrete made of the different matrices, a non-linear analytical homogenisation model for the chemical-mechanical behaviour of concrete is required to be implemented. This model must be able to manage the solid phases of cement paste versus the chemical state of concrete, and this must be reflected in the mechanical properties. Furthermore, during the chemical damage processes (leaching, carbonation, NaCl ingress…in the hydrated cement paste), this model should also consider the amount and nature of aggregates on macroscopic residual mechanical properties.

The specific case of reinforced concrete

Until now, the phenomenon modeling of reinforcement corrosion was decoupled from the chemical state of the concrete. Hence the lock to be lifted in this chemo-mechanical model will consist in predicting the progress of steels corrosion as a function of the chemical state of the concrete at the interface and in localised cracks, deducing its effect in terms of steel anchorage and their contribution on reinforced concrete mechanical performances.

Another phenomenon to be considered and incorporated into this model is the cracking of reinforced concrete, along with predicting its impact on the transport properties (permeability, diffusion coefficient, water retention curve…) of the concrete.

The implementation solution

The implementation in a Thermo-Hydro-Chemo-Mechanical finite element code able to compute the evolution of a tunnel during several thousand years seems a relevant solution. Once implemented, it will allow a more accurate prediction of the lifetime of radioactive waste disposal structures, but also the simulation of their very long-term behaviour under natural mechanical loading and physicochemical degradation caused by the host rock water. Different chemistry of binders could be considered to perform comparative studies of envisioned solutions.

The following knowledge general gaps were identified through the development of this SOTA:

- What is the impact of various chemical degradation phenomena on the mechanical behaviour of massive cementitious materials?
- What is the impact of microbially induced processes in the chemo-mechanical behaviour of cementitious materials (by considering the recent material development and the chemical/structural evolution during the lifecycle of the concrete)? Do these processes change the expected chemical evolution without microbiological activity?
- How to model the long-term mechanical behaviour of cementitious materials during hydraulic transients or fully saturated media with respect to the chemical evolution with and without microbial activity?
- How to achieve a comprehensive model based description of the multi-scale modelling process?

Based on this SOTA review, the MAGIC WP was built to increase the confidence in chemo-mechanical simulations by reducing uncertainties in input data and understanding of key coupled processes (for both young and aged materials). Specific conditions for waste disposal (microbial activity, chemical and mechanical stress, variable saturation, etc…) are taken into account by addressing implementation needs and safety aspects, e.g. regarding selection of materials, dimensioning, and (long-term) behaviour of seals and plugs.

5. Appendix A

Natural water compositions in the host rocks

- Composition of water representative of crystalline rock environment

Synthesis of contributions

The chemical compositions of pore water in crystalline rocks are conditioned by the properties of the rock. A pore water sample comes from the groundwater flowing in the (micro) fractures (the porosity of the crystalline rock is less than 1%).

The Bukov URL (Czech Republic) was built on the 12th level of former uranium mine of Rožná. The determination of the chemical composition of the pore water was analysed for drill core in the laboratory, by installing a packer inside an intact borehole and by high-pressure extraction techniques. The results show that all examined pore water samples contain sodium. The pore water samples from the laboratory contain mainly carbonates, whereas the pore water samples from the in situ experiments contain chlorides and sulphates in addition to carbonates (Bukovska et al., 2020). The groundwater has a very low salinity as the majority of species have a concentration below mmol/L (Figure 1-1Figure 5-1).

Figure 5-1 shows a comparison of out-diffusion experiment with groundwater chemical composition on the 12th level, groundwater chemical composition, sampled in-situ and finally with model representation of water/mineral phases equilibrium (Model HH). Model HH with the additive NaCl steps represents the reaction of equilibrated solution with fluid inclusions/external source of NaCl (Bukovska et al., 2020).

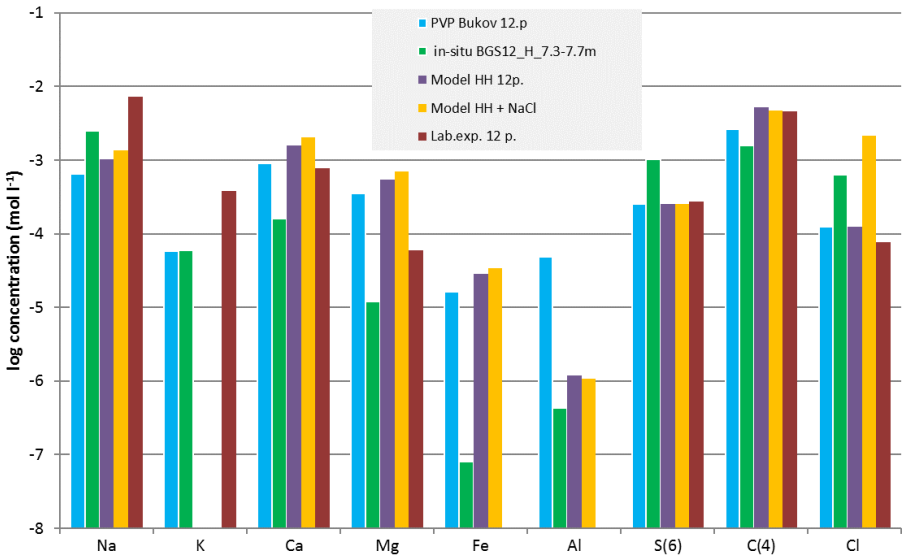

Figure 5-1: Chemical composition of the crystalline host rock groundwater.

The chemical composition of groundwater in the Rožná mine galleries is influenced by two primary factors. The first one is vertical location of groundwater inflow the mine; the second one is the influence of oxidative environment in mine galleries.

Table 5-1 gives the mean composition of the Bukov URL used in the research programs (S25 groundwater).

Table 5-1: The chemical composition (main anions and cations) of S25 groundwater

	Cl^-	SO_4^{2-}	SiO_3^{2-}	HCO_3^-	pH	TOC
S25 groundwater composition	**(mg/l)**	**(mg/l)**	**(mg/l)**	**(mg/l)**		**(mg/l)**
	20.4	45.5	21.5	89.0	9.5	1.89
	Na	**K**	**Mg**	**Ca**	**Fe**	**Al**
	(mg/l)	**(mg/l)**	**(mg/l)**	**(mg/l)**	**(mg/l)**	**(mg/l)**
	56.6	0.702	0.215	1.57	0.434	0.345

The pore solution composition can vary in function to the crystalline rock considered (Neeft et al., 2020). As example, Table 5-2 indicates the pore water chemistries in granitic host rocks pore water chemistries for granitic rocks in Czech.

Table 5-2: Measured pore water chemistries in granitic rocks (Neeft et al., 2020)

Parmeter	Unit	Czech (600 m)	Czech (1000 m)
Temperature	°C	25	25
pH	-log(H^+)	8.2	9.4
Na^+	mmol/kg	0.865	3.81
K^+	mmol/kg	0.0537	0.0179
Ca^{2+}	mmol/kg	0.864	0.0324
Mg^{2+}	mmol/kg	0.342	0.00412
Fe^{2+}	mmol/kg	0.00179	0.00179
Al^{3+}	mmol/kg	0.00371	0.00371
SiO_2 (aq)	mmol/kg	0.520	0.481
Cl^-	mmol/kg	0.0931	0.528
SO_4^{2-}	mmol/kg	0.219	0.109
HCO_{3-}	mmol/kg	2.68	5.048

The lab tests conducted at GRS are related to the disposal system T1 (Disposal system in clay formation of larger thickness) appropriate to the RESUS project (Reinhold et al., 2013). A salt content around 150 kg/m^3 is estimated for the disposal area. The pore water of the disposal system T1 is comparable with the pore water of Schacht Konrad (Table 5-3; Herold et al., 2020). The measurement conditions and analysis methods are not detailed in the available references (see above).

Table 5-3: Parameter for "Konrad-solution" at 25°C (Herold et al., 2020)

Component	Mass [mmol/l]
Sodium	3380.721
Potassium	5.422
Calcium	223.040
Magnesium	113.598
Chloride	3823.541
Sulphate	8.661
Additional parameter	
pH	7.9
Density	1155 kg/m^3
Viscosity	2.0 mPa·s

Table 5-4 gives the composition of salts for production of a synthetic “Konrad-solution” at GRS lab.

Table 5-4: Composition for synthetic “Konrad-solution” at 25°C

Chemical	Formula	Mass [g/l]
Sodium chloride	NaCl	150.08
Magnesium chloride hexahydrate	$MgCl_2 \cdot 6\ H_2O$	19.414
Sodium sulfate-10-hydrate	$Na_2SO_4 \cdot 10\ H_2O$	30.94
Potassium chloride	KCl	0.459
Calcium chloride hexahydrate	$CaCl_2 \cdot 6\ H_2O$	96.072
Silicium	Si	6.58
Aluminium	Al	30.89

According to the European standard NF EN 206/CN (2014) such a geological medium is ranked in the exposure class XA_2. This is a moderately aggressive chemical environment for concrete due to the presence of sulfates and magnesium.

- Composition of water representative of clayey rock environment

Porewater in equilibrium with the argillaceous surrounding rock of either the French Callovo-Oxfordian argilite (Bure - France), the Toarcian argillite of Tournemire (France), the Opalinus clay of Mont Terri (Switzerland) or the Boom clay (Belgium and the Netherlands) has a multi-ionic composition (HCO_3^-, Cl^-, SO_4^{2-}, Mg^{2+}). For example, in the Bure URL (France), the data coming from *in situ* measurements at five different depths between -430 m and -505 m with three experimental set-ups [2] indicate that the groundwater contains high levels of sulphate and chloride ions, which leads to an exposure class XA_2 according to the European standard NF EN 206/CN (2014).

Table 1-5 shows the mean values and maximum deviations for measured concentrations of major species and pH for Callovo-Oxfordian pore water. These are averages for PAC1002 (Vinsot et al., 2008), POX1201 and EPT1201 during the post-drilling period and OPA pore water (Mäder 2018; Wersin et al., 2020) based on Measured compositions (mmol/L) of water circulated in the BCI-4 B and C borehole at the Mt. Terri Underground Rock Laboratory.

Table 5-5: Chemical composition of the clayey host rock groundwater.

Parameter	Cox pore water PAC1002 ; POX1201; EPT1201	Opalinus Clay water from Mont Terri
pH	7.0 ± 0.3	7.24 – 7.78* (± 0.05)
Ionic strength (meq/L)	0.08 (± 5 %)	
Chloride (mmol/L)	39.5 (± 6 %)	271.45 (± 5 %)
Sulfate (mmol/L)	12.6 (± 4 %)	13.5 (± 5 %)
TIC** (mmol/L)	4.1 (± 31 %)	2.45 (± 5 %)
Sodium (mmol/L)	47.6 (± 3 %)	239.55 (± 5 %)
Calcium (mmol/L)	5.4 (± 8 %)	15.15 (± 5 %)
Magnesium (mmol/L)	4.5 (± 6 %)	16.1 (± 5 %)
Potassium (mmol/L)	0.6 (± 12 %)	1.4 (± 5 %)
Strontium (mmol/L)	0.2 (± 11 %)	0.5 (± 5 %)
Silica (mmol/L)	0.4 (± 72 %)	0.12
Ammonium (mmol/L)	0.2 (± 30 %)	< 0.8 (± 5 %)
Bromine (mmol/L)	0.081 (± 14 %)	0.5 (± 5 %)
Fluorine (mmol/L)	0.033 (± 32 %)	
Iodine (mmol/L)	0.029 (± 15 %)	0.02 (± 5 %)

*Lower pH: stable values measured after short storage time. Higher pH: stable values reached after long storage time

** TIC: Total Inorganic Carbon

The data in the second column of Table 5-5 come from a large number of data acquired from several holes and therefore have a good representativity of the Cox pore water composition. The measured pore water compositions for clay host rocks can be influenced by experimental artefacts such as the difference in partial pressure of CO_2, the accuracy of redox potential measurements and the oxidation of the host rock (when exposed to air, for example during the measurements).

The chemical analysis of the Opalinus clay pore water is possible by sampling the water accumulated at the bottom of dry bores with compressed gas flushing. The Opalinus clay pore water of Mount Terri differs from the Cox pore water by its higher content of chloride, sodium and magnesium (Mazurek and de Haller, 2017).

Given the inherent spatial heterogeneities of the clay formation, the Opalinus (OPA) Clay pore solution from exactly the same location as for the mock-up OPA/concrete interface systems studied in Task 2 of the MAGIC WP, i.e., the location of the Cement-clay Interaction (CI) experiment at the Mt. Terri Underground Rock Laboratory (URL), is taken as the reference.

The composition of the OPA pore solution is approximately known at the location of the HE-D Niche (CI-D location) at the Mt. Terri URL. It was measured based on the pore solution sampling, carried out in 2016 at this site, from the observation interval in borehole BCI-4 (U. Mäder 2018). The measured composition of water circulated in the borehole of BCI-4 is shown in Table 1-5. For the lab synthesis of an analogue pore solution, the composition from the BCI-4 samples was adjusted to atmospheric pCO_2, by reducing alkalinity and maintaining calcite equilibrium. This resulted also in a somewhat higher pH value, compared to the in-line measurement performed during sampling.

It is important to mention that the Swiss experience deals mainly with cases where the clayey pore solution diffuses into the cement-based parts of the EBS. The conditions relevant for the Swiss repositories never deal with the case of a cement-based component of the EBS being completely saturated as if submerged into the pore solution.

In the case of Boom clay, the chloride concentration strongly depends on the borehole location. The chloride concentration is 26 mg L^{-1} at the URF HADES in Mol and up to 3,100 mg L^{-1} in the Essen boreholes (De Craen et al., 2006). For comparison, the chloride concentration variations in the pore water of the Opalinus clay at Mont Terri (Switzerland) reaches a maximum of 12 to 14 g/L.

The natural production of water *via* the boreholes present in the underground laboratory is generally low (~ 20 ml per day and per m^2 of surface for the Cox for example). Thus, all partners developed specific protocols for the synthesis of the pore water.

6. Appendix B

Relative to the Part 1.3

PSI, EMPA

Special effect of the charged surfaces of cement minerals- double layer effects, potential and charge reversal

The formation of the electrical double layer at a mineral surface is controlled by the surface charge of cement particles formed as result of protonation deprotonation reactions (e.g. C-S-H). Macroscopically, the interaction of solutes with mineral surface is described using thermodynamic surface complexation models (SCM) (Lyklema, 1995). In such models, the surface of the mineral is represented by a planar or at best a spherical interface. The surface reactive sites, typically oxygen atoms with uncompensated bond charge balance, are the source of the surface charge due to the protonation/de-protonation and ion adsorption reactions. Depending on the SCM approach used, the ions at contact with the surface are considered either as part of the diffuse double layer or as part of the surface (Figure 6-1). Several extensive reviews of the SCM and their historical development exist in the literature (Kulik, 2009; Lutzenkirchen, 2002). The effect of the ion-ion interaction on the surface complexation reactions and protolysis is typically considered in a mean-field approximation (e.g. as an average relative electrostatic potential resulting from the superposition of all single ion potentials).

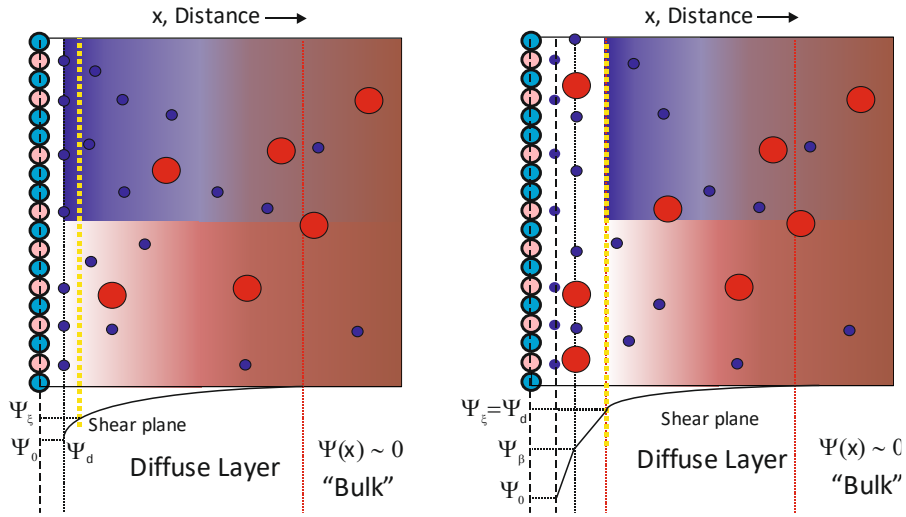

Figure 6-1: Schematic representations of the modified Gouy–Chapman (MGC) model (left) and the triple layer (TL) model (right) (Lyklema, 1995). Surface sites are shown by pink (negatively charged, (-)) and light blue (zero charged) spheres surrounded by black circles. The net negative surface charge emerges due to deprotonation of surface sites, controlled by the pH in solution. The distribution of ions charge in the diffuse layer is described by the Poisson Boltzmann equation for external electrostatic potential$\Psi(x)$.

In the MGC model, the surface potential is equal to the contact potential of the diffuse double layer$\Psi_0 \equiv \Psi_d$. The TL model assigns the location of surface sites and inner-sphere complexes, the outer-sphere complexes and the contact of the diffuse layer to three distinct surface plains with corresponding net charge densities $(\sigma_0, \sigma_\beta, \sigma_d)$. Inner-sphere complexes are located in the 0-plane. The $\sigma_0$charge density is the sum of the charges contributed by surface sites and the inner-sphere complexes. The β -plane indicates the location of outer-sphere surface complexes, whereas the d-plane marks the beginning of the diffuse layer. These charged planes form two sequential capacitors with the capacitance C_1 and C_2, respectively. The potentials at each plane are thus linearly related: $\Psi_0 - \sigma_0/C_1 = \Psi_\beta = \Psi_d - \sigma_d/C_2$. The MGC model can be formally deduced from TL model setting the capacitance to infinity. The shear plane

indicates a virtual boundary between “immobile” ions bound to the surface and “mobile” ones in the aqueous solution. The choice of the shear plane position is not constrained by SCM parameters and has to be tuned to independent data on ions mobility. In TL models the shear plane is often assumed to co-inside with d-plane. Figure adapted from (Churakov and Prasianakis, 2018).

In the MGC model (Figure 6-1), the amphoteric reactive sites at mineral surface participate in protonation/de-protonation reactions, and the mobile ions are distributed in the diffuse layer according to the Poisson Boltzmann equation. The surface potential is assumed to be equal to the contact potential in electrolyte at the interface. The standard state of the surface reaction is defined for the neutral surface and the intrinsic acidity of the surface sites. The effective surface complexation constant depends on the mean electrostatic potential due to the surface charge. The finite dimensions of the surface sites and aqueous ions do not enter into model parameters explicitly, but, in principle, can be accounted for via the activity coefficient.

The TL model assumes that the (de)protonated surface sites, inner-sphere complexes and outer-sphere complexes are located within a set of individual planes at increasing distance to the surface (Figure 6-1). The distribution of ions between the sorption sites is obtained by the speciation calculations. In the currently most widely accepted TL model CD-MUSIC (Hiemstra and Van Riemsdijk, 1996) the formula charge on each surface complex is distributed between 0, β and *d* planes according to the mineral specific constants. These charged planes form a series of parallel capacitors. The electrostatic potential in each plane contributes to the activity coefficients. Free model parameters are the surface complexation constants. Due to potentially strong correlations with the surface complexation constants, the capacitance of two layers is not fitted but fixed constantly at some physically meaningful values. The capacitance can be further broken down into the di-electric permittivity of the media and the distance between charged planes. It is, however, difficult to obtain an unambiguous estimation of all model parameters (Sverjensky, 2001; 2005). Neither capacitance density nor the dielectric permittivity of the interfacial region can be directly measured (Cheng and Sprik, 2014). The model has been applied with success to a large number of systems (Sahai and Sverjensky, 1997; Sverjensky, 2006). The thickness of the sorption layers can, in principle, be estimated based on various spectroscopic methods (Hofmann et al., 2016). The distribution of ions between inner- and outer-sphere complexes may depend on the nature of the surface and on the electrostatic properties of bulk minerals, e.g. magnitude and the structural position of surface charges. The location of ions in the inner- and outer-sphere complexes is a complex result of a balance between the surface-ion and ion solvent interaction.

In the simplest approximation, the effect of electrical double layer at the mineral electrolyte interface in taken into account in reactive transport simulations using either Poisson Boltzmann or Donnan equilibrium models. In the Poisson Boltzmann model, the distribution of ions at the interface is obtained solving the Poisson equation assuming Boltzmann distribution of ions for a given electrostatic potential:

$$\nabla^2\phi(x) = -\frac{F}{\varepsilon}\sum_i z_i\, C_i(x) \qquad 6\text{-}1$$

$$C_i(x) = C_i^B \Gamma_i(x)\, exp\left(\frac{-z_i F\varphi(x)}{RT}\right) \qquad 6\text{-}2$$

where $\phi(x)$ is the local potential as a function of the distance to the surface, C_i^B the ion concentration in the bulk solution unaffected by the surface charge, $\Gamma_i(x)$ the ratio of the activity coefficients in bulk solution and in the double layer at position x, z_i the charge number of the ion, F the Faraday constant, R the universal gas constant, and T the temperature. These equations are solved together with the electro-neutrality and the boundary conditions for the mineral surface charge. The activity ratio $\Gamma_i(x)$ is usually not known and assumed to be unity in most of the simulations. Solving the Poisson Boltzmann equation for a symmetric electrolyte and a single planar charged surface leads to the Gouy-Chapman (GC) model and modified GC model if ion adsorption in a Stern layer is taken into account.

In the Donnan approach the concentration dependencies of ion distributions at a charged interface or in a pore enclosed by charged surfaces are replaced by a uniform concentration of solutes. The equilibrium

with the bulk electrolyte is described by the equalization of the chemical potential for the species in the Donnan volume and in the bulk electrolyte:

$$\mu_i^{B,0} + RT\ ln\ a_i^B = \mu_i^{D,0} + RT\ ln\ a_i^D + z_i F \varphi_m \quad 6\text{-}3$$

where $a_i^B\ and\ a_i^D$ are activities, and φ_m is the Donnan potential. The superscripts *B and D* are referred to as bulk and Donnan solution, respectively (Alt-Epping et al., 2018).

This description leads to the Donnan equilibrium concentration:

$$C_i^D = C_i^B \Gamma_i\ exp\left(-\frac{z_i F \varphi_m}{RT}\right) \quad 6\text{-}4$$

The Donnan potential φ_m depends on the surface charge and the solution composition, but in contrast to the Poisson Boltzmann concept is constant in the entire Donnan domain. It is obtained from balancing the charge over the Donnan porosity through

$$\sum_i z_i C_i^D = -Q \quad 6\text{-}5$$

where Q is the net surface charge per volume of Donnan solution (typically negative for clays). The net charge may be smaller (or larger) than the basic clay layer charge originating from isomorphic substitution, in response to a partial shielding (or an addition) of charges by more strongly bound surface ions (e.g., a Stern layer) or protons.

Poisson-Nernst-Planck equation

In present of diffuse double layer, the transport of charged species becomes electrochemically coupled since the local charge conservation must be maintained at all times, when the global boundary condition implies zero electrical current.

These effects are taken into account by Nernst-Planck equation, which describes the transport of charged particles (ions) in presence of electrical field. Transport is therefore described by the combined effect of an ionic concentration gradient (or a gradient of the chemical potential μ [J]) and a gradient of the electrical potential Φ [J C^{-1}]. Based on that the Nernst-Planck equation is an extension of Fick's laws where in addition the diffusing particles are influenced by electrostatic forces. In the frame of the Nernst-Planck formalism the diffusive flux $\vec{j}_i$ [mol m^{-2} s^{-1}] of the i-th ion species in the liquid is according to Pivonka et al. (2009):

$$\vec{j}_i = -\boldsymbol{D}_i \left(\vec{\nabla} C_i + \frac{z_i F}{RT} C_i \vec{\nabla} \Phi\right) \quad 6\text{-}6$$

The first term in the brackets describes Fickian diffusion of the *i*-th ion species down its individual concentration gradient; the second term accounts for transport along the gradient of the electrostatic potential Φ [V = J C^{-1}] dependent on the charge of the ion. In Equation 1-27 C_i [mol m^{-3}] is the concentration of the *i*-th species in the mobile phase and $\boldsymbol{D}_i$ [m^2 s^{-1}] is individual diffusion coefficient. *F* [C mol^{-1}] is the Faraday constant and z_i the valence ($|z_i|$ is the charge number) of the *i*-th ion type, *R* [J K^{-1} mol^{-1}] represents the gas constant and *T* [K] the temperature.

For practical purposes, the Equation 1-27 has to be solved with appropriate initial and boundary conditions based on the physical problem to be modelled (Figure 6-2). Consideration of electrostatic effects is particularly important in the presence of a salt concentration gradient and highly charged mineral surfaces. In such surfaces the electro-chemical coupling can result in the transport of tracers against concentration gradients (Hax Damiani et al., 2020).

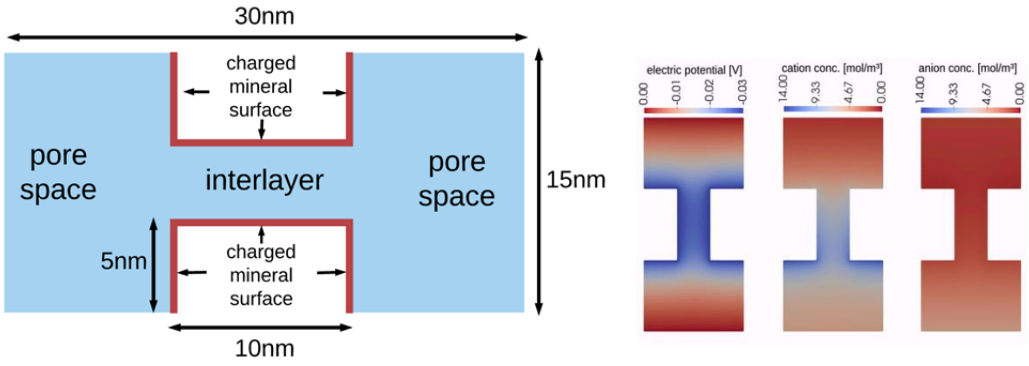

Figure 6-2: Simulation of a steady state ion distribution in a nanoscale pore with charged surfaces resembling the surface charge of illite/smectite particles. At the beginning of the simulations, two reservoirs separated by narrow pores are filled with 5 mol/m³ and 1 mol/m³ NaCl solution, respectively. Results of the calculation show a redistribution of cationic and anionic species and formation of diffused double layer as a result of the salt concentration gradient and the electrostatic potential due to the presence of the charged mineral surface (Hax Damiani et al., 2020).

Molecular scale limitations of classical Poisson-Nernst-Planck equation

In a most simple representation the negative structural charge results in formation of diffuse double layer at the interface as shown in Figure 6-2 for the simple Poisson Boltzmann equation and in Figure 6-3 for the more elaborate GC model. The electrostatic potential of the negatively charge surface results in accumulation of positive ions at the mineral surface (Stern layer). The Stern layer dimensions are comparable with the diameter of a hydrated ion. The potential at the surface of the first adsorbed cationic layer is still negative. This region is essentially anion-free due to the strong electrostatic repulsion. Beyond this region, ions are distributed according to the Poisson Boltzmann equation (consistent with classical Nernst-Planck description). The concentration of cations exponentially increases and the concentration of anion exponentially decreases towards the surface.

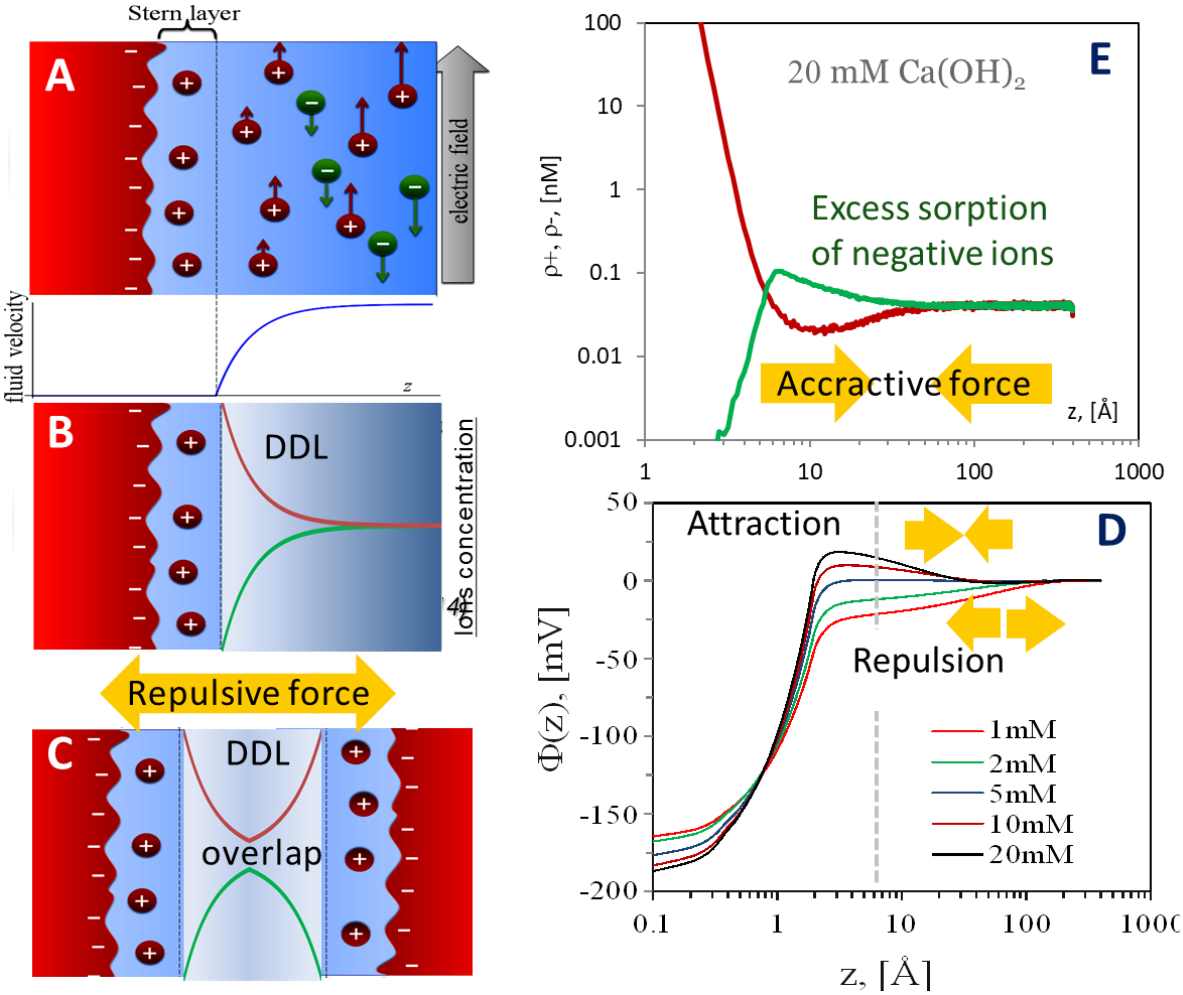

Figure 6-3: Conceptualisation of modified GC model and ζ-potential measurements of effective surface charge (A). Ions in the Sterner layer are tightly attached to the surface and contribute to the net surface charge. In an applied electric field, the colloidal particles of C-S-H move in direction of the field strength or opposite to it depending on the surface charge. (B) Concentration profile of positive and negative species in DDL according to Poisson Boltzmann equation. PB-model predicts negative effective potential due to depletion of anionic species and limited sorption of cation. Accordingly, PB-model always predicts a net repulsive force between charged surface at short distances, if noticeable overlap of DDLs takes place (C). Reactive Monte Carlo simulations of C-S-H surface charge indicate strong dependence of surface ζ-potential as function of pH and concentration of divalent cations (e.g. Ca) (Churakov and Labbez, 2017; Churakov et al., 2014; Jonsson et al., 2005; Labbez et al., 2009). Simulations and measurements demonstrate that with increasing Ca concentration the surface potential change from negative to positive. In a 20mM $Ca(OH)_2$ solution (e.g.) in equilibrium with portlandite, positive ζ-potential (surface overcharge), leads to co adsorption of anionic species (E). Furthermore, the ion-ion correlation leads to attractive force between C-S-H surfaces at short distances, the phenomena that are not captured by PB-theory.

Both the Donnan and Poisson Boltzmann approaches rely on several fundamental assumptions, which limits the applicability and the extrapolation range of the theory. Essentially, both approaches neglect ion-ion correlation effects and the finite sizes of the solvent and solute species. This strictly limits the reliability of the approximation to low ionic strength and low charged ions. These effects have been closely looked at in cement systems (Churakov and Labbez, 2017; Churakov et al., 2014; Jonsson et al., 2005; Labbez et al., 2009), The PB theory is known to fail for 2:1 electrolytes, e.g. solutions dominated by divalent cations. In these systems, the strong cation–surface interaction leads to an overcharging of the mineral surface and co-adsorption of anions. Fig. 6 shows predictions of the ion distribution by the Poisson-Boltzmann theory and Monte Carlo simulations. Strong disagreement is observed in the surface of the 2:1 electrolyte. Poisson Boltzmann equations predict a larger extent of

the diffuse double layer and fail to reproduce the co-uptake of the anionic species. Thus, Poisson Boltzmann overestimates the anion exclusion effects.

The ion-ion correlation aspects can in principle be included into the Poisson Boltzmann and Donnan approaches via activity coefficient. Recently, a modified formulation of Poisson Boltzmann Nernst-Planck equation (MPB-NP) has been developed, which takes into account the contribution of the ion activities and the gradients from Monte Carlo simulations (Yang et al., 2019):

$$\boldsymbol{J}_i = -D_{i,0}\left(\nabla C_i + \frac{ez_iC_i}{kT}\nabla\psi + \frac{C_i}{kT}\nabla\mu_i^{ex}\right) \quad 6\text{-}7$$

$$kTln\left(C_{i,\infty}\right) = kTln\left(C_i(x)\right) + ez_i\psi(x) + \left(\hat{\mu}_i^{ex} + kTln\left(\frac{\gamma_i(x)}{\gamma_{i,\infty}}\right)\right) = kTln\left(C_i(x)\right) + ez_i\psi(x) + \mu_i^{ex}(x) \quad (4.20)$$

$$\frac{1}{kT}\mu_i^{ex}(x) = -\frac{ez_i}{kT}\psi^{GCMC}(x) - ln\left(\frac{C_i^{GCMC}(x)}{C_{i,\infty}}\right) \quad 6\text{-}8$$

The difference to the conventional approach is that the gradient of the chemical potential is evaluated from the Monte Carlo simulations and implemented into transport simulations via Eq. 13. This approach enables to reproduce the exact electrostatic potential and concentration profiles at the charged mineral surface and their effect on the effective diffusion coefficient (Figure 6-4). This MPB-NP model was applied to study ion transport in gel pores of C-S-H particles as function of inter-particle distance and to derive the effective diffusion coefficients of water sodium and chlorine ions in the aggregates of C-S-H particle. Eventually, a multiscale modelling approach was used to access Cl transport in heterogeneous cement paste (Figure 6-5). The effective diffusivities in C-S-H gel pore obtained with MPB-NP model were to estimate the Cl mobility C-S-H aggregate and cement paste in 3D using continuum scale diffusive transport.

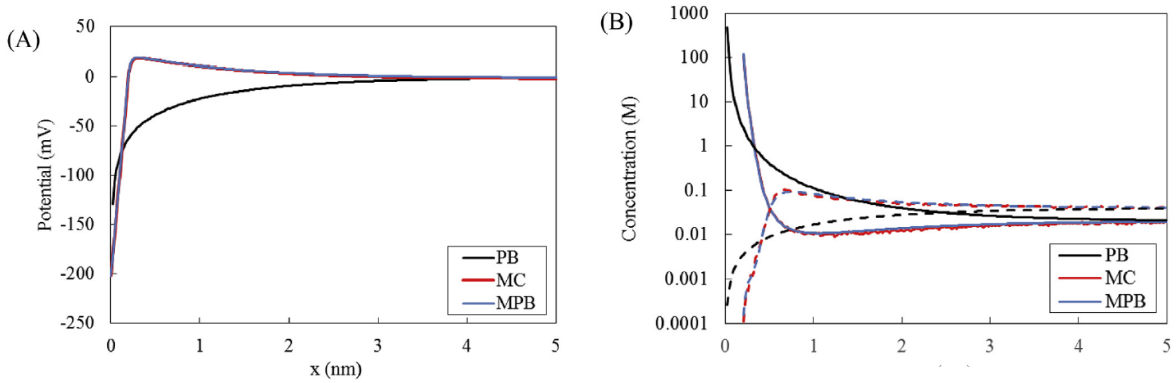

Figure 6-4: The electrical potential (A) and ion concentration distribution (B) with respect to the distance normal to the surface of charged surface calcium-silicate-hydrates. The red lines represent predictions of the Monte Carlo simulations, which account for the ion-ion correlations and the finite size of the ions. Black lines are results from the conventional Poisson Boltzmann Nernst -Planck theory (PB-NP) modelling chain. Blue lines are predictions of a modified PNP model (MPB). Solid and dashed lines represent cationic and anionic species, respectively. The system corresponds to a mix of 10 mol/m^3 NaCl with 20 mol/m^3 $Ca(OH)_2$. Adopted from (Yang et al., 2019)

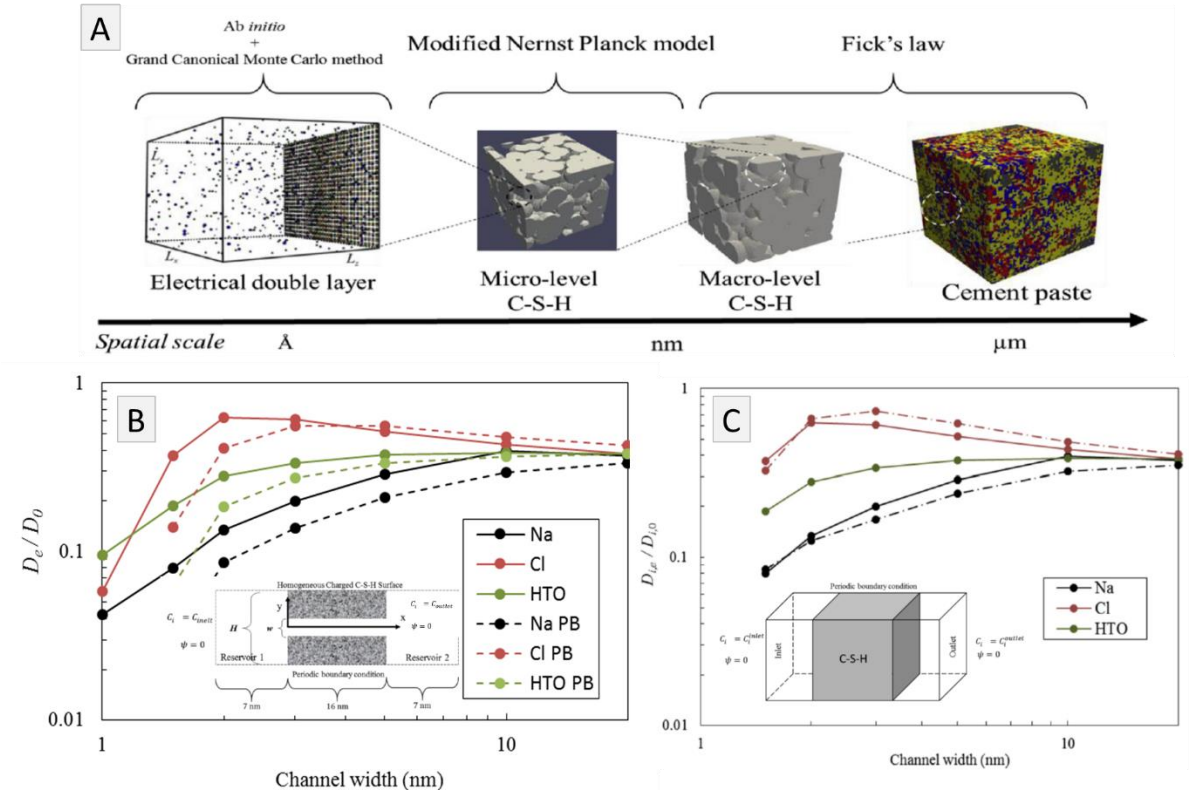

Figure 6-5: A: Multiscale modelling approach for the assessment of diffusive mobility of water and cation in cement paste taking into account molecular scale interaction of ions with surface of C-S-H phases and the heterogeneous microstructure of cement paste (Yang et al., 2019).. The normalised effective diffusion coefficients for Na^+, H_2O and Cl^- obtained with the classical PB-NP model (dashed lines) and the modified MPB-NP model, taking into account the activity of the cationic and anionic species (B). Estimation of diffusion parameter at the scale of cement grains (anhydrous phases).

Lattice Boltzmann method

The lattice Boltzmann method (LB) is a special discretization of the Boltzmann equation and originates from the gas kinetic theory. The LB method is vitally applied for reactive transport processes at pore

scale. The advantages of the method include simple discretisation approach on a regular grid, locality of numerical operation enabling efficient parallelisation using domain decomposition.

The elementary variables are the so-called populations or distribution functions f_i which represent the probability of finding in space a particle with a given velocity. To every distribution function corresponds a discrete velocity vector (Succi, 2001). Depending on the dimensions and number of discrete velocities, there exist different lattice models. For two-dimensional simulations the standard D2Q9 square lattice with 9 discrete velocities is implemented. The projection of this lattice in 3D results in the D3Q27 cubic lattice with 27 discrete velocities (Figure 6-6).

These lattices require communication and exchange of information only within the next neighbouring nodes. This has the advantages of (a) simple implementation of complex geometry boundary conditions, and (b) efficient parallelization of the algorithm for use in high performance computing facilities.

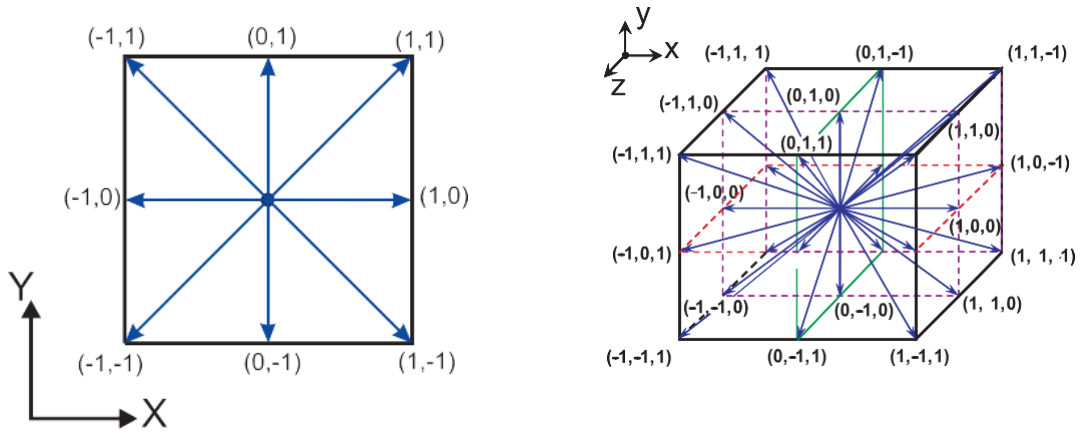

(a) D2Q9-lattice (b) D3Q27-lattice

Figure 6-6: Lattice models: (a) two dimensional 9-velocity lattice (D2Q9); (b) three dimensional 27-velocity lattice (D3Q27). Only next-neighbours communication is required for these space-filling lattices.

The lattice BGK equation is a discrete variant of the Boltzmann equation and can be written as:

$$f_i(x + c_i\delta t, t + \delta t) = f_i(x,t) + \frac{1}{\tau'}\left[f_i^{eq} - f_i(x,t)\right] \qquad 6\text{-}9$$

where i is the index of the lattice velocity vectors, i = 0...8 for D2Q9 lattice and i = 0...26 for D3Q27 lattice, $\boldsymbol{c}_{i\alpha} = c_i\boldsymbol{e}_\alpha$ are the discrete lattice velocities, the direction vector of velocity $\mathbf{e}_\alpha$ is given as,

$$\boldsymbol{e}_\alpha = \begin{cases} (0,0) & \alpha = 0 \\ (cos\theta_\alpha, cos\theta_\alpha)\ c_i & \alpha = 1,3,5,7 \\ (cos\theta_\alpha, cos\theta_\alpha)\sqrt{2}\ \ c_i & \alpha = 2,4,6,8 \end{cases} \qquad 6\text{-}10$$

where α is the coordinate index ($\alpha = x, y, z$), and $c_i = \delta x/\delta t$ is the lattice discrete velocity speed. Here, δx and δt are the lattice spatial step (spacing between consecutive nodes) and lattice time step, respectively. For a single component LB model δx=1 and δt=1 in lattice units. Parameter τ is the relaxation time that controls the viscosity of the fluid and the diffusivity of the solutes in a passive scalar approach; f^{eq} is the equilibrium distribution function and the most commonly used form is:

$$f_i^{eq}(\rho,u) = \omega_i \rho \left[1 + 3\left(\frac{c_i.u}{c^2}\right) + \frac{9}{2}\left(\frac{c_i.u}{c^2}\right)^2 - \frac{3}{2}\left(\frac{u}{c}\right)^2\right] \quad 6\text{-}11$$

where the weight factors ω_i for D2Q9 lattice model are $\omega_0 = 4/9$, $\omega_{1,2,3,4} = 1/9$, $\omega_{5,6,7,8} = 1/36$. Every species has each own population set. The local density ρ and the local velocity u are calculated as the first moments of the distribution functions:

$$\rho = \sum_{i=0}^{8} f_i, \qquad u_\alpha = \frac{\sum_{i=0}^{8} c_{i\alpha} f_i}{\rho} \quad 6\text{-}12$$

For multicomponent simulations the model can be scaled up to an arbitrary number of species using a passive scalar approach (Molins et al., 2020; Prasianakis et al., 2018; 2017). Dissolution-precipitation reactions leading to the change of microstructure and the alteration properties of porous media are followed by either kinetic rate equations or equilibrium approach. Particular strength of the approach is that effective permeability and a diffusivity test can be conducted by applying a differential pressure and a differential concentration along the sides of the evolved geometries using the same lattice Boltzmann solver.

Nucleation processes at pore scale

Reactive transport within porous media is governed by several mechanisms that are also dependent on the porosity, connectivity and the degree of confinement. The mineral dissolution and precipitation reactions can alter the transport pathways and affect the microstructural evolution either promoting or reducing the mass transport rates. Depending on the size of the pores different mechanisms compete during mass transport and phase change. For example, at small scales (few nm), the electrostatic forces have a very strong influence in transport and in some cases may totally restrict the transport of ions depending on the surface charge. Reaction kinetics and crystallization paths are also dependent on the pore sizes. Very often for the initiation of precipitation, a threshold supersaturation must be achieved, before which, the solution remains in a metastable state.

The classical nucleation theory or its extended variants may be used to model such processes. The model developed by Prieto (2014) can be used to calculate the Supersaturation-Nucleation-Time (SNT) dynamics. Through describing crystallisation in porous media, it is essential to distinguish between homogeneous and heterogeneous nucleation mechanism. Heterogeneous (HET) nucleation assumes growth of new phase on the existing substrate of the same of another phase. Contrarily, in homogeneous (HON) nucleation process no initial seeds or template are present; crystallisation is initiated with formation of the first crystal nuclei from a homogeneous aqueous solution. Once stable crystals are formed crystallisation proceeds by the growth on existing substrate. For both HET and HON, the nucleation rate, J [m^3/s], varies exponentially with the free energy change ΔG_c associated with the formation of a nucleus of critical size:

$$J = \Gamma \exp\left(-\frac{\Delta G_c}{kT}\right) \quad 6\text{-}13$$

where k is the Boltzmann constant, T is the absolute temperature and Γ a pre-exponential factor. The nucleation energy barrier is highly dependent upon the interfacial tension σ and saturation index SI. This barrier is higher for HON compared to HET. In Figure 6-7, a schematic plot of the total Gibbs free energy (ΔG) for HON and HET is shown as a function of the radius of spherical nuclei. As soon as a critical nucleus is formed and the energetic barrier is exceeded (at the maximum of the ΔG curve), further growth of the nucleus is more favourable than starting disaggregation and precipitation. Compared to HET, a higher activation barrier has to be exceeded for HON nucleation to occur, which further explains why homogeneous nucleation requires higher levels of supersaturation to occur. The exact relation reads:

$$\Delta G_c = \frac{\beta v^2 \sigma^3}{(kT\ ln(SI))^2} \qquad 6\text{-}14$$

where β is a geometry factor, σ is the interfacial tension, v is the volume of a single spherical monomer of the mineral. The pre-exponential factor Γ represents the rate of attachment of monomers controlled by diffusion and is a function of the diffusion coefficient of the monomers, the number of nucleation sites, the number of monomers that form a critical nuclei and the degree of supersaturation. The appearance of many nuclei and their growth are responsible for the breakdown of the solution metastability. This process can be quantified with the induction time t_i, the time that the system remains in a metastable state before the onset of precipitation.

$$t_i = \left(\frac{1}{JV_p}\right) \qquad 6\text{-}15$$

where V_p is the volume of the local pore under consideration.

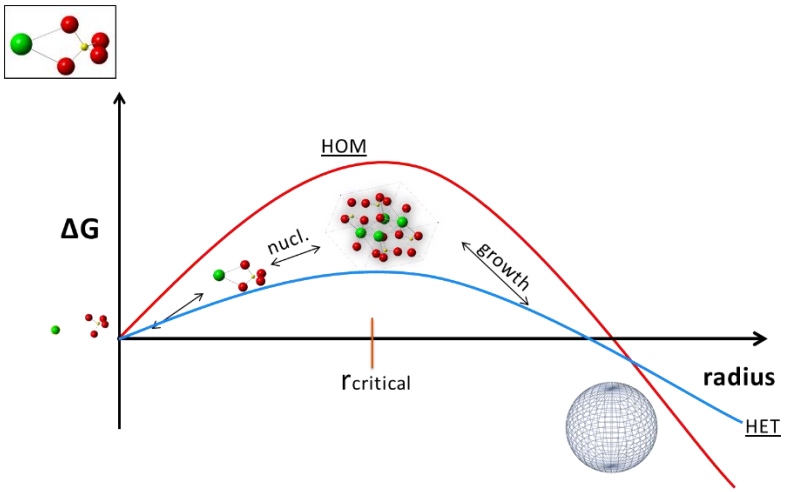

Figure 6-7: Schematic of the Gibbs free energy (ΔG) for homogeneous (HON) and heterogeneous (HET) nucleations as a function of the radius of spherical nuclei. As soon as a critical nucleus is formed ($r_{critical}$) and the energetic barrier is exceeded (at the maximum of the ΔG curve) further growth of the nucleus is more favourable than its disaggregation and precipitation starts. (Prasianakis et al., 2017)

The validity of the classical nucleation theory for the description of precipitation processes in confinement has been recently tested against microfluidic experiments in which nucleation and growth of barite crystal and barite celestite solid solution have been observed as function of sup saturation degree in solution and dimensions of confinement (Poonoosamy et al., 2021; 2019; Prasianakis et al., 2017).

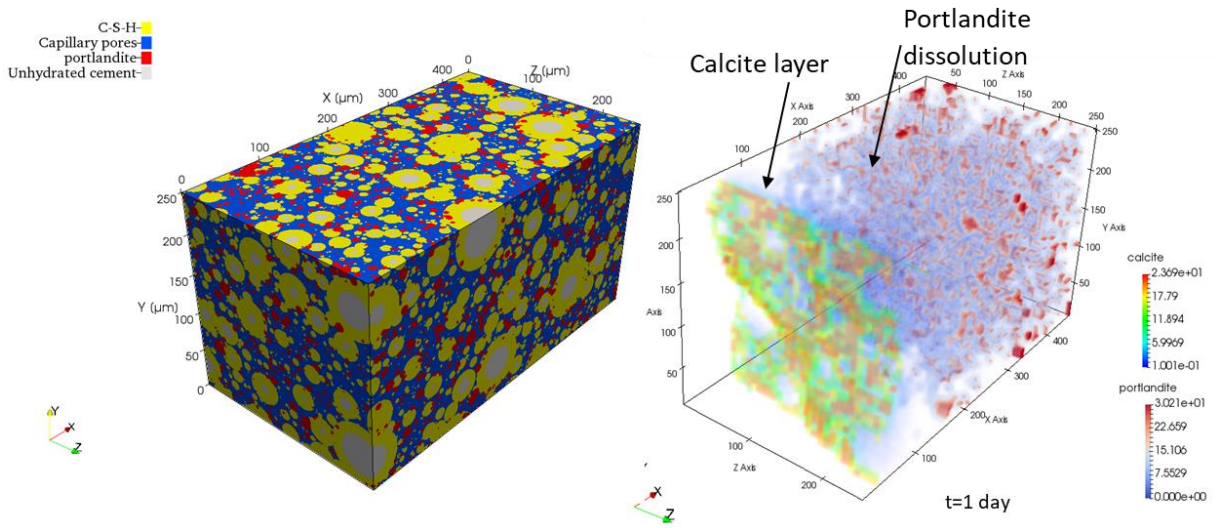

Figure 6-8: Initial distribution of portlandite and C-S-H in cement phase (left) and the evolution of portlandite dissolution front followed by carbonate precipitation front after 1 day of reaction time (Right). The simulations are performed in a 250 μm × 250 μm × 450μm with 435 μm^3 grid resolution (Patel et al., 2021).

Application of Machine learning for thermodynamic coupling

Major computational efforts in reactive transport simulations are related to the calculations of thermodynamic equilibrium and geochemical speciation. The reason for that is the large number of involved species, and the need to perform chemical calculations at each mesh point and every time step. Geochemical speciation calculations are used to find the quantities of chemical species in the system under the assumption of local equilibrium. This type of calculations can be done using the Law of Mass Action (LMA) (as in PhreeqC (Parkhurst, 1995)) or Gibbs Energy Minimization (GEM) (as in GEMS-Selektor (Kulik et al., 2012)). In a reactive transport code, reactions and mass transport are usually coupled in one of three main ways: by directly implementing the chemical speciation routines within the code (Xu et al., 2011), by using a pre-calculated look-up table that contains speciation calculations (Huang et al., 2018; Poonoosamy et al., 2019), or for more complex chemical systems by coupling the mass transport code to an external geochemical software (Kosakowski and Watanabe, 2014). The look-up table approach is in general faster but requires the pre-calculation of the full geochemical system, and the accuracy depends on the resolution of the look-up table. On the other hand, a direct calculation solving the chemical system will give an exact result, whereas it will be slower due to the involved calculations. In a reactive transport simulation, the number of geochemical calculations scales linearly with the number of computational grid points and the involved time steps.

Artificial neural networks (NN) are computational models that can represent complex relationships between input and output data in multidimensional spaces (Jain et al., 1996). Different NN's types are assembled to exhibit specific behaviour depending on their architecture, and the type of problem to be solved. The main challenge of machine learning algorithms is to sufficiently train a NN using an existing training set of input and output data, such that the NN can be used to forecast accurate output values for data that do not belong to the training dataset. Meanwhile, it should be noted that there is no optimum predefined number of neurons or an a-priori guarantee that a trained NN with a specific number of neurons can predict the output with the desired accuracy.

The feedforward type of NN's is used for the pore-level simulations. This is one of the simplest but most efficient network type, suitable for solving complex regression problems. The neural networks used in this study were obtained by a supervised learning approach in order to encode the thermodynamic equilibrium depending on the composition of the solution, with the data that GEMS provides. The mean squared error loss function is used.

The NN training is using the backpropagation technique introduced by (Rumelhart et al., 1986). The right balance between the size of the network and its resulting accuracy was pursued. For that, several networks were tested, by varying the number of neurons per hidden layer, the number of hidden layers and the activation functions of the neurons. Moreover, several training algorithms were tested. It is noted, that a common issue in this type of networks is the element mass conservation between input and output of the networks, which cannot be fully preserved and which at the moment is source of uncertainty (Guérillot and Bruyelle, 2020; Jatnieks et al., 2016). However, the resulting networks trained in this work achieve an excellent accuracy which is not affecting the simulation results similar to (Prasianakis et al., 2020).

6.1 References for appendixes

See references of Part 1.